Photo-Triggerable Laminin Mimetic Peptides for Directional Neural Regeneration

Max Planck Graduate Center
mit der Johannes Gutenberg-Universität Mainz

JOHANNES GUTENBERG UNIVERSITÄT MAINZ

Aleeza Farrukh

Dissertation

Zur Erlangung des Grade eines

“Doctor rerum naturalium (Dr. rer. nat.)”

der Fachbereiche:

• 08 – Physik, Mathematik und Informatik

• 09 – Chemie, Pharmazie und Geowissenschaften

• 10 – Biologie

• Universitätsmedizin

der Johannes Gutenberg-Universität

Mainz, July 2017

Photo-Triggerable Laminin Mimetic Peptides for Directional Neural Regeneration

Aleeza Farrukh

geb. in Karachi, Pakistan

Dissertation

Max Planck Institute for Polymer Research, Mainz, Germany
INM – Leibniz Institute for New Materials, Saarbrücken, Germany

Mainz, July 2017

I hereby declare that I wrote the dissertation submitted without any unauthorized external assistance and used only sources acknowledged in the work. All textual passages which are appropriated verbatim or paraphrased from published and unpublished texts as well as all information obtained from oral sources are duly indicated and listed in accordance with bibliographical rules. In carrying out this research, I complied with the rules of standard scientific practice as formulated in the statutes of Johannes Gutenberg-University Mainz to insure standard scientific practice.

Aleeza Farrukh

Abstract

The restoration of neuronal activity after injury or during aging requires neuron repopulation at the site of injury, directional regeneration of new nerves and oriented generation of new synapses. The ECM protein Laminin is abundant in neuronal microenvironment and is known to be involved in directing neuronal migration, differentiation and neurite development. In this thesis, a strategy for *in vitro* directional neurite growth in soft hydrogels is presented. It is based on the spatiotemporal control of the availability of Laminin adhesive motifs within synthetic hydrogels using light as an external guiding trigger.

Different variants of Laminin mimetic peptides containing the IKVAV were selected as ligands to mediate control over axonal growth on biomaterials. The photo-cleavable groups 3-(4,5-dimethoxy-2-nitrophenyl)-2-butanol (DMNPB), 6-nitroveratryl alcohol (NVOC) and 2,2'-((3'-(1-hydroxypropan-2-yl)-4'-nitro-[1,1'-biphenyl]-4-yl)azanediyl)bis(ethan-1-ol) (HANBP) were inserted at the K rest of the peptide to temporally block IKVAV bioactivity. Poly(acrylamide) (PAAm) hydrogel films with varied stiffness from 0.2-70 kPa were used as 2D substrates to study IKVAV-guided directional growth of axons. Two novel acryl monomers carrying methylsulfone (MS) side chains were developed to tune specific coupling of thiol terminated IKVAV to the PAAm gel at physiological conditions. The ability of the photoactivatable IKVAV-containing peptides to trigger and support neurite outgrowth was studied and compared in different cell biology experiments using neural progenitor cells from mouse embryo. The ability of the photoactivatable IKVAV-containing peptides to trigger and support spatial organization of neurons was demonstrated by using masked irradiation. The *in-situ* light exposure of IK(HANBP)VAV by scanning lasers allowed spatially directed neurite development in 2D cell cultures.

In the last part of the Thesis, an attempt to extend the photoactivation strategy to 3D environments was made by using two-photon activatable chromophores. The *p*-methoxynitrobiphenyl (PMNB) photoremovable group was introduced at aspartic acid residue of RGD sequence, a common adhesive motif used for cell attachment to biomaterials. Degradable hydrogels modified with RGD(PMNB)fC peptide were developed and 3D resolved spatial photoactivation inside the gel using two-photon laser guided migration of fibroblasts L929 within the 3D network was established. These results demonstrate that photoactivatable adhesive peptides can be used for spatiotemporal activation of attachment, migration and directional growth of cells in 2D and 3D cultures and provide a tool to control and pattern cell processes in relevant biomedical applications.

Zusammenfassung

Die Wiederherstellung der neuronalen Aktivität nach Verletzung oder während des Alterns erfordert die Repopulation von Neuronen an der Verletzungsstelle, die gerichtete Regeneration von neuen Nerven und die orientierte Generation von neuen Synapsen. Das ECM Protein Laminin ist üppig innerhalb der neuronalen Mikroumgebung exprimiert. Hier ist es maßgeblich an der gerichteten Migration und Differenzierung von Neuronen sowie der neuralen Entwicklung beteiligt. In dieser Arbeit wird eine Strategie für ein gerichtetes Axonwachstum innerhalb eines weichen Hydrogels *in vitro* vorgestellt. Das Wachstum basiert auf der durch externes Licht raumzeitlich kontrollierbaren Verfügbarkeit und räumlichen Lokalisation von Lamininadhäsionsmotiven innerhalb des synthetischen Hydrogels.

Zur Vermittlung eines kontrollierbaren axogonalen Wachstums auf Biomaterialien wurden verschiedene Varianten des mimetischen Lamininpeptids, die die Sequenz IKVAV enthalten, als Liganden ausgesucht. Die lichtabspaltbare Gruppen 3-(4,5-dimethoxy-2-nitrophenyl)-2-butanol (DMNPB), 6-nitroveratryl alcohol (NVOC) und 2,2'-((3'-(1-hydroxypropan-2-yl)-4'-nitro-[1,1'-biphenyl]-4-yl)azanediyl)bis(ethan-1-ol) wurden des Peptids eingeführt, um die IKVAV-Bioaktivität zeitlich zu blockieren. Polyacrylamid- (PAAm) Hydrogele mit unterschiedlichen Steifigkeiten von 0,2-70 kPa wurden als 2D-Substrate verwendet, um das IKVAV-gesteuerte, gerichtete Axonwachstum zu untersuchen. Zwei neue Acryl-Monomore, die Methylsulfon- (MS) Seitenketten enthalten, wurden entwickelt und ermöglichen unter physiologischen Bedingungen die spezifische Kupplung von Thiol-modifizierten IKVAV an die PAAm-Gele. Die Fähigkeit von lichtaktivierbaren IKVAV-enthaltenen Peptiden zur Erzeugung und Unterstützung eines Axonauswuchs wurde in verschiedenen zellbiologischen Experimenten untersucht und verglichen. Hierzu wurden neurale Progenitorzellen gewonnen aus Mausembryonen verwendet. Unter der Verwendung von Maskenbelichtung und abrasternden Lasern konnte die Möglichkeit der räumlichen Neuronorganisaton auf der Oberfläche über licht-aktivierbare Peptide demonstriert werden. Die *in situ* Belichtung von IK(HANBP)VAV erlaubte die räumlich-gerichtete Axonentwicklung in 2D-Zellkulturen.

Im letzten Teil der Arbeit wird der Versuch, die Strategie der Lichtaktivierbarkeit in 3D-Umgebungen mittels 2-Photon-Aktivierung zu erhöhen, beschrieben. Es *p*-methoxynitrobiphenyl (PMNB) wurde verwendet, um die Asparaginsäure innerhab der RGD-Sequenz, eines bekannten Zell-Adhäsionsmotiv auf Biomaterialien, zu schützen. Es wurden abbaubare, mit RGD(PMNB)fC-Peptid modifizierte Hydrogele wurden entwickelt und 3D-aufgelöste räumliche Lichtaktivierung innerhalb des Gels unter Verwendung eines 2-Photonen-Laserscanners, ermöglichte eine Fibroblasten L929migration innerhalb des 3D-Netzwerks initiierte, wurde hergestellt. Diese Ergebnisse demonstriert, dass licht-aktivierbare, adhäsive Peptide verwendet werden können, um raumzeitlich Zellanhaftung, Migration und direktes Wachstum in 2D- und 3D-Kulturen zu steuern. Dies stellt ein Werkzeug zur Kontrolle und Strukturierung von Zellprozessen in relevanten biologischen Anwendungen dar.

Abbreviations

δ	Chemical shift
ε	Molar extinction coefficient
λ_{max}	Wavelength of the absorbance maximum
v	Frequency
φ	Chemical yield
Φ	Quantum yield
AAm	Acrylamide
AA	Acrylic acid
APS	Ammonium persulfate
APTS	3-(Trimethoxysilyl)propyl acrylate
APTES	(3-Aminopropyl)triethoxysilane
ANBP	*p* –dimethylaminonitrobiphenyl
Ala	Alanine
Arg	Arginine
Asp	Aspartic acid
Ar	Organic/Aromatic Residue
AU	Absorbance units
AcOH	Acetic acid
BSA	Bovine serum albumin
Boc	Tert-butoxycarbonyl protecting group
^{t}Bu	Tertiary butyl ester
c	Concentration
$CDCl_3$	Deuterated chloroform
cyclo[RGDfK]	Cyclic (arginine-glycine-aspartic acid-D-phenylalanine-lysine)
cyclo[RGDfC]	Cyclic (arginine-glycine-aspartic acid-D-phenylalanine-cysteine)
cyclo[RGD(DMNPB)fK]	Cyclic (RGDfK) caged with 3-(4,5-dimethoxy-2-nitro-phenyl)- 2-butyl ester at the carboxylic side chain of the aspartic acid
cyclo[RGD(coum)fC]	Cyclic (RGDfC) caged with (7-(N,N-diethylamino)-coumarin-4-yl)methyl at the carboxylic acid side chain of the aspartic acid
cyclo[RGD(coum)fK]	Cyclic (RGDfK) caged with (7-(N,N-diethylamino)-coumarin-4-yl)methyl at the carboxylic acid side chain of the aspartic acid
Cys	Cysteine
d	Day
d	Doublet (NMR)

DAPI	(4',6-Diamidino-2-phenylindole, dihydrochloride)
DCM	Dichloromethane
DCX	Doublecortin
DLS	Dynamic light scattering
DEACM	(7-(N,N-diethylamino)-coumarin-4-yl)methanol
DIPEA	Diisopropylethylamine
DIV	Days in vitro
DMAP	4-dimethylaminopyridine
DMEM	Dulbecco's Modified Eagle Medium
DMF	N,N-dimethylformamide
DMNPB	3-(4,5-dimethoxy-2-nitrophenyl)-2-butanol
DMSO	Dimethylsulfoxide
DPPA	Diphenylphosphorylazide
E	Young´s Modulus
EDC	1-ethyl-3-(3-dimethylaminopropyl)carbodiimide
ECM	Extracellular matrix
eq.	Molecular equivalent
ESI-MS	Electrospray ionization mass spectroscopy
EtOH	Ethanol
EtOAc	Ethylacetate
E 14.5	Mouse embryonic day 14.5
FAK	Focal adhesion kinase
FBS	Fetal bovine serum
FCS	Fetal calf serum
FGF	Fibroblast growth factor
Fmoc	9-fluorenylmethoxycarbonyl protecting group
G´	Storage Modulus
GFP	Green fluorescent protein
Gly	Glycine
GPC	Gel permeation chromatography
h	Hour
HANBP	2,2'-((3'-(1-hydroxypropan-2-yl)-4'-nitro-[1,1'-biphenyl]-4-yl)azanediyl)bis(ethan-1-ol)
HBTU	O-benzotriazole-N,N,N’,N’-tetramethyl-uronium-hexafluorophosphate
HeLa	Henrietta Lacks cell line (Human epithelial cell line)

HEPES	4-(2-hydroxyethyl)-1-piperazineethanesulfonic acid)
HOBt	1-hydroxybenzotriazol
HPLC	High performance liquid chromatography
HUVEC	Human umbilical vein endothelial cells
Hz	Hertz
Ile	Isoleucine
J	Coupling constant in Hz (NMR)
LED	Light emitting diode
Lys	Lysine
M	Molarity (mol/l)
m	Multiplet (NMR)
MAL	Maleimide
MeOH	Methanol
MES	2-(N-morpholino)ethanesulfonic acid
Milli-Q	Deionized, filtered ultrapure water
min	Minute
MS	Methyl Sulfone
MMP	Matrix metalloproteinase
MW	Molecular weight
Mw	Molecular weight distribution
mol%	Molar percentage
NaCl	Sodium chloride
NaOH	Sodium hydroxide
$NaHCO_3$	Sodium bicarbonate
NB	Nitrobenzyl
NH_2	Amino group
NGF	Nerve growth factor
NPCs	Neural progenitor cells
NVOC	6-Nitroveratryl alcohol
NHS	N-hydroxysuccinimide
NMR	Nuclear magnetic resonance
NSCs	Neural stem cells
o	Ortho
OH	Hydroxyl
OMe	Methoxy
PD	Polydispersity index

PDL	Poly-D-Lysine
PMNB	*p*-methoxynitrobiphenyl
p	Para
Pbf	Nα-(2,2,4,6,7)-pentamethyldihydro-benzofuran-5-sulfonyl
PBS	Phosphate buffered saline
PEG	Poly(ethylene glycol)
Phe	Phenylalanine
q	Quartet (NMR)
R	Organic residue
s	Singlet (NMR)
SAM	Self-assembled monolayer
sec	Second
SMI	Anti-Neurofilament marker
SEM	Scanning electron microscopy
sulfo-SANPAH	(sulfosuccinimidyl-6-(4'-azido-2'-nitrophenylamino)hexanoate)
Ser	Serine
r.t.	Room temperature
TFA	Trifluoroacetic acid
TEMED	Tetramethylethylenediamine
TFE	2,2,2-trifluoroethanol
THF	Tetrahydrofuran
TLC	Thin layer chromatography
TRITC	Tetramethylrhodamine B isothiocyanate
Tris	Tris(hydroxymethyl)aminomethane / 2-amino-2-hydroxymethyl-1,3-propanediol
UV	Ultraviolet
UV/VIS	Linear optical absorption spectroscopy in the ultraviolet and visible spectral region
Val	Valine
VIS	Visible spectral range
wt%	Weight percentage
X	Leaving group
^{1}H-NMR	Proton NMR spectroscopy
^{13}C-NMR	Carbon NMR spectroscopy

All other abbreviations, as physical and chemical units, have their usual meaning if not stated otherwise.

Index

Motivation **1**

1. Background and Literature Review **6**

1.1 The extracellular matrix (ECM) **6**

1.2 Cell-matrix Interactions **8**

1.2.1 Biochemical interaction **8**

1.2.2 The integrin trans-membrane receptor family **9**

1.2.3 Biophysical interaction and mechanotransduction **12**

1.3 Biomimetic extracellular matrices **13**

1.3.1 Peptidomimetics of adhesive proteins **14**

1.3.2 Hydrogels as 2D and 3D Matrices **20**

1.3.3 Dynamic changes in the physical properties of hydrogels by degradation **27**

1.4 Light-induced changes in the biochemical properties of synthetic biomaterials **29**

1.5 Photo-cleavable protecting groups for light-triggered biochemical activity **30**

1.5.1 The NVOC photo-cleavable protecting group **33**

1.5.2 The DMNPB photo-cleavable protecting group **36**

1.5.3 The nitrobiphenyl (ANBP and PMNB) photo-activatable two photon protecting groups **39**

2. Synthesis of photoactivable laminin mimetic peptides **49**

2.1 Introduction **49**

2.2 Molecular design of a photoactivatable laminin peptides **51**

2.2.1 Selection of laminin peptidomimetic **51**

2.2.2 Selection of caging site **55**

2.2.3 Synthesis of caged IK-12 variants **56**

2.3 Photochemical properties of caged IK-12 derivatives **60**

2.4 Synthesis of IK(HANBP)VAV **62**

2.5 Photolysis studies on thin hydrogel films **64**

2.6 Conclusions **66**

3. New routes for biofunctionalization of P(AAm) gels with cell adhesive ligands **69**

3.1 Introduction **69**

3.2 Synthesis of methylsulfone acrylamides **72**
3.3 Synthesis and physicochemical properties of P(AAm-MS) hydrogels **74**
3.4 Surface functionalization of copolymer P(AAm-X) **80**
3.5 Biocompatibility of P(AAm-MS) hydrogels **85**
3.6 Conclusions **87**

4. Differentiation of neural progenitor cells on bifunctionalized soft P(AAm-MS-AA) gels **90**
4.1 Introduction **90**
4.2 Preparation and physicochemical characterization of P(AAm-MS-AA) hydrogels **93**
4.3 Orthogonal coupling of two different ligands to P(AAm-MS-AA) hydrogels **99**
4.4 Differentiation of neural progenitor cells on bifunctionalized P(AAm-MS-AA) **105**
4.5 Influence of substrate stiffness on differentiation of neural progenitor cells culture **110**
4.6 Bifunctional hydrogels platform to controls fate of Adult NSCs **115**
4.7 Conclusions **117**

5. Photo-activatable Laminin peptidomimetics for directional neuronal growth **120**
5.1 Introduction **120**
5.2 Bioactivity of Laminin Peptidomimetics **121**
5.2.1 Bioactivity of IKVAV variants **121**
5.2.2 Bioactivity of IK-12 photoactivatable variants **126**
5.3 Directional neuronal migration on IK-12(HANBP) patterned substrates **129**
5.4 Neuronal differentiation and localization on light-activated IK(HANBP)VAV hydrogels **131**
5.5 *In-situ* activation of IK-12(HANBP) for light guided axon growth **136**
5.6 Conclusions **138**

6. Two photon photoactivatable c[RGD(PMNB)fC] for spatially controlled cell migration in 3D **141**
6.1 Introduction **141**
6.2 Synthesis of two photon activatable RGD(cage)fC **144**

6.2.1 Selection of chromophores and synthesis of photoactivatable variants of aspartic acid **144**
6.2.2 Synthesis of photoactivatable RGDfC peptide. **146**
6.2.3 Physicochemical properties of RGD(Cage)fC derivatives **148**
6.3 Photochemical properties of RGD(PMNB)fC **149**
6.4 Spatiotemporally controlled cell adhesion and migration in 2D cell culture **151**
6.5 Cell migration in 3D pathways defined by 2P activation **153**
6.5.1 Synthesis and physicochemical properties of thiol/maleimide PEG hydrogels for cell encapsulation **153**
6.5.2 3D patterning of cell adhesive ligands in PEG hydrogels **156**
6.5.3 Cell migration on gels after two-photon activation of RGD(PMNB)fC **157**
6.6 Conclusions **159**

7. Conclusion and Outlook **162**
8. Appendix **164**
List of Scientific Contributions **211**

Motivation

In recent years the biomaterials field is flourishing thanks to impressive progress in the understanding of how cells and materials interact from a biological perspective. The development of tunable biomaterials for tissue engineering or cell therapies able to mediate controlled and personalized interactions between cells and materials open new avenues for regenerative medicine and therapeutic applications. The biocompatibility and immunogenicity of biomaterials for *in vivo* use are relevant pre-requisites for biomaterials application, and relevant synthetic polymers have been developed over the last decades to reasonably fulfill these requirements. Increasing attention is now paid to the physical properties (stiffness, topography, viscoelasticity, toughness) and biochemical functionalization of artificial biomaterials to match those of natural tissues. The dynamic variation of these properties continuously occurs in natural tissues, and plays a fundamental role in basic cellular processes such as adhesion, migration, proliferation, or differentiation. Classical biomaterials, however, do not allow dynamic variation of properties or adaptation.

The extracellular environment surrounding the cells *in vivo* comprises scaffolding and adhesive proteins, growth factors and neighboring cells. Biomaterials nowadays are designed to capture the mechanical and adhesive properties of the natural scaffold, named the extracellular matrix (ECM). Typically, hydrogels incorporating adhesive ligands are used for this purpose. In many cases those adhesive ligands are peptidomimetics of the adhesive sites of the natural ECM adhesive proteins, which allow more easy and quantitative bioconjugation to artificial biomaterials, as well as controlled degradability or activity depending on the chemical design. The properties of the ECM are dynamic: cells continuously remodel the composition and biophysical properties of the ECM by secreting new components or proteases to degrade them. Such control is difficult to realize in artificial materials and approaches using responsive polymers have been reported. Biomaterials changes in response to electric or magnetic fields, chemicals, pH, or temperature have been realized. More recently, light has also been used to control biomaterials properties and cell-matrix interactions. Light response is particularly interesting in a biomedical context, as light is readily available in biological setups and increasingly used in the clinics. It allows selective targeted activation of light-responsive molecules and can be easily tuned.

In this Thesis, a strategy to light-direct cell-materials interactions *in vitro* is presented, and particularized for directing the growth and differentiation of neurons using specialized biomaterials and photoactivatable mimics of ECM adhesive proteins. Photoactivatable, IKVAV-containing Laminin peptidomimetics will be developed and applied to biofunctionalized hydrogels and support neuronal cell cultures upon light exposure. This platform enables light guided spatial arrangement of adhesive ligands to direct cell attachment and *in situ* guide neurites extension using scanning lasers. These novel biomaterials allow external control on adhesion and extension of neurites and finally directed axon growth.

This Thesis has the following objectives:

- Synthesis and characterization of phototriggerable laminin mimetic peptides by introducing unnatural amino acids in the peptide sequence containing a photoremovable protecting group. In particular peptides containing the 5-mer sequence IKVAV, which has been reported to be the shortest functional sequence sensed by neurons, will be developed.
- Different photoremovable protecting groups will be explored for derivatizing the peptides and selected on the basis of photolytic efficiency, hydrolytic stability and water solubility.
- The ability of photoactivatable mimetic peptides to be recognized by the corresponding cell membrane receptors before and after activation and guide cellular behavior will be studied and compared.
- Model hydrogel biomaterials will be developed for cell studies. Soft polyacrylamide hydrogels with tunable stiffness and adhesive ligands will be prepared. Optimization of ligand concentration and substrate stiffness for neuronal cell cultures will be attempted, as both parameters are known to be crucial in *in vitro* cultures of neurons.
- The adhesive and directional cues for directional regeneration of axon and dendrites in primary neuronal progenitor cultures will be investigated.

In the last part of the Thesis, this approach will be extended to 3D cell culture systems. For this purpose, the classical RGD binding motif from fibronectin will be used and modified with two-photon activatable photocleavable groups. Light-activated cell adhesion and migration within 3D biodegradable PEG hydrogels will be

demonstrated by two-photon scanning and photocleavage of the chromophore. The following objectives will be addressed:

- Synthesis of two-photon photoactivatable RGD derivatives with high photolytic efficiency and hydrolytic stability.
- Functionalization of 3D PEG hydrogels with two-photon photoactivatable RGD and optimization of composition for cell encapsulation.
- Spatiotemporally defined activation of attachment and migration of fibroblasts within the 3D hydrogel network using a scanning laser at long wavelengths.

The thesis is organized as follows:

Chapter 1- Background and literature Review; describes fundamentals of cell-ECM interactions *in vivo;* summarizes state-of-the-art literature on biomimetic hydrogels with bio-mechanical and biochemical features to regulate dynamic interactions *in vitro*; describes 2D and 3D cell culture platforms and light-activatable chemistries for single and two-photon activation.

Chapter 2 describes the selection and synthesis of several photoactivatable IKVAV peptidomimetic variants from laminin protein containing different chromophores and different amino acid sequences. The physicochemical and photochemical properties of the obtained photoactivatable variants will be compared. The IK(HANBP)VAV variant, with improved solubility, hydrolytic stability, and photo efficiency will receive particular attention.

Chapter 3 entails the development of a methylsulfone acrylate monomer for functionalization of polyacrylamide hydrogels to support cell cultures. The copolymers of methyl sulfone acrylate with acrylamide will be presented for specific conjugation of thiolated biomolecules to the hydrogel. The synthesis of the acrylate monomer, the physicochemical characterization, biofunctionalization of the copolymer and the cell culture experiments on the hydrogel will be described.

Chapter 4- The poly(acrylamide)-based hydrogel platform for differentiation of neural progenitor and stem cells will be described. Soft poly(acrylamide) hydrogels copolymerized with acrylic acid and methylsulfone acrylate for orthogonal bifunctionalization of hydrogel networks will be presented. The characterization of

terpolymer, selective and specific surface functionalization and application for neural culture will be described.

Chapter 5 describes the bioactivity of IKVAV variants in neural cultures. The application of the photoactivatable laminin peptidomimetics from chapter 2 for spatial neuronal migration and *in situ* activation for light guided neurite extension is described.

Chapter 6 describes the design, synthesis and photochemical properties of two-photon activatable RGD peptides. The design of a 3D hydrogel for cell encapsulation and spatiotemporally controlled adhesion and migration with 3D resolution will be presented.

Chapter 7 summarizes the most important conclusions from the presented work and gives a brief outlook on future directions.

Chapter 8- Appendix provides all the experimental protocols, NMR, HPLC, ESI-MS data, cell culture protocols and surface functionalization strategies as well as related supplementary data.

Chapter 1

Background and Literature Review

1.1 The extracellular matrix (ECM)

The extracellular matrix (ECM) is the scaffold surrounding the cells in tissue. This material provides mechanical support to the cells and also plays a relevant role in regulating cell behavior by biochemical signaling.[1] The biochemical and structural properties of ECM are specific for different tissue types, attributed to mutual remodeling of ECM components regulated by cell-matrix interactions.[2] The ECM undergoes dynamic tuning of production and degradation of it components and cells respond to these modulation.[3]

ECM is integral for various physiological process such as embryogenesis angiogenesis, morphogenesis and wound healing. The integrity of ECM is indispensable for proper tissue functioning. Malfunction of ECM results in failure in regulation of cell proliferation, apoptosis, adhesion and differentiation. This results in various pathological disorders such as tissue fibrosis, tumor progression and genetic syndromes such as Williams-Beuren syndrome, Ehlers-Danlos syndrome (EDS) and Marfan syndrome (MFS).[1b, 3-4] ECM is formed by complex macromolecules comprising mesh of fibers (collagen, elastin), proteoglycans and adhesive proteins (laminin, fibronectin) (Figure 1).[5] Different components of ECM and their functions are described in the following sections.

a) Structural proteins

Structural proteins are the major component of ECM. They are water insoluble fibrous proteins, provide tensile strength, regulate cell adhesion and facilitate migration during tissue development. Collagen is major part of structural protein and comprise 30% of total protein mass in multicellular animals.[5a] Fibroblast predominantly, secretes collagen, pull on collagen fibrils, to organize and align them into sheets, cables and fibers. Fibrillins and elastin fibers are also part of mesh fibers and enhance strength and resilience of collagen fibers.

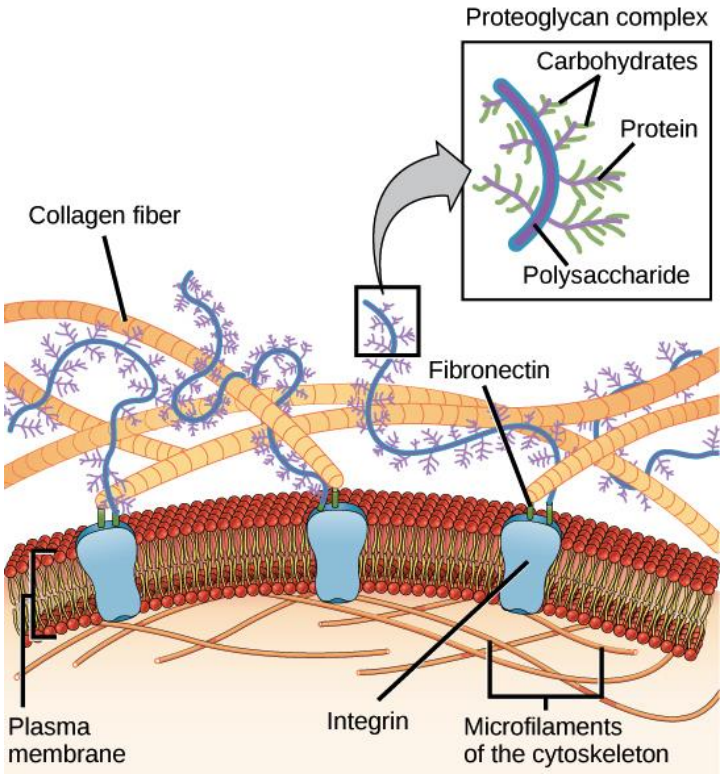

Figure 1. Components of extracellular matrix. Copyrights Biology-Open Stax.

b) Proteoglycans

Proteoglycans are highly hydrated component of ECM and connective tissues. They fill interstitial space and provide mechanical cushion. They comprise a protein core to which repeating sulfated disaccharide units, known as glycosaminoglycans (GAGs) are attached.[5d] These repeating units inherit high surface charge, they assemble to form high molecular weight chains that swell and hydrate the ECM, and provide a platform for the diffusion of small molecules in ECM. The most important proteoglycans are heparan sulfate, keratin sulfate and chondroitin sulfate.[5b]

c) Adhesive proteins

Adhesive matrix proteins provide binding sites for cells and growth factors; and play key role in organization of other ECM components. Laminin and fibronectin are major ECM adhesive proteins. In addition to providing physical strength to matrix, they regulate cell shape, attachment, and migration. Therefore, these protein tune signal-transduction, cellular response, and integrin mediate cell attachment. Fibronectin is a glycoprotein that regulates attachment of cell to matrix components as collagen (types I, II, III, and V) and polysaccharides.[6] The 11-different types of fibronectin defined by different fibronectin modules which contain binding sites for other ECM

components such as fibrin, collagen and heparan sulfate proteoglycans (HSPGs). A tripeptide unit Arg-Gly-Asp (RGD) is major binding site of fibronectin for interaction with integrin receptor on cell surface. During cell-fibronectin interaction forces excreted by cell, directs fibrillogenesis i.e conversion of soluble form of fibronectin to fibrillar fibronectin.[4, 7] This mechanoregulatory interaction with integrin binding sites on cell play important role in cell adhesion and migration.

Laminins are multi-adhesive matrix proteins present in all basal lamina secreted by epithelial and mesenchymal cells.[8] It is responsible for binding of matrix components such as collagen and polysaccharides to organize ECM and show receptors mediated signaling between ECM and cell surface by interaction with integrin and dystroglycan.[5d, 9] Laminins are involved in cell type–specific functions in processes such as adhesion, differentiation, migration, phenotype maintenance, and resistance to apoptosis. Laminin is a heterotrimeric protein contain α chain (~400 kDa), β chain (~210 kDa), and γ chain (~200 kDa).[10] The α, β, and γ chains form disulfide bonds and arrange in cross structure (Figure 6).[10] On the basis of genetically distinct forms of α, β, and γ chains approximately 16 different laminin isoforms are identified. Almost 9 different form of integrin can bind to Laminin as $\alpha_1\beta_1$, $\alpha_2\beta_2$, $\alpha_6\beta_1$, $\alpha_6\beta_4$, $\alpha_7\beta_1$, $\alpha_9\beta_1$, $\alpha_v\beta_3$, $\alpha_3\beta_1$ and $\alpha_4\beta_1$, result in distinct tissue-specific functions.[11]

1.2 Cell-matrix interaction

Cell-Matrix interaction encompasses reciprocal biochemical and biomechanical signaling between cellular components and microenvironment. This dynamic interaction on one hand modulates fate of cell such as proliferation and differentiation while on the other hand tunes the properties of ECM.[12] The resulting site specific heterogeneity of ECM translates in to different functional tissue. The cell-ECM connection involves mechanical signaling through physical and topographical features of ECM and chemical signaling by cell adhesion molecules (CAMs).

1.2.1 Biochemical interaction

The dynamic signaling between cell and it is surrounding is regulated by binding of CAMs such as integrins, mucins, immunoglobin super family (Ig), cadherins, and selectins with matrix proteins, neighboring cells and growth factors.[13] These binding

interactions transduce signaling pathway and regulate physiological features such as development of blood brain barriers, axonal guidance and tissue homeostasis. These receptors bind to identical receptor through homophilic interactions (e.g cadherin receptors) or to a different type of cell adhesion molecules by heterophilic interaction (e.g integrin receptor), as depicted in Figure 2. The adhesion receptors primarily depend on Ca^{+} ions for attachment, although binding of immunoglobin superfamily is Ca^{+} independent.

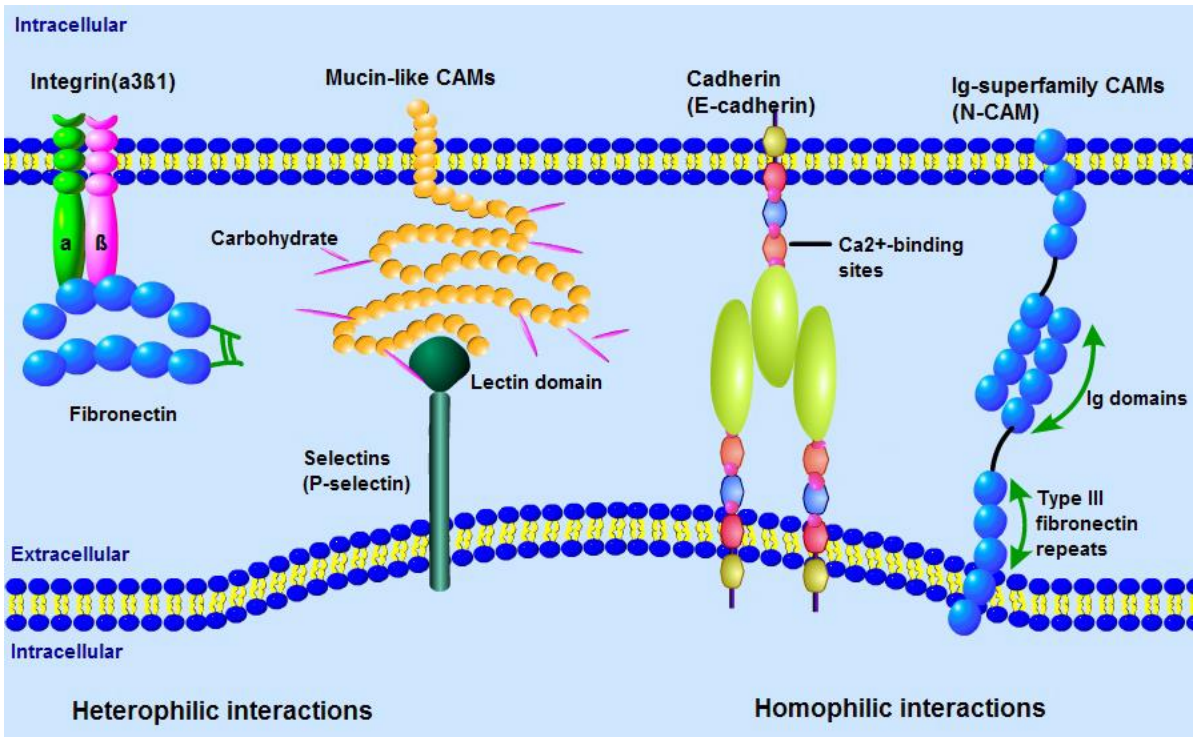

Figure 2. Four major classes of CAM. Reproduced after permission

1.2.2 The integrin trans-membrane receptor family

Integrins are transmembrane glycoprotein receptors. They mechanically connect intracellular and extracellular components and mediate cell-ECM interaction. They are bidirectional heterodimeric receptors with two non-covalently bounded alpha and beta subunits. There are 24 different types of integrins combining by 18 alpha and 8 beta units.[14] Integrins interact with ECM ligands and this interaction can initiate cascade of signal transduction, controlling cellular process such as cytoskeleton organization, adhesion, migration, and survival. The well-known adhesion motif of fibronectin; RGD mainly binds with $\alpha_5\beta_1$, $\alpha_8\beta_1$ and $\alpha_v\beta_3$. The laminin shows strong interaction with $\alpha_3\beta_1$, $\alpha_4\beta_1$, $\alpha_6\beta_1$, $\alpha_7\beta_1$, $\alpha_6\beta_4$ while major collagen integrin receptors

are $\alpha_1\beta_1$, $\alpha_2\beta_1$, $\alpha_{10}\beta_1$, $\alpha_{11}\beta_1$.[11b, 15] The integrin-ligand complex is a conundrum involving interaction of one integrin to various receptor or vice versa however each interaction mediate distinct functional response.[15] Thus malfunction of integrin receptor disrupt cellular functions causing diseases such as osteoporosis, inflammation, thrombosis and metastasis.[14]

Integrins have three major domains, large extracellular domain, transmembrane domain and cytoplasmic domain. Extracellular domain is about 80–150 kDa and interact with extracellular matrix proteins, while the short transmembrane domain (TM) of integrin, embedded in cell membranes comprise helical coils of about 25–29 amino acid units. The cytoplasmic domains interact with cytosolic components and usually contain 10–70 amino acid residues, while it could reach up to 1000 amino acids units in certain cases. However the GFFKR and HDR(R/K)E motif in cytoplasmic domain is conserved for alpha and beta subunit respectively. The arginine (R) from alpha and aspartic acid (D) from beta unit form salt bridge between both chains during integrin resting conformation.[16]

Integrin extracellular domains in resting state are present in low-affinity or bent conformations and upon interaction with binding ligand shift to high affinity or straight conformation.[16] TM domain during activation state undergoes dissociation of transmembrane helices, resulting in stabilization and straightening of active conformation.[14] The cytoplasmic domain during activation interacts with cytoskeletal protein and facilitates signaling proteins, leading to stabilization of focal adhesion complex.[1b]

Integrin regulates bi-directional signal transduction, either by binding with ECM ligand *outside-in* signaling or in certain cell types initiate signaling from cytoplasm to ECM *inside-out* signaling.

a) *Inside-Out* signaling

Inside-out integrin activation generally occur in blood cells such as platelets or leukocytes, in response to external cues as injury, vasculature or inflammation. Moreover, during morphogenesis *inside-out* signaling assist long distant cell migration and enables onset of signal transduction by cell once it come close to ligand. This signaling pathway disrupt salt bridge between α and β subunit of cytoplasmic domain and directs interaction with cytoskeleton component; talin which bind with kindlins to form focal adhesion (Figure 3). This multimerization on

cytoskeleton lead to reorganization of transmembrane domain resulting in its binding with ECM ligand. [14]

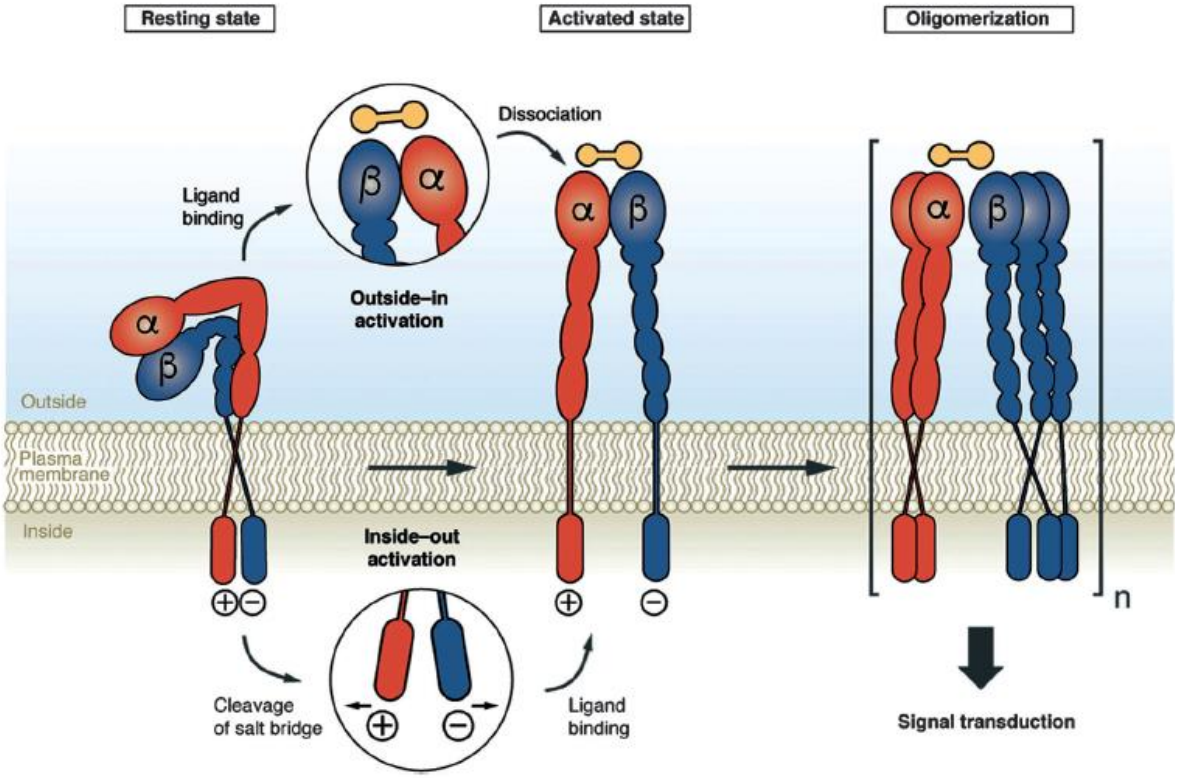

Figure 3. Schematic representation of Integrin activation and signaling. Reproduced with permission from Wiley publications.[14]

b) *Outside-In* signaling

In this scenario integrins undergo activation on attachment of extracellular domain with ECM ligands, leading to signal transduction. Most adherent cells activate by this signaling pathway, results in cell adhesion, differentiation, polarization and apoptosis. This intracellular signal mediates mechano-transduction by assembly of the cytoskeleton and focal adhesion formation. Focal adhesion (FA) is a multiprotein complex, form in response to integrin activation in plasma membrane, leading to assembly of actin fibers. In course of *outside-in* signaling, integrin cytoplasmic domain interacts with actin cytoskeleton via talin, actinin and filamin, which further binds with cytoskeleton proteins such as kindlins, paxillin, integrin-linked kinase (ILK) and vinculin (Figure 4).[17] This binding results in strengthening of cytoskeleton, transduction of intracellular signaling, transmission of forces on ECM and formation

of FA complex.[18] Consequently, integrin receptors are key for modulation of cell-matrix interaction.

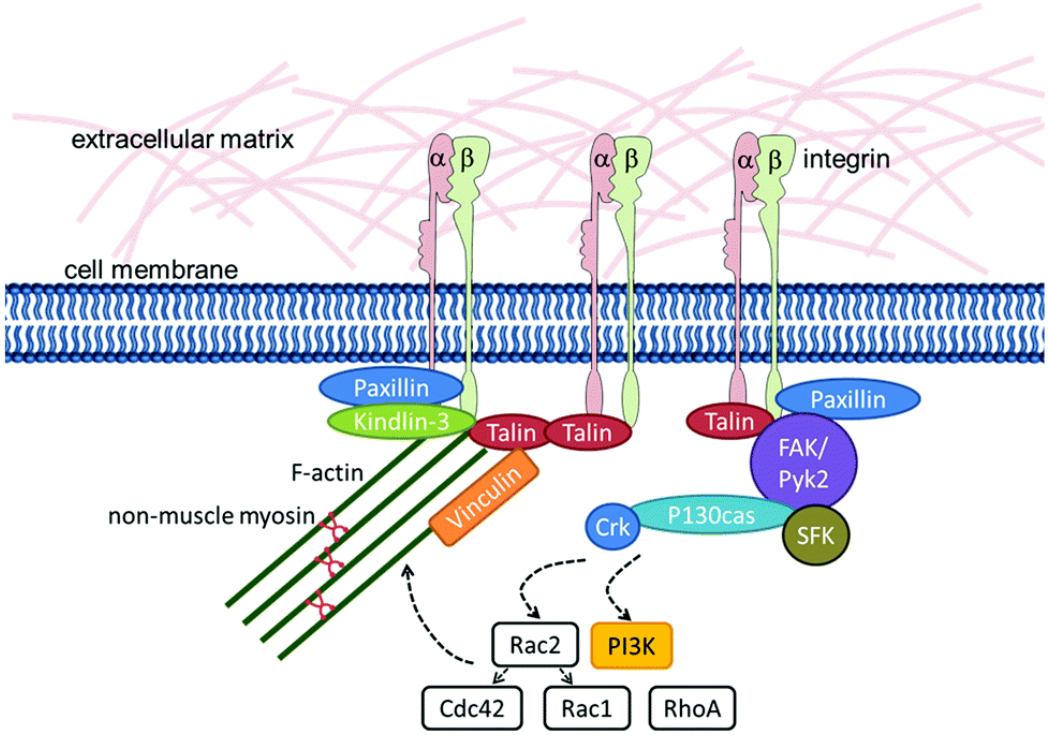

Figure 4. Composition of focal adhesion complex. Published with permission Royal society of chemistry.[1b]

1.2.3 Biophysical interaction and mechanotransduction

Mechanotransduction is the ability of cell to sense physical forces exerted by its microenvironment and reciprocal biological response of cells.[19] Mechanotransduction is a vital phenomenon for development of cytoskeleton of cell, maintenance of cell shape and elasticity of ECM. The mechanical microenvironment of cell is composed of endogenous forces generated by the cells on the ECM by cytoskeletal contractility, or exogenous forces applied by neighboring cell and ECM stiffness. The integrins are important force transduces which mechanically link ECM with cell cytoskeleton.[2]

Cells sense physical features of ECM as stiffness, porosity, topographic and in response to these mechanical cues undergo adhesion, division and migration. The cell senses the physical features of its environment through traction forces generated by actomyosin contractility transmitted to ECM by integrin receptors. In response to external tension cell assemble focal adhesion complex, initiate internal cell signaling pathways as (RhoA, ROCK, YAP/TAZ) and organize cytoskeleton.[12, 20] The focal

adhesion complex is the mechano-sensing that connects cytoskeleton, nuclear matrix, nuclear envelope and the ECM.[12, 18] The focal adhesion aligns in the direction of actin stress fibers and their size linearly correlate with force exerted by the cells. The mechanotransduction is responsible for various cellular process such as adhesion, polarization and differentiation.[12, 20] This interplay of mechanical cue defines tissue specific cell integrity by determining cell differentiation during development resulting in different functional organs.[3] This control over cell fate emerge into stiffness of body tissue from soft blood cells to stiff osteocytes originating from same stem cell during embryogenesis.[1a]

1.3 Biomimetic extracellular matrices

Dynamic cell-ECM interaction regulates various physiological process *in vivo* and are henceforth crucial for survival.[5a-c] The cellular niche involves cell-cell interaction, cell-ECM interaction, growth factors and hormones, as depicted in Figure 5.[21] To recapitulate ECM dynamics, modulation of ligands spatial presentation, controlled release of growth factors and mechanical parameters need to be tune.[22] The *in-vitro* models of biomimetic ECM are widely explored to modulate and investigate effect of specific ECM parameter on cellular process. Biomimetic ECMs are used as scaffold for tissue engineering, drug screening, as pharmacological study model and in regenerative medicine.

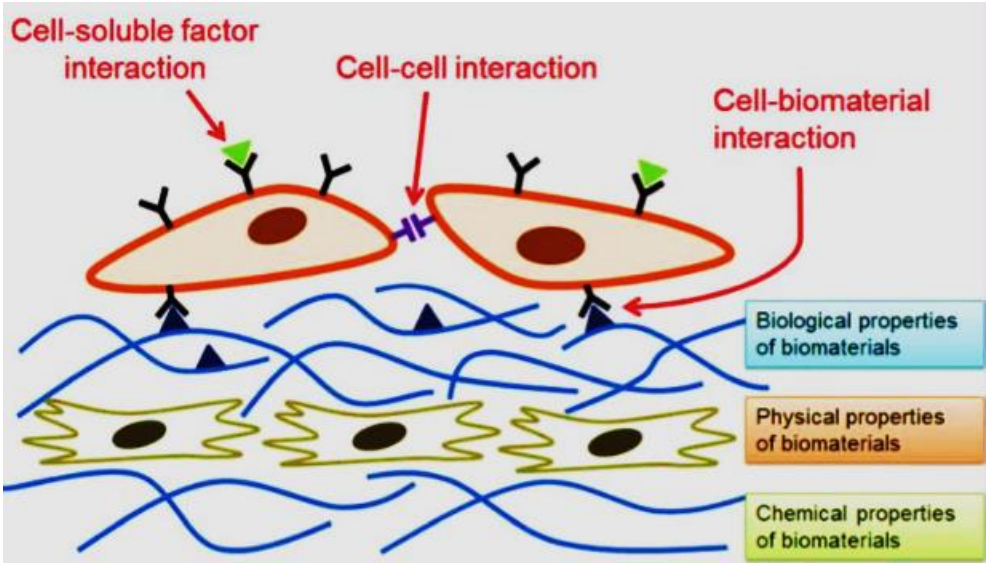

Figure 5. Schematic representation of cellular niche; cell-cell interaction, cell-matrix interaction, and growth factors. Reproduced with permission from American chemical society.[21]

1.3.1 Peptidomimetics of adhesive proteins

Peptidomimetics are short sequences mimicking the structure of the active site of a particular protein. Peptidomimetics of adhesive proteins mimic the adhesive site of the native ECM protein and are easier to handle than the full protein for biomaterials applications. These short peptides are widely incorporated into biomaterials to recapitulate defined cellular response. In this section, an overview of peptidomimetic sequences from Laminin (IKVAV) and Fibronectin (RGD) is entailed.

a) IKVAV as a mimetic peptide from Laminin

Laminin; a heterotrimeric glycoprotein is a major component of the basement membrane and responsible for cell adhesion, migration, neurite outgrowth, metastasis and angiogenesis. Laminin plays important part in neural development during growth and it is expressed in very early stages of embryogenesis. The Laminin mimetic peptides YIGSR, IKVAV, RKRLQVQLSIRT have been reported to support adhesion of neural cells and neurite out-growth.[23] The YIGSR and RKRLQVQLSIRT assist neural cells adhesion while IKVAV sequence is reported to accelerate neurite extension.[24] IKVAV (Ile-Lys-Val-Ala-Val) motif is present on globular region of long alpha chain in Laminin-1 and was first identified in 1984 (Figure 6).[25] This sequence promotes diverse functions as neurite outgrowth, angiogenesis and collagenase IV production. IKVAV binding site is recognized by brain receptor known as 110 kDa laminin-binding protein receptor and promote neurite outgrowth. The 110 kDa receptor is found in neural crest cell during embryogenesis, localized in adult brain and its expression is upregulated during brain injury.[26] The 110 kDa receptor is a member of transmembrane β-amyloid precursor proteins (APPs) associated with brain development. The APPs expression is also upregulated during brain injury and especially in Alzheimer disease.[27] The recognition of IKVAV as binding site by 110 kDa receptor and APPs highlights its role in brain development.

The IKVAV containing laminin peptidomimetic chains (AASIKVAVSADR) form β-sheet and assemble into amyloid-like fibrils.[25] The IKVAV sequence display integrin specific response and bind with $\alpha_3\beta_1$, $\alpha_4\beta_1$ and $\alpha_6\beta_1$ integrin to assist spreading, differentiation and migration of neural cells.[23, 28] The IKVAV is predicted to interact with integrins in divalent cation independent manner as no effect on binding efficiency was observed on addition of EDTA to culture medium.[29] The activity of

IKVAV sequence depends on peptide conformation and reversing the peptide sequence (VAVKI) results in loss of IKVAV activity.[30] The lysine amino acid residue has been reported as active site for IKVAV and substitution of Lys with other amino acids results in lack of neurite outgrowth activity.[25]

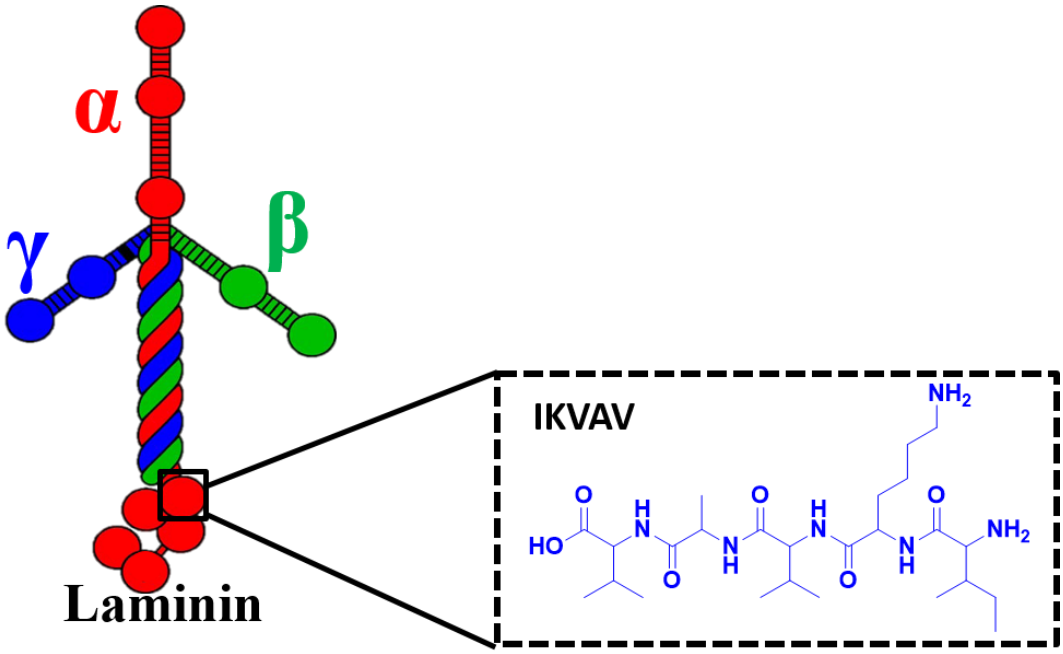

Figure 6. Structure of Laminin, highlighting IKVAV motif. Adapted with permission from Springer link.[11a]

Various reports have proven the relevance of IKVAV in promoting development and differentiation of neuronal cells. IKVAV functionalized surface supports differentiation of embryonic neural stem cell (NSCs) into neuronal cells over the glial phenotype.[31] Poly(ester carbonate) functionalized IKVAV model support cell proliferation and neurite outgrowth *in vivo*.[32] The 3D hyaluronic acid–poly(ethylene glycol) hydrogel formed by Diels-Alders reaction, coupled with IKVAV peptide support neurite outgrowth and long axonal process.[33] Similarly the IKVAV grafted 3D silk fibroin-based hydrogel promote differentiation of progenitor cells into neuronal cell.[34] Moreover an IKVAV functionalized collagen hydrogel support differentiation of dorsal root ganglion (DRS) into neuronal cells.[35] The electrical conducting phosphorylcholine polymer functionalized with IKVAV support neurite outgrowth, axonal length and stimulate secretion of proteins from primary Schwann cells on electrical stimulation.[36]

The IKVAV sequence incorporated into self-assembled peptide amphiphiles (PAs) promotes neural developments. The IKVAV modified self-assembled PAs nanofibers in 3D preferentially promotes neuronal cell growth over glial cells (Figure 7).[37]

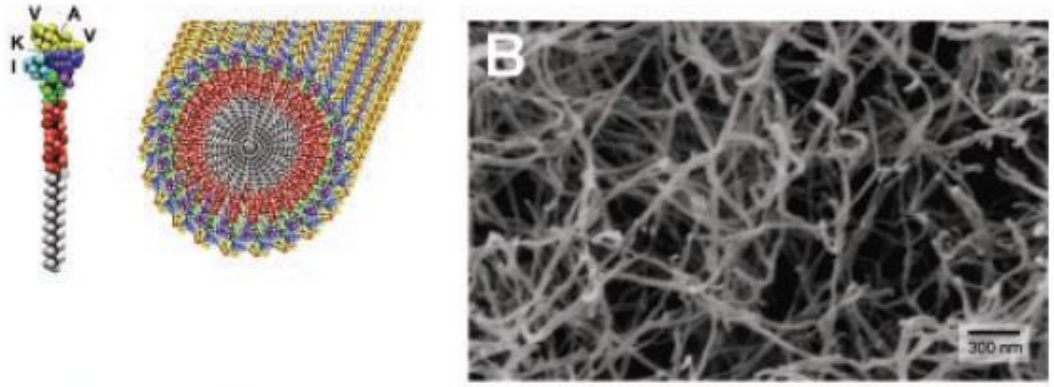

Figure 7. IKVAV-containing peptide amphiphile molecule and its self-assembled nanofiber.[37] Reprinted with permission from AAAS Science.

The IKVAV functionalized implantation especially for spinal cord regeneration showed promising results. The IKVAV nanofibers employed in *in vivo* mouse spinal cord injury model, enhance cell viability at the site of injury and promote development of motor neurons.[34, 38] Similarly, the inert commercially available PuraMatrix® hydrogel used for cochlear implants (CI) was functionalized with IKVAV. The cell viability and outgrowth of spiral ganglion neurites has reported to be enhanced by coupling of IKVAV peptide on PuraMatrix® hydrogel in comparison to unmodified hydrogel.[39]

IKVAV functionalized aligned nanofibers and surface topography directs guided neurite development for neural connectivity. The IKVAV functionalized aligned nanofibers promotes directional growth and migration of neural progenitor cells. The progenitor cells on aligned fibers differentiate into neuronal cells and develop synaptic connections *in vivo*.[40] The poly-L-lactic acid (PLLA) tube filled with IKVAV unidirectional nanofibers was used for guided axonal growth.[36] The admantane-conjugated IKVAV and aligned electrospun cyclodextrin nanofibers (CDNFs) recently reported to promote neuronal differentiation and oriented neurite extension.[41] IKVAV functionalized nanorod-structured on silicon wafers prepared by wet etching has been reported for directional neurite outgrowth.[42] The advancement in IKVAV grafted substrates underline its importance as potential candidate for neural outgrowth and axonal guidance.

b) RGD mimicking peptide

The tripeptide sequence RGD (Arg-Gly-Asp) is a binding domain of different ECM protein as fibrinogen, fibronectin, vitronectin, and laminin promoting cell adhesion, migration and proliferation.[43] RGD mainly binds $\alpha_5\beta_1$ and $\alpha_v\beta_3$ type integrins in various studies supporting cell adhesion, differentiation, angiogenesis, and tumor growth (Figure 8).[14, 44]

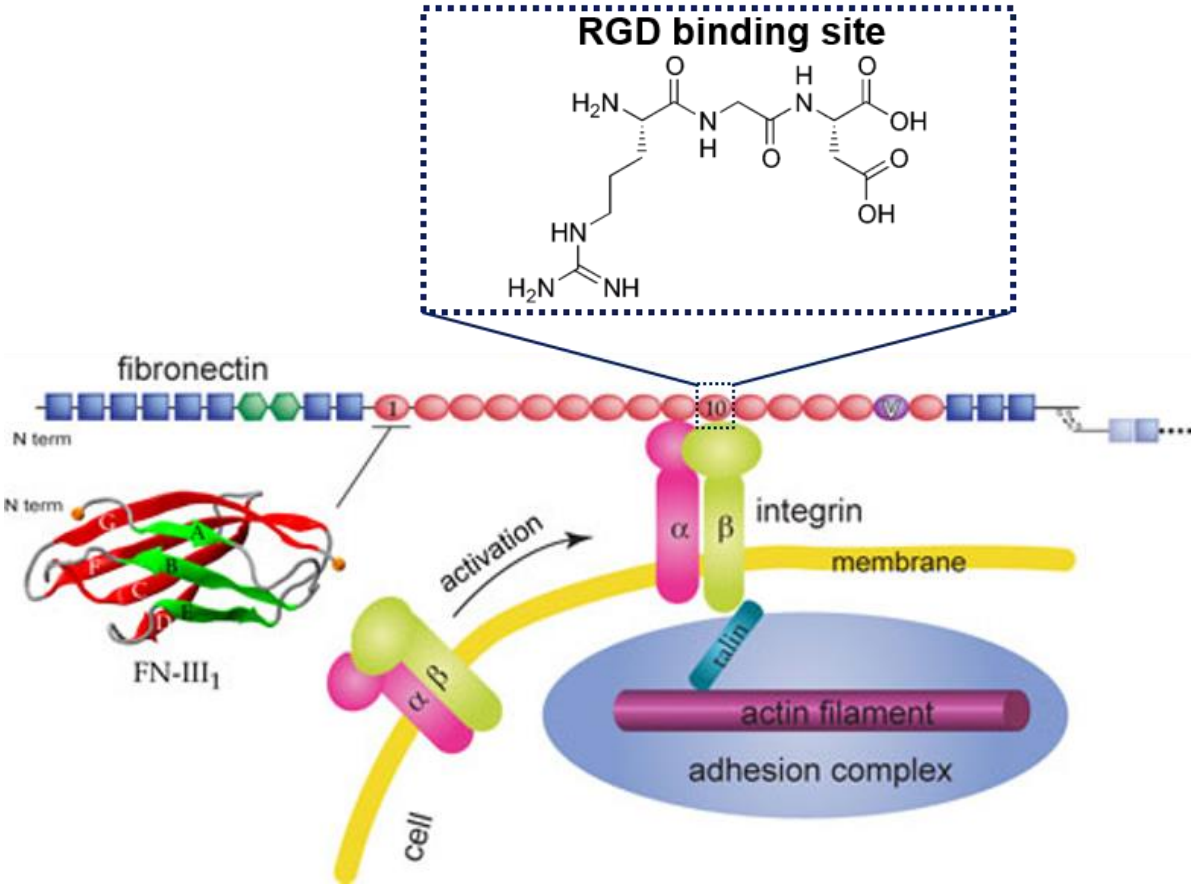

Figure 8. Schematic representation of RGD binding domain on Fibronectin. Reprinted after permission from Royal chemical society.[45]

The aspartic acid unit (D) in RGD interact with divalent cations hence act as integrin selective binding site by facilitating ion-dependent adhesion (Figure 9).[46] The order and length of the peptide core is crucial for its activity. To maintain the same activity profile, RGD sequence has been modified via cyclization, N-methylation (Cilengitide) or substitution with similar sized synthetic molecules. The conformationally constrained cyclic version RGDfV was designed by Kessler *et al.* to enhance the activity of RGD sequence *in vitro*. The change in chirality of one amino acid by substitution D-phenylalanine (f) instead of L-phenylalanine in RGDfV improves the

conformational rigidity.[47] The cyclic RGDfV enhances the proteolytic resistance of peptide and shows 20 to 100 folds improvement in binding affinities to integrin receptors.[47a, 48] The RGD sequence is conserved and change in the position of amino acid in RGD to RDG or RAD results in loss of bioactivity.[49]

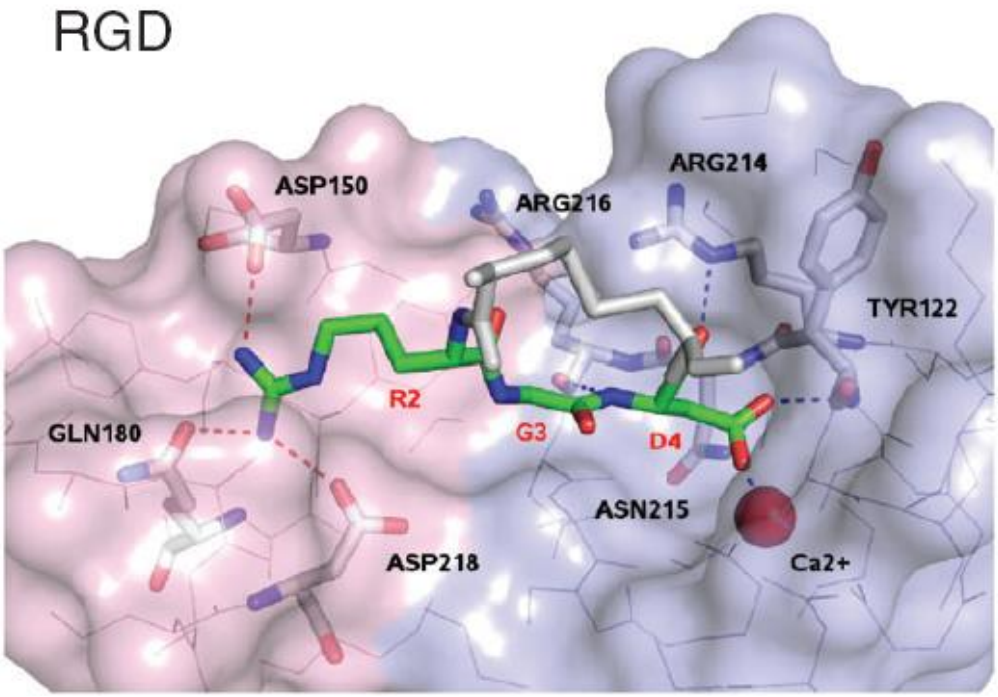

Figure 9. Model for the interaction between RGD-binding site and $\alpha_v\beta_3$ integrin binding pocket. The RGD residues are shown in green, cysteine in gray while nitrogen and oxygen atoms are shown in blue and red, respectively. Ca^{2+} bound to the adhesion site represented by a red sphere. Dotted lines denote hydrogen bonds between ligands and integrin.[50] Reprinted with permission from Journal of Biological Chemistry.

The specificity of integrin binding site in RGD is explored in different accounts by insertion of photocaged moieties at aspartic acid lead to recognition failure by cell. The photoactivatable caging groups were reported to control cell adhesion and release by blocking RGD active site. The cells fail to adhere on RGD in presence of DMNPB chromophore inserted at aspartic acid residue (Figure 10A).[51] The spatiotemporal photoactivation of RGD by removal of caging group, results in restoration of activity lead to cell attachment. The HUVEC cells are reported to show spatially defined attachment on the patterned irradiated area (Figure 10B).

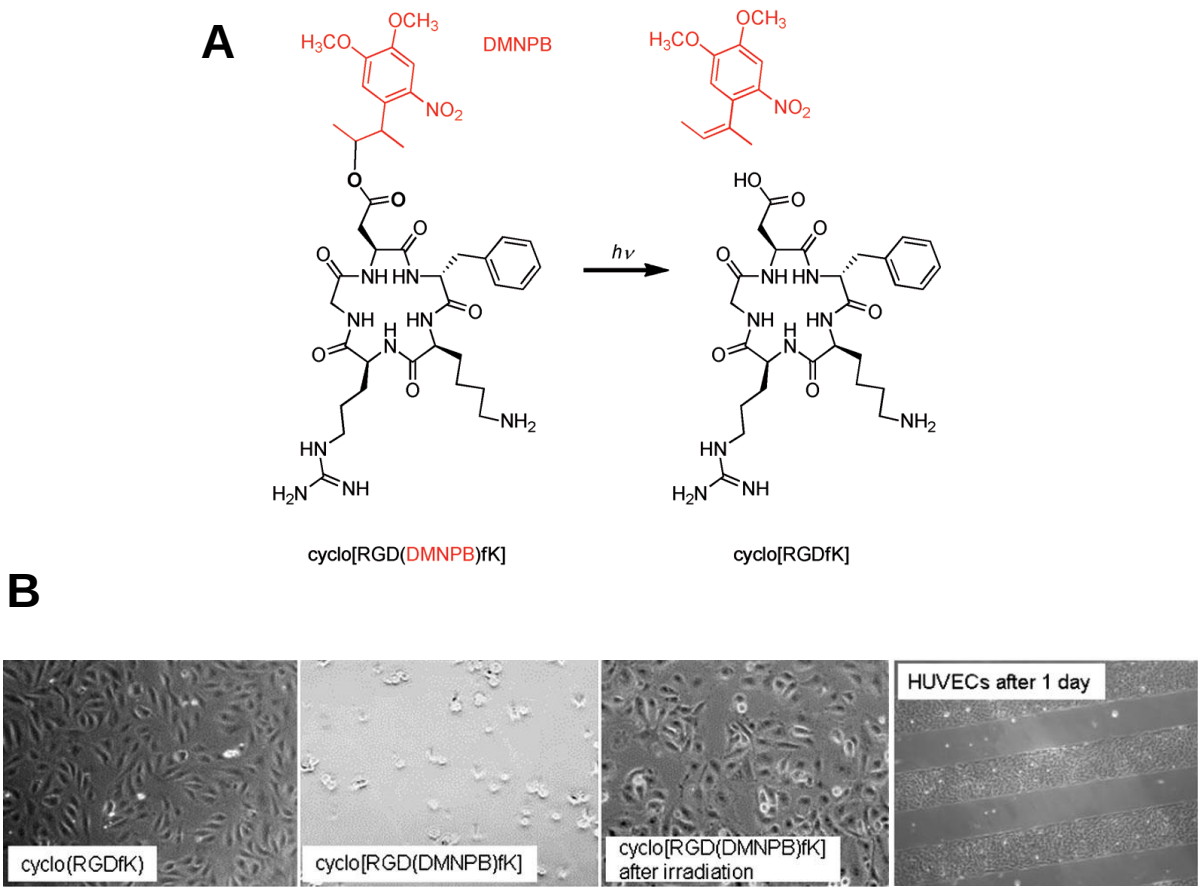

Figure 10. (A) Structure of RGD with DMNPB cage introduced at aspartic acid residue, (B) HUVECs cells seeded on c(RGDfK), and on c[RGD(DMNPB)fK] functionalized substrates before and after irradiation. Patterns of HUVECs cells on c[RGD(DMNPB)fK] after masked irradiation.[44] Reprinted with permission from Wiley.

The $\alpha_v\beta_3$ integrin binding affinity for aspartic acid in RGD was explored by QCM microbalance.[44] The $\alpha_v\beta_3$ show no binding on the surface of RGD in the presence of DMNPB cage aspartic acid and negligible change in dissipation or frequency was observed in QCM. The *in-situ* photo-activation of RGD lead to considerable change in frequency signal due to binding interaction of $\alpha_v\beta_3$ integrin with RGD. The spatiotemporal control over RGD activity is further extended in 3D cell culture by reports of binding active motif through thiol-ene click chemistry and gel formation by azide-alkyne click reaction. The photo degradation of hydrogel promote specific cell adhesion and migration in 3D gels.[52]

1.3.2 Hydrogels as 2D and 3D matrices

Hydrogels are polymeric network, containing high content of water, porosity, and mechanical tunability similar to *in-vivo* ECM matrix.[22] Consequently, hydrogels are explored for cell culture due to flexibility of regulating their chemical and mechanical properties hence creating biomaterials for regenerative medicinal applications. Various materials are used to prepare hydrogels for cell culture, classified into natural and synthetic polymers, established by their source. Hydrogels can be crosslinked by covalent or non-covalent interaction depending on precursors, permitting accessible regulation of rigidity. The synthetic gels are antifouling and cytocompatible such as polyacrylamide (P(AAm), poly(2-hydroxy ethyl methacrylate) (PHEMA), poly(vinyl)alcohol (PVA) and polyethylene glycol (PEG) hydrogels. These polymeric networks are inert and by chemical modifications defined densities of bioactive functionalities can be introduced. Their mechanical properties can also be tuned over a wide range of stiffness (0.1 - 750 kPa).

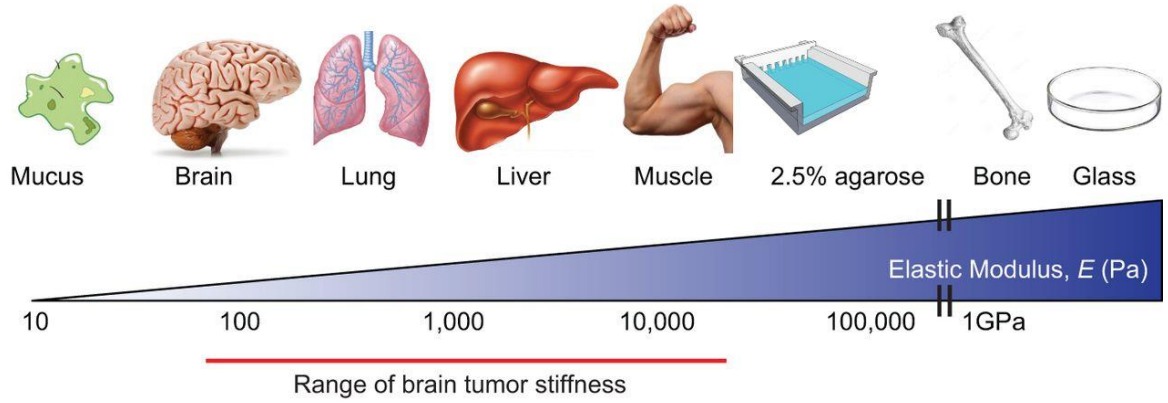

Figure 11. Schematic representation of mechanical properties in various tissues. Republished with permission from Company of biologist.[53]

The tissue stiffness in body varies over wide range from 0.1-1kPa for brain to GPa range for bone tissue highlighting prerequisite of stiffness modulation in designing of biomaterials (Figure 11).[54] The cell, cultured on stiff glass or polystyrene substrate display uncharacteristic flat morphology, different genetic expression and can lose differentiation potential emphasizing relevance of choosing proper substrate for cell culture.[55] Stiffness play important role in defining cell phenotype, and based on substrate stiffness, stem cells can differentiate into distinct lineage as observed during development of mesenchymal stem cells (MSCs) into neuroglial, adipocytes

and osteocytes. The MSCs were cultured on polyacrylamide gels (0.1- 1kPa) mimicking brain tissue develop in to neurogenic cells, on gel mimicking muscle stiffness (8–17 kPa) into myocytes while cell show osteogenic differentiation on hard gels (25–40 kPa).[56] Other studies also supported this finding depicting substrate stiffness as major feature for tuning MCSs differentiation invalidating effect of other parameters as porosity or protein binding density.[57]

In addition to cell differentiation, cell adhesion and spreading is likewise defined by substrate stiffness as depicted by low adherence of fibroblasts and endothelial on soft (<2 kPa) substrate while display spreading and amplification of actin fibers on stiff surface (> 2kPa).[58] Similar studies show enhanced spreading of human lung fibroblast on 20kPa[59] while liver endothelial cells on 10 kPA P(AAm) hydrogels.[60] The hMSCs failed to proliferate on soft P(AAm) hydrogel (250 Pa),[61] likewise the pericytes show better proliferation on stiff 15 kPa substrate.[62] The cell also displays durotaxis and show migration towards increasing stiffness. The MSCs on P(AAm) hydrogel with gradient of stiffness from 1-12 kPa show migration towards stiffer region.[63] This behaviors was also recently observed during collective migration of endothelial cells on stiffness gradient.[64] The substrate stiffness also influences cell-cell interactions. The endothelial cells cultured on stiff substrate failed to form cell-cell assembly and prefer cell-substrate interactions.[65]

Hydrogel based 2D cell culture systems are attractive due to their relatively simple preparation and easy modulation but it is insufficient to mimic 3D *in-vivo* cellular niche.[66] The cells in 2D show apical-basal polarization and adhere in horizontal plan in contrast to *in vivo* environment where many cells are confined and can adhere in all dimensions (Figure 12). Thus, cells in 2D culture can respond very differently to different stimuli such as growth factors or pharmacological drugs. 3D cell culture models can better recapitulate *in-vivo* environment than 2D system and cell maintain their pluripotency in 3D culture.[55] The cells are encapsulated in 3D gel network and cell migrate through the network by microtubules and proteolytic degradation comparable to *in vivo* conditions. Various natural and synthetic polymer are used for 3D cell culture such as alginates, hyaluronic acid, collagen, matrigel, PEG, fibrin hydrogels. Besides hydrogels, nanofibrous scaffolds offer ECM fibrillar topology for 3D but suffer from mechanical instability to sustain mechanotransduction. Cells can easily migrate through natural polymeric system

due to relatively less cross-linked polymer and possibility of proteolytic degradation of network. In synthetic or highly cross-linked natural polymeric network, cell migrates by biodegradation of polymeric network.

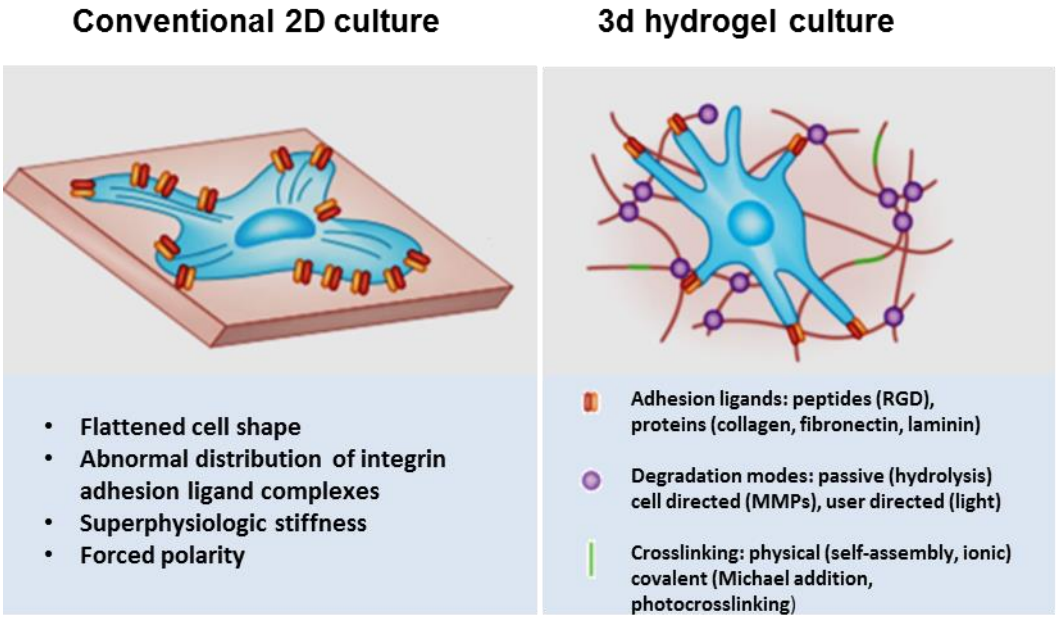

Figure 12. Schematic representation cell microenvironment in 2D and 3D cell culture. Figure adapted after permission from Nature Publication**.**[55]

The phenotypic difference observed between 2D and 3D cell culture can lead to variation in signaling pathway and protein expression. This was first observed in human breast epithelial cells culture, which in 2D develop as tumor cell while in 3D revert to normal cell, under influence of native niche.[67] The phenotypic difference were also observed in enhance chondrogenic differentiation of embryonic stem cell in 3D cell culture in comparison to 2D model.[68] The prospect of modulation of cellular niche in 3D cell culture augmented in enhance cell viability, phenotypic fate and proliferation. The polyacrylamide hydrogel as 2D cell culture model and polyethylene glycol hydrogels as 3D cell encapsulation platform are described below:

a) Polyacrylamide hydrogels

Polyacrylamide P(AAm) hydrogels are widely used for 2D cell culture due to their cytocompatibility, transparency, tunable stiffness, and ease of preparation from inexpensive chemicals. These gels are prepared by free radical vinyl addition polymerization of acrylamide and bis-acrylamide crosslinker, initiated by ammonium persulfate (APS) and catalyzed by tetramethylethylene- diamine (TEMED) (Figure 13).

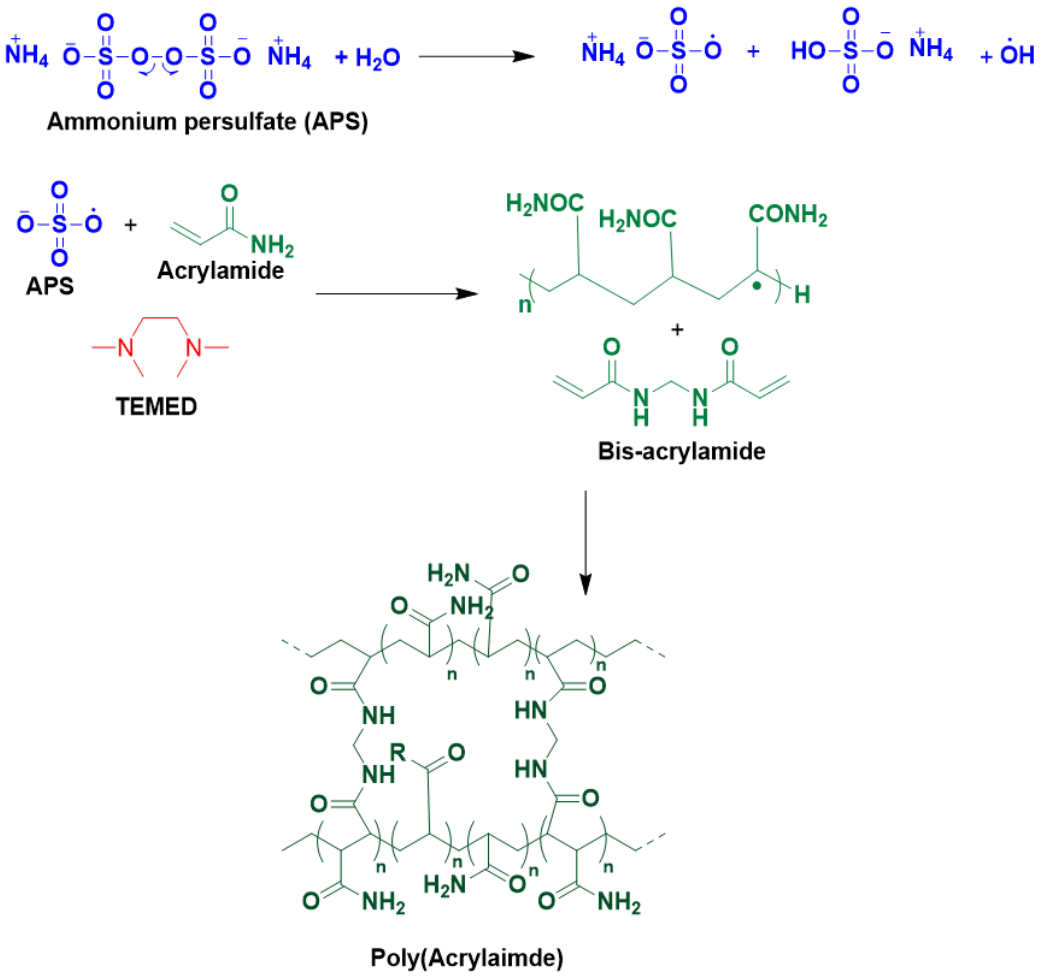

Figure 13. Free radical polymerization mechanism for polyacrylamide hydrogel preparation.

P(AAm) hydrogels are inert and therefore cell can specifically interact with the bonded ligand. The pendant amide group in P(AAm) are non-reactive hence impart challenge for surface modification. These hydrogels are functionalized by physical coating of biomolecules on surface suffer from batch to batch variation and non-uniform distribution of ligand. Chemical activation with hydrazine hydrate, periodate, UV or γ-rays, or photoactivable cross linker sulfo-SANPAH (sulfosuccinimidyl-6-(4'-azido-2'-nitrophenylamino) hexanoate) are used for covalent binding on the surface.[69] These methods endure low reproducibility, harmful irradiation and toxic chemicals. The co-polymerization of P(AAm) gel with reactive polymers are recently explored for surface modification, without effecting the biocompatibility. The co-monomers ought to be non-toxic and compatible with radical polymerization. The acrylic acid (AA) copolymerized P(AAm) gels functionalized with RGD peptide by activation of carboxyl group were successfully employed for MSCs culture.[56, 70]

The ease of stiffness modulation (0.1-100kPa) by adjusting crosslinker and monomer ratio, underline relevance of P(AAm) hydrogels in cell culture for mechano-regulation.[58] The differentiation of stem cells is regulated by rigidity of ECM during mechanotransduction correspondingly *in-vitro* stem cells fate is influenced by substrate stiffness. The MSCs differentiation into different phenotypic lineage exclusively based on surface stiffness.[56] Similarly differentiation of human adipose derived stromal cells into adipogenic or osteogenic lineage is primarily governed by stiffness, independent of porosity or ligand density.[57, 71] Similar findings were observed during myogenic and osteogenic differentiation of MSCs on poly(AAm-co-AA) hydrogels in the presence of BMP-2 mimetic peptide. The cells were failed to differentiate into osteogenic phenotype on soft gels (0.5 to 3.5 kPa) even in the presence of BMP-2 peptide, highlighting stiffness effect. [70]

b) Polyethylene glycol hydrogels

The PEG hydrogels are biocompatible and are widely used for bio-conjugated 3D cell encapsulation, due to its non-fouling and low inflammatory profile *in vivo*.[66] PEG hydrogels are inert therefore, cell adhesive ligand can be introduced during crosslinking hence uniformly distributed throughout the gel network. Inert hydroxyl terminal group in PEG can easily modified into various reactive end functional groups such as maleimides, acrylates, vinyl sulfones, thiols, norbornenes, azide and alkynes (Figure 14A). Branched PEG macromers with of 4 or 8 arm chains, functionalized with reactive end group, enhance possibility to adjust properties of hydrogel (Figure 14B).[66] PEG hydrogels can be crosslinked by via free-radical UV polymerization of PEG diacrylate, but this results in low cell viability. Alternatively Michael-addition between reactive functional group such as thiol-maleimide/vinyl-sulfone is more promising due absence of free-radicals and phototoxicity.[66] These gels can be prepared quickly at physiological range in the presence of cells with additional benefit of *in situ* bioligand incorporation during gelation. The 3D platform of PEG hydrogels functionalized with RGD formed by bioconjugation of PEG dithiol with 4-arm PEG maleimide for cell encapsulation. This system show faster gelation and functionalization in comparison to thiol- vinyl sulfone system.[66] Apart from traditional Michael addition reaction, PEG hydrogel prepared by Diels−Alder reaction between PEG tetrazine macromer and dinorbornene crosslinker support *in-situ* hMSCs encapsulation and growth.[72] Sequential strain promoted azide-alkyne copper free

click reaction (SPAAC) between 4-arm PEG azide and 4-arm-cyclooctyne at physiological range provide another platform for 3D cell encapsulation. The orthogonal azide-alkyne click reaction and photo-regulated thiol-ene reaction support *in situ* tuning of biochemical and biomechanical properties of the system by specific binding of bioligand enabling spatial patterning.[73]

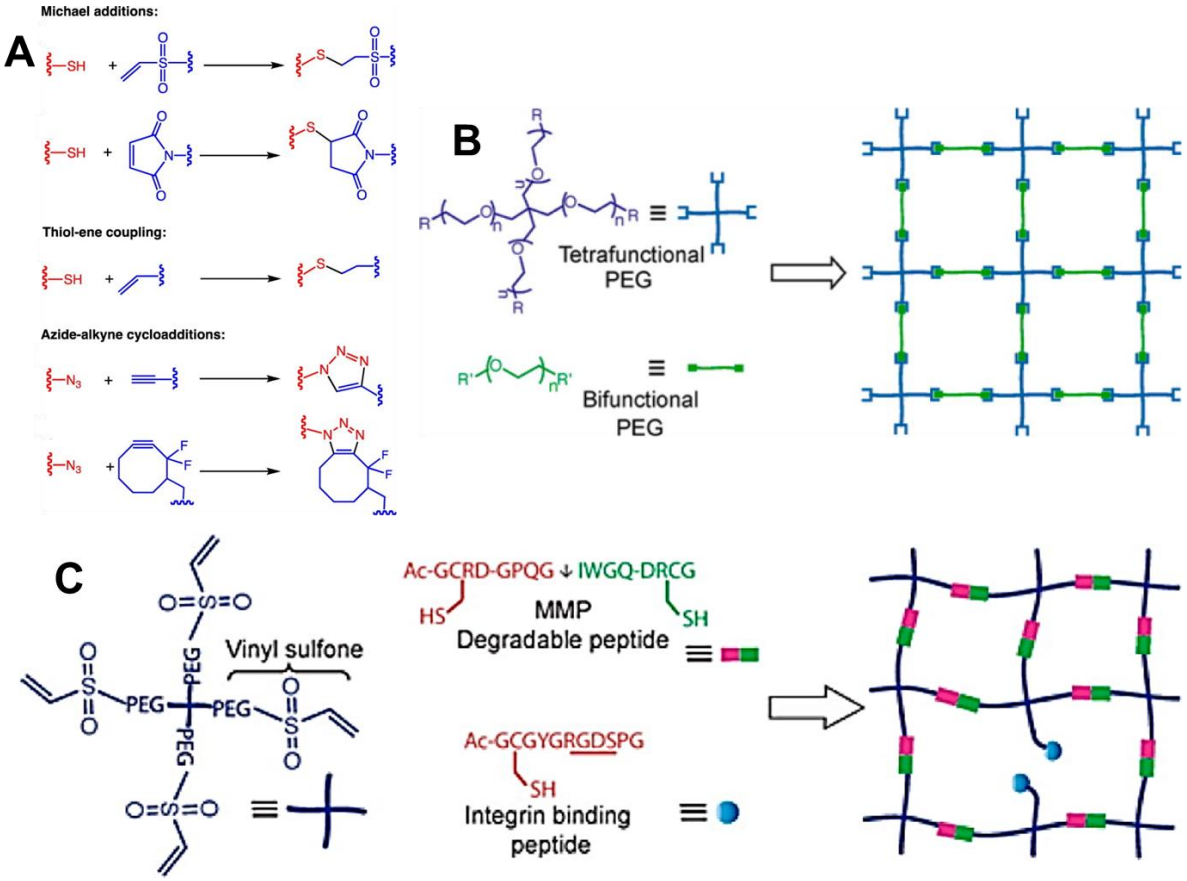

Figure 14. Schematic representation (A) PEG bioconjugation cross-linking reaction, (B) Multi-arm PEG macromer forming hydrogel network (C) *In-situ* PEG hydrogel formation by thiol-vinyl sulfone reaction, functionalization with RGD ligand, and thiol containing MMP sequence for enzymatic degradation. Adapted with permission from American Chemical Society.[74]

The PEG gels are non-biodegradable therefore proteolytic crosslinking peptide sequence are added to make them penetrable and degradable by cells. The crosslinking and degradability of PEG gels can be controlled by tuning amounts of monomer and degradable crosslinking sequence (Figure 14C). These peptide sequence are recognized by extracellular proteolytic enzymes on cell known as matrix metalloproteinases (MMPs).

The MMPs allow cell to move *in vivo* by degradation of ECM and they are over expressed during cancer metastasis and angiogenesis. There are 24 zinc containing endopeptidases (MMPs) discovered in human divided into 5 categories. The gelatinases, collagenases, matrilysins, stromelysins and membrane-type MMPs are responsible for degrading all components of ECM.[75] The commonly used cross-linking peptide (CLP) susceptible to MMPs for PEG hydrogels are highly degradable sequence GCRDVPMS↓MRGGDRCG (VPM) and slowly degradable sequence GCRDQGWI↓GQPGDRCG (GPQ). The degradability can also be adjusted by mixing degradable CLP with non-degradable CLP such as using non-degradable GCRDGDQGIAGFDRCG (GDQ) for crosslinking.

c) Physicochemical properties of hydrogels

The designing of biomimetic ECM requires mechanically resilient network, emphasizing flexibility of tuning material mechanical properties. Stiffness, swelling and porosity are major defining features for biomimetic scaffolds. Consequently, all these parameters are evaluated and characterized while designing of mimetic biomaterials.

i. Stiffness

Stiffness of substrate is most important parameter of mechanotransduction, defined as intrinsic resistance of material towards deformation.[56, 58] The stiffness of hydrogel is measured by either rheology, tensile testing or by AFM experiments. Stiffness is defined in term of elastic modulus (E) explained as amount of force required to deform a substance in Pascal or N/m^2.[53] The elastic modulus is calculated from shear modulus (G) and Poisson ratio (v for hydrogels = 0.45–0.5) by following equation.[55]

$$E = 2 G (1+ v)$$

ii. Swelling

Swelling ratio of hydrogel defines the capacity of hydrogel to hold water and it is related with cross-linking, porosity, pH and charge sensitives of polymeric network[76] The gels with charged groups along the chain or lower crosslinking hold more water and show higher swelling ratio. The swelling ratio (SR) of the hydrogels are generally measured by gravimetric analysis from weight of swollen gel (W_S) and weight of dry gel (W_d).

iii. Porosity

The ECM matrix is a mesh like network with pores for transportation of nutrient, growth factors and for gaseous exchange. Therefore, porosity is essential for biomimetic hydrogels especially in cell encapsulated 3D gel for supply of nutrients from medium, removal of waste products and gaseous exchange. Porosity is defined as maximum size of solute that can diffuse in hydrogel, measured by mesh size (ξ) and depends on crosslinking density of polymeric chains.[77]

1.3.3 Dynamic changes in the physical properties of hydrogels by degradation

Hydrogels of natural origin such as collagen, alginates, hyaluronic are degraded by cell-mediated enzymatic degradation involving proteases. Synthetic polymer networks like PVA can be degraded by hydrolysis, while special biodegradable sequences have to be introduced in PEG matrices to assist their enzymatic degradation.[78]

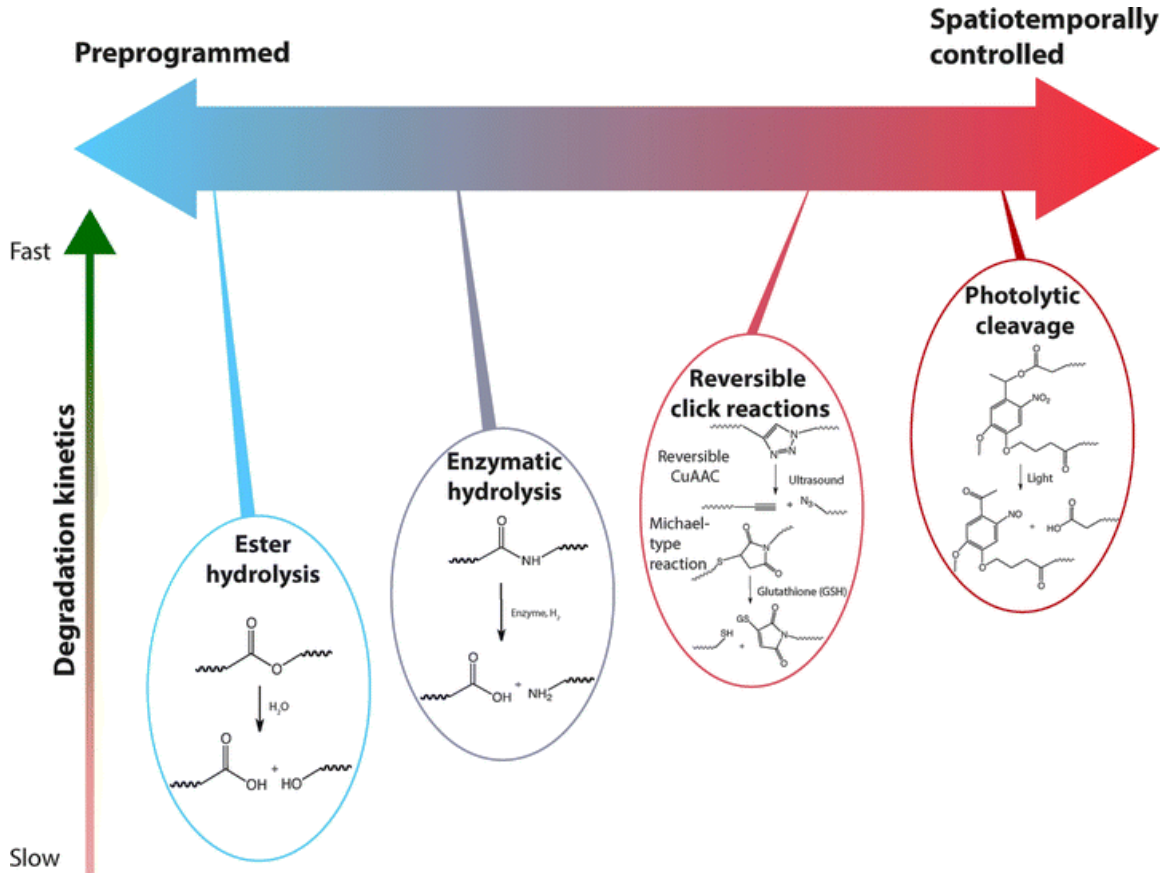

Figure 15. Strategies for controlling biomaterial dynamics by stimuli responsive hydrolysis, enzymatic activity or photolytic cleavage. Reproduced after permission from Royal chemical society.[43]

The degradability of hydrogel changes the properties of matrix such as stiffness, swelling, pore size, and integrity. The modulation of degradation facilitates application of hydrogels for drug or growth factor release and attractive for tissue regeneration.[79] The Figure 15 highlights commonly employed strategies for controlling dynamics of biomaterials.

The reported enzyme mediated degradation of methacrylated gelatin (GelMA) hydrogels by collagenase MMPs from cells *in vivo* result in controlled release of VEGF from the hydrogels to mediate angiogenesis.[80] Similarly the cell mediated degradation of hyaluronic acid (HA) hydrogels were designed to follow differentiation of hMSCs.[81] The physically crosslinked gels can undergo reverse gelation due to pH, ionic strength or temperature. The alginates hydrogels crosslinked by non-covalent interactions with Ca^{2+} ions undergo degradation by changing Ca^{2+} ions concentration. Hydrolytic degradation due to change in pH disrupt ester bond and allow degradation of polymers. The reverse click reaction retro Diels alders by using ultrasonication or pH also change matrices properties.

The stimuli responsible (temperature, light) polymeric networks are more successful in modulating material properties. Light induce spatial degradation in 3D by introduction of photocleavable cross linker as ONB are reported in this term. Recently Anseth *et al.* presented photoinitiated degradation of PEG hydrogel system by using allyl sulfide in radical addition–fragmentation chain transfer (AFCT) process. The symmetric allyl sulfide was introduced in between bis-(PEG_3-azide) crosslinker and later on photoinitiated free radicals degradation of ally sulfide dissolve the hydrogel.[82] The 3D temperature tunable such as gelatin hydrogels with electrospun microfibers of poly(*N* -isopropylacrylamide) (PNIPAM) is reported. The polyNIPAM fibers were slowly degraded by cell culture temperature yield thermo-tunable hydrogels.[83]

The incorporation of photodegradable crosslinking group simplified spatially control degradation of PEG network as depicted by guided cell migration in PEG azide-cyclooctyne click hydrogels.[52] The photo degradability is presented in polymeric network by introduction of photocleavable cross linking (ONB) sequence. Similar photolytic patterning system is presented by crosslinking of PEG tetracycloctyne via click reaction with photo- and enzyme labile diazide crosslinker and azide-containing integrin-binding peptide (Figure 16).[84]

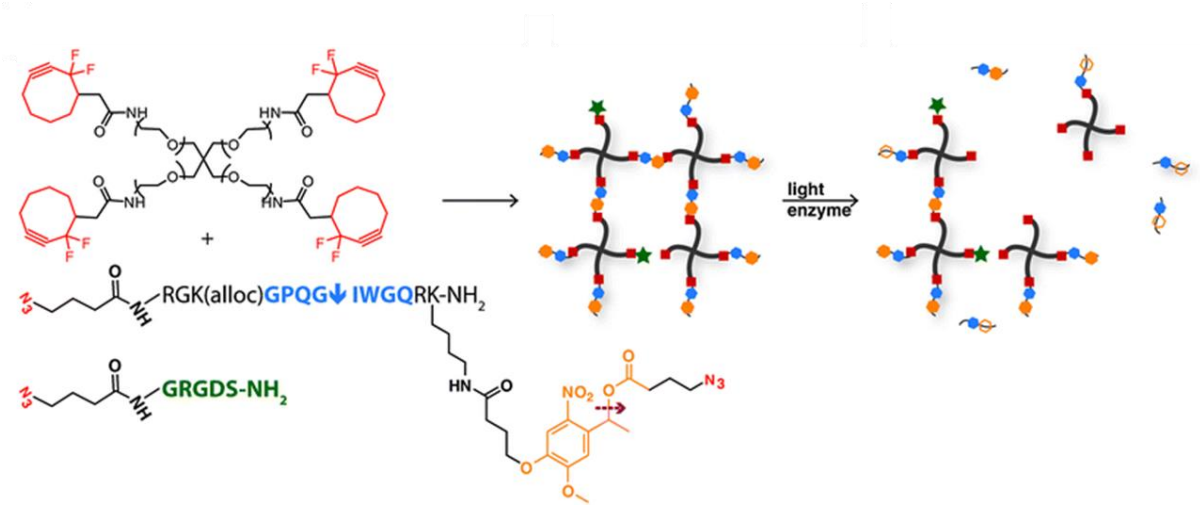

Figure 16. Photo-regulated hydrogel. Reprinted with permission from Royal chemical society.[84]

The two-photon laser scanning (TPLS) photolithography was employed in a similar strategy for spatially regulated 3D guided migration assisted by RGD ligand.[85] Photo-regulated spatial modulation of material rigidity is as well depicted in hydrazone formation between PEG-hydrazine and *in-situ* light generated aldehyde from 2-nitrobenzyl alcohol poly(ethylene glycol) (PEG). The crosslinking density and reaction kinetic was controlled by light dose, modulating matrix stiffness and rapid gel formation at physiological condition with high cell viability.[86]

1.4 Light-induced changes in the biochemical properties of synthetic biomaterials

Photo-responsive materials are ideal candidates for providing spatiotemporal control over activation of chemical cues at cell friendly wavelength, in a non-invasive manner and in the absence of chemical additive.[87] Most examples of phototriggerable biomaterials are based on the use of photocleavable protecting groups or “cages” attached to biologically relevant ligands. These chromophores undergo cleavage at cell-compatible wavelengths in UV-Visible or visible range (above 320 nm). In this way the bioactivity of the molecule is restored and a non-toxic photolytic byproduct is released.[87] The photoremovable group should encompass efficient photolytic yield, hydrolytic stability, water solubility higher extinction coefficient and primarily it should be inert towards biological system.[46, 88] Additionally selection of binding site and ease of introduction of suitable photo-

responsive caging group defines design of photoresponsive biomaterial. Following section encompass properties of various photocleavable groups in detail.

1.5 Photo-cleavable protecting groups for light-triggered biochemical activity

Photo-protecting groups (PPGs) were first used as protecting group in organic synthesis and undergo uncaging in the presence of light at specific step.[89] The photocage group bind to active site of biomolecule and render it inactive, upon irradiation, photolysis lead to irreversible removal of caging group and re-activation of biomolecule as depicted in Figure 17.[90]

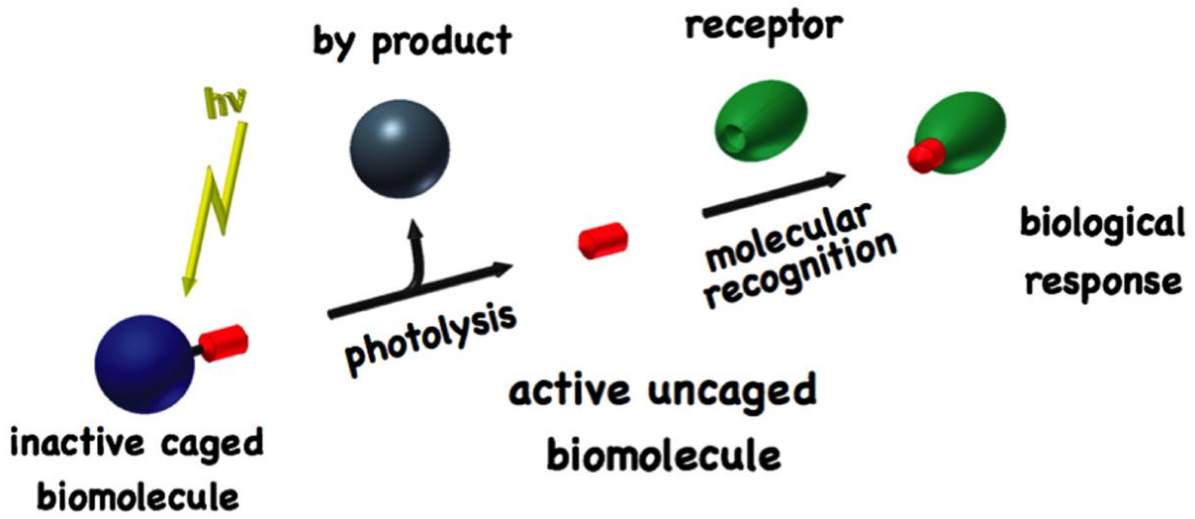

Figure 17. Schematic representation of photo-regulation. Copy rights belongs to The optical society.[91]

Diverse range of photoactive groups are available as o-nitroaryl, coumarin, azobenzene, benzophenone, dinitroindoline, anthraquinone, p-hydroxy phenacyl and dimethoxy benzoin ester derivatives.[92] These photocleavable families are activatable over wide wavelength range (220-890 nm). The fundamental parameters for classifying photoprotective groups (PPGs) comprise absorption maximum, photolysis efficiency, extinction coefficient, non-reactive side products, synthetic effort and hydrolytic stability.[93]

The o-nitroaryl family is most widely use photoactive group employed in various solid phase and organic synthesis reactions.[89] This was the first group used in 1960 as PPGs for selective conjugation of primary amine to the hydroxyl groups of agaroses

in the presence of ONB-protected cysteine. The o-nitroaryl based photolabile groups such as Nitroveratryloxycarbonyl (NVOC), (4,5-dimethoxy-2-nitrophenyl)butan-2-oxycarbonyl (DMNPB) and *p* –dialkylaminonitrobiphenyl (ANBP) are used in various biomaterials. These different ONB based photolabile groups can be activated over wide range (345 – 800 nm) attributed to introduction of substituted groups.

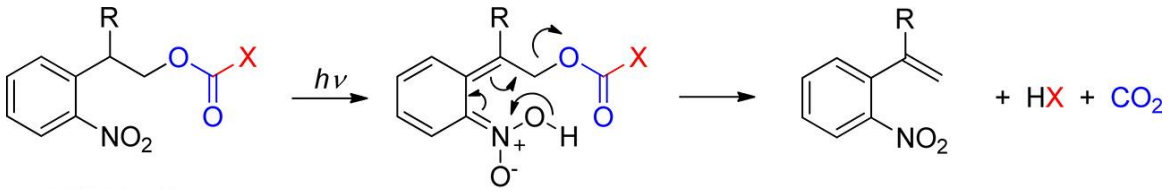

Figure 18. Photolysis of 2-Nitro-2-Phenethyl Derivatives.[94]

The ONB derivative undergoes photolysis and release nitrostyrene side product by beta-elimination mechanism (Figure 18). The substitution on aromatic ring and at benzylic carbon tune the photochemical properties of chromophore. The insertion of methyl group at benzylic carbon increase quantum yield of DMNPB (Φ = 0.26) vs NVOC (Φ = 0.042). The extension of the aromatic core to a biphenyl group and the substitution with a methoxy in *p*-methoxynitrobiphenyl (PMNB, GM 3.2) or *p*-dialkylaminonitrobiphenyl (ANBP, GM 11) renders chromophores with a reasonable two-photon cross section that can be used for photoactivating with 3D resolution. The introduction of substituent also influences hydrolytic stability and solubility of chromophore. The addition of electron donating group at meta position in ONB ring (e.g -OMe in DMNPB lead to enhance stability and red shift in cleavage wavelength (λ_{max} shift from 345 nm to 365 nm).[95] These caging groups substituted at active site of wide range of biomolecules are employed for development of photoactive biomaterials (Figure 19).

The cage is introduced into biomaterial by reaction at active motif via reactive chloroformate, halide or carboxylic acid caged derivatives. The photolabile moieties are inserted at amine group as carbamate, to carboxylic acids as ester or carbonate and binding with alcohol or thiol moiety is carried out by ether/thioether or carbonate link.[93]

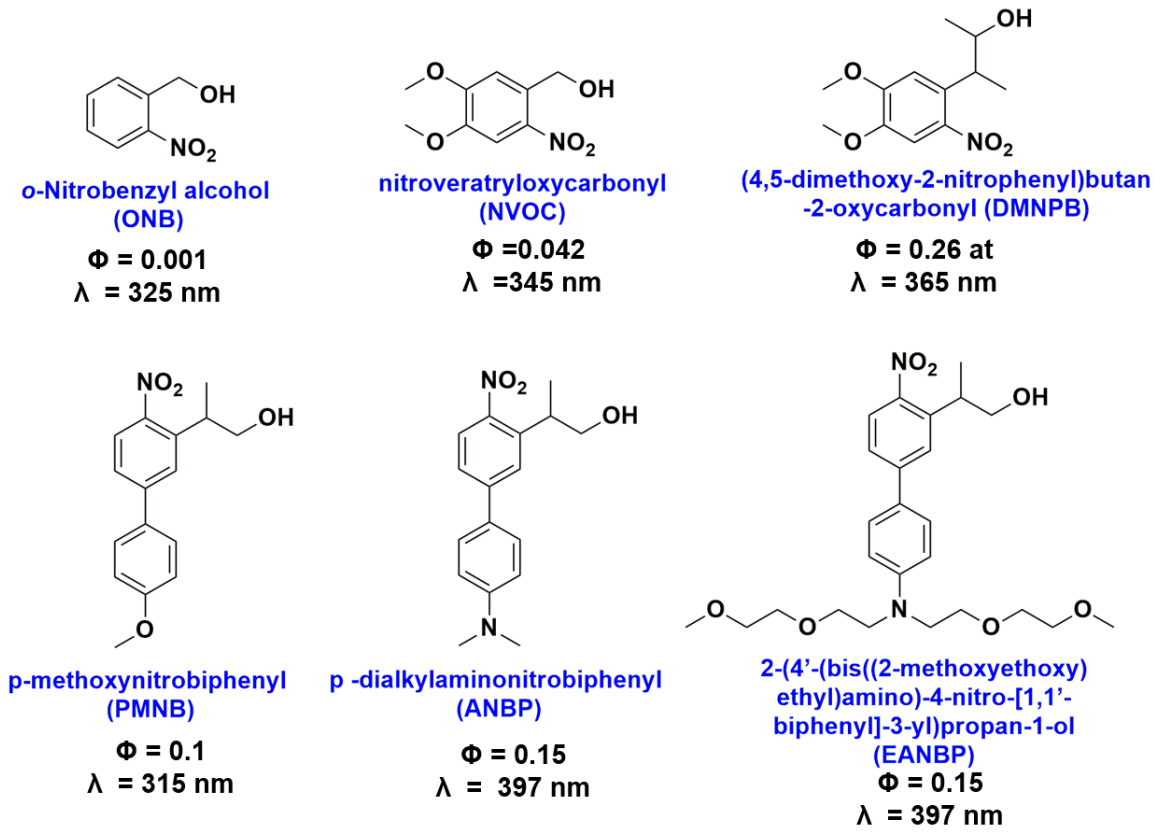

Figure 19. Structure and quantum yield of common o-nitroaryl groups by single photon activation. Adapted with permission.[94]

The availability of different caging group enables orthogonal wavelength selective activation of different photo protective group one by one. A four level wavelength selective activation is reported by photolysis of organosilane functionalized with benzoin (BNZ), 7-(diethylamino)coumarin-4-yl)methyl (DEACM), 7-nitroindoline (DNI, BNI), and p-hydroxyphenacyl (pHP) derivatives. The photoinduced orthogonal elimination was performed in following order DEACM/DNI/BNZ/pHP at 435/420/360/275 nm respectively.[90] The similar approach was presented for solid phase synthesis of DNA. The sequential removal of DEACM, NDBF [1-(3-nitrodibenzofuran-1-yl)ethyl], NPP [2-(o-nitrophenyl) propyl)], and pHP at 505, 440, 365, and 313 nm receptively, allow selective activation of oligonucleotides during DNA solid phase synthesis (Figure 20).[96]

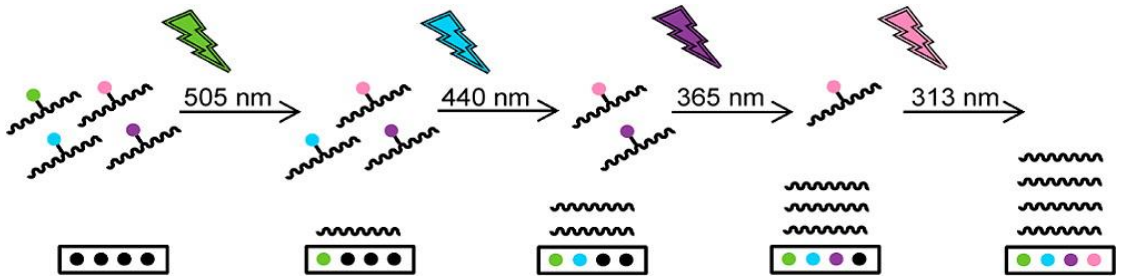

Figure 20. Schematic representation of four levels of wavelength-selective uncaging for DNA synthesis. Reproduced after permission from American chemical society.[96]

1.5.1 The NVOC photo-cleavable protecting group

NVOC (6-Nitroveratryl alcohol) is o-nitrobenyzl (ONB) based photolabile caging group, initially used as protecting group in solid-phase peptide synthesis.[94] NVOC chloroformate is commercially available and readily react with amine terminated biomolecules, therefore most widely used in various applications.[94] It can be activated at near UV range (340-365 nm, ε= 6210 $M^{-1}cm^{-1}$ at λ_{max} 365 nm), hence also introduce as orthogonal photolabile group with other chromophores such as DEACM for wavelength selective activation.[90]

Photo-triggerable NVOC is used as tool in various applications such as in SPPS, in photodegradable polymeric networks, to tune surface wettability and for drug delivery. The introduction of NVOC on biomimetic sequence enabling their photo regulation is highlighted from numerous reports. NVOC inserted at Lys99 amino in antigenic peptide derived from moth cytochrome c (MCC) was used for spatiotemporal activation of T cells. The antigenic peptides are present on the surface of target cells and facilitate recognition of cells by T-cell receptors (TCR). The TCR failed to recognize NVOC protected MCC antigenic peptide. The photo-activation of antigenic peptide results in detection of target cell by T-cells as visualized by increase in calcium ion flex (Figure 21).[97]

The delivery of cytotoxic drugs to tumor cells without their harmful effect on normal cells is a challenge in tumor therapy. Stimuli responsive drug release such as in response to magnetic field, light or temperature are targeting in this direction. Photo-triggerable 2´,7-Caged Paclitaxel was developed by insertion of cage NVOC at 2 and 7 position, for selective drug release. Paclitaxel is an anti-cancer drug, act by freezing tubulin assembly, lead to inhibition of mitosis and dead of tumor cells. The photoactivable version helps in spatiotemporal activation enabling control over microtubule dynamics in *in vitro* and *in vivo* applications.[98]

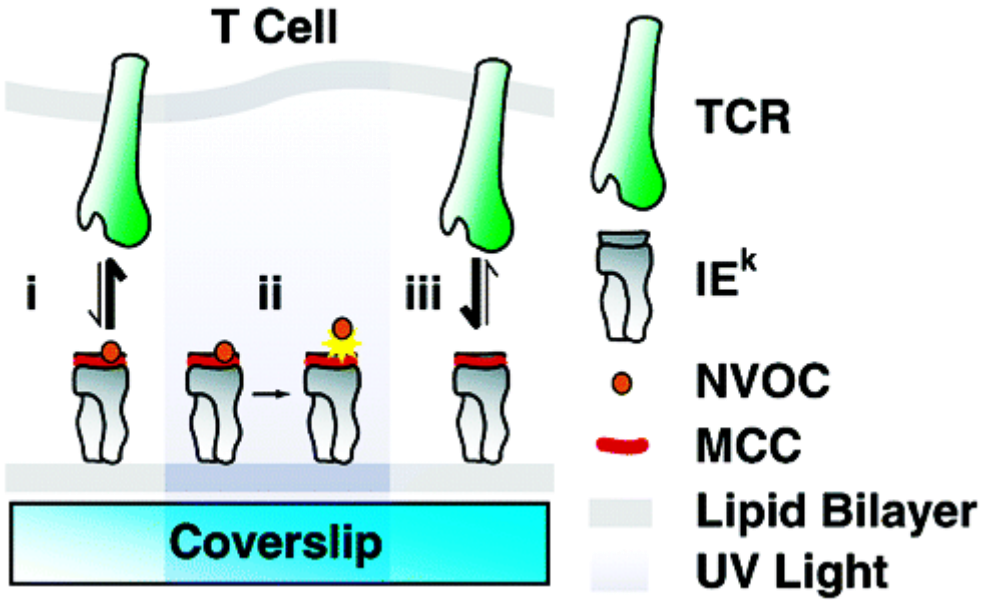

Figure 21. Photoactivated TCR binding: (i) The strong binding between TCR and antigenic MCC peptide on target cell, (ii) The insertion of NVOC on antigenic peptide block the recognition by TCR (iii) Near-UV light cleaves the NVOC chromophore and restore binding between TCR and MCC antigenic peptide. Reprinted with permission from American chemical society.[97]

The application of NVOC crosslinker in polymeric network for degradation is demonstrated in PEG photodegradable hydrogel system.[52] In addition photocleavable poly(methyl acrylate) network was designed by introduction of NVOC between two polymeric chains. Photochemical activation by exposure to UV light released carboxylic acid terminated polymeric chain and o-nitrosobenzaldehyde.[99] The PPG are also use for modulation of surface properties, such as NVOC caged silane surface are used for photolithography, by spatial activation of amine terminated surface upon uncaging of caged NVOC group. This tool enable sub-wavelength chemical structuring by specific binding of adhesive proteins and biomolecules limited at photoactivated area.[100] The introduction of NVOC for wavelength selective surface modification was achieved by orthogonal activation of NVOC and 3,5 dimethoxybenzoin (Bzn). This photo selective surface modification was carried out by either by selective activation of NVOC at 411 nm or by activation Bzn at 254 nm, followed by surface modification with target molecules [101]

The light activated gene expression in Fibroblat (3T3) cells in response to NVOC caged doxycycline (NVOC-Dox) in tetracycline dependent transcription activation by transactivator/transrepressor (TET-ART) system has been reported. The TET-ART transcription is regulated by activation/deactivation of tetracycline or its derivative doxycycline (Dox). The transrepressor remained bonded to transcription machinery in the caged version, inhibiting expression of gene while photoactivated release of doxycycline blocks transpressor leading to gene expression (Figure 22).[102]

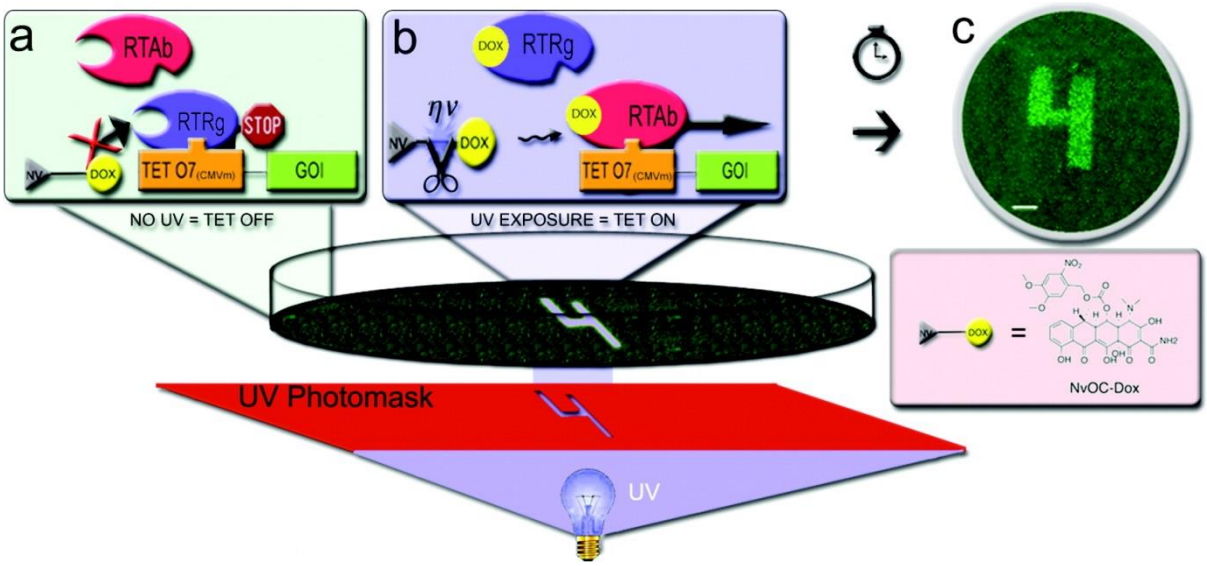

Figure 22. Light-directed gene patterning with Retro TET-ART a) No expression of GFP by Retro-Tet ART system in the presence of NVOC-Dox b) A photomask was used to selectively irradiate cells in a desired pattern by liberating dox resulting in release of the transrepressor and recruitment of the transactivator to the Tet operator, (c) GFP pattern by photo-induced gene expression (scale bar = 1 mm). Reprinted with permission from American Chemical Society.[102]

The photodegradable NVOC groups in the macromer backbone were reported by Griffin *et al.* for photodegradation in 3D to control release of hMSCs. [103] The hMSCs expressing GFP or RFP were encapsulated in hydrogels with different rate of photodegradation. The hydrogels were placed adjacent to each other with isolated cell populations. The photodegradation of hydrogels by cleaving NVOC chromophore enables control release and mixing of two cell populations as depicted in Figure 23.

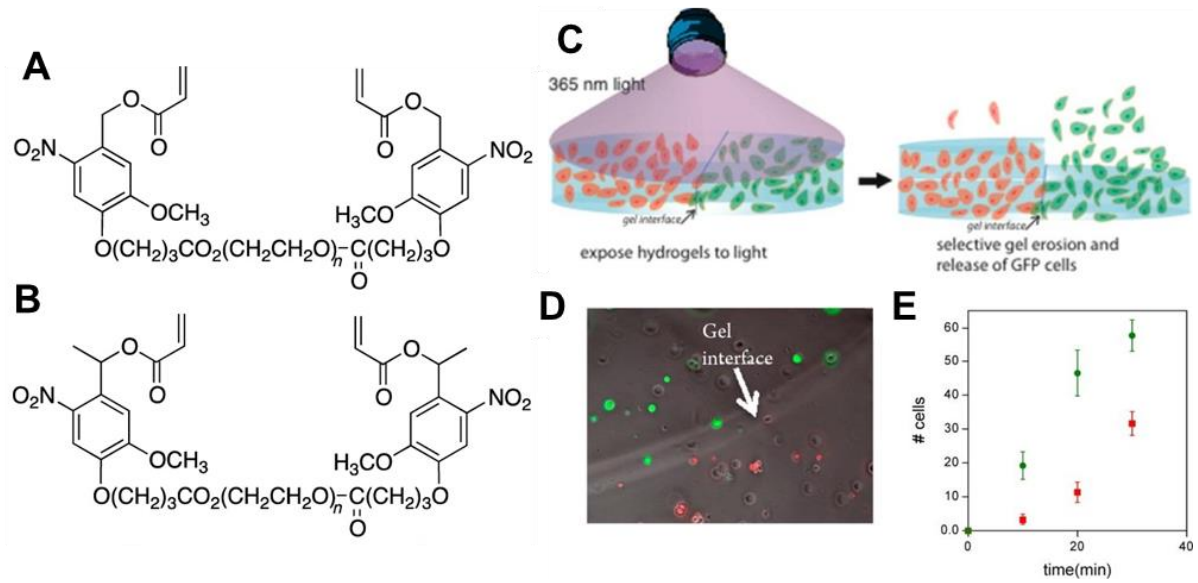

Figure 23. Selective release of cells in adjacent gels with NVOC crosslinker in (A) and (B) macromer possessing different degradation rate, (C) RFP-expressing hMSCs and GFP-expressing hMSCs were encapsulated within hydrogels made with (A) or (B), where the two hydrogels were in direct contact with each other, (D) The interface between hydrogels before exposure, (E) Irradiation of gel at 365 nm results in selective release of GFP cell population over RFP. Reprinted after permission from American Chemical society.[103]

1.5.2 The DMNPB photo-cleavable protecting group

DMNPB 3-(4,5-dimethoxy-2-nitrophenyl)-2-butanol is a o-nitrophenethyl family photolabile caging with wavelength activation at (346 - 365 nm, ε= 4100 $M^{-1}cm^{-1}$ at λ_{max} 346 nm). Structurally, DMNPB have substituted methyl group on benzylic carbon, enhancing its photolytic properties and hydrolytic stability. The photolytic properties of this 2-(o-nitrophenyl)propyl group is based on donor-acceptor mechanism. The DMNPB is an effective PPG, widely used in biomaterial to control and tune cellular response and for selective drug delivery. DMNBP is employed for development of photoactivable biomimetic sequence primarily RGD peptide for modulating cell adhesion and migration. RGD peptide show specific integrin mediating response, therefore DMNPB cage was introduced at integrin binding site, making it unrecognizable by cell, on photoactivation the bioactivity was restored.[46] [44] In addition the caged RGD(DMNPB)fK was used to selectively control cell migration with subcellular spatiotemporal resolution *in-vitro* by non-invasive photoactivation (Figure 24).[49, 104]

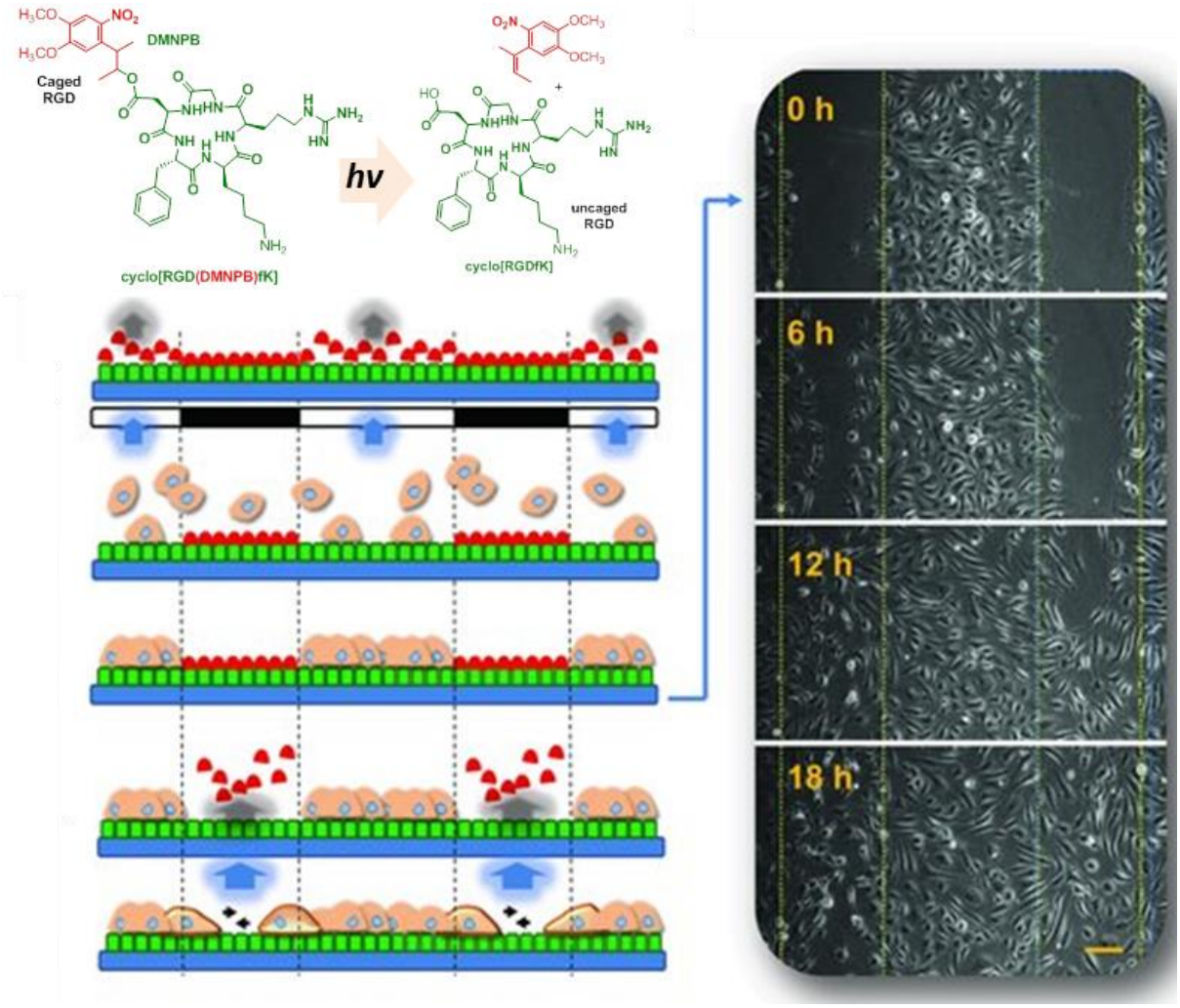

Figure 24. Photo-activatable migration assay by surface functionalization with caged RGD. Reprinted after permission.[104]

DMNPB is also used as photolyzable crosslinker between the surface and the adhesive site for tuning control release of cells from the surface.[105] The gold surface was decorated with DMNPB linker attached with RGD through ethylene glycol chain. The cell attached to the surface by recognizing RGD sequence. The HUVEC cells were selectively detached from surface by photodegradation of linker as shown in Figure 25.

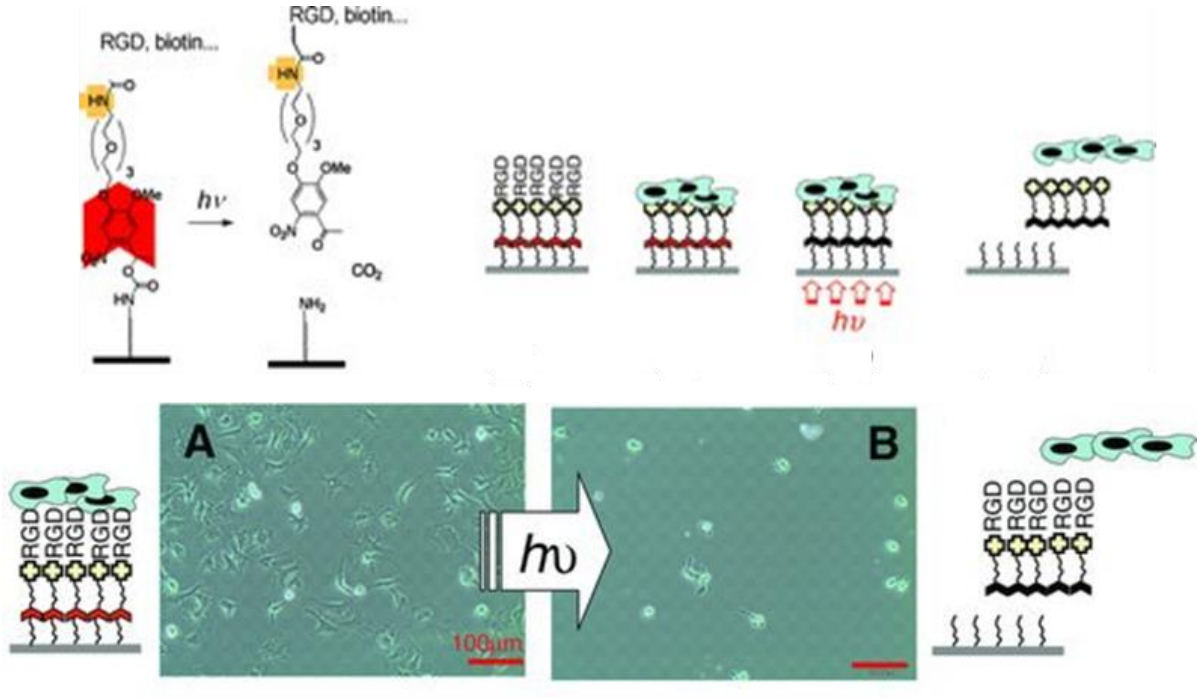

Figure 25. Schematic of phototriggered cell detachment, (A) The HUVECs attached RGD-modified substrates (B) Controlled cell release by photodegradation of light sensitive linker. Reproduced after permission.[105]

The DMNPB was applied for selective delivery of metal based anticancer prodrug [Ru(dppz)2(CppH)](PF6)2 by suppressing it activity. This Ru II complex is cytotoxic toward both normal (MRC-5) and cancerous cells (HeLa and U2OS), therefore introduction of photolabile DMNBP cage, block the cytotoxicity masking its activity. The spatiotemporal activation at tumor site reactivate the drug activity targeting primarily tumor cells.[106]

The DMNPB photocaged RGD was applied *in vivo for* light-activated regulation of cell adhesion. The temporal control over photo-triggered activation of adhesive peptides, suppresses the inflammation and rejection of implanted biomaterial. The PEG hydrogels decorated with RGD(DMNPB)fC peptide were implanted in mouse (Figure 26). The light-triggered transdermal spatiotemporal activation of RGD peptide trigger in vivo cell adhesion and vascularization on activated area. [49]

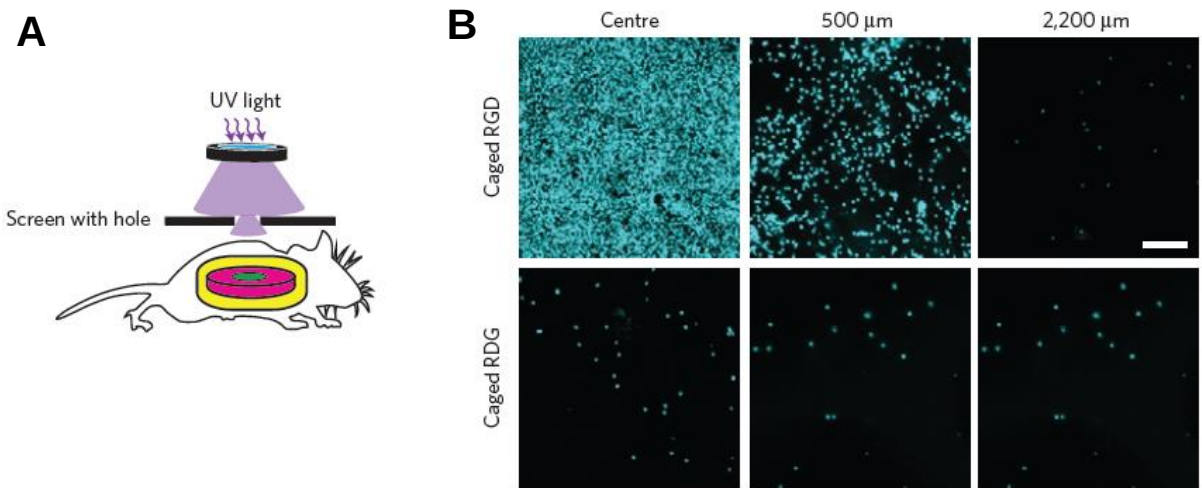

Figure 26. Light-triggered patterning of *in vivo* (A) Transdermal UV light exposure set-up through a mask, (B) Explanted hydrogels displaying adherent cells on photoactivated caged RGD and scrambled caged RDG hydrogels. The cell nuclei are stained with DAPI and scale bar is 40µm. Copyright 2014 Nature Publishers.[49]

1.5.3 The nitrobiphenyl (ANBP and PMNB) photo-activatable two-photon protecting group

UV assisted photoactivatable caging groups application in biomaterial is limited by associated phototoxicity, absorption and dispersion of UV by tissue and relatively low sub-micrometer and sub-millisecond resolution.[107]

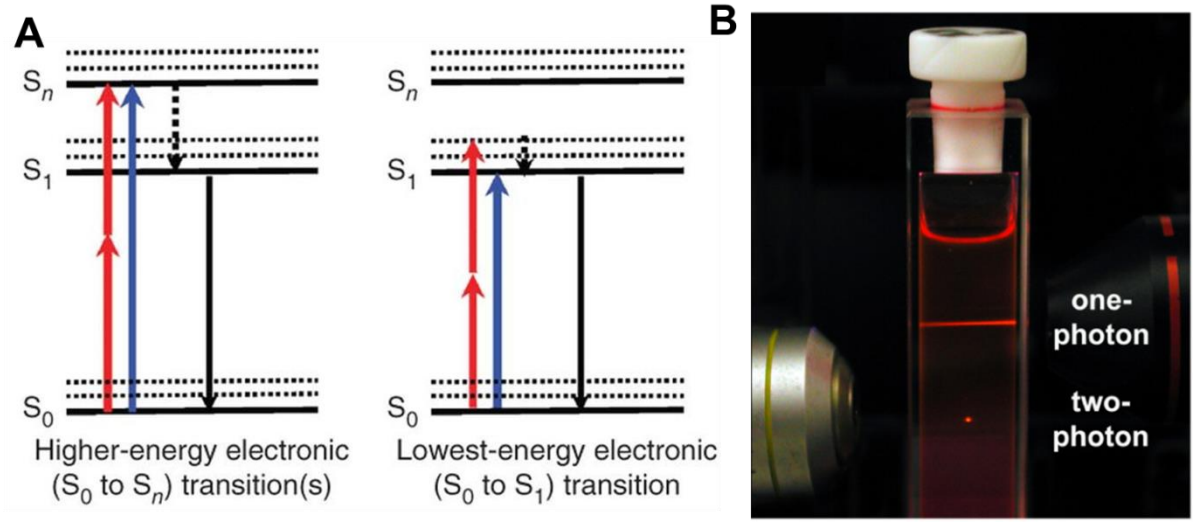

Figure 27. Comparison between and 1P and 2P activation A) Jablonski diagram of energy transitions [108] (B) Spatial resolution[91]

Recently two-photon based activation in near infra-red region (720-990 nm), is becoming relevant due to added advantage of reduced photodamage, higher penetration and fine spatial resolution. The photocleavage reaction by two photon laser is based on absorption of two similar energy photons, leading to cleavage or bond rearrangements (Figure 27).[93] The properties of two photon photolabile group depend on two photon absorption spectra (2PA), cross section (σ2), quantum yield (φ), and on two-photon excitation (2PE) action cross sections (σ2' = σ2 x φ). The two-photon cross section defines probability of simultaneous absorption of two photons to reach molecular transition energy and it is measured in in Goeppert-Mayer units, 1 GM = 10^{-50} cm^4 s.[108]

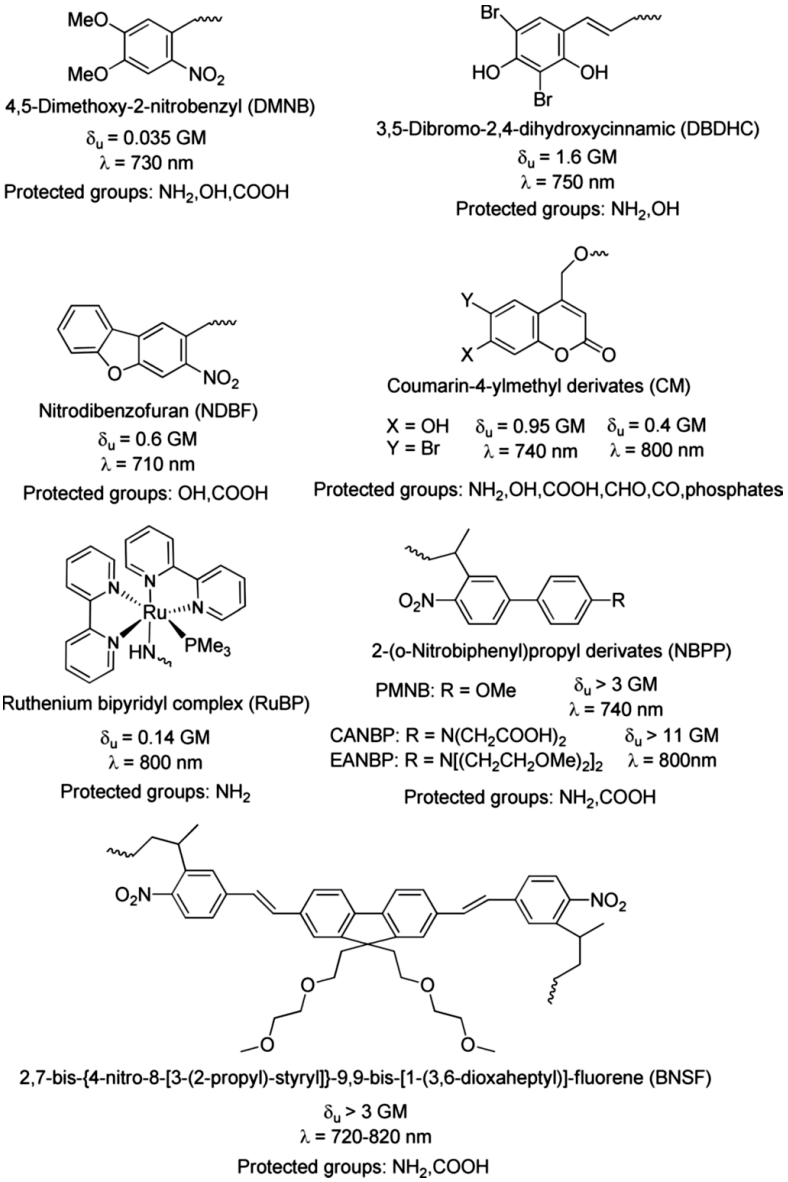

Figure 28. Structure and photolysis properties of common two photon photolabile groups. Reproduced after permission from Wiley.[109]

N-acyl-7-nitroindolines (710 nm) [110], 5-Aryl-dimethylamino quinoline (730 nm) [111], hydroxycoumarin, hydroxyquinoline, o-Hydroxycinnamate,[109] ruthenium–bipyridyl complexes [107], and ortho-nitrobiphenyl derivatives are photoactivatable at two photon range, as summarized in Figure 28. The member of o-nitroaryl family such as o-nitrobenzyl and o-nitrophenethyl show low two-photon cross section efficiency, therefore another aromatic was substituted at meta to phenethyl moiety to extend the conjugation. This biphenyl based extended conjugation significantly enhance the photolysis properties of nitro-phenethyl derivatives, by donor-acceptor platform. This lead to PMNB and ANBP photolabile groups with TP photolysis efficiency of 3.1 GM at =740 nm and 11 GM at 800 nm respectively.

PMNB cage was reported for targeted drug delivery of anticancer prodrug aminoferrocene. The aminoferrocene complex gets converted into unstable derivatives and Fe ions in the presence of reactive oxygen species (ROS). The high concentration of ROS in tumor cell support the catalysis, but during transport it could affect non-cancerous cells as well. Therefore insertion of PMNB cage render its bioactivity and later photoactivated at target site (Figure 29).[112]

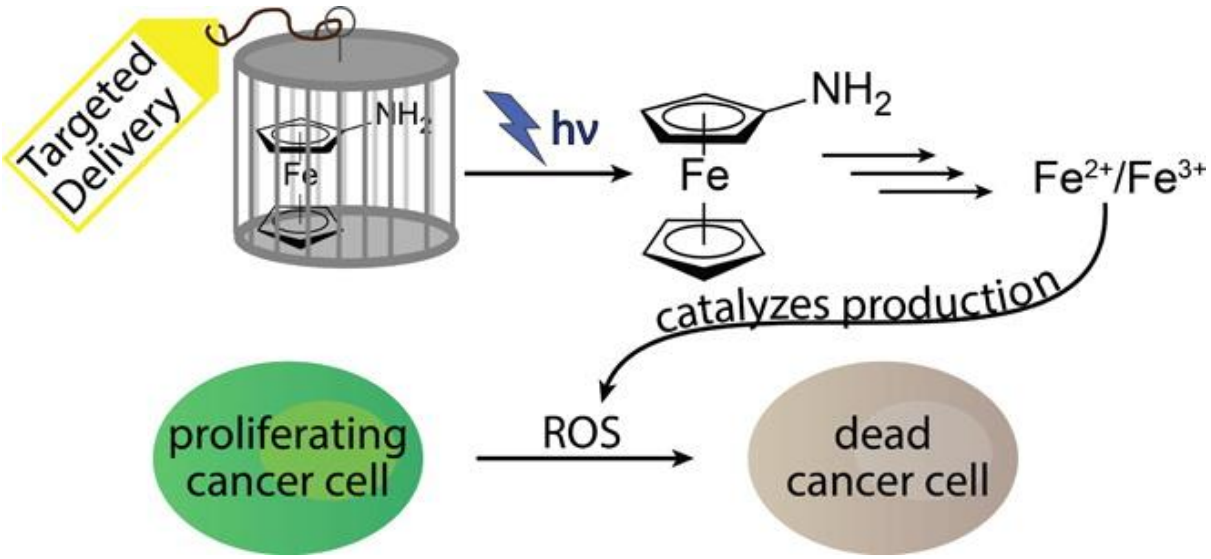

Figure 29. Photoregulated site selective drug delivery. Reproduced after permission from American chemical society.[112]

Sequential activation approach is used for controlling material properties as crosslinking and depolymerization. The photoregulated polymerization can be achieved either by sequential 1P and 2P activation or by selective 2P activation.

The orthogonal photolithography of polyurethane was performed by combing 1P and 2P activation using 1-(2-nitrophenyl)-1,2-ethanediol, NP(OH) 2 (λ_{max} 275 nm) and PMNB (λ_{max} 780 nm) respectively.[113] While polymerization of polyurethane based polymer was sequentially tuned in 2D and 3D, by pre-modification of monomer chains with photolabile two photon ANBP (λ_{max} 820 or 520 nm) and PMNB(λ_{max} 780 nm or 365 nm) chromophores (Figure 30).[114]

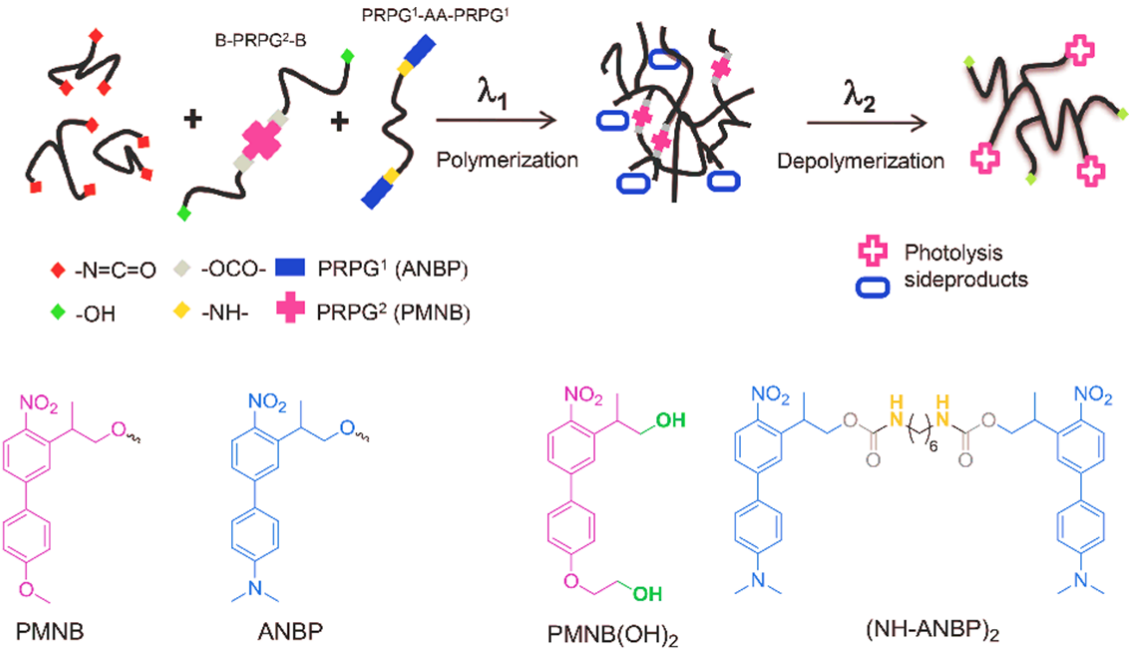

Figure 30. Wavelength selective polymerization strategy. Reproduced after permission from Wiley.[114]

Wavelength selective activation in spatiotemporally controlled DNA hybridization in 3D was accounted by combination of ANBP (980 nm) and DEACM (840 nm) two-photon activatable chromophores.[115] Photocontrol hybridization of DNA and RNA nucleic-acid-based technique enable development of large array of oligonuclieotides, based on caged nucleotides.

The potential biomedical application of 2P chromophore demand enhancement of 2P uncaging efficiency, longer activation wavelength and high water solubility. Therefore photolysis efficiency and hydrolytic stability of ANBP was enhanced by substitution of dimethyl by dialkoxyamine (ENABP) leading to 11 GM cross-sections at 800 nm and high water solubility.[88, 116] Neurotransmitter GABA caged with ENABP was employed for photoregulated spatial release of GABA in intact brain slice. The further improvement in cross section efficiency is reported by introduction of acetylene

residue between biphenyl chain, extending π interaction conjugation. This diphenylacetylene show 1.8 time enhanced photolysis and applied to control intracellular protein dimerization by photo-regulating subcellular level release of gibberellic acid (GA).[117] The GA act as intracellular chemical inducers of dimerization (CIDs) by connecting TAG protein with protein of interest.

References

[1] aF. Gattazzo, A. Urciuolo, P. Bonaldo, *Biochimica et Biophysica Acta (BBA)-General Subjects* **2014**, *1840*, 2506-2519; bC. Lee-Thedieck, J. P. Spatz, *Biomaterials Science* **2014**, *2*, 1548-1561.

[2] A. Page-McCaw, A. J. Ewald, Z. Werb, *Nature reviews Molecular cell biology* **2007**, *8*, 221-233.

[3] P. Lu, K. Takai, V. M. Weaver, Z. Werb, *Cold Spring Harbor perspectives in biology* **2011**, *3*, a005058.

[4] C. Bonnans, J. Chou, Z. Werb, *Nature reviews Molecular cell biology* **2014**, *15*, 786-801.

[5] aH. K. Kleinman, R. J. Klebe, G. R. Martin, *J cell biol* **1981**, *88*, 473-485; bH. Lodish, A. Berk, L. Zipursky, P. Matsudaira, D. Baltimore, J. Darnell, *Lodish, H., Berk, A., Zipursky, SL & et al. 4th Molecular Cell Biology. New York: WH Freeman and Company* **2000**, Section 22.24; cC. Frantz, K. M. Stewart, V. M. Weaver, *J Cell Sci* **2010**, *123*, 4195-4200; dM. D. Henry, J. S. Satz, C. Brakebusch, M. Costell, E. Gustafsson, R. Fassler, K. P. Campbell, *Journal of Cell Science* **2001**, *114*, 1137-1144.

[6] aD. Guarnieri, S. Battista, A. Borzacchiello, L. Mayol, E. De Rosa, D. Keene, L. Muscariello, A. Barbarisi, P. A. Netti, *Journal of Materials Science: Materials in Medicine* **2007**, *18*, 245-253; bK. M. Yamada, in *Fibronectin*, Academic Press, New York, **1989**, pp. 47-121.

[7] S. Stenman, A. Vaheri, *The Journal of experimental medicine* **1978**, *147*, 1054-1064.

[8] A. Domogatskaya, S. Rodin, K. Tryggvason, *Annual review of cell and developmental biology* **2012**, *28*, 523-553.

[9] E. Hohenester, P. D. Yurchenco, *Cell adhesion & migration* **2013**, *7*, 56-63.

[10] H. Kleinman, R. C. Ogle, F. Cannon, C. Little, T. Sweeney, L. Luckenbill-Edds, *Proceedings of the National Academy of Sciences* **1988**, *85*, 1282-1286.

[11] aM. Durbeej, *Cell and tissue research* **2010**, *339*, 259; bA. M. Belkin, M. A. Stepp, *Microscopy research and technique* **2000**, *51*, 280-301.

[12] C. C. DuFort, M. J. Paszek, V. M. Weaver, *Nature reviews Molecular cell biology* **2011**, *12*, 308-319.

[13] G. M. Edelman, *Science* **1983**, *219*, 450-457.

[14] C. Mas-Moruno, R. Fraioli, F. Rechenmacher, S. Neubauer, T. G. Kapp, H. Kessler, *Angewandte Chemie* **2016**, *55*, 7048–7067.

[15] C. S. Stipp, *Expert reviews in molecular medicine* **2010**, *12*, e3.

[16] M. B. Srichai, R. Zent, in *Cell-Extracellular Matrix Interactions in Cancer*, Springer, **2010**, pp. 19-41.

[17] M. Hammerschmidt, D. Wedlich, *Development* **2008**, *135*, 3625-3641.

[18] B. Geiger, J. P. Spatz, A. D. Bershadsky, *Nature reviews Molecular cell biology* **2009**, *10*, 21-33.
[19] E. K. Paluch, C. M. Nelson, N. Biais, B. Fabry, J. Moeller, B. L. Pruitt, C. Wollnik, G. Kudryasheva, F. Rehfeldt, W. Federle, *BMC biology* **2015**, *13*, 47.
[20] A. N. Gasparski, K. A. Beningo, *Archives of biochemistry and biophysics* **2015**, *586*, 20-26.
[21] A. Higuchi, Q.-D. Ling, S.-T. Hsu, A. Umezawa, *Chemical Reviews* **2012**, *112*, 4507-4540.
[22] A. M. Rosales, K. S. Anseth, *Nature Reviews Materials* **2016**, *1*, 15012.
[23] J. E. Frith, R. J. Mills, J. E. Hudson, J. J. Cooper-White, *Stem cells and development* **2012**, *21*, 2442-2456.
[24] aM. Mochizuki, D. Philp, K. Hozumi, N. Suzuki, Y. Yamada, H. K. Kleinman, M. Nomizu, *Archives of biochemistry and biophysics* **2007**, *459*, 249-255; bY. Yamada, K. Hozumi, A. Aso, A. Hotta, K. Toma, F. Katagiri, Y. Kikkawa, M. Nomizu, *Biomaterials* **2012**, *33*, 4118-4125.
[25] M. Yamada, Y. Kadoya, S. Kasai, K. Kato, M. Mochizuki, N. Nishi, N. Watanabe, H. K. Kleinman, Y. Yamada, M. Nomizu, *FEBS letters* **2002**, *530*, 48-52.
[26] S. H. Gee, R. Blacher, P. Douville, P. Provost, P. Yurchenco, S. Carbonetto, *Journal of Biological Chemistry* **1993**, *268*, 14972-14980.
[27] M. C. Kibbey, M. Jucker, B. S. Weeks, R. L. Neve, W. E. Van Nostrand, H. K. Kleinman, *Proceedings of the National Academy of Sciences* **1993**, *90*, 10150-10153.
[28] aD. Thid, M. Bally, K. Holm, S. Chessari, S. Tosatti, M. Textor, J. Gold, *Langmuir* **2007**, *23*, 11693-11704; bV. M. Freitas, V. F. Vilas-Boas, D. C. Pimenta, V. Loureiro, M. A. Juliano, M. R. Carvalho, J. J. Pinheiro, A. C. Camargo, A. S. Moriscot, M. P. Hoffman, *The American journal of pathology* **2007**, *171*, 124-138.
[29] S. Kasai, Y. Ohga, M. Mochizuki, N. Nishi, Y. Kadoya, M. Nomizu, *Peptide Science* **2004**, *76*, 27-33.
[30] M. Nomizu, W. H. Kim, K. Yamamura, A. Utani, S.-Y. Song, A. Otaka, P. P. Roller, H. K. Kleinman, Y. Yamada, *Journal of Biological Chemistry* **1995**, *270*, 20583-20590.
[31] D. Thid, K. Holm, P. S. Eriksson, J. Ekeroth, B. Kasemo, J. Gold, *Journal of Biomedical Materials Research Part A* **2008**, *84*, 940-953.
[32] D. Xing, L. Ma, C. Gao, *Macromolecular bioscience* **2014**, *14*, 1429-1436.
[33] D. Xing, L. Ma, C. Gao, *Journal of Bioactive and Compatible Polymers* **2017**, 0883911516684654.
[34] W. Sun, T. Incitti, C. Migliaresi, A. Quattrone, S. Casarosa, A. Motta, *Journal of tissue engineering and regenerative medicine* **2017**, *11*, 1532-1541.
[35] H. Hosseinkhani, Y. Hiraoka, C.-H. Li, Y.-R. Chen, D.-S. Yu, P.-D. Hong, K.-L. Ou, *ACS chemical neuroscience* **2013**, *4*, 1229-1235.
[36] Y. Akizawa, Y. Morita, Y. Hsu, T. Yamaoka, E. Nakamachi, in *ASME 2016 International Mechanical Engineering Congress and Exposition*, American Society of Mechanical Engineers, **2016**, pp. V003T004A073-V003T004A073.
[37] G. A. Silva, C. Czeisler, K. L. Niece, E. Beniash, D. A. Harrington, J. A. Kessler, S. I. Stupp, *Science* **2004**, *303*, 1352-1355.
[38] aV. M. Tysseling-Mattiace, V. Sahni, K. L. Niece, D. Birch, C. Czeisler, M. G. Fehlings, S. I. Stupp, J. A. Kessler, *Journal of Neuroscience* **2008**, *28*, 3814-3823; bH. Cui, M. J. Webber, S. I. Stupp, *Peptide Science* **2010**, *94*, 1-18.

[39] C. Frick, M. Müller, U. Wank, A. Tropitzsch, B. Kramer, P. Senn, H. Rask-Andersen, K.-H. Wiesmüller, H. Löwenheim, *Colloids and Surfaces B: Biointerfaces* **2017**, *149*, 105-114.
[40] E. J. Berns, S. Sur, L. Pan, J. E. Goldberger, S. Suresh, S. Zhang, J. A. Kessler, S. I. Stupp, *Biomaterials* **2014**, *35*, 185-195.
[41] S. Hamsici, G. Cinar, A. Celebioglu, T. Uyar, A. B. Tekinay, M. O. Guler, *Journal of Materials Chemistry B* **2017**, *5*, 517-524.
[42] Y.-P. Lu, C.-H. Yang, J. A. Yeh, F. H. Ho, Y.-C. Ou, C. H. Chen, M.-Y. Lin, K.-S. Huang, *International journal of pharmaceutics* **2014**, *463*, 177-183.
[43] P. M. Kharkar, K. L. Kiick, A. M. Kloxin, *Chemical Society Reviews* **2013**, *42*, 7335-7372.
[44] M. Wirkner, S. Weis, V. San Miguel, M. Álvarez, R. A. Gropeanu, M. Salierno, A. Sartoris, R. E. Unger, C. J. Kirkpatrick, A. del Campo, *ChemBioChem* **2011**, *12*, 2623-2629.
[45] M. Gao, M. Sotomayor, E. Villa, E. H. Lee, K. Schulten, *Physical Chemistry Chemical Physics* **2006**, *8*, 3692-3706.
[46] S. Petersen, J. M. Alonso, A. Specht, P. Duodu, M. Goeldner, A. del Campo, *Angewandte Chemie International Edition* **2008**, *47*, 3192-3195.
[47] aM. Aumailley, M. Gurrath, G. Müller, J. Calvete, R. Timpl, H. Kessler, *FEBS letters* **1991**, *291*, 50-54; bM. Gurrath, G. Müller, H. Kessler, M. Aumailley, R. Timpl, *European Journal of Biochemistry* **1992**, *210*, 911-921.
[48] R. Haubner, R. Gratias, B. Diefenbach, S. L. Goodman, A. Jonczyk, H. Kessler, *Journal of the American Chemical Society* **1996**, *118*, 7461-7472.
[49] T. T. Lee, J. R. García, J. I. Paez, A. Singh, E. A. Phelps, S. Weis, Z. Shafiq, A. Shekaran, A. Del Campo, A. J. García, *Nature materials* **2015**, *14*, 352-360.
[50] aA. Spitaleri, S. Mari, F. Curnis, C. Traversari, R. Longhi, C. Bordignon, A. Corti, G.-P. Rizzardi, G. Musco, *Journal of Biological Chemistry* **2008**, *283*, 19757-19768; bA. Corti, F. Curnis, *J Cell Sci* **2011**, *124*, 515-522.
[51] S. Petersen, J. M. Alonso, A. Specht, P. Duodu, M. Goeldner, A. del Campo, *Angew Chem Int Ed Engl* **2008**, *47*, 3192-3195.
[52] C. A. DeForest, K. S. Anseth, *Nature chemistry* **2011**, *3*, 925-931.
[53] J. M. Barnes, L. Przybyla, V. M. Weaver, *Journal of Cell Science* **2017**, *130*, 71-82.
[54] B. Mammadov, M. Sever, M. O. Guler, A. B. Tekinay, *Biomaterials Science* **2013**, *1*, 1119-1137.
[55] S. R. Caliari, J. A. Burdick, *Nature methods* **2016**, *13*, 405-414.
[56] A. J. Engler, S. Sen, H. L. Sweeney, D. E. Discher, *Cell* **2006**, *126*, 677-689.
[57] J. H. Wen, L. G. Vincent, A. Fuhrmann, Y. S. Choi, K. C. Hribar, H. Taylor-Weiner, S. Chen, A. J. Engler, *Nature materials* **2014**, *13*, 979-987.
[58] J. Thiele, Y. Ma, S. Bruekers, S. Ma, W. T. Huck, *Advanced Materials* **2014**, *26*, 125-148.
[59] X. Huang, N. Yang, V. F. Fiore, T. H. Barker, Y. Sun, S. W. Morris, Q. Ding, V. J. Thannickal, Y. Zhou, *American journal of respiratory cell and molecular biology* **2012**, *47*, 340-348.
[60] A. Juin, E. Planus, F. Guillemot, P. Horakova, C. Albiges-Rizo, E. Génot, J. Rosenbaum, V. Moreau, F. Saltel, *Biology of the Cell* **2013**, *105*, 46-57.
[61] J. P. Winer, P. A. Janmey, M. E. McCormick, M. Funaki, *Tissue Engineering Part A* **2008**, *15*, 147-154.

[62] S. Lee, A. Zeiger, J. M. Maloney, M. Kotecki, K. J. Van Vliet, I. M. Herman, *Journal of Physics: Condensed Matter* **2010**, *22*, 194115.
[63] L. G. Vincent, Y. S. Choi, B. Alonso-Latorre, J. C. del Álamo, A. J. Engler, *Biotechnology journal* **2013**, *8*, 472-484.
[64] R. Sunyer, V. Conte, J. Escribano, A. Elosegui-Artola, A. Labernadie, L. Valon, D. Navajas, J. M. García-Aznar, J. J. Muñoz, P. Roca-Cusachs, *Science* **2016**, *353*, 1157-1161.
[65] B. N. Mason, J. P. Califano, C. A. Reinhart-King, in *Engineering Biomaterials for Regenerative Medicine*, Springer, **2012**, pp. 19-37.
[66] E. A. Phelps, N. O. Enemchukwu, V. F. Fiore, J. C. Sy, N. Murthy, T. A. Sulchek, T. H. Barker, A. J. García, *Advanced Materials* **2012**, *24*, 64-70.
[67] O. W. Petersen, L. Rønnov-Jessen, A. R. Howlett, M. J. Bissell, *Proceedings of the National Academy of Sciences* **1992**, *89*, 9064-9068.
[68] M. W. Tibbitt, K. S. Anseth, *Biotechnology and bioengineering* **2009**, *103*, 655-663.
[69] C. Pande, A. Sharma, *Journal of applied polymer science* **2002**, *84*, 2613-2620.
[70] O. F. Zouani, J. Kalisky, E. Ibarboure, M.-C. Durrieu, *Biomaterials* **2013**, *34*, 2157-2166.
[71] B. Trappmann, J. E. Gautrot, J. T. Connelly, D. G. Strange, Y. Li, M. L. Oyen, M. A. C. Stuart, H. Boehm, B. Li, V. Vogel, *Nature materials* **2012**, *11*, 642-649.
[72] D. L. Alge, M. A. Azagarsamy, D. F. Donohue, K. S. Anseth, *Biomacromolecules* **2013**, *14*, 949-953.
[73] C. A. DeForest, E. A. Sims, K. S. Anseth, *Chemistry of materials* **2010**, *22*, 4783-4790.
[74] M. A. Azagarsamy, K. S. Anseth, *ACS macro letters* **2013**, *2*, 5-9.
[75] aD. G. Vartak, R. A. Gemeinhart, *Journal of drug targeting* **2007**, *15*, 1-20; bU. Eckhard, P. F. Huesgen, O. Schilling, C. L. Bellac, G. S. Butler, J. H. Cox, A. Dufour, V. Goebeler, R. Kappelhoff, U. auf dem Keller, *Matrix Biology* **2016**, *49*, 37-60.
[76] O. Okay, in *Hydrogel sensors and actuators, Vol. 6*, Springer, **2009**, pp. 1-14.
[77] J. R. Tse, A. J. Engler, *Current protocols in cell biology* **2010**, *47*, 10-16.
[78] Š. Selimović, J. Oh, H. Bae, M. Dokmeci, A. Khademhosseini, *Polymers* **2012**, *4*, 1554-1579.
[79] R. Y. Tam, L. J. Smith, M. S. Shoichet, *Accounts of Chemical Research* **2017**.
[80] T. Lai, J. Yu, W. Tsai, *Journal of Materials Chemistry B* **2016**, *4*, 2304-2313.
[81] S. Khetan, M. Guvendiren, W. R. Legant, D. M. Cohen, C. S. Chen, J. A. Burdick, *Nature materials* **2013**, *12*, 458-465.
[82] T. E. Brown, I. A. Marozas, K. S. Anseth, *Advanced Materials* **2017**, *29*.
[83] J. B. Lee, X. Wang, S. Faley, B. Baer, D. A. Balikov, H. J. Sung, L. M. Bellan, *Advanced healthcare materials* **2016**, *5*, 781–785.
[84] A. M. Kloxin, K. J. Lewis, C. A. DeForest, G. Seedorf, M. W. Tibbitt, V. Balasubramaniam, K. S. Anseth, *Integrative Biology* **2012**, *4*, 1540-1549.
[85] S.-H. Lee, J. J. Moon, J. L. West, *Biomaterials* **2008**, *29*, 2962-2968.
[86] M. A. Azagarsamy, I. A. Marozas, S. Spaans, K. S. Anseth, *ACS macro letters* **2015**, *5*, 19-23.
[87] C. Brieke, F. Rohrbach, A. Gottschalk, G. Mayer, A. Heckel, *Angewandte Chemie International Edition* **2012**, *51*, 8446-8476.

[88] A. Specht, F. Bolze, L. Donato, C. Herbivo, S. Charon, D. Warther, S. Gug, J.-F. Nicoud, M. Goeldner, *Photochemical & Photobiological Sciences* **2012**, *11*, 578-586.
[89] C.-L. Ciana, C. G. Bochet, *CHIMIA International Journal for Chemistry* **2007**, *61*, 650-654.
[90] V. San Miguel, C. G. Bochet, A. del Campo, *Journal of the American Chemical Society* **2011**, *133*, 5380-5388.
[91] S. Piant, F. Bolze, A. Specht, *Optical Materials Express* **2016**, *6*, 1679-1691.
[92] I. Ahmed, L. Fruk, *Molecular BioSystems* **2013**, *9*, 565-570.
[93] D. Warther, S. Gug, A. Specht, F. Bolze, J.-F. Nicoud, A. Mourot, M. Goeldner, *Bioorganic & medicinal chemistry* **2010**, *18*, 7753-7758.
[94] P. Klán, T. Šolomek, C. G. Bochet, A. l. Blanc, R. Givens, M. Rubina, V. Popik, A. Kostikov, J. Wirz, *Chemical Reviews* **2013**, *113*, 119.
[95] M. J. Hansen, W. A. Velema, M. M. Lerch, W. Szymanski, B. L. Feringa, *Chemical Society Reviews* **2015**, *44*, 3358-3377.
[96] A. Rodrigues-Correia, X. M. Weyel, A. Heckel, *Organic letters* **2013**, *15*, 5500-5503.
[97] A. L. DeMond, T. Starr, M. L. Dustin, J. T. Groves, *Journal of the American Chemical Society* **2006**, *128*, 15354-15355.
[98] R. A. Gropeanu, H. Baumann, S. Ritz, V. Mailänder, T. Surrey, A. Del Campo, *PloS one* **2012**, *7*, e43657.
[99] M. E. Lee, E. Gungor, A. M. Armani, *Macromolecules* **2015**, *48*, 8746-8751.
[100] aM. Álvarez, J. M. Alonso, O. Filevich, M. Bhagawati, R. Etchenique, J. Piehler, A. del Campo, *Langmuir* **2011**, *27*, 2789-2795; bM. Álvarez, A. Best, A. Unger, J. M. Alonso, A. del Campo, M. Schmelzeisen, K. Koynov, M. Kreiter, *Advanced Functional Materials* **2010**, *20*, 4265-4272.
[101] A. del Campo, D. Boos, H. W. Spiess, U. Jonas, *Angewandte Chemie International Edition* **2005**, *44*, 4707-4712.
[102] D. J. Sauers, M. K. Temburni, J. B. Biggins, L. M. Ceo, D. S. Galileo, J. T. Koh, *ACS chemical biology* **2010**, *5*, 313-320.
[103] D. R. Griffin, A. M. Kasko, *Journal of the American Chemical Society* **2012**, *134*, 13103-13107.
[104] M. J. Salierno, A. J. García, A. Del Campo, *Advanced Functional Materials* **2013**, *23*, 5974-5980.
[105] M. Wirkner, J. M. Alonso, V. Maus, M. Salierno, T. T. Lee, A. J. García, A. Del Campo, *Advanced Materials* **2011**, *23*, 3907-3910.
[106] T. Joshi, V. Pierroz, C. Mari, L. Gemperle, S. Ferrari, G. Gasser, *Angewandte Chemie International Edition* **2014**, *53*, 2960-2963.
[107] G. Bort, T. Gallavardin, D. Ogden, P. I. Dalko, *Angewandte Chemie International Edition* **2013**, *52*, 4526-4537.
[108] M. Drobizhev, N. S. Makarov, S. E. Tillo, T. E. Hughes, A. Rebane, *Nature methods* **2011**, *8*, 393-399.
[109] J. Cui, V. S. Miguel, A. del Campo, *Macromolecular rapid communications* **2013**, *34*, 310-329.
[110] K. A. Hatch, A. Ornelas, K. N. Williams, T. Boland, K. Michael, C. Li, *Biomedical Optics Express* **2016**, *7*, 4654-4659.
[111] C. Tran, P. Dunkel, H. Dhimane, D. Ogden, P. I. Dalko, *Optical Materials Express* **2016**, *6*, 2207-2212.
[112] A. Leonidova, P. Anstaett, V. Pierroz, C. Mari, B. Spingler, S. Ferrari, G. Gasser, *Inorganic chemistry* **2015**, *54*, 9740-9748.

[113] L. García-Fernández, A. Specht, A. del Campo, *Macromolecular rapid communications* **2014**, *35*, 1801-1807.
[114] L. García-Fernández, C. Herbivo, V. S. M. Arranz, D. Warther, L. Donato, A. Specht, A. del Campo, *Advanced Materials* **2014**, *26*, 5012-5017.
[115] M. A. Fichte, X. M. Weyel, S. Junek, F. Schäfer, C. Herbivo, M. Goeldner, A. Specht, J. Wachtveitl, A. Heckel, *Angewandte Chemie* **2016**, *128*, 9094-9098.
[116] L. Donato, A. Mourot, C. M. Davenport, C. Herbivo, D. Warther, J. Léonard, F. Bolze, J. F. Nicoud, R. H. Kramer, M. Goeldner, *Angewandte Chemie International Edition* **2012**, *51*, 1840-1843.
[117] K. M. Schelkle, T. Griesbaum, D. Ollech, S. Becht, T. Buckup, M. Hamburger, R. Wombacher, *Angewandte Chemie International Edition* **2015**, *54*, 2825-2829.

Chapter 2

Synthesis of Photoactivatable Laminin Mimetic Peptides

2.1 Introduction

Laminin is an abundant protein in the neural niche fundamental for neuronal migration, differentiation and neurite outgrowth.[1] Laminin binds to beta-1 integrin membrane receptors such as $\alpha_3\beta_1$, $\alpha_4\beta_4$ and $\alpha_6\beta_1$ responsible for neural attachment, development and neurite extension. Laminin mimetic peptides YIGSR, IKVAV, RKRLQVQLSIRT have been used to functionalize biomaterials to support adhesion of neural cells and neurite out-growth.[2]

In many neuronal tissues (spinal cord, optical nerve, cortex) neurites extend along certain directions. The pathfinding and orientation of the neurites built neural circuitry and allows transmission of nerve impulse in a particular direction.[3] The spatial organization of adhesive proteins like Laminin in the natural niche is relevant for the direction of neural growth.[4] The spatial arrangement determines the availability and density of adhesive biomolecules at specific areas and, therefore the direction along which neurons will attach and organize. In *in vitro*, spatial arrangement of adhesive proteins allows localization of cells in particular patterns.[5] This can be achieved by microcontact printing, electro-spinning, photolithograpy, electro-activation or thermoregulation as depicted by Figure 1.[5b, 5c, 6] In A. del Campo group, spatial organization upon light activation has been demonstrated based on photoresponsive peptidomimetics.[5a, 7] A photoremovable protecting group (cage) is covalently attached to the adhesive peptidomimetic at a relevant binding site. In this way, the bioactivity of the peptide is temporally inhibited. The site selective photo-illumination at appropriate wavelength releases the cage and unblocks the active site. The light provides non-invasive control over bioactivity at cell friendly conditions. The photoactivation can also regulate temporal activation and interaction with cells.[8]

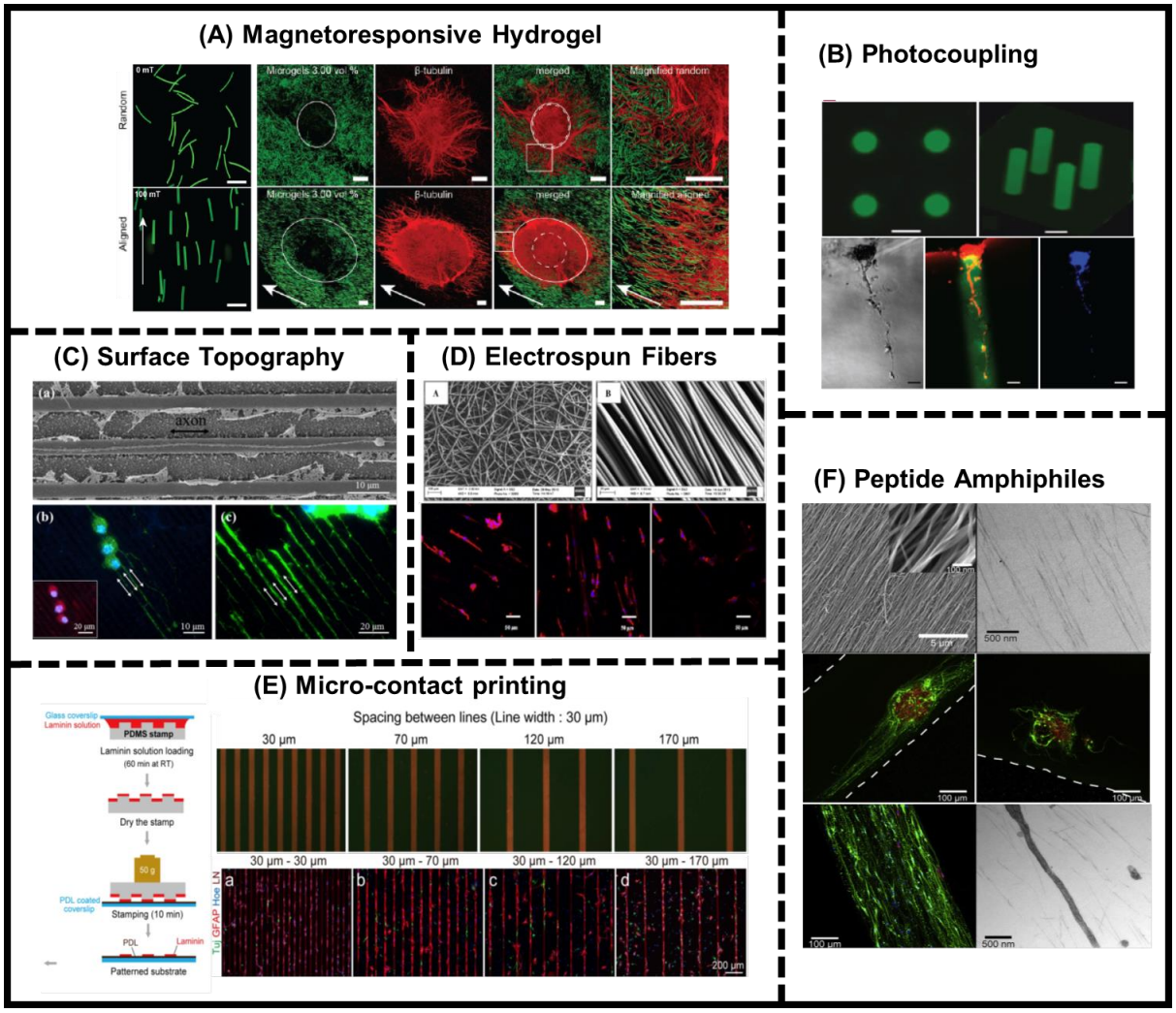

Figure 1. Various approaches for directional neural growth (A) Magnetoresponsive PEG based microgel developed by incorporation of iron oxide nanoparticles for directional growth of dorsal root ganglion[9] (B) Bio-adhesive channels in agarose gel created by release of photo-protecting NVOC group and subsequent thiol-maleimide reaction for binding ligands. The Primary rat dorsal root ganglia cells show directional growth within GRGDS functionalized channels in agarose[10] (C) Nanostructure on silicon wafer created by wet etching and modified with Laminin for direction growth of PC12 cells[11] (D) Electro-spun aligned poly-ε-caprolactone microfibers for aligned extension of PC12 cells[12] (E) Microcontact printed Laminin strips for differentiation of aNSCs[13] (F) Aligned IKVAV containing peptide amphiphile (PA) nanofibers for directional growth of neural progenitor cells and hippocampal neurons respectively. The TEM image show hippocampal neurite on aligned gel oriented parallel to the aligned PA nanofibers.[5b]

In this chapter, a photoactivatable derivative of IKVAV; the laminin peptidomimetic is presented.[14] Different variants containing 5-12 amino acid and different photolabile protecting groups at the Lysine (K) residue will be discussed in terms of solubility, stability and photo-efficiency. The ability of this peptide to control direction of axon growth will be described in Chapter 5 Section 5.3 – 5.5.

2.2 Molecular design of a photoactivatable Laminin peptides

2.2.1 Selection of Laminin peptidomimetic

Literature search (Chapter 1 Section 1.3.1a) lead to the selection of IKVAV motif as potential candidates to develop a photoactivatable laminin adhesive peptide.[15] The IKVAV sequence is highly hydrophobic due to uncharged amino acids and shows low water solubility. Different variants of IKVAV have been developed in order to improve its solubility. This includes introduction of polar amino acids residue, charged amino acids and ethylene glycol chains into peptide sequence (Table 1). Reported data do not allow meaningful comparison of solubility differences to identify best candidate. Therefore, all candidates were synthesized and their solubility was evaluated.

All peptides were synthesized manually by Fmoc solid-phase peptide synthesis (SPPS) except CCRRIKVAVWLC and CSRARKQAASIKVAVSADR were purchased. The SPPS strategy involves sequential addition of amino acids to a growing resin, extending chain of linear peptide by repeated coupling cycles (Figure 2). The acid sensitive trityl-linker (TCP) resin with either Arg(Pbf)-Fmoc or Val-Fmoc loading were used to start synthesis depending on desired sequence. The peptide sequence was grown from C to N terminal, with Fmoc deprotection of N-terminal for addition of each amino acid, under basic conditions (20% piperidine). The cleavage of peptide from resin and deprotection of side chain protecting groups was performed in acidic conditions. The peptides were purified by reverse phase high performance liquid chromatography (RP-HPLC) and characterize by ESI-MS.

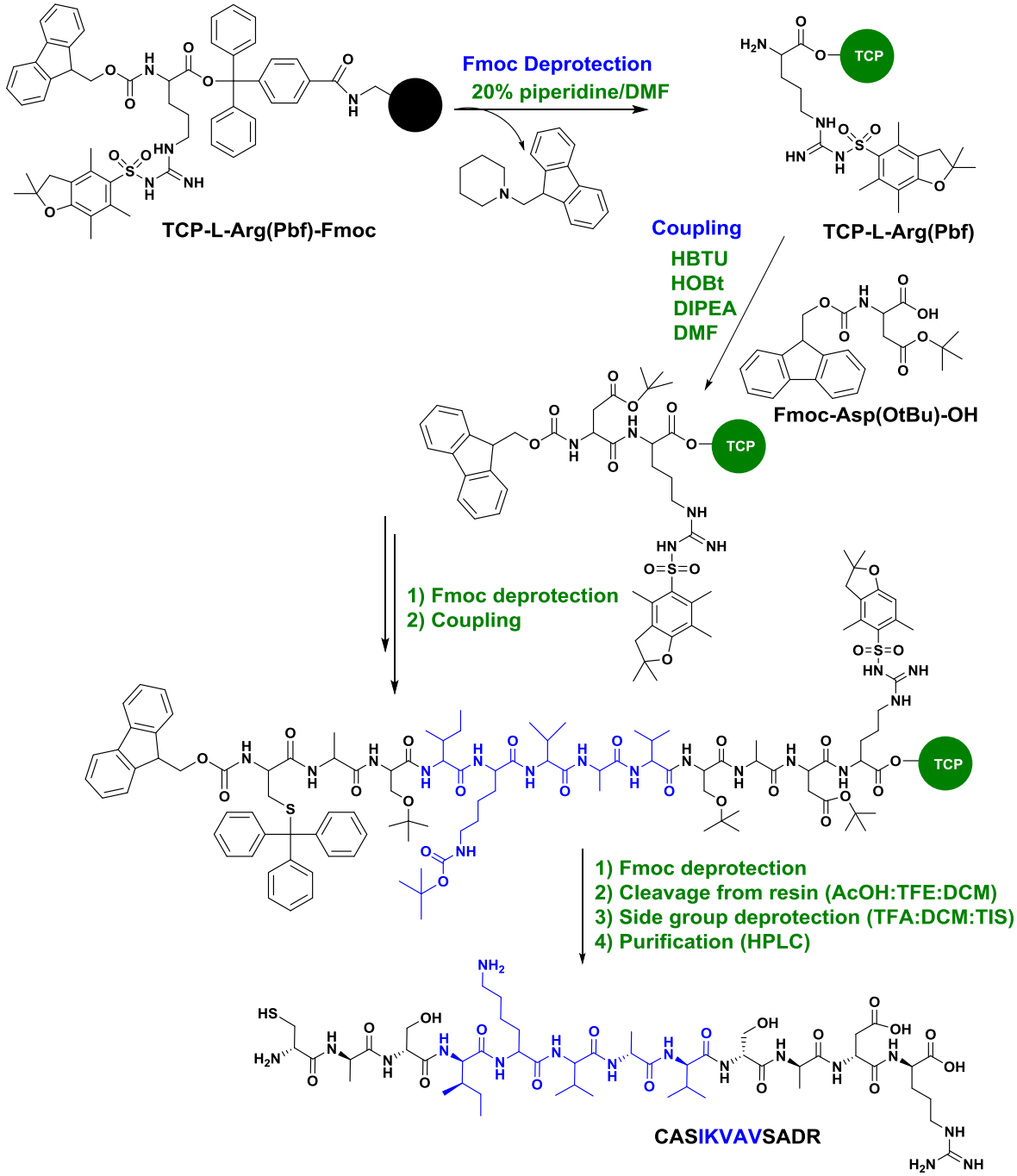

Figure 2. The representative synthesis of IK-12 peptide by SPPS.

The coupling cocktail for each amino acid during peptide synthesis involves side chain protected respective amino acid, DIPEA as base and coupling agents as HBTU/HOBt. The base and coupling agents activate the carboxyl acid moiety of amino acid to be coupled which form amide bond by nucleophilic attack of amine on carbonyl carbon (Figure 3). The DIPEA abstract proton and form carboxylate ion, which attacks electro-deficient carbonium ion of HBTU. The deprotonated amine attack on carbonyl carbon and displace HOBt forming amide bond.

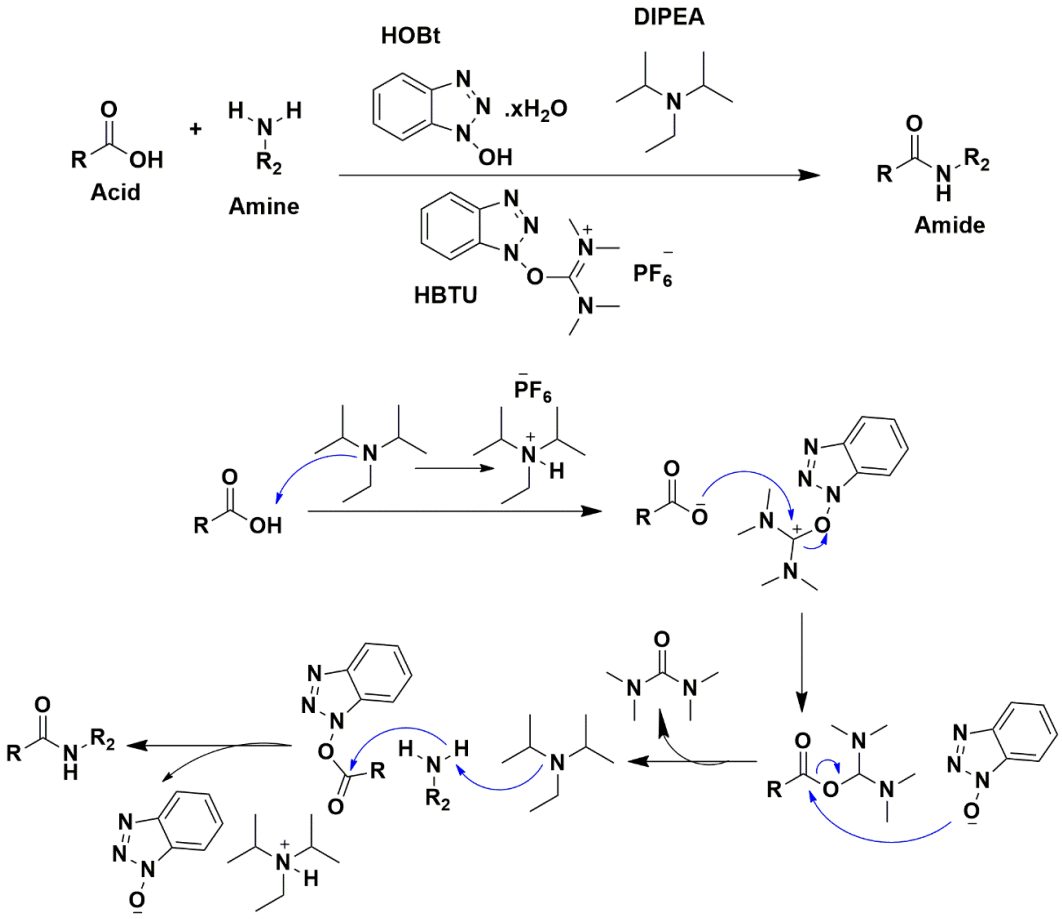

Figure 3. Mechanism of amide bond formation catalyzed by HOBt and HBTU coupling agents.

The solubility of the peptides was evaluated on the basis of DLS measurements of peptide solutions in PBS at 0.2 mgmL^{-1} concentration. This concentration was selected based on optimized working concentration of peptides for later cell culture experiments. The Table 1 summarizes the results of these studies. IKVAV formed microscopic aggregates at the tested conditions. The introduction of polar amino acid in CSIKVAV (CS-IK) and the addition of short ethylene glycol chain as in (EG_2)IKVAV (EG_2IK) improved the solubility of the peptide and decreased the size of aggregates to 1 µm and 370nm respectively. It is important to note that aggregates are still significantly larger than the expected size of a single peptide chain (<1 nm). The presence of anionic amino acids in the peptide structure, as in CEEIKVAV (CE2IK) and CEEEEIKVAV (CE4IK), favored solubility. The increase in net negative charge of the chain reduced the size of the aggregates to 260 and 120 nm respectively.

Table 1: Summarizing of different IKVAV variants

Peptide Sequence	Abbreviation	Methodology	Net Charge (pH 7.0)	DLS
IKVAV	IK-5	Non-polar amino acids	1	> 1 µm
(EG_2)-IKVAV	(EG_2)-IK	Ethylene glycol chain	1	370 nm
CSIKVAV	CSIK	Polar amino acids	0.9	1 µm
CEEIKVAV	CE2IK	Negative charged amino acid (E)	-1.1	260 nm
CEEEEIKVAV	CE4IK	Negative charged amino acid (E)	-3.1	120 nm
CSIKVAVSADR	IK-12	Charged amino acids	0.9	590 nm
CCRRIKVAVWLC	CIKC	Positively charged amino acids	2.8	> 1 µm
CSRARKQAASIKVAVSADR	IK-19	Charged amino acids	3.9	400 nm

Positively charged sequences like CCRRIKVAVWLC (CIKC) were also evaluated. However, this peptide shows micrometric sized aggregates in solution. The addition of cationic tail in IK-19 reduced the size of aggregates and enhances water solubility. This long sequence was truncated to IK-12 sequence maintaining net positive charge. IK-12 showed less aggregation than IKVAV. The different IKVAV variants helps in decreasing the size of aggregates but no single strategy was efficient in completely breaking the aggregation.

In addition to the solubility tests, the bioactivity of the peptides was evaluated in cell culture experiments. These are described in Chapter 5 Section 5.2. The neural culture experiments showed that IK-19 and IK-12 support neuronal development comparable to standard LN and LN/PDL functionalized biomaterial.

Based on the results from solubility and bioactivity (Chapter 5 Section 5.2) tests, the CASIKVAVSADR (IK-12) sequence was selected for the development of light-responsive motifs. IK-12 sequence lacks the cationic tail of IK-19. This prevents non-specific attachment of cell on the IK-12 surface due to electrostatic charge interactions between positive charge peptide and negatively charge cells. IK-12 formed aggregates of 590 nm size, larger than IK-19. However, IK-12 showed comparable bioactivity to IK-19 and LN (Chapter 5, Section 5.2). IK-12 is a shorter peptide and requires less synthetic effort. Therefore IK-12 was selected as most appropriate peptide for preparing photoactivatable laminin derivatives.

2.2.2 Selection of caging site

The selection of caging site depends on the binding domain of the selected motif recognized by integrins. While the photocage, is selected on the basis of synthetic effort and ease of introduction at active site. The caging group should encompass hydrolytic stability, water solubility and primarily it should be inert towards biological system.[16] The photochemical by products generated after uncaging should be non-reactive and non-toxic. In IKVAV the isoleucine and lysine amino acids are reported to be crucial for binding to integrins. The substitution of these residue results in loss of IKVAV activity.[17] The lysine residue is an ideal caging site, since the amine side group can be easily reacted with chromophores to render a caged lysine. Preliminary activity tests with a scrambled version of IK-12 where lysine (K) was replaced by glutamate (E) CSIEKAVASADR (IE-12) confirmed that Lys residue in IK-12 was relevant for bioactivity (Chapter 5, Section 5.3). Therefore, caged IK-12 derivatives with a photocleavable protecting group at the Lys were attempted.

Three different photoremovable protecting groups were explored to cage the amine group of the lysine amino acid: the NVOC [18], DMNPB,[5a, 7a, 19] and HANBP[20]. NVOC belongs to the *o*-nitrobenzyl family and is a well-established caging group for amines. The DMNPB is *o*-nitrophenethyl group selected on the basis of reported higher stability and photolysis efficiency. The *o*-nitrobiphenyl donor–acceptor based chromophore HANBP has shown enhanced photolysis efficiency vs the previous candidates, and imparts better water solubility.[20] This class of chromophore is reported to show appreciable two photon cross section which could be relevant for future application in 3D cultures. [21]

2.2.3 Synthesis of caged IK-12 variants

The caged derivative of lysine was synthesized by insertion of chromophores on lateral amine chain. The fmoc protected alpha amine in lysine (Fmoc-Lys-OH) facilitates selective substitution at side chain. The NVOC was easily introduced by using commercially available NVOC-chloroformate in a single step in slightly basic conditions. The crude product was purified by solvent extraction and obtained in 91% yield.

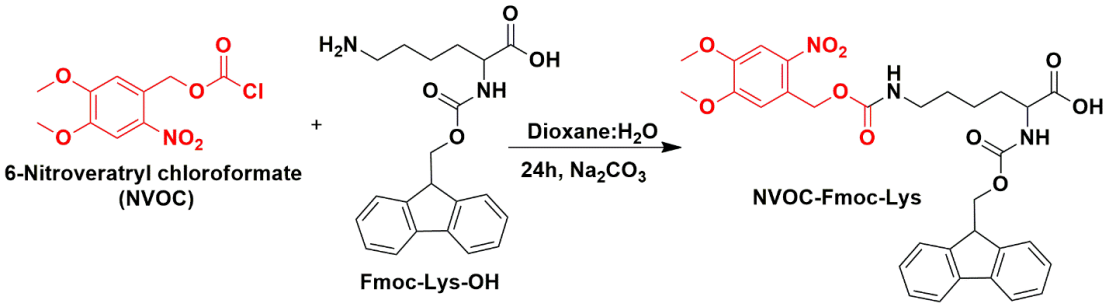

Scheme 1. Synthesis of Fmoc-Lys(NVOC)-OH from NVOC chloroformate.

The DMNPB caging group was synthesized by following a reported protocol.[7a] It involves 4 steps starting from substitution of methyl on benzylic carbon in 3,4-dimethoxy-acetophenone. The ketone is subsequently reduced to hydroxy by using sodium borohydride. The hydroxyl group in DMNPB was converted to activated chloroformate by triphosgene (**a**). The DMNPB chloroformates was introduced to Lysine yielding carbamate link (**b**). The pure product was obtained in gram scale with 87% yield (overall 42% yield) by HPLC purification.

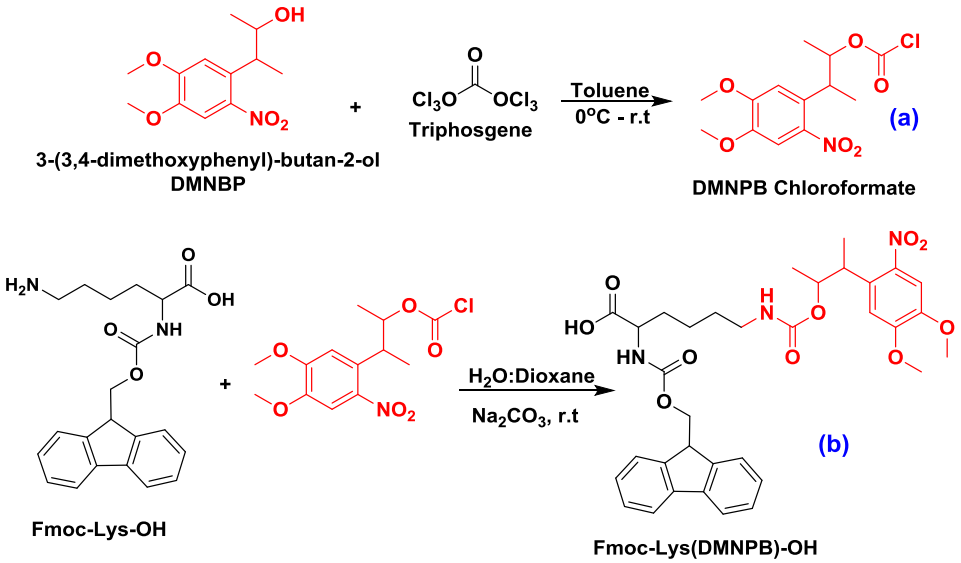

Scheme 2. Synthesis of Fmoc-Lys(DMNPB)-OH by using DMNPB chloroformate

The HANPB was synthesized by microwave assisted Suzuki coupling reaction adapted from reported pathway.[20] The acylation at *ortho* position in *p*-bromo nitro benzene yield tert-butyl 2-(5-bromo-2-nitrophenyl)acetate **(a)**. The methyl iodide was used to substitute methyl at benzylic position in **(a)** to enhance the photo-efficiency. The reduction of ^{t}Bu ester in **(b)** to hydroxy and subsequent borylation of **(c)** using pinacolatodiboron yield *o*-nitrophenethyl pinacolato borate complex **(d)**. The reduction of **(b)** was performed by DIBAL-H, as strong inorganic hydrides ($LiAlH_4$) can reduce the nitro group into amine. The phenethyl alcohol in **(d)** was converted to chloroformate by triphosgene **(e)** and substituted at lysine before Suzuki coupling to yield **(f)**. This pathway was adopted to avoid competition from N-substituted free hydroxyl groups in biphenyl unit. The iodo N-phenyldiethanolamine **(g)** was obtained in single step after iodination. The ethanol amine groups were kept as free hydroxy in contrast with original report to enhance the water solubility. The microwave assisted Suzuki coupling between iodo N-phenyldiethanolamine **(g)** and Fmoc-Lysine-borane complex **(f)** yield HANBP caged lysine. The product was purified by flash column chromatography and obtained in gram scale with 82% yield (Overall yield 43%). The products were fully characterized by ^{1}H-NMR, ^{13}C-NMR and ESI-MS (Appendix Section 8.2.3).

The ^{1}H-NMR of compound **(a)** after acylation of bromo-nitrobenzene show clear signal for ^{t}Bu ester (1.41 ppm), the methylation at benzylic carbon in **(b)** yield a doublet and quartet for methyl and benzylic carbon respectively (1.57 and 4.21 ppm). The reduction by DIBAL-H **(c)** result in disappearance of ^{t}Bu ester signal and appearance of a new multiplet of methylene carbon (3.78 ppm). The nitro-substituted pinacolato borate **(d)** shows a strong multiplet from methyl groups (1.31-134 ppm). The conversion of chloroformate intermediate was confirmed by TLC and product was used for coupling with Fmoc-Lys-OH without isolation due to expected instability of chloroformate. The Fmoc-Lysine pinacolato borate **(f)** display representative signals of Fmoc in aromatic range (7.28-7.72 ppm) as well as signals from methylene chain of lysine (1.24- 3.80 ppm). The palladium catalyzed Suzuki coupling result in disappearance of signals of pinacolato borate complex and display new aromatic signals (6.50 and 7.61 ppm) as well as methylene signals (3.80 and 4.20 ppm) in **(h)**. The ESI-MS showed $[M+Na]^{+}$ signal for final product at 777.58 Da.

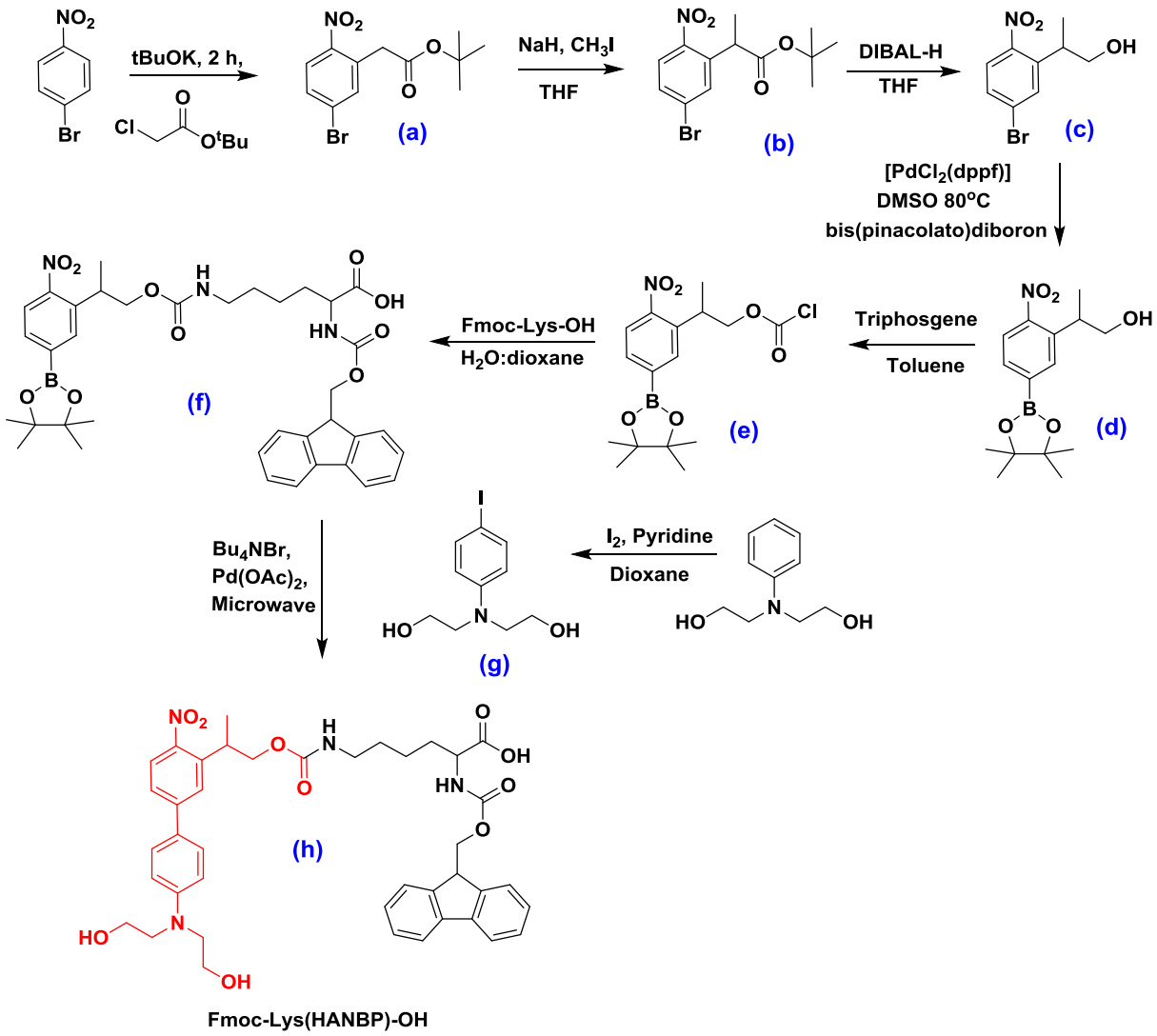

Scheme 3. Synthetic pathway for Fmoc-Lys(HANBP)-OH

The synthesized caged lysine was incorporated into the corresponding peptide sequence during solid-phase peptide synthesis (Figure 4). The peptides were started from TCP Arg(Pbf)-Fmoc resin in order to introduce the caged peptide close to the end of sequence and avoid hydrolysis of caging group with repeated deprotection and coupling cycles during SPPS. The caged IK-12 was also attempted to synthesized in two halves with 8-mer linked with resin (TCP-RDASVAVK-NH_2) and coupling with 4-mer (COOH-ISAC-NH_2) to introduce cage in the end. However, this pathway gave very low yield (18%) and 8-mer peptide was recovered as major product. The caging chromophores were stable during SPPS and no hydrolysis was observed during cleavage of peptide from the resin and deprotection of side chain protecting groups. The peptides were purified by RP-HPLC. The final products were

obtained in high purity (> 95%), good amounts (mg scale) and reasonably good yields (48-59%).The caged IK-12 variants, named IK-12(NVOC/DMNPB/HANPB) showed a reduced solubility (~ 0.75 mg/mL) *vs.* IK-12 (1 mg/mL), but were still soluble at working concentrations (0.2-0.5 mg/mL) required for hydrogel modification in the biological application.

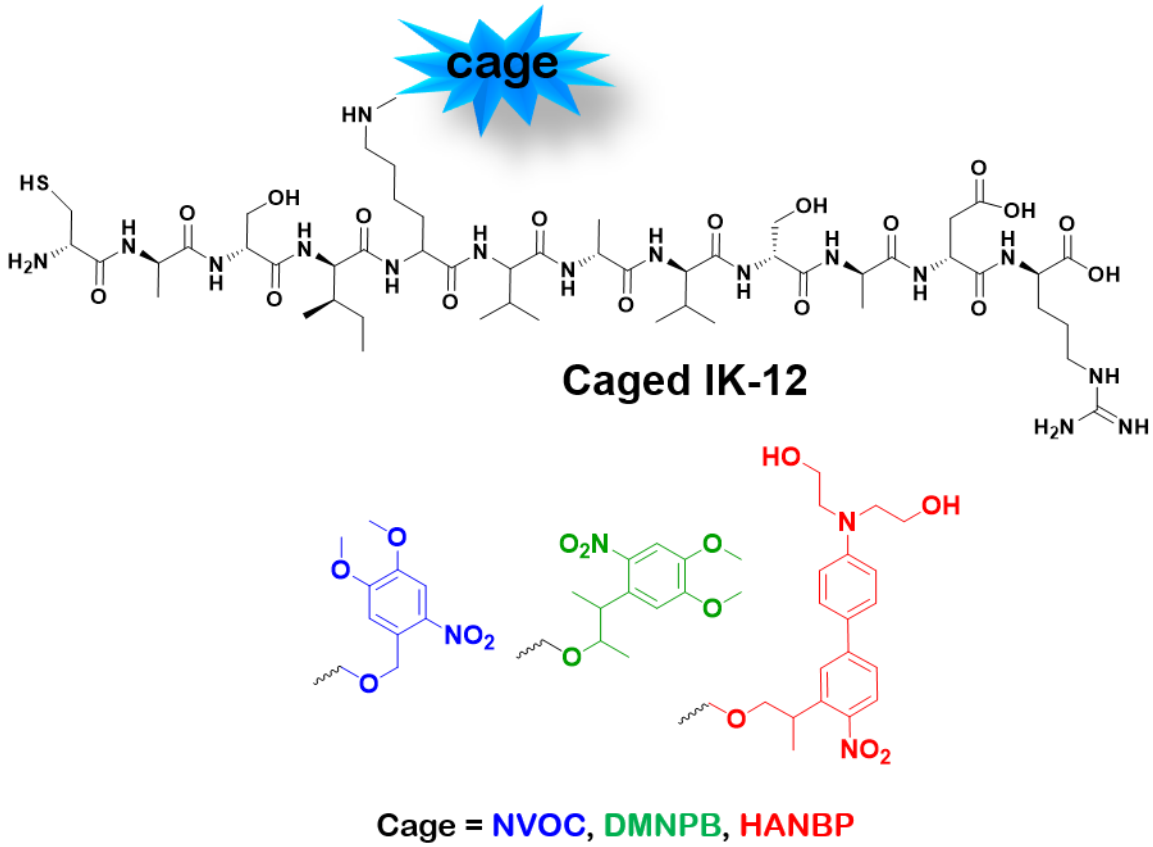

Figure 4. Chemical structure of caged IK-12(NVOC/DMNPB/HANPB) peptides.

2.3 Photochemical properties of caged IK-12 derivatives

The photosensitivity of photoactivable molecules depend on the extinction coefficient and the quantum yield of the photochemical reaction. Quantum yield (Φ) refer to number of molecule release per photon absorbed at irradiation wavelength λ. The quantum yield is typically less than 1 as not all absorb photon results in a chemical reaction.[22] Molar extinction coefficient (ε) of a molecule is its tendency to absorb light at irradiation wavelength λ per molar concentration. In a biological context, the wavelength range within which the photoreaction can take place, and the photochemical yield, are also relevant parameters. The activation wavelength above

320 nm and efficient photocleavage of caging group with subsequent release of biomolecules is desired. The UV spectrum of the photosensitive molecule provides information regarding the absorption spectrum and the extinction coefficient. Figure 5 shows the UV spectra of IK-12(NVOC/DMNPB/HANPB). The absorption maxima, λ_{max}, are located at 350, 365 and 490 nm respectively. The reported extinction coefficients (ε) in literature for NVOC: 6210 $M^{-1}cm^{-1}$ at 365 nm[23], for DMNPB: 4100 $M^{-1}cm^{-1}$ at 346 nm [5a], and for HANBP: 7500 $M^{-1}cm^{-1}$ at 397 nm.[20] The quantum yields (Φ) for the different chromophores available from literature data for NVOC: Φ = 0.0013 at 345 nm, for DMNPB 0.26 at 365 nm and for HANBP 0.15 at 397 nm.[16b, 22]

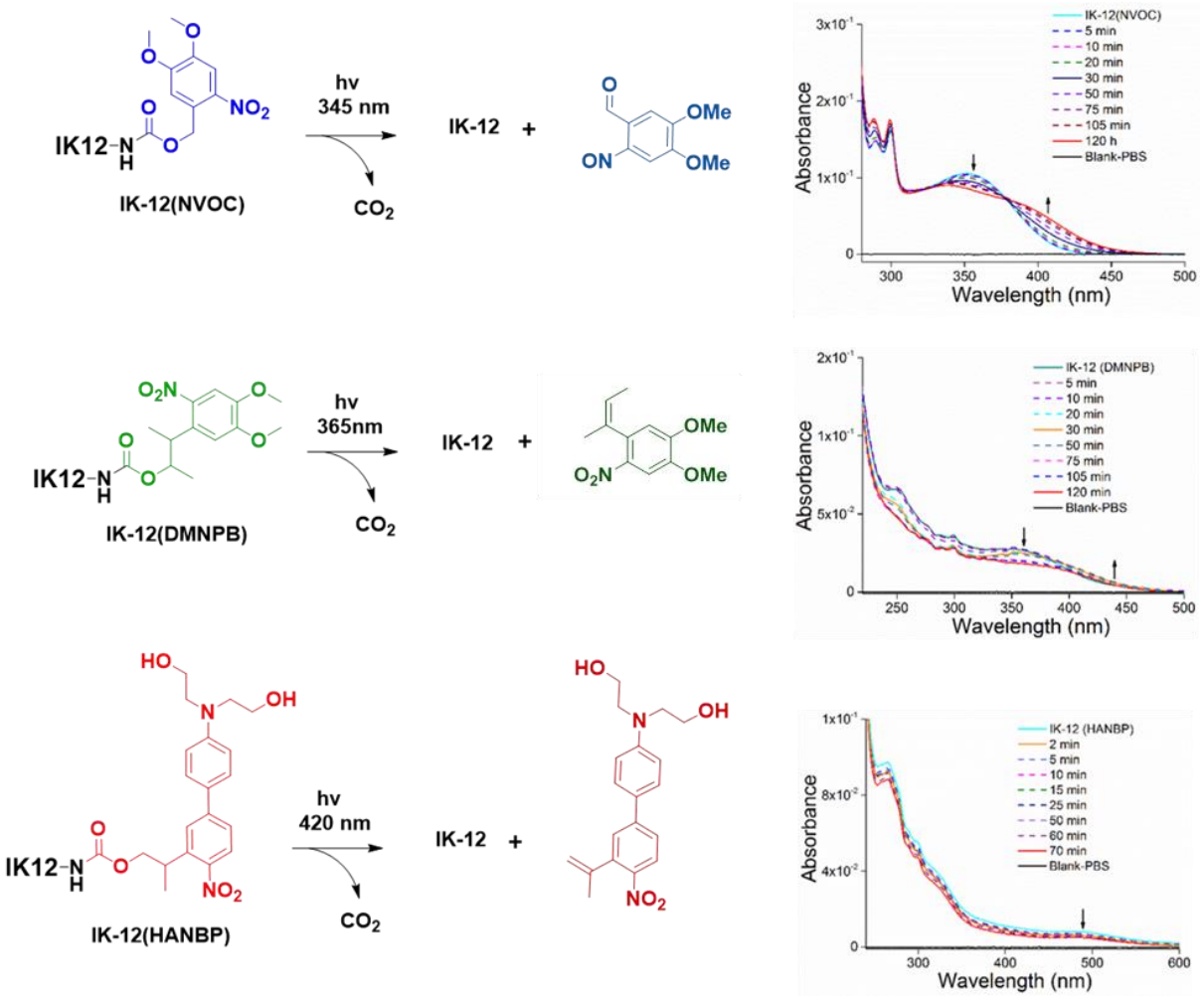

Figure 5. Photochemical reaction expected for IK-12(NVOC/DMNPB/HANPB) and corresponding photolysis UV-vis spectra measured in solution at increasing exposure times.

The photolysis of IK-12(NVOC/DMNPB/HANPB) peptides was followed by UV spectroscopy by irradiation at their λ_{max}, 345 nm for NVOC, 365 nm for DMNPB, and 420 nm for HANBP. Photoconversion values were calculated from the decrease in UV absorbance of 1mM peptide solutions in phosphate buffer (pH 7.4) at selected wavelengths with increasing irradiation times. The photochemical yield was quantified from analytical HPLC characterization of the irradiated solutions and ESI-MS measurements.

Irradiation of solutions of IK-12(NVOC/DMNPB/HANPB) leads to visible changes in their UV spectrum. In IK-12 NVOC the intensity of the absorption band at 345 nm decreases while a new maximum at 410 nm appears with increases in intensity with exposure times. The irradiated solution was subjected to analytical HPLC to quantify the photolysis products. Upon irradiation, the intensity of IK-12(NVOC) peak decreases while the signal for IK-12 appears at increasing intensity with increasing exposure time. HPLC curves before and after irradiation is included in Appendix Section 8.4.2. IK-12 DMNPB showed a drop in absorbance at 350 nm and an increase in intensity at lower wavelengths. The HPLC profile confirmed the release of IK-12 upon exposure. The UV-vis spectra of IK-12(HANBP) solution showed little changes with illumination. This is because the spectrum of the photolyzed product does not significantly changes vs IK-12(HANBP). However, the photolysis was confirmed by analytic HPLC and mass spectrometry characterization of the irradiated solutions, where the signals corresponding to free IK-12 became clearly visible with increasing exposure. The shift in λ_{max} after irradiation for IK-12(DMNPB) and IK-12(HANBP) was not very evident due to release of large IK-12 chain aggregates. The proposed photolysis reaction proceed through β-1 elimination, as previously predicted in the literature,[20] [5a] [24] since the photolyzed side product (o-nitro phenyl alkene M+1 = 356 + H^{+1}) was observed in ESI-MS results (Figure 6). The irradiation at comparable intensity yield 15, 12 and 48% of uncaged IK-12 peptide in 30 min for NVOC, DMNPB and HANPB respectively calculated from analytic HPLC profile.

In summary, all variants of IK-12(NVOC/DMNPB/HANPB) undergo photolysis at respective wavelength and release IK-12. The solubility and hydrolytic stability of NVOC/DMNPB/HANPB chromophores were comparable. The photolysis efficiency at comparative irradiation conditions can be classified as HANBP>NVOC>DMNPB.

The HANBP show the higher photolysis efficiency and most successfully release uncaged IK-12 in short time.

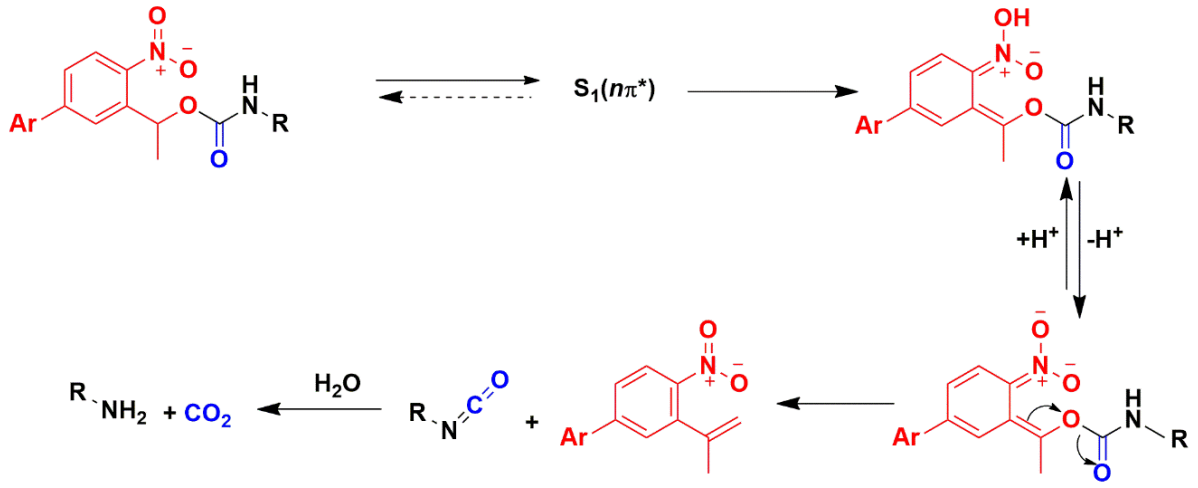

Figure 6. Proposed mechanism for photolysis of IK-12 (HANBP)

2.4 Synthesis of IK(HANBP)VAV

The experiments with caged IK-12 derivatives evident the higher photolysis efficiency and better water solubility of HANBP group than NVOC and DMNPB chromophore. Therefore, attempts to introduce HANPB in the short IK(HANBP)VAV sequence were performed. This peptide shows poor solubility and strong aggregation. Modification with HANBP was expected to enhance the solubility of the peptide and eventually prevent aggregation. It is important to note that the IKVAV is the active sequence within IK-12 peptide and a soluble, photoactivatable IKVAV would save synthetic effort vs. the IK-12 derivative.

IK(HANBP)VAV peptide was synthesized analogously to IK-12(HANBP). The IK(HANBP)VAV motif showed very good water solubility (15 mg/mL) and form no aggregates in water at 0.2 mgmL^{-1}. The polarity of the HANPB chromophore and possibly a conformational change in the peptide forced by the presence of the biphenyl core could be the reasons for preventing aggregate formation. The IK(HANBP)VAV solution showed a λ_{max} = 490 nm similar to IK-12(HANBP) and a shift in λ_{max} from 490 nm to 400 nm upon exposure at 420 nm (Figure 7).

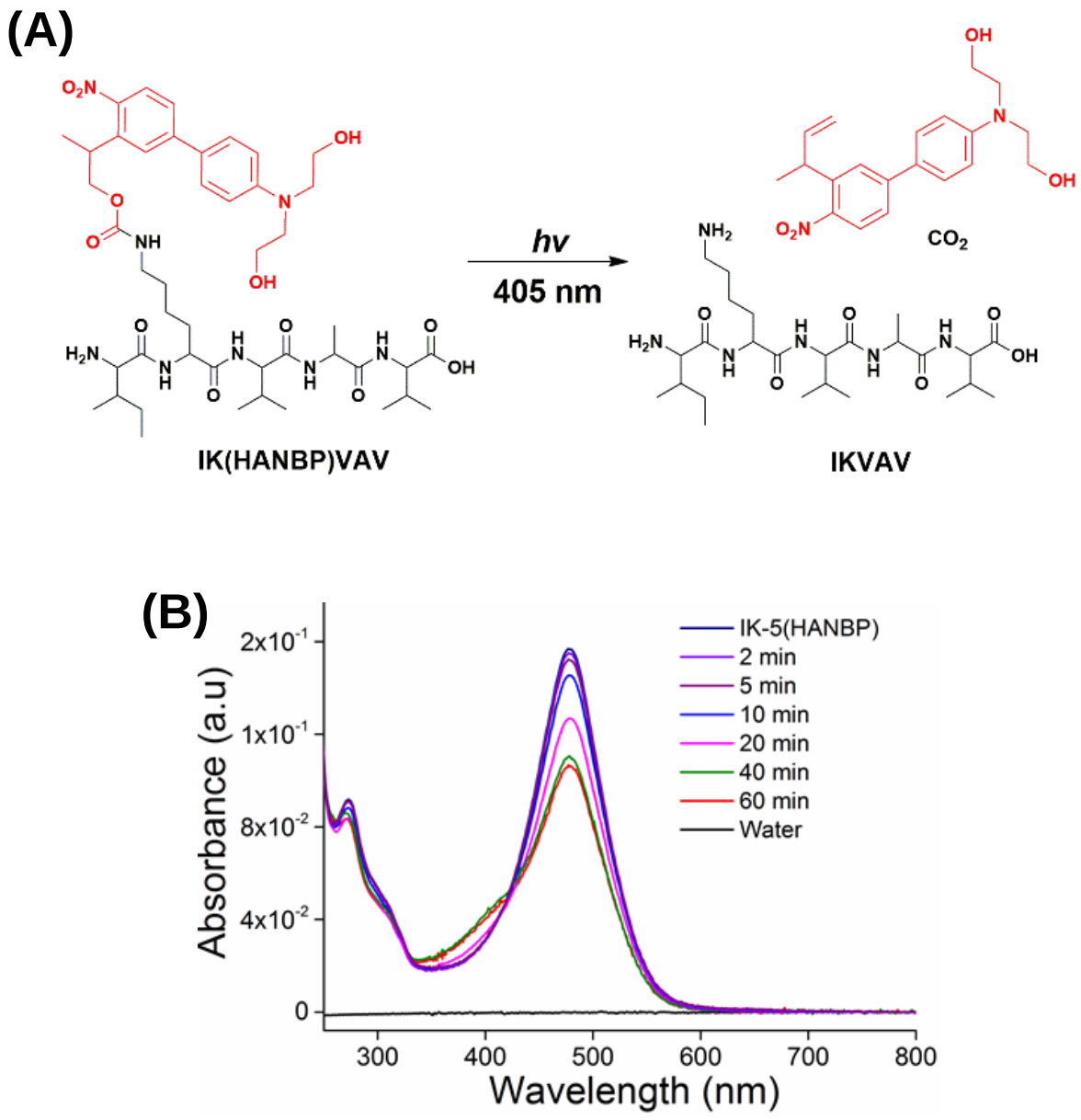

Figure 7. (A) Photolysis of IK(ANBP)VAV at 420 nm (B) UV spectra of IK(ANBP)VAV (0.9 mM in PBS, pH 7.4) irradiated at 420 nm during various time points

The HPLC analysis of the irradiated solution showed the disappearance of the IK(HANBP)VAV signal and the parallel appearance of active IKVAV (83%) in 30 mins (Figure 8). The short IK(HANBP)VAV showed highest water solubility and photochemical efficiency in comparison to all IKVAV uncaged and caged variants. This sequence is expected to trigger more specific biological response due to absence of any additional amino acid units. The photocaged IK(HANBP)VAV is a promising candidate for light guided neural growth.

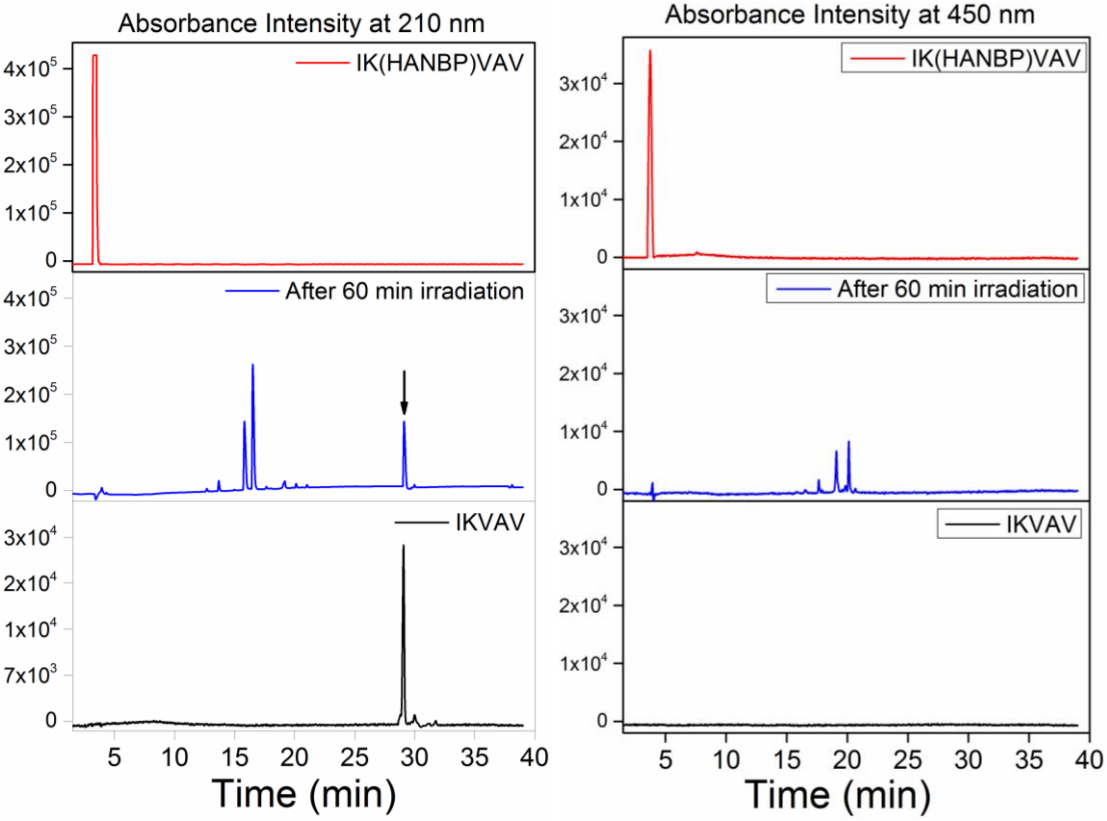

Figure 8. Analytical HPLC chromatograms of IK(ANBP)VAV (0.9 mM) solution before and after irradiation at 420 nm for 60 min. The HPLC profile is shown for 210 and 450 nm absorbance channels. For comparison HPLC profile of IKVAV at different channels is shown as well.

2.5 Photolysis studies on thin hydrogel films

IK-12(NVOC/DMNPB/HANPB) and IK(HANPB)VAV peptides will be used later to modify hydrogels and the photoactivation step will take place in the immobilized form (Chapter 5 section 5.3 - 5.5). Therefore, photolysis experiments were also performed in thin films of P(AAm-*co*-AA) hydrogels. These experiments provide information about the minimum irradiation dose required to activate the peptides to support neuronal culture. The caged IK-12 and IKVAV peptides were coupled through terminal amine to the hydrogels films supported on quartz substrates. Detailed gel preparation protocol and surface functionalization is mentioned in Chapter 4 section 4.2 and Appendix Section 8.5. The hydrogels were irradiated for increasing times, followed by a washing step with PBS to remove photolyzed by-products (Figure 9 A-C). The signal corresponding to the chromophore starts to disappear with irradiation due to release of chromophore.

The initial peptide concentration in the hydrogel was calculated from absorbance values by applying the Beer-Lambert law, $c = A/l\varepsilon$. The values for the extinction coefficients of the chromophores were (NVOC: 6210 $M^{-1}cm^{-1}$ at 365 nm[23], DMNPB: 4100 $M^{-1}cm^{-1}$ at 346 nm [5a], and HANBP: 7500 $M^{-1}cm^{-1}$ at 397 nm.[20] The optical depth in this experiment corresponds to the thickness of the hydrogel films, which was adjusted to 0.007 cm in all gels (Chapter 4 section 4.2) and measured by fluorescence microscopy (Appendix Section 8.11).[25] The obtained concentration, as calculated from UV spectra of the modified hydrogel films, was similar in all three caged variants.(IK12-NVOC: 0.39 mM, -DMNPB: 0.33 mM, -HANBP: 0.36 mM). The photolysis yield on thin film was 17%, 14% and 48% for IK12-NVOC, -DMNPB and -HANBP respectively after 15 minutes of irradiation. The photolysis yield was relatively low but 15 min pre-irradiated samples were selected for investigation of bioactivity of the caged peptide as longer irradiation time are not suitable for biological studies in the presence of cells (Chapter 5 section 5.3).

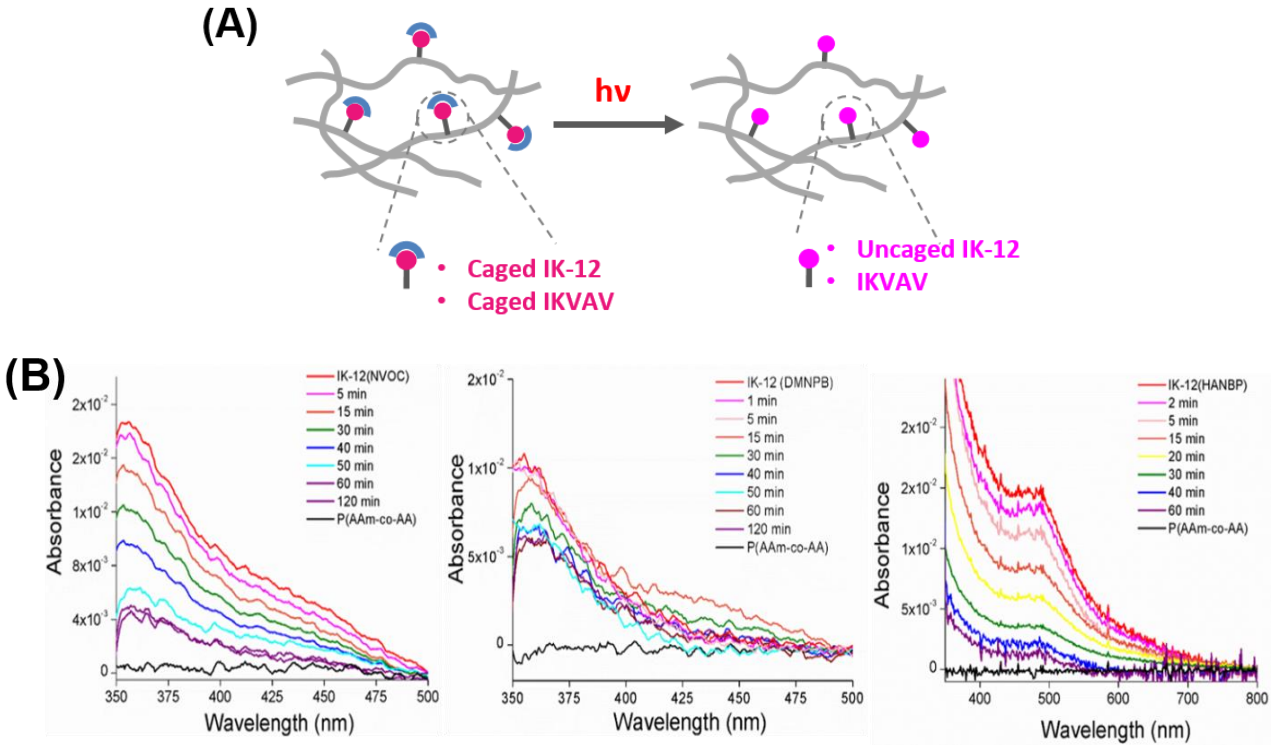

Figure 9. (A) Schematic representation of IK-12 (NVOC/DMNPB/HANPB) and IK(HANBP)VAV on hydrogel films after irradiation, (B) UV-Vis spectra of thin hydrogel films modified with caged IK-12 after light exposure for increasing times. Irradiation was performed at λ_{max}: 345 nm for NVOC, 365 nm for DMNPB, and 420 nm for HANBP.

The photolysis of IK(HANBP)VAV on thin hydrogel films was evaluated in a similar way. Irradiation was performed at 420 nm. A clear decay in UV absorbance was observed just after 2 min of irradiation (Figure 10). The IK(HANBP)VAV show enhanced photolysis yield and 86% uncaging was obtained after irradiation for 7 min. Therefore, for biological experiments with photocaged IK(HANBP)VAV 7min of irradiation dosage was selected. The IK(HANBP)VAV show higher photolysis efficiency in comparison to all other cage variants IK-12 (NVOC/DMNPB/HANPB). These results are in accordance with photolysis studies in solution.

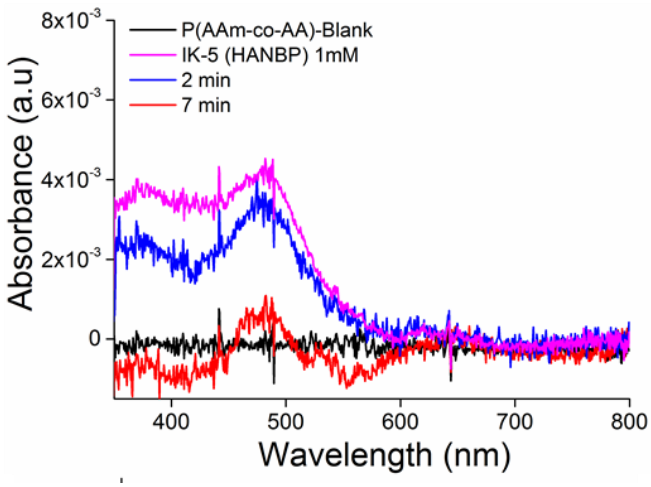

Figure 10. UV spectra of IK(ANBP)VAV functionalized P(AAm-*co*-AA) hydrogel, irradiated at 420 nm at different time-points (after washing).

2.6 Conclusions

Photo-responsive derivatives of the laminin peptidomimetic IKVAV were successfully synthesized. Different IKVAV containing peptide derivatives with either charged amino acid residue or with ethylene glycol unit were analyzed to reduce the aggregation of IKVAV in water. The positively charged IK-12 and IKVAV were selected for synthesis of photoactivatable variants. These were developed by attaching a photoremovable chromophore at the Lys residue of the sequence, which is critical for binding. The three different chromophores (NVOC, DMNPB and HANBP) attached to the lysine amino acid residue were synthesized in high purity and good yield. The lysine with NVOC, DMNPB and HANBP were introduced into positively charged IK-12 peptide sequence by SPPS. In addition, short IKVAV sequence with HANBP chromophore was synthesized by introducing cage at Lysine

amino acid. The caged peptides showed reasonable solubility in water and promising photolytic properties in solution and on hydrogel surface for application in biological experiments.

References

[1] aW. Lee, C. W. Frank, J. Park, *Advanced Materials* **2014**, *26*, 4936-4940; bW.-L. Lei, S.-G. Xing, C.-Y. Deng, X.-C. Ju, X.-Y. Jiang, Z.-G. Luo, *Cell research* **2012**, *22*, 954-972.

[2] J. E. Frith, R. J. Mills, J. E. Hudson, J. J. Cooper-White, *Stem cells and development* **2012**, *21*, 2442-2456.

[3] aM. A. Wolman, V. K. Sittaramane, J. J. Essner, H. J. Yost, A. Chandrasekhar, M. C. Halloran, *Neural development* **2008**, *3*, 6; bM. Pesaresi, R. Soon-Shiong, L. French, D. Kaplan, F. Miller, T. Paus, *Neuroimage* **2015**, *115*, 191-201.

[4] A. Domogatskaya, S. Rodin, K. Tryggvason, *Annual review of cell and developmental biology* **2012**, *28*, 523-553.

[5] aS. Petersen, J. M. Alonso, A. Specht, P. Duodu, M. Goeldner, A. del Campo, *Angew Chem Int Ed Engl* **2008**, *47*, 3192-3195; bE. J. Berns, S. Sur, L. Pan, J. E. Goldberger, S. Suresh, S. Zhang, J. A. Kessler, S. I. Stupp, *Biomaterials* **2014**, *35*, 185-195; cV. M. Tysseling-Mattiace, V. Sahni, K. L. Niece, D. Birch, C. Czeisler, M. G. Fehlings, S. I. Stupp, J. A. Kessler, *Journal of Neuroscience* **2008**, *28*, 3814-3823; dB. Mammadov, R. Mammadov, M. O. Guler, A. B. Tekinay, *Acta biomaterialia* **2012**, *8*, 2077-2086; eH. Koh, T. Yong, C. Chan, S. Ramakrishna, *Biomaterials* **2008**, *29*, 3574-3582.

[6] R. Fricke, P. D. Zentis, L. T. Rajappa, B. Hofmann, M. Banzet, A. Offenhäusser, S. H. Meffert, *Biomaterials* **2011**, *32*, 2070-2076.

[7] aM. Wirkner, S. Weis, V. San Miguel, M. Álvarez, R. A. Gropeanu, M. Salierno, A. Sartoris, R. E. Unger, C. J. Kirkpatrick, A. del Campo, *ChemBioChem* **2011**, *12*, 2623-2629; bS. Piant, F. Bolze, A. Specht, *Optical Materials Express* **2016**, *6*, 1679-1691.

[8] M. J. Salierno, A. J. García, A. Del Campo, *Advanced Functional Materials* **2013**, *23*, 5974-5980.

[9] J. C. Rose, M. Cámara-Torres, K. Rahimi, J. Köhler, M. Möller, L. De Laporte, *Nano Letters* **2017**.

[10] Y. Luo, M. S. Shoichet, *Nature materials* **2004**, *3*, 249-253.

[11] Y.-P. Lu, C.-H. Yang, J. A. Yeh, F. H. Ho, Y.-C. Ou, C. H. Chen, M.-Y. Lin, K.-S. Huang, *International journal of pharmaceutics* **2014**, *463*, 177-183.

[12] W. Zhu, F. Masood, J. O'Brien, L. G. Zhang, *Nanomedicine: Nanotechnology, Biology and Medicine* **2015**, *11*, 693-704.

[13] S. Joo, J. Y. Kim, E. Lee, N. Hong, W. Sun, Y. Nam, *Scientific reports* **2015**, *5*, 13043.

[14] aB. Zhu, S.-C. Luo, H. Zhao, H.-A. Lin, J. Sekine, A. Nakao, C. Chen, Y. Yamashita, H.-h. Yu, *Nature communications* **2014**, *5*; bM. Durbeej, *Cell and tissue research* **2010**, *339*, 259.

[15] aK.-i. Tashiro, G. C. Sephel, B. Weeks, M. Sasaki, G. R. Martin, H. K. Kleinman, Y. Yamada, *Journal of Biological Chemistry* **1989**, *264*, 16174-16182; bM. Aumailley, V. Nurcombe, D. Edgar, M. Paulsson, R. Timpl, *Journal of Biological Chemistry* **1987**, *262*, 11532-11538.

[16] aS. Petersen, J. M. Alonso, A. Specht, P. Duodu, M. Goeldner, A. del Campo, *Angewandte Chemie International Edition* **2008**, *47*, 3192-3195; bA. Specht, F. Bolze, L. Donato, C. Herbivo, S. Charon, D. Warther, S. Gug, J.-F. Nicoud, M. Goeldner, *Photochemical & Photobiological Sciences* **2012**, *11*, 578-586.

[17] M. Yamada, Y. Kadoya, S. Kasai, K. Kato, M. Mochizuki, N. Nishi, N. Watanabe, H. K. Kleinman, Y. Yamada, M. Nomizu, *FEBS letters* **2002**, *530*, 48-52.

[18] V. San Miguel, C. G. Bochet, A. del Campo, *Journal of the American Chemical Society* **2011**, *133*, 5380-5388.

[19] T. T. Lee, J. R. García, J. I. Paez, A. Singh, E. A. Phelps, S. Weis, Z. Shafiq, A. Shekaran, A. del Campo, A. J. García, *Nature Materials* **2015**, *14*, 352-360.

[20] L. Donato, A. Mourot, C. M. Davenport, C. Herbivo, D. Warther, J. Léonard, F. Bolze, J. F. Nicoud, R. H. Kramer, M. Goeldner, *Angewandte Chemie International Edition* **2012**, *51*, 1840-1843.

[21] L. García-Fernández, C. Herbivo, V. S. M. Arranz, D. Warther, L. Donato, A. Specht, A. del Campo, *Advanced Materials* **2014**, *26*, 5012-5017.

[22] P. Klán, T. Šolomek, C. G. Bochet, A. l. Blanc, R. Givens, M. Rubina, V. Popik, A. Kostikov, J. Wirz, *Chemical Reviews* **2013**, *113*, 119.

[23] F. Buhr, J. Kohl-Landgraf, C. Hanus, D. Chatterjee, A. Hegelein, E. M. Schuman, J. Wachtveitl, H. Schwalbe, *Angewandte Chemie International Edition* **2015**, *54*, 3717-3721.

[24] S. Walbert, W. Pfleiderer, U. Steiner, *Helvetica Chimica Acta* **2001**, *84*, 1601-1611.

[25] A. Farrukh, J. I. Paez, M. Salierno, A. del Campo, *Angewandte Chemie* **2016**, *128*, 2132–2136.

Chapter 3

New Routes for Biofunctionalization of P(AAm) Gels with Cell Adhesive Ligands[1]

3.1 Introduction

Polyacrylamide P(AAm) hydrogels are standard materials for cell culture to study cell response to the biochemical and mechanical properties of the their microenvironment.[1] These gels are cytocompatible and transparent under microscope. They can be prepared in a range of stiffness varying between 0.1 and 100kPa from simple starting chemicals.[2] Proteins do not absorb onto P(AAm) gels and, therefore, these gels can be used as model surfaces to study the interaction of cells with specifically immobilized ligands. The low reactivity of the pendant amide group, however, make effective ligand coupling to P(AAm) gels difficult.

Generally, P(AAm) gels are functionalized using the photoreactive sulfoSANPAH bifunctional linker (Figure 1a). The aryl azide group on one end of sulfo-SANPAH generates a reactive intermediate upon activation with light. The generated free radicals react with P(AAm) backbone through non-specific chemical reactions. The -NHS group on other terminal of sulfo-SANPAH reacts with amine groups in biomolecules. The free radicals on sulfo-SANPAH can also react with the ligand in a non-specific manner, making it difficult to control the surface density and activity of the immobilized ligands. Other methods for surface coupling to P(AAm) gels involve the use of gamma or UV rays, or toxic chemicals such as hydrazine hydrates, periodate and glutaraldehyde.[3] The hydrazine (Figure 1b) reacts with P(AAm) by substitution of amine to hydrazine and forms hydrazone with biomolecules. The unreactive biomolecules are oxidized with periodate into aldehyde, which later forms hydrazone with activated P(AAm)/Hydrazine hydrate.

[1]The content of this chapter was published in Angewandte Chemie International Edition (2016), Volume 128 (6), page 2132–2136, A. Farrukh, J. I. Paez, M. Salierno, A. del Campo, “Bioconjugating Thiols to Poly(acrylamide) Gels for Cell Culture Using Methylsulfonyl Co-monomers”

These bioconjugation strategies for P(AAm) gels have low reproducibility and poor standardization of surface functionalization protocols among different cell biology labs.

Copolymerization of a co-monomer containing reactive side groups in small ratio is another option for functionalization of P(AAm) (Figure 1d). AAm have been reported to be co-polymerized with acrylic acid, *N*-(3-aminopropyl)-methacrylamide or N-hydroxethyl acrylamide for surface functionalization without affecting properties of P(AAm).[4]

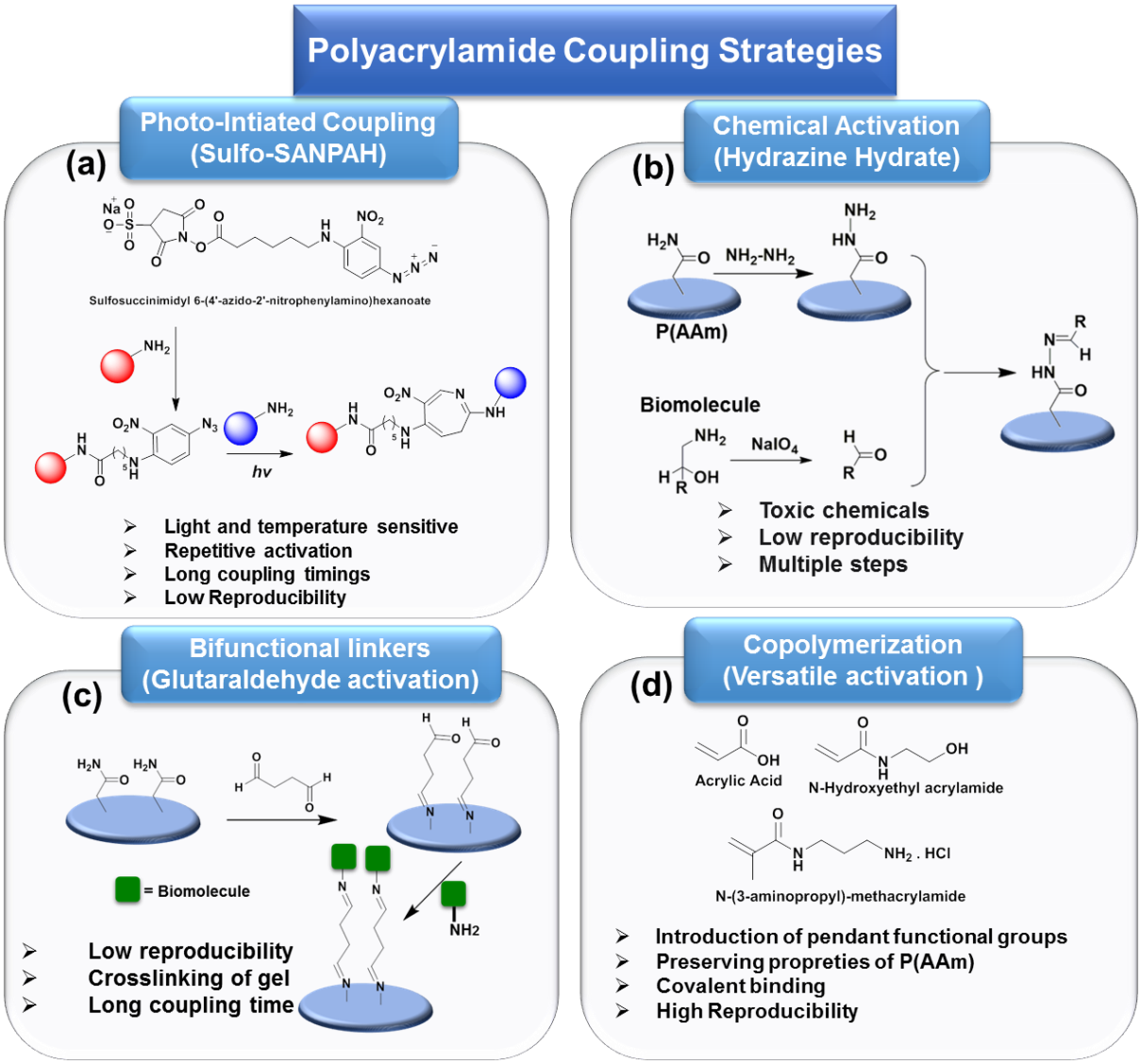

Figure 1. Polyacrylamide surface functionalization strategy

Thiol moieties are widely used as functional groups in biological experiments for conjugation of small molecules to surfaces. No straightforward strategies are currently available for thiol functionalization on P(AAm) surface. The most common routes for coupling thiol modified molecules to surfaces involve thiol-maleimide, thiol-vinyl sulfone, thiol-ene, or thiol-yne reactions.[5] However, maleimide and –ene/yne functional groups are not compatible with the free radical polymerization of P(AAm) and, therefore, they cannot be introduced in the polymer composition.

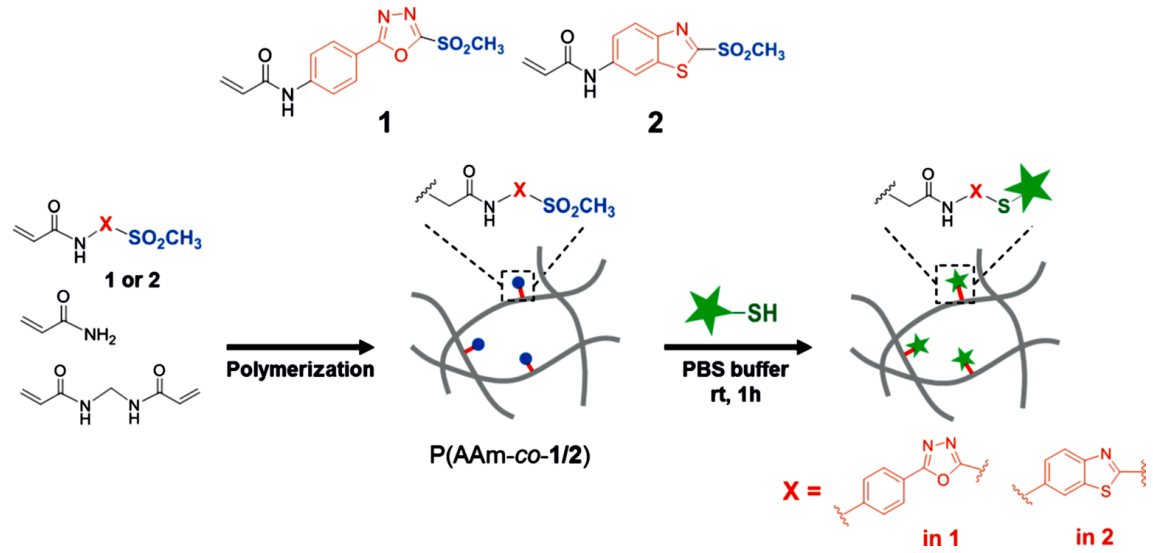

Figure 2. Schematic representation of copolymerization of P(AAm-co-**1** or **2**) by free radical polymerization and subsequent use for thiol- bioconjugation.

Heteroaromatic methylsulfone (MS) derivatives have been reported to undergo chemo-selective labeling of thiols in native proteins to inhibit disulfide pair formation under physiological conditions.[6] These reagents react with thiols by nucleophilic substitution of methylsulfone moieties forming a stable adduct. The substitution reaction is very fast (5-60 min) with high yields (45-99%) and takes place at physiological conditions (PBS, r.t). The structure of methylsulfone derivatives are not expected to interfere with free radical polymerization. Therefore, incorporation of these heteroaromatic methylsulfone in P(AAm) network could be a promising strategy for thiol bio-conjugation. In this chapter, a methylsulfone functionalized P(AAm-MS) gels for specific coupling of thiol containing bioactive ligands to P(AAm) gels under mild conditions is presented. This bioconjugation strategy involves insertion of the thiol reactive co-monomer in P(AAm) gel during polymerization reaction (Figure 2). Phenyl oxadiazole methylsulfone and benzothiazol methylsulfone

were selected as thiol-reactive groups on the basis of their fast kinetics (5-30 mins), excellent reaction yield (>87 %) and inertness towards free radical reaction.[7] This chapter entails selection, synthesis and co-polymerization of methysulfone acrylates with P(AAm) hydrogels for cell culture.

3.2 Synthesis of methylsulfone acrylamide

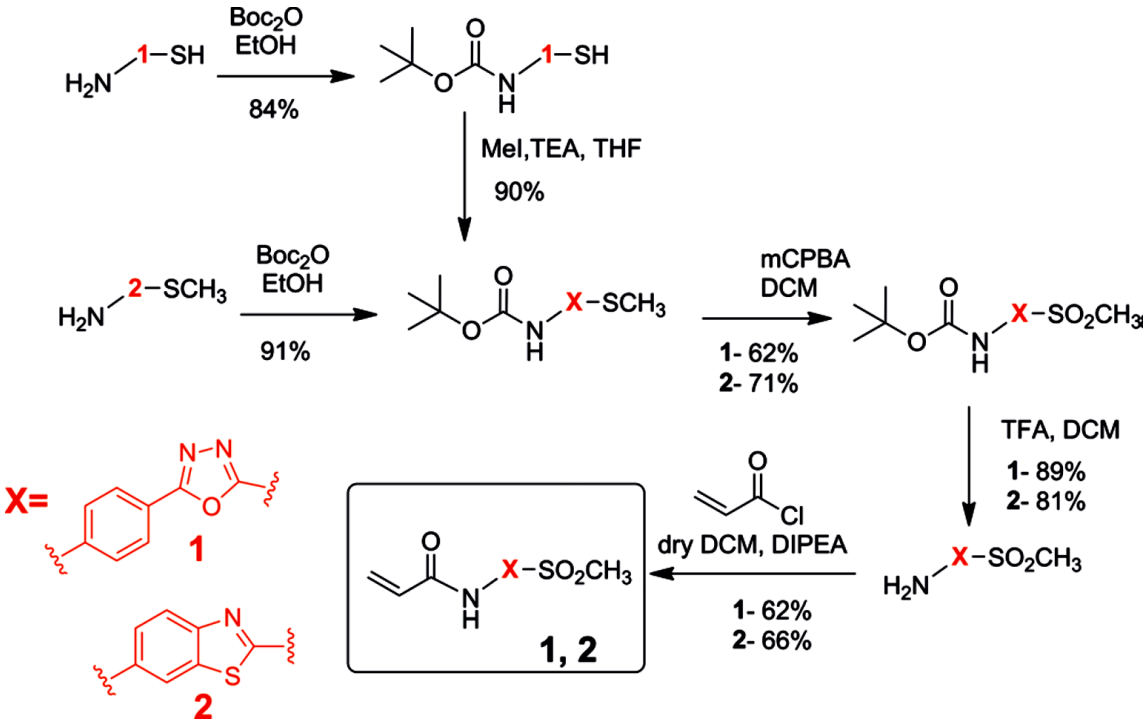

Scheme 1. Synthetic pathway for the methylsulfone acrylates **1** and **2**.

Phenyl oxadiazole methylsulfone and benzothiazol methylsulfone were selected to prepare thiol-reactive acrylates.[7] The monomers were prepared by following literature reports for different steps. The phenyl oxadiazole (**1**) and benzothiazole (**2**) acrylates were prepared from easily available starting materials 5-(4-aminophenyl)1,3,4-oxadiazole-2-thio and 2-(methylthio)benzo[*d*]thiazol-6-amine respectively (Scheme1). The heteroaromatic amine in thiol derivatives of phenyl oxadiazole and benzothiazole were Boc- protected to avoid N-methylation or oxidation of amine with mCPBA.[8] The heteroaromatic thiols were S-methylated (-SMe) and subsequently oxidized to the corresponding sulfone derivative by mCPBA.[9] The introduction of acrylate functionality was achieved by Boc-deprotection of heteroaromatic amine and further reaction with acryloyl chloride.[10] The details of synthesis and characterization data are described in Appendix Section

8.6. The final acrylates were obtained in gram scale with good yields (62-66%). The NMR spectra of final product proved the identity and high purity of the purified products. The singlet in ^{1}H-NMR at 3.43 and 3.47 ppm is distinctive for methyl moiety in acrylates **1** and **2,** respectively, confirming methylsulfone functionality. The doublets signals at 5.74-6.34 ppm correspond to vinyl groups in final product. The compounds **1** and **2** showed 2 mgmL^{-1} solubility in water and remained stable during 6 months as solids or in DMF solution kept in the fridge. The UV spectra of compounds **1** and **2** in water solution at various concentrations are shown in Figure 3.

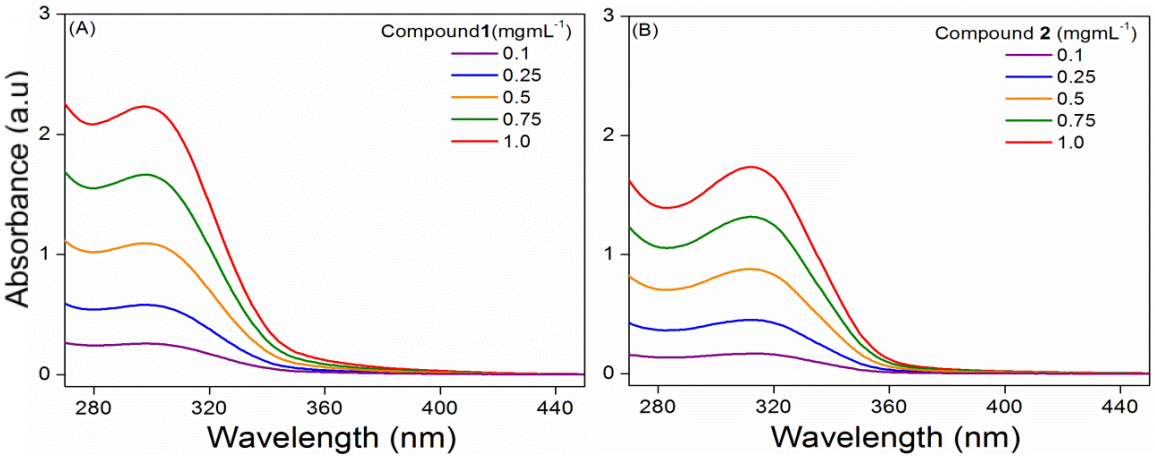

Figure 3. UV-Vis spectra of compounds **1** and **2** with varying concentration (mg mL^{-1}) in water.

The compounds **1** and **2** show absorption bands with λ_{max} at 300 and 313 nm, respectively. The extinction coefficient was calculated from the absorption spectra of solutions at increasing concentrations. The following relationship from Lambert-Beer law was used to calculate extinction coefficient:

$$\varepsilon = \frac{A}{cl}$$

Where **A** is absorption at λ_{max}, ***c*** is molar concentration of solution and **l** is path length in cm. The obtained values of the extinction coefficient for compound **1** and **2** at 21 °C were 512 and 493 M^{-1}cm^{-1}, respectively.

3.3 Synthesis and physicochemical properties of P(AAm-MS) hydrogels

The methylsulfone derivatives **1** and **2** were first tested for their ability to copolymerize with P(AAm). 2 mol% of monomer **1** dissolved in DMF was copolymerized with 98 mol% AAm in PBS using APS as initiator and TEMED as catalyst to obtain linear copolymer. After 15 min of polymerization, the reaction was stopped by opening the polymerization vials to air. The obtained polymers, control P(AAm) and P(AAm-*co*-**1**) were dissolved in D_2O, and analyzed by ^1H NMR following the signals corresponding to unreacted monomer, in particular the signal of the alkene group (5.6-6.2 ppm). After 15 min of polymerization, AAm was almost completely consumed in the P(AAm) homopolymer and P(AAm-co-**1**), as denoted by decrease in intensity of signals corresponding to the alkene protons (Figure 4B-C). Moreover, new broad signals corresponding to CH and CH_2 groups (1.5-2.3 ppm,) and amide $–NH_2$ (6.8-7.7 ppm) from the formed polymer backbone were observed. The percentage of conversion of monomer into polymer was calculated from the decrease in intensity of the alkene signals (5.60-5.84 ppm). Dimethylsulfone (singlet at 3 ppm) was used as internal standard to eliminate dilution errors. The conversion percentage was calculated from following expression.

$$\textbf{Conversion}\ (\%) = \mathbf{100} - \left(\frac{\boldsymbol{I_t\ x\ 100}}{\boldsymbol{I_0}}\right)$$

Where I_t corresponds to the integral of alkene protons at time *t* and I_0 corresponds to the integral of alkene protons at time t=0 (before addition of the initiator). The obtained conversion (%) after 1h for the homopolymer P(AAm) was 99.4%, while for the copolymer P(AAm-*co*-**1**) was found to be 97.2%. The slight drop in polymerization yield was attributed to the presence of monomer **1**.

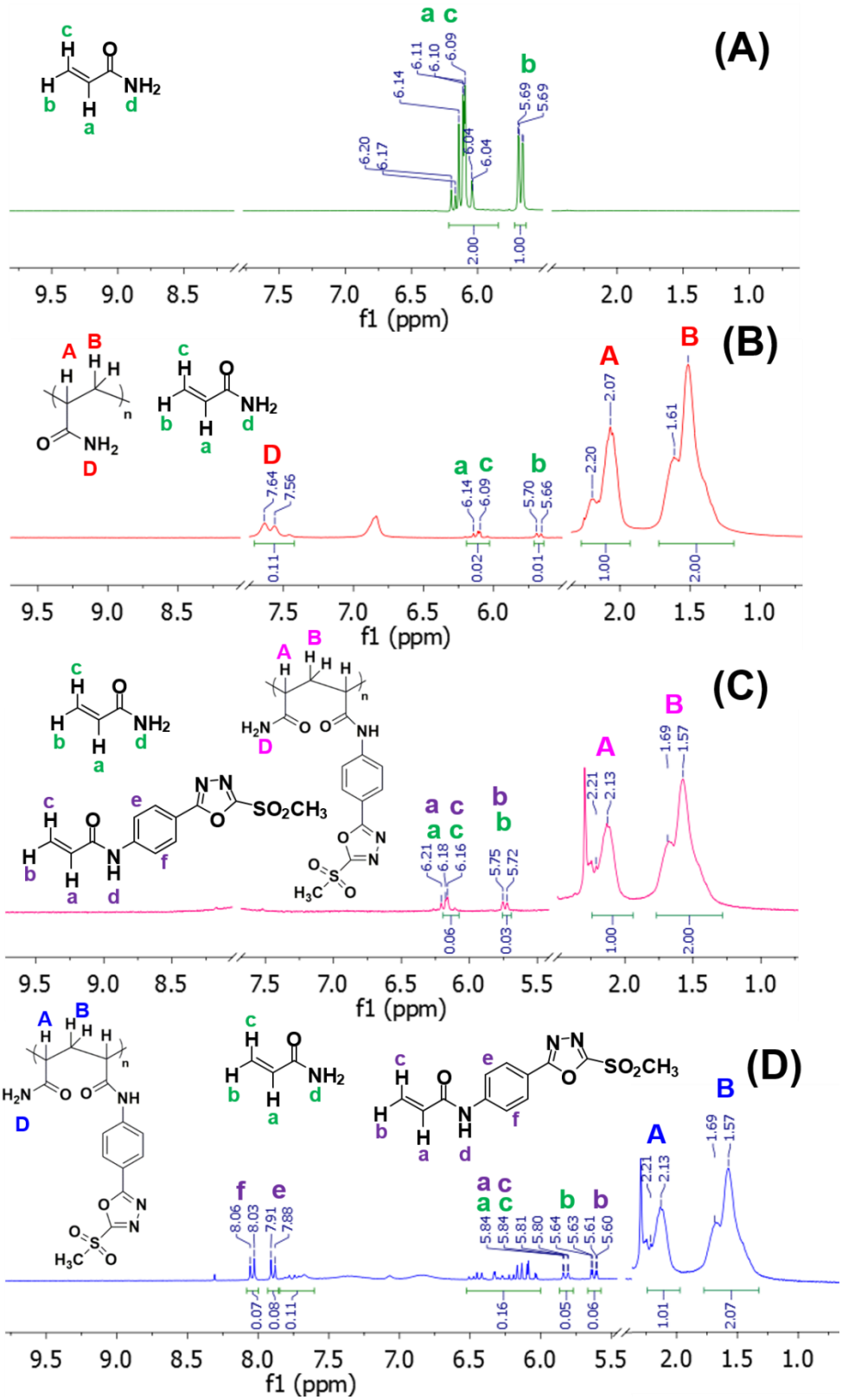

Figure 4. ^{1}H NMR (D_2O, 300 MHz) of (A) AAm without initiator, (B) linear P(AAm) and (C) linear P(AAm-*co*-**1**) (98:2 mol%), (D) linear P(AAm-*co*-**1**) (50:50 mol%). Samples B-D were measured after 15 min of polymerization.

The signals for monomer **1** were not visible from NMR due to very low initial concentration of acrylate (1.67 mol%). Therefore, the NMR of linear polymer was also performed at initial 50:50 mol% ratio for AAm:**1**. The copolymerization with higher ratio of monomer **1** provided a similar outcome (Figure 4D). New broad signals from polymer backbone (1.5-2.3) appeared and weak signals from unreacted AAm were visible. Weak signals from remaining acrylate **1** were observed as well for aromatic (8.0 and 7.9 ppm) and alkene protons (6.0-6.5 and 5.8 ppm). The ratio of unreacted monomers, AAm:monomer **1** (0.05:0.06), was the same as in the feeding ratio, indicating that both monomers were statistically incorporated into the copolymer chain.

The linear copolymers obtained by polymerizing 2mol% of **1** or **2** with 98 mol% of AAm, were subjected to GPC analysis to follow the effect of MS comonomer on the molecular weight of the final polymers and the molecular weight distribution. The copolymers showed molecular weights slightly lower and polydispersity indexes slightly higher than the control homopolymer P(AAm) polymerized under identical conditions. These results are in accordance with NMR data and confirm the compatibility of the monomers with the free radical polymerization and their suitability to obtain copolymers of P(AAm) with reactive side groups (Figure 5).

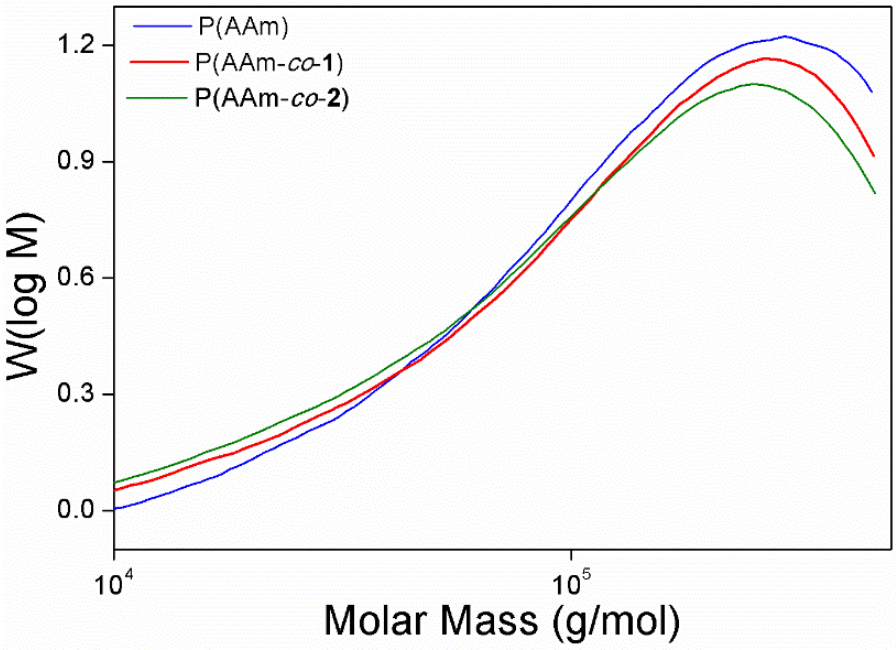

Figure 5: GPC plot showing molecular mass distribution of linear analogs.

The methylsulfone acrylates **1** or **2** (<2 mol%) were then incorporated into P(AAm) networks to form reactive hydrogels. **1** and **2** were copolymerized with AAm and N,N-methylene-bis-acrylamide as crosslinker. The polymerization was initiated by APS and catalyzed by TEMED under oxygen free conditions at room temperature. Thin films of polymeric networks were obtained by polymerizing the mixture between APTS and Sigmacote® functionalized glass surfaces. The glasses were coated with commercially available Sigmacote® solution to make the glass hydrophobic in order to prevent binding of hydrogel. The glasses were silanized by APTS solution to introduce acrylate functionality for covalent binding of hydrogel to the surface (Scheme 2).

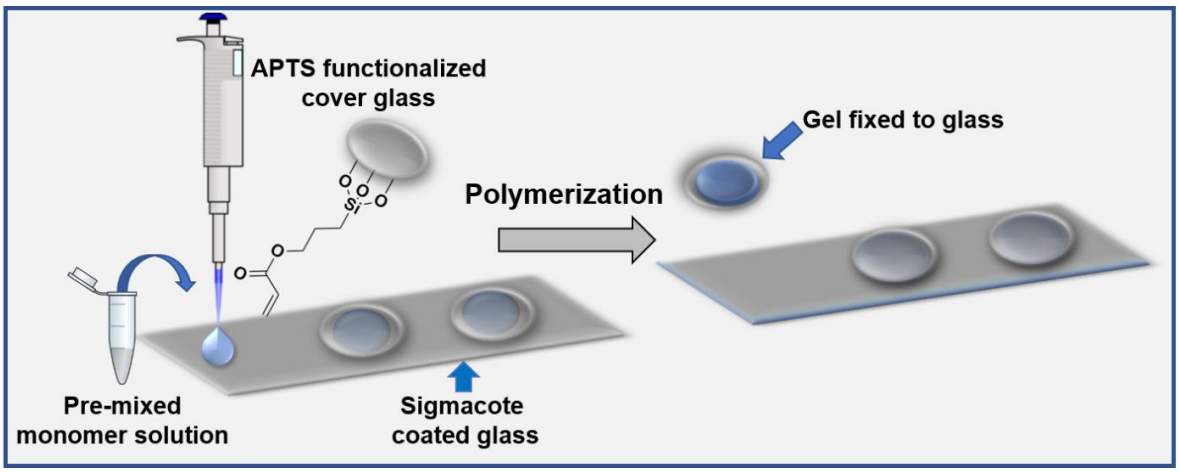

Scheme 2. Preparation steps for thin films of hydrogel on glass. A drop of the polymerization solution is placed on hydrophobic Sigmacote slides (rectangular) and covered by APTS-coated cover slips (circular). The thin film hydrogel forms between both glasses and covalently attaches to the APTS modified cover slip.

Once the gels were synthesized and washed three times with water, the incorporation of the monomers to the network was tested by measuring the UV spectrum of the gels mounted on the glass surface. The UV spectra of monomers **1** and **2** thin films are shown in Figure 6. The absorption band with λ_{max} at 301 and 313 nm was consistent with the spectra of the monomers in solutions. This result confirms successful incorporation of the monomers to the polyacrylamide network.

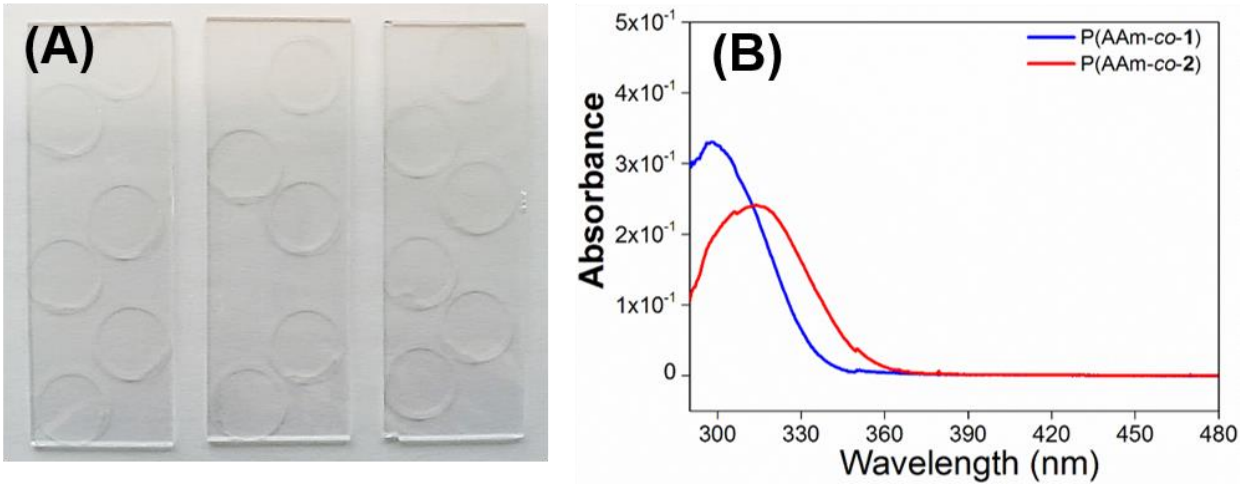

Figure 6. Picture displaying (A) hydrogels on glass slides (B) UV/Vis spectra of obtained thin films displaying absorbance of monomer **1** and **2**.

In order to characterize the physico-chemical properties of the copolymer networks P(AAm-*co*-**X**, X= **1** or **2**), the swelling degree, porosity and stiffness of hydrogels were measured and compared with those of P(AAm). The stiffness of hydrogel films was measured by dynamic mechanical analysis in a plate-plate rheometer. The elastic modulus was calculated from the measured storage modulus (G´) by using Poisson values of 0.5 typical for hydrogels.[11] The stiffness of copolymer P(AAm-*co*-**X**) was slightly less than homopolymer P(AAm), but still within acceptable range. The decrease in polymerization can be attributed to different polymerization kinetics of both monomers, presence of DMF in polymerization mixture and difference in solubility of monomers in DMF/PBS solvent.

The swelling of hydrogel depends on the cross-linking degree of the network, porosity and the hydrophilicity. The swelling of the hydrogels was determined by comparing the amount of water uptake by hydrogel in bulk polymer samples. The swelling ratio slightly increased (<20%) by addition of comonomer due to decrease in crosslinking in the polymeric network in P(AAm-*co*-**X**). This slight increase in swelling was due to the addition of monomer **1** or **2**, as anticipated from NMR and GPC results but no significant change was observed (Table 1).

Table 1. Physical properties of P(AAm) and P(AAm-co-X) hydrogels.

Polymer	Mw g/mol	Mn g/mol	Polydispersity (PD)	Swelling Ratio [mg water/mg gel]	Elastic Modulus (kPa)
P(AAm)	173296	75194	2.30	13.8	11.6
P(AAm-*co*-**1**)	166470	69852	2.38	16.6	9.9
P(AAm-*co*-**2**)	160763	65073	2.47	17.4	9.7

The surface topography of P(AAm) was imaged by SEM and compared with copolymers P(AAm-*co*-**X**). Hydrogels were prepared and examined in bulk and as thin films. The hydrogels were cryo dried and coated with Au for imaging. The hydrogel appears to form fibrous network in bulk state with varied pore size in the nm range (~50-200nm), in accordance with reported literature (Figure 7a).[12] The topography on thin films was significantly different. Higher pore sizes in the µm range (10-30µm) were observed, possibly due to stretching of the network during freeze drying (Figure 7b).[12a] The stretching of polymeric network during freeze drying of swollen hydrogel was anticipated with observed difference in swollen thickness from 70µm measured by FSC to 134 µm determined by SEM. The topography of soft hydrogel networks depends on sample preparation protocol and measurement technique. These results do not allow to decide about real topography of the swollen gel. It is, however, important to point out, that no significant differences in topography were observed between P(AAm) and P(AAm-*co*-**X**), indicating that the copolymerization reaction does not influence hydrogel morphology.

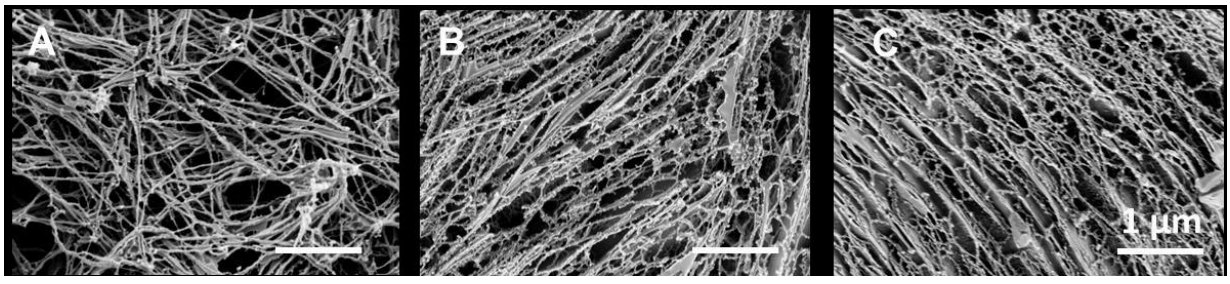

Figure 7a. SEM images of fracture site of freeze dried (A) P(AAm), (B) P(AAm-*co*-**1**) and (C) P(AAm-*co*-**2**) hydrogels prepared in an Eppendorf tube.

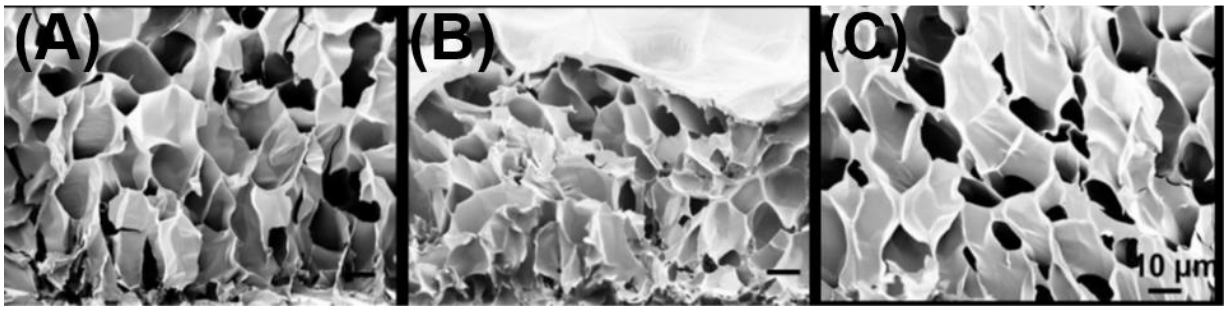

Figure 7b. SEM images of freeze dried (a) P(AAm), (b) P(AAm-*co*-**1**), and (c) P(AAm-*co*- **2**) hydrogel films on glass substrates. The images show the fracture site.

3.4 Surface functionalization of copolymer P(AAm-X)

The reactivity of P(AAm-co-**X**) with thiol-containing molecules was tested using a cysteine containing peptide with a chromophore to be followed by UV spectroscopy. The RGD(DMNPB)fC peptide, previously synthesized in the group, was used for this purpose.[13] The gels were incubated with increasing concentration of RGD(DMNPB)fC in PBS (pH 7.4) for 1h at room temperature followed by washing with water. The appearance of an absorption band at λ_{max} = 350 nm was visible in both copolymer networks, confirming successful coupling (Figure 8A-B). The band showed increasing intensity with increasing incubation concentration of the chromophore. The peptide coupling density was calculated from the absorbance value and the experimentally obtained extinction coefficients using the Beer-Lambert law at λ_{max}. The optical pathway was the thickness of the hydrogel as measured by fluorescence confocal microscopy (Appendix Section 8.11). The efficiency of the coupling reaction was then calculated as described in Appendix Section 8.5.3. A coupling yield of >90% was obtained for both monomers. This yield was similar to reported yields in solution.[7] This indicates that the network structure did not seem to affect the binding efficiency of methyl sulfone moieties with thiol molecules. The chemical reaction was completed in 1h and no further increase was observed in chemical yield with longer reaction times (Figure 8C-D). The highest coupling efficiency was observed at pH ≈ 7.4 in accordance with reported conditions, and chemical yields were reduced at lower pH (Figure 8E). The drop in reaction efficiency was due to protonation of thiolate moiety at acidic pH, which reduces its nucleophilicity.

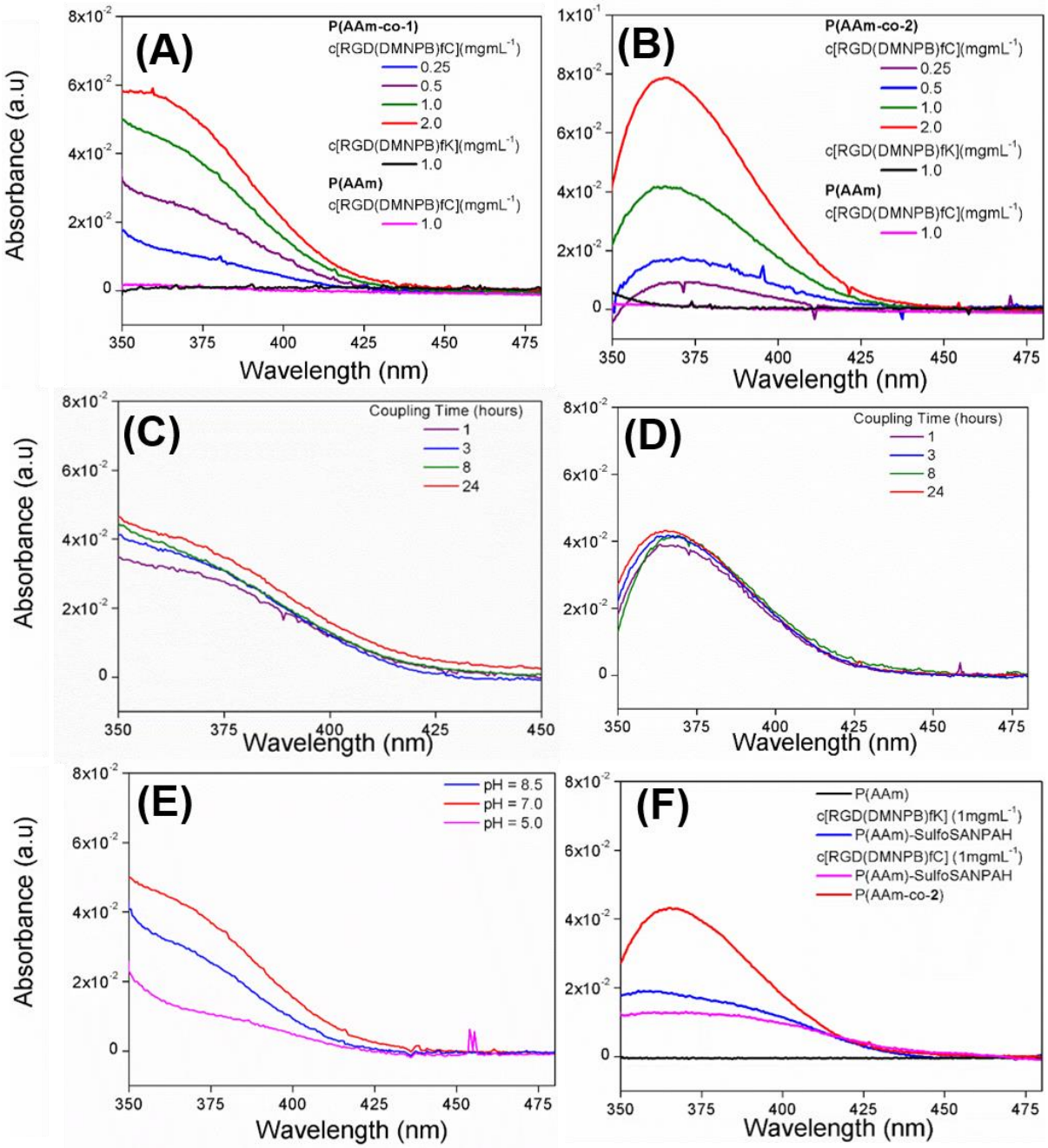

Figure 8. UV/Vis spectra of thin films hydrogel, (A-B) incubation with increasing concentrations of c[RGD(DMNPB)fC] for 1 h, (C-D) increasing reaction times with c[RGD(DMNPB)fC] (1 mg mL^{-1}), (E) pH dependent coupling of RGD(DMNPB)fC (1 mg mL^{-1} in water) to P(AAm-*co*-**1**) gel. The pH of the peptide solution was adjusted by adding 0.1 M $NaHCO_3$ or CH_3COOH solutions, (F) P(AAm)/sulfo-SANPAH and P(AAm-*co*-**2**) gels after 1 h of incubation with ligands.

The specificity of the coupling reaction for thiol groups was tested in a range of control experiments. The incubation of RGD(DMNPB)fC solutions with P(AAm) hydrogel gel in the absence of co-monomers showed no absorbance in UV. Incubation with the amine containing chromophore RGD(DMNPB)fK failed to bind with the surface, indicating no reactivity of the methylsulfone groups with amine groups (Figure 8A and B).

The binding of biomolecules on gels was stable and no drop in absorbance was observed by keeping hydrogels for 6 weeks in PBS. The stability of bound peptide c[RGD(DMNPB)fC)] (0.5mgmL$^{-1)}$ on P(AAm-*co*-**1**) was compared in cell culture medium in the presence of serum for 3 and 10 days. Experimental details are in Appendix Section 8.7.11.

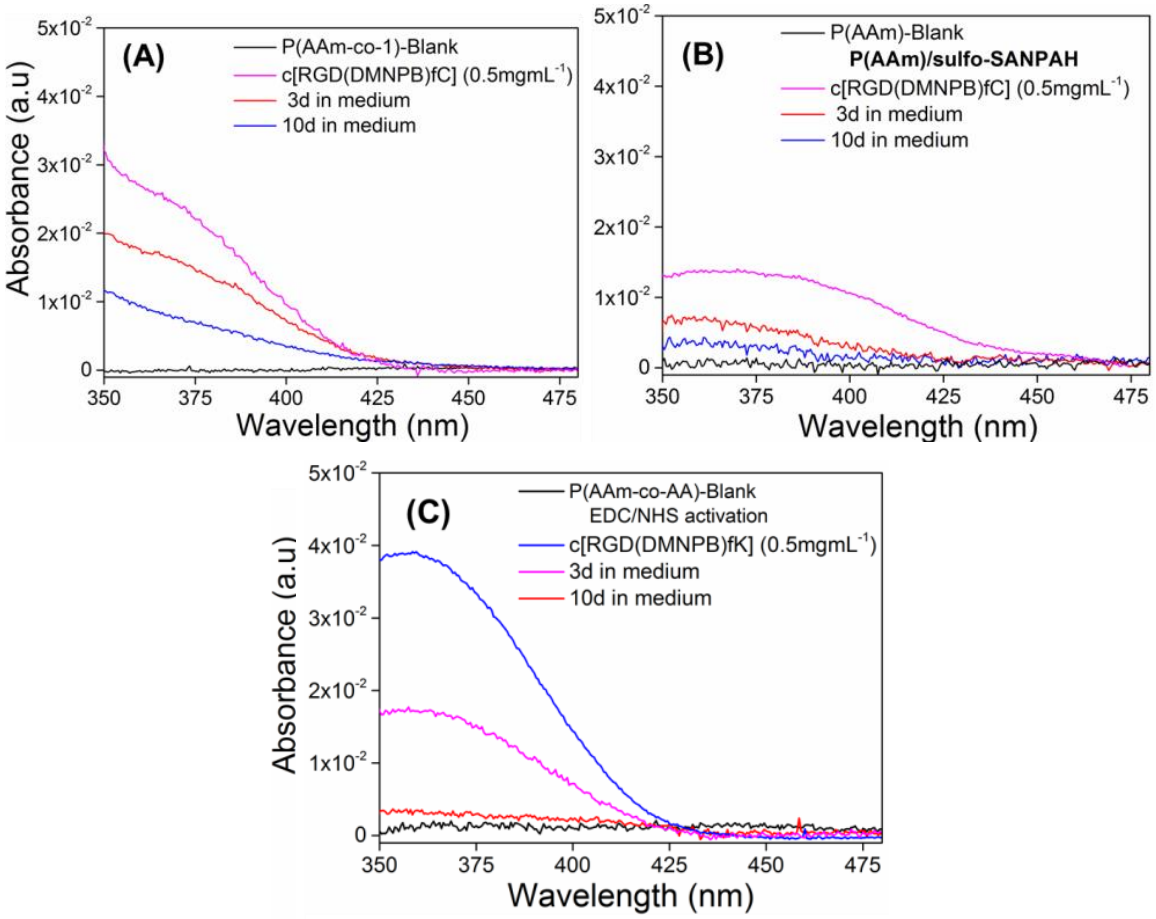

Figure 9. UV/Vis spectra of c[RGD(DMNPB)fC)] on hydrogel (A) P(AAm-co-**1**), (B) P(AAm)/sulfo-SANPAH and c[RGD(DMNPB)fK)] on (C) P(AAm-co-AA)/EDC after incubation with cell culture medium containing FBS for 3 and 10 days.

A decrease in UV absorption was observed with time due to hydrolysis of peptide by proteolytic enzymes secreted by cells. The stability was also compared with sulfo/SANPAH and amide coupling after EDC activation on P(AAm-*co*-AA) hydrogels. The methylsulfone gels retained 50% of bound peptide estimated from change in UV profile of DMNPB chromophore with time in comparison to other surface binding strategies such as sulfo-SANPAH or EDC/NHS chemistry (Figure 9 B-C).

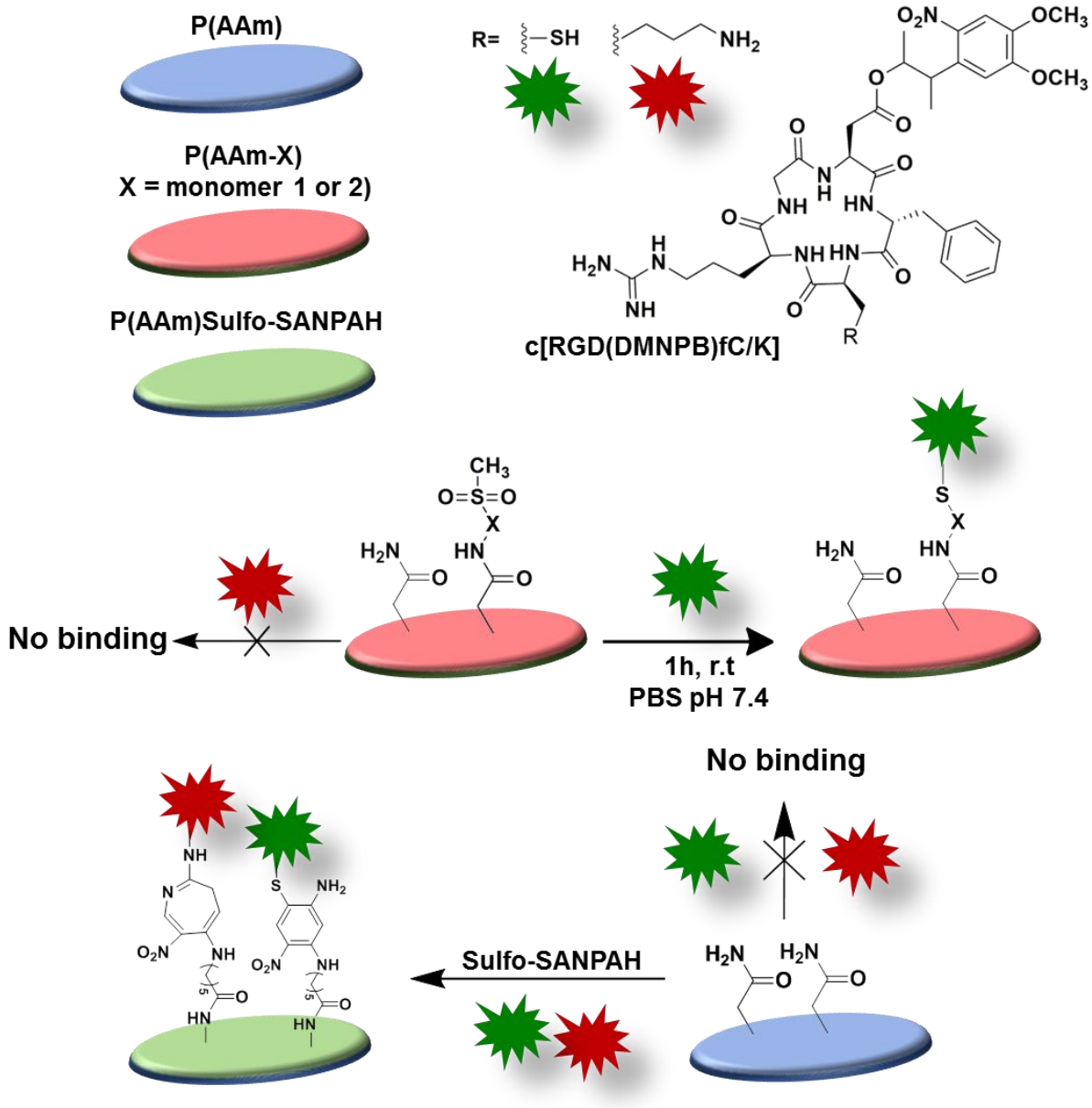

Scheme 3. Summarization of various surface functionalization routes on P(AAm), P(AAm-*co*-**X**) and P(AAm)/Sulfo-SANPAH hydrogels.

The coupling efficiency of P(AAm-co-**X**) hydrogels was compared with the coupling of the same molecule to P(AAm) hydrogels using sulfo-SANPAH. The coupling of RGD(DMNPB)fC to P(AAm) *via* sulfo-SANPAH showed three times less binding efficiency than coupling to P(AAm-co-**2**). RGD(DMNPB)fK was also successfully coupled to P(AAm)/sulfo-SANPAH, indicating no selectivity of the photoactivated aryl-azide group between amine and thiol groups and, therefore, the lack of selectivity of the sulfo-SANPAH coupling method (Figure 8 F). In addition to low binding efficiency and non-specificity towards ligands, P(AAm)/sulfo-SANPAH required 24 h incubation to achieve the binding efficiency of P(AAm-co-X) gels, and also required several coupling and washings steps. These results show that P(AAm-MS) gels are suitable substrates for thiol binding, providing easier, faster, more selective, and more stable couplings in comparison to other commonly used functionalization strategies like sulfo-SANPAH.

The ability of P(AAm-*co*-**X**) hydrogels to bind larger molecules, like proteins, was also tested. P(AAm-*co*-**1**) hydrogels incubated with rhodamine labeled fibronectin (1 $mgmL^{-1}$) showed a clear absorbance maximum at 560 nm, while no binding of fibronectin was observed on P(AAm) gels (Figure 10 A). Thus, P(AAm-*co*-**X**) gels allow specific immobilization of proteins containing thiol residues.

Site-specific coupling of biomolecule is essential for their bioactivity as a non-specific binding, especially anchoring through the active site of a ligand, can result in loss of bioactivity. The impact of site-specific immobilization was highlighted by comparison of streptavidin/biotin complex coupling on P(AAm-*co*-**1**) and P(AAm)/sulfo-SANPAH hydrogels. The gels were incubated overnight with streptavidin (0.1 $mgml^{-1}$), followed by coupling with Atto 425-biotin (0.3 $mgmL^{-1}$). The UV spectra showed higher absorbance of Atto 425 on MS hydrogels, while surprisingly very low absorbance was observed on P(AAm)/sulfo-SANPAH. In sulfo-SANPAH coupling, higher density of streptavidin was expected on the surface as streptavidin contains 25 amine groups while only 4 thiol moieties are available for P(AAm-*co*-**1**) coupling. The low binding on sulfo-SANPAH gels was attributed to either low binding efficiency of streptavidin in P(AAm)/sulfo-SANPAH gels or to loss of streptavidin activity due to non-specific immobilization. Further investigation of binding by first pre-mixing of streptavidin/biotin lead to significantly higher absorbance in P(AAm)/sulfo-SANPAH hydrogels while almost same intensity was observed in P(AAm-*co*-**1**) system (Figure

10B). This indicates that binding of streptavidin by sulfo-SANPAH blocks the active site for biotin recognition, while in P(AAm-*co*-**1**) the specific binding through thiol preserves the bioactivity.

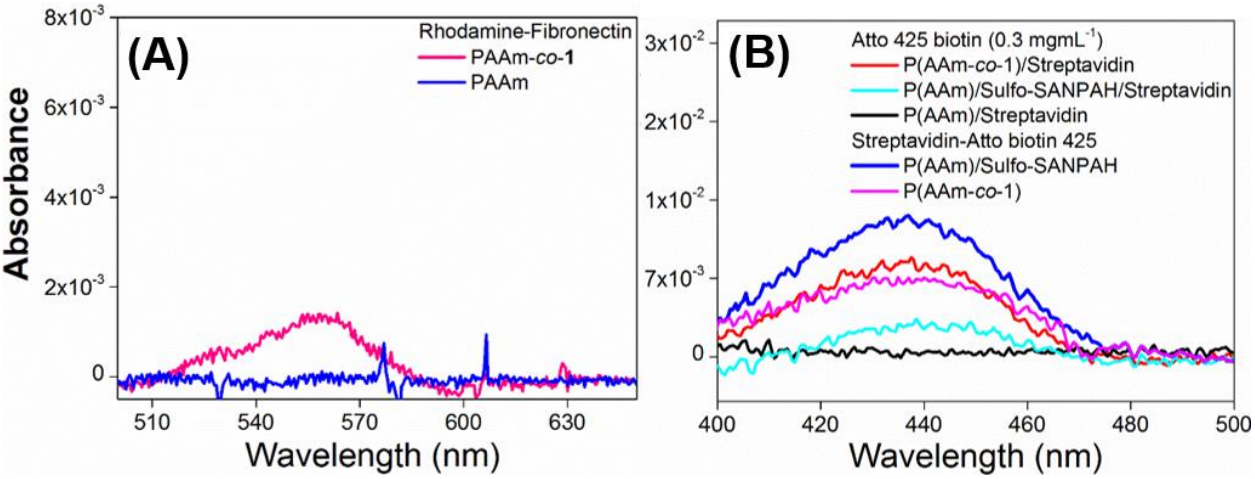

Figure 10. UV-vis spectra (A) Coupling of rhodamine labeled fibronectin on P(AAm-*co*-**1**) gel, (B) P(AAm)/sulfo-SANPAH and P(AAm-*co*-**1**) gels functionalization first with streptavidin followed by Atto 425 biotin complexation, or gels after coupling of pre-prepared streptavidin-Atto-biotin 425 complex.

3.5 Biocompatibility of P(AAm-MS) hydrogel

The presence of the new monomers in the P(AAm-*co*-**X**) hydrogels can compromise the biocompatibility of the material. Therefore, experiments were performed to test the cytocompatibility of the new gels using HeLa cell line. For this purpose, gels were functionalized with the cell adhesive ligand c[RGDfC] and with fibronectin protein. Functionalization of the gels with adhesive molecules is necessary to support attachment of cells to the hydrogel surface, which occurs *via* integrin membrane receptors that identify the binding sites on the adhesive molecules. Functionalization protocols were taken from the extensive reported literature dealing with P(AAm) gels as model substrates for cell culture and the study of cell-materials interactions.[4b, 14] The details of cell culture protocols and cell viability tests are described in the Appendix section 8.8.

Cells cultured on P(AAm-co-**X**) gels modified with the adhesive molecules showed good attachment, spreading and proliferation. Cells remained viable during 3 days on the surface with 95 and 93% viability for P(AAm-co-**1**) and P(AAm-co-**2**), respectively (Appendix Section 8.8.2). The control experiment on hydrogels without

surface functionalization with the adhesive ligands or functionalized with the amine peptide c[RGDfK] showed no cell attachment. These results confirm that P(AAm-co-**X**) gels support cell culture and specific attachment of cells *via* functional immobilized ligands (Figure 11).

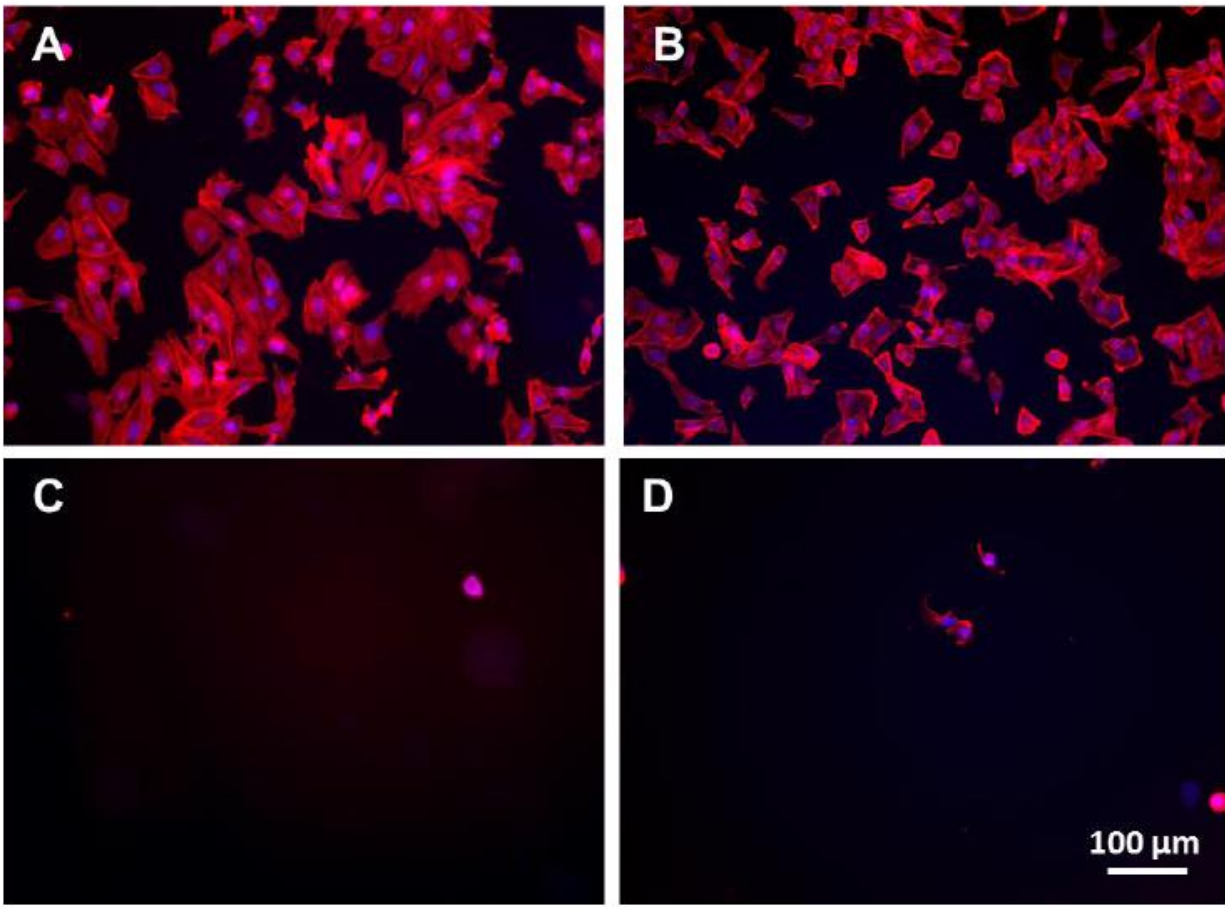

Figure 11. Epifluorescence images of HeLa cells 24 hours after seeding on P(AAm-*co*-**1**) gel functionalized with (A) c[RGDfC] and (B) fibronectin, (C) without functionalization and (D) after incubation with c[RGDfK].

The superior performance of P(AAm-*co*-**X**) gels vs P(AAm)/sulfo-SANPAH was tested by analyzing the variation of the morphology of cells attached on c[RGDfC] functionalized hydrogels. The effect of non-functional ligand binding on cell response was observed by immobilizing same concentration of c[RGDfC] on P(AAm)/sulfo-SANPAH and P(AAm-*co*-**1**) gels. Peptide density (8 µM) was estimated in both cases, through Lambert-Beer's law from UV absorbance profile of RGD(DMNPB)fC (Appendix Section 8.8.3). The equal concentration of peptide on surface was achieved by using initial concentration of (20 µgmL^{-1}) for P(AAm-*co*-**1**) and (100

µgmL^{-1}) for P(AAm)/sulfo-SANPAH. The HeLa cells showed significantly lower spreading after 6h on the peptide immobilized with sulfo-SANPAH than on P(AAm-*co*-**1**) gels. The cell spreading improved after 24h in both cases but spreading area in P(AAm-*co*-**1**) was much larger. This difference is translated in distribution of stress fibers and organization of cytoskeleton (Figure 12). The low cell spreading kinetics was due to low density of functional c[RGDfC] on sulfo-SANPAH activated hydrogels as binding concentration, stiffness and swelling were similar for both platforms.

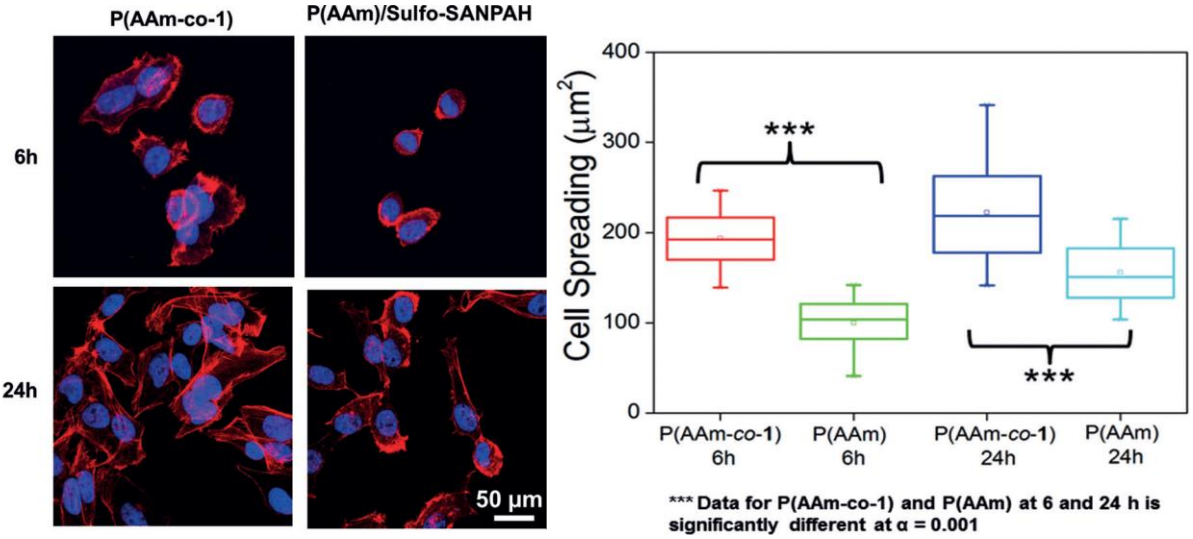

Figure 12. Confocal images of HeLa cells cultured on P(AAm-*co*-**1**) or P(AAm)/sulfo-SANPAH gels functionalized with c[RGDfC] after 6 or 24 hours. The statistical analysis using one-way ANOVA displaying significant differences between samples at alpha=0.001 level and Tukey contrast

3.6 Conclusions

The polyacrylamide hydrogels for thiol bioconjugation were designed by copolymerization with heteroaromatic methylsulfonyl acrylate. The copolymerized hydrogels P(AAm-*co*-**1**) or P(AAm-*co*-**2**) showed precise coupling of thiols by nucleophilic aromatic substitution, within few minutes (10- 60 min) under physiological conditions (r.t., PBS pH 7.4). The properties of P(AAm) system as transparency, stiffness, swelling or protein repellency remained unaffected in the copolymers. These gels exhibit higher quantitative and functional immobilization of ligands in comparison to sulfo-SANPAH activation. These methylsulfone derivatized hydrogels ensure specific coupling of thiol-terminated biomolecules with superior quantitative control over surface density. The P(AAm-*co*-**X**) gels show high binding

reproducibility and stability to see interplay of ligand density and stiffness on cell attachment and behavior.

References

[1] A. K. Denisin, B. L. Pruitt, *ACS applied materials & interfaces* **2016**, *8*, 21893-21902.

[2] aB. Trappmann, J. E. Gautrot, J. T. Connelly, D. G. T. Strange, Y. Li, M. L. Oyen, M. A. Cohen Stuart, H. Boehm, B. Li, V. Vogel, J. P. Spatz, F. M. Watt, W. T. S. Huck, *Nat. Mater.* **2012**, *11*, 642-649; bR. S. Fischer, K. A. Myers, M. L. Gardel, C. M. Waterman, *Nature protocols* **2012**, *7*, 2056-2066.

[3] aC. Pande, A. Sharma, *Journal of applied polymer science* **2002**, *84*, 2613-2620; bV. Damljanovic, B. C. Lagerholm, K. Jacobson, *BioTechniques* **2005**, *39*, 847; cP. Moshayedi, L. da F Costa, A. Christ, S. P. Lacour, J. Fawcett, J. Guck, K. Franze, *Journal of Physics: Condensed Matter* **2010**, *22*, 194114; dT. Grevesse, M. Versaevel, G. Circelli, S. Desprez, S. Gabriele, *Lab on a Chip* **2013**, *13*, 777-780.

[4] aS. Seiffert, W. Oppermann, *Macromolecular Chemistry and Physics* **2007**, *208*, 1744-1752; bO. F. Zouani, J. Kalisky, E. Ibarboure, M.-C. Durrieu, *Biomaterials* **2013**, *34*, 2157-2166; cW. F. Lee, C. H. Shieh, *Journal of applied polymer science* **1999**, *71*, 221-231; dN. Dafader, M. Adnan, M. Haque, D. Huq, F. Akhtar, *African Journal of Pure and Applied Chemistry* **2011**, *5*, 111-118.

[5] aM. H. Stenzel*, Vol. 2*, ACS Publications, **2012**, pp. 14–18; bM. A. Azagarsamy, K. S. Anseth, *ACS macro letters* **2013**, *2*, 5-9; cC. Boyer, J. Liu, L. Wong, M. Tippett, V. Bulmus, T. P. Davis, *Journal of Polymer Science Part A: Polymer Chemistry* **2008**, *46*, 7207-7224; dS. Chatani, D. P. Nair, C. N. Bowman, *Polymer Chemistry* **2013**, *4*, 1048-1055.

[6] D. Zhang, N. O. Devarie-Baez, Q. Li, J. R. Lancaster Jr, M. Xian, *Organic letters* **2012**, *14*, 3396-3399.

[7] N. Toda, S. Asano, C. F. Barbas, *Angewandte Chemie International Edition* **2013**, *52*, 12592-12596.

[8] T. Vilaivan, *Tetrahedron letters* **2006**, *47*, 6739-6742.

[9] N. Toda, S. Asano, C. F. Barbas, *Angew. Chem., Int. Ed.* **2013**, *52*, 12592-12596.

[10] J. M. Rodriguez, A. D. Hamilton, *Angewandte Chemie* **2007**, *119*, 8768-8771.

[11] J. Thiele, Y. Ma, S. Bruekers, S. Ma, W. T. Huck, *Advanced Materials* **2014**, *26*, 125-148.

[12] aJ. H. Wen, L. G. Vincent, A. Fuhrmann, Y. S. Choi, K. C. Hribar, H. Taylor-Weiner, S. Chen, A. J. Engler, *Nat. Mater.* **2014**, *13*, 979-987; bB. Trappmann, J. E. Gautrot, J. T. Connelly, D. G. Strange, Y. Li, M. L. Oyen, M. A. C. Stuart, H. Boehm, B. Li, V. Vogel, *Nature materials* **2012**, *11*, 642-649.

[13] T. T. Lee, J. R. García, J. I. Paez, A. Singh, E. A. Phelps, S. Weis, Z. Shafiq, A. Shekaran, A. del Campo, A. J. García, *Nature Materials* **2015**, *14*, 352-360.

[14] aR. L. Saunders, D. A. Hammer, *Cellular and molecular bioengineering* **2010**, *3*, 60-67; bP. Rajagopalan, W. A. Marganski, X. Q. Brown, J. Y. Wong, *Biophysical journal* **2004**, *87*, 2818-2827; cC. A. Reinhart-King, M. Dembo, D. A. Hammer, *Langmuir* **2003**, *19*, 1573-1579.

Chapter 4

Differentiation of Neural Progenitor Cells on Bifunctionalized Soft Poly(AAm-MS-AA) gels[1]

4.1 Introduction

Neural progenitor cells are responsible for development and regeneration of nerve tissue during the embryonic and adult stages. Neural progenitor cells undergo several division cycles and differentiate into either glial or neuronal lineages. The fate of neural progenitor cells *in vivo* is controlled by various intrinsic and extrinsic factors, such as genetic coding, gradient of signaling molecules, composition and mechanical properties of the extracellular matrix and cell-cell interactions.

Typically, neural progenitor cells are cultured on poly-D-lysine (PDL) coated plastic/glass surfaces. The positive charges of the PDL interact electrostatically with the cell membrane and support cell attachment to the plastic surface.[1] The PDL-membrane interaction is enough to physically retain progenitor cells on the substrate, but it does not capture the biochemical information of the natural microenvironment required by progenitor cells to undergo division or differentiation. ECM proteins possess specific active sites that interact with membrane integrin receptors and trigger specific responses. Laminin (LN) is a relevant ECM protein in the neuronal microenvironment. LN possesses active sites that trigger neuronal development, proliferation and migration.[2] In fact, LN is often mixed with PDL to condition cell culture plates for neuronal cultures.[3] The physical co-adsorption of the two molecules can lead to low binding, poor reproducibility, lack of spatial orientation or leaching of the coating during washing steps. Selective, covalent binding of the molecules is expected to provide more homogenous and stable coatings, and eventually allow specific orientation of ligands for more effective binding.[4]

[1]The content of this chapter is reprinted by permission of American chemical Society, published in *Biomacromolecules* (2017), Volume 18, page 906-913. A. Farrukh, J. I. Paez, M. Salierno, W. Fan, B. Berninger, A. del Campo, "Bifunctional poly(acrylamide) hydrogels through orthogonal coupling chemistries"[5]

In the last years, soft polyacrylamide P(AAm) hydrogels have been widely employed as culture substrates for neural cells.[6] Soft P(AAm) hydrogels (Young's Modulus 0.1- 1kPa) mimic the mechanical properties of brain better than glass (with Young's Modulus in the GPa range).[6b, 6c, 7] In fact, neurons seem to sense the stiffness of P(AAm) hydrogels and show differences in growth and phenotypic differentiation in response to stiffness changes.[6d, 8] P(AAm) hydrogels have also been used for mechanosensing studies of astrocytes and to investigate formation and activity of cortical neuronal networks.[9] In all these cases, the P(AAm) gels are usually biofunctionalized by physically adsorbing PDL or LN, or by attaching them covalently using hydrazine hydrate, periodate or sulfo-SANPAH based strategies. As explained in Chapter 3, section 3.1, all these methods provide limited control over surface functionalization and compromise reproducibility.[10]

P(AAm) hydrogels are chemically stable and limited options are available for the specific covalent functionalization. Copolymerization with reactive monomers is an effective strategy to allow specific modification of P(AAm) gels with biomolecules. Copolymerization with methylsulfone acrylate (MS) for bioconjugation of thiol containing biomolecules, as presented in Chapter 3, is one possibility. Copolymerization with acrylic acid (AA) has also been reported in the literature.[11] The carboxylic group of AA allows specific binding of amine terminated biomolecules upon activation with well-established EDC/NHS chemistry.[11]

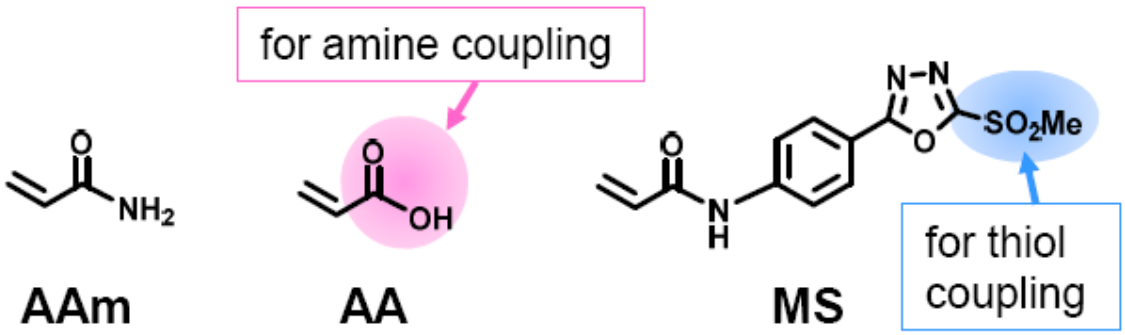

Scheme 1. Bifunctional modification of P(AAm) hydrogels by copolymerizing with methylsulfone acrylates (MS) and acrylic acid (AA) for independent coupling of thiol and amine containing biomolecules respectively.

In order to introduce two different biomolecules in an orthogonal way, a ter-polymer P(AAm-MS-AA) containing the two functional monomers (MS and AA) is presented in this chapter. This system allows orthogonal coupling of amine terminated biomolecules to the same hydrogel (Scheme 1).[5, 12] This chapter includes designing, characterization and functionalization of bifunctional P(AAm-MS-AA) terpolymer hydrogels. P(AAm-MS-AA) hydrogels with tuned stiffness (0.2 – 70 kPa) will be orthogonally functionalized with a cysteine-terminated laminin peptidomimetic coupled to MS monomer and with PDL coupled to EDC/NHS activated AA monomer. The following sections present the optimization of gel composition to direct differentiation of neural stem cells (NSCs) and neural progenitor cells (NPCs). The neural progenitor cells which were isolated from cerebral cortex of mouse embryo (E14.5) are referred as eNPCs and stem cells isolated from subependymal zone (SEZ) of adult mouse (8-12 weeks) titled as aNSCs.

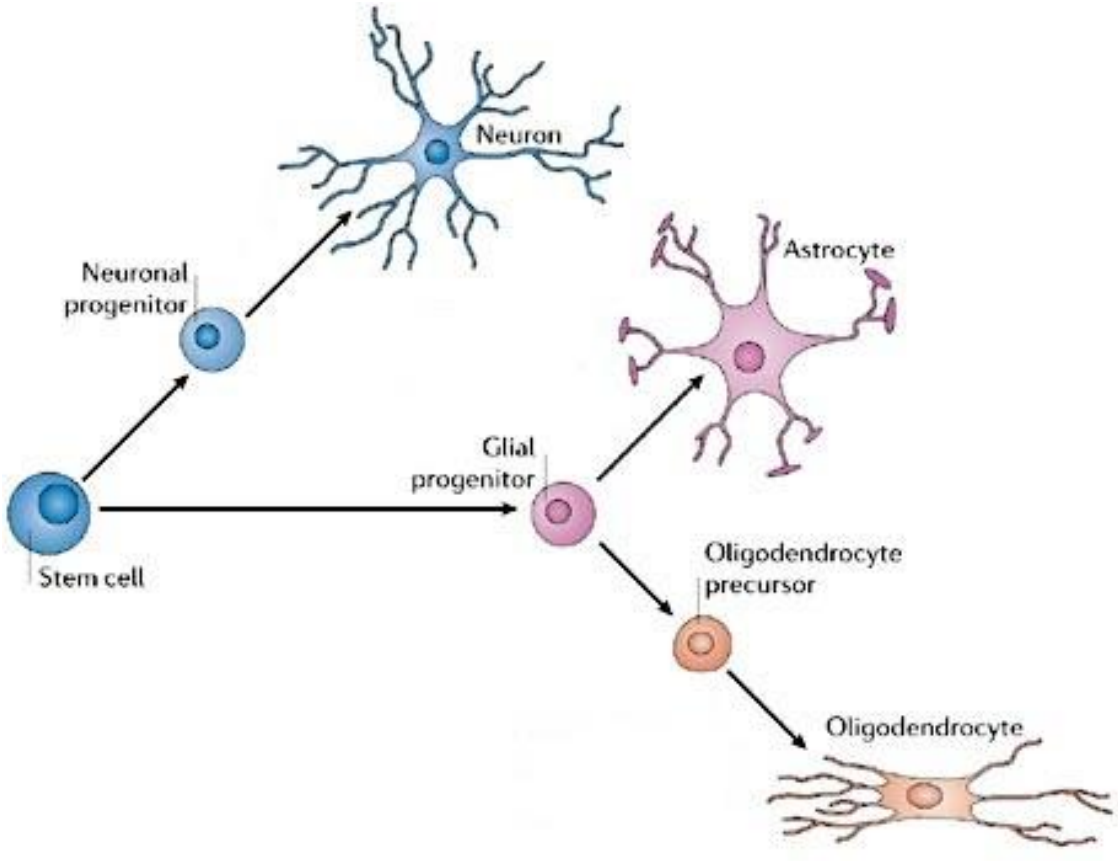

Scheme 2. Differentiation of stem cells into glial and neuronal progenitor cells. The former will give rise to astrocytes and oligodendrocyte, the latter to neuronal lineage. This figure is reprinted with permission from Nature publishing group. [14]

During development stem cells undergo division cycles either by symmetric division into two daughter stem cells or asymmetric division lead to a daughter stem cell and neuronal/glial progenitor cells. *In vivo* the multipotent undifferentiated neural progenitor cell undergoes limited number of division and differentiates into neurons, astrocytes, and oligodendrocyte lineage (Scheme 2).[13] The fate of progenitor cell *in vitro* depends on cell culture medium, substrate stiffness and surface. The fate of NSCs and NPCs will be regulated towards neuronal differentiation by selective surface functionalization of substrate with tunable stiffness.

4.2 Preparation and physiochemical characterization of P(AAm-MS-AA) hydrogels

The bifunctional hydrogels P(AAm-MS-AA) were synthesized by free radical copolymerization of acrylamide (AAm) with acrylic acid (AA) and phenyl oxadiazole methylsulfonyl acrylate (MS). AAm has been shown to effectively copolymerize with MS and AA monomers in binary mixtures. Preliminary experiments were performed first to test the copolymerization reaction of the three monomers. The linear copolymer was prepared by mixing AA (8.8 mol%) and MS (2.2 mol%) with AAm (89 mol%) monomer in PBS in the presence of APS (initiator) and TEMED (catalyst) without crosslinker. The polymerization was carried out for 15 min at room temperature under oxygen free conditions. The obtained copolymers were dissolved in D_2O for NMR studies. The incorporation of the monomers into P(AAm-MS-AA) and control P(AAm-AA) polymers was evaluated by ^1H NMR characterization of the final polymers (Figure 1 B). The broad signal for polymer backbone appears at (1.5-1.7 and 2.1-2.3 ppm) along with the corresponding decrease in intensity of monomer signals. The doublets from vinyl moieties (5.5-6.3 ppm) of the rest monomer in the reaction mixture were used to calculate the incorporation of monomer into polymer. The percentage of conversion was calculated from disappearance of alkene protons (5.5 - 5.8 ppm) of AA and AAm acrylates by following expression.

$$\boldsymbol{Conversion}\ (\%) = \mathbf{100} - \left(\frac{\boldsymbol{I_t}\ \boldsymbol{x}\ \mathbf{100}}{\boldsymbol{I_0}}\right)$$

I_t corresponds to the integral of alkene protons at time *t* and I_0 corresponds to the integral of alkene protons at time t=0 (before polymerization). The ^{1}H NMR spectra of linear P(AAm-AA) and P(AAm-MS-AA) shows consumption of AA monomer and AAm after 15 min of polymerization (Figure 1 B). The obtained conversion for P(AAm-AA) and P(AAm-MS-AA) was 98.7% and 97.3% respectively. The signal for MS monomer were not visible in NMR therefore the measurement was performed with higher concentration of MS acrylate. The polymerization was carried out with AAm:MS:AA with 50:40:10 mol% for 15 min in PBS. Both MS and AA monomers are effectively incorporated in the terpolymer. In P(AAm-MS-AA) copolymer aromatic signals at 8.0 and 7.9 ppm corresponds to presence of methylsulfone acrylate. The ratio of the comonomers in the polymer roughly corresponds to feeding ratio of monomers (AAm:AA:MS 40:10:50).

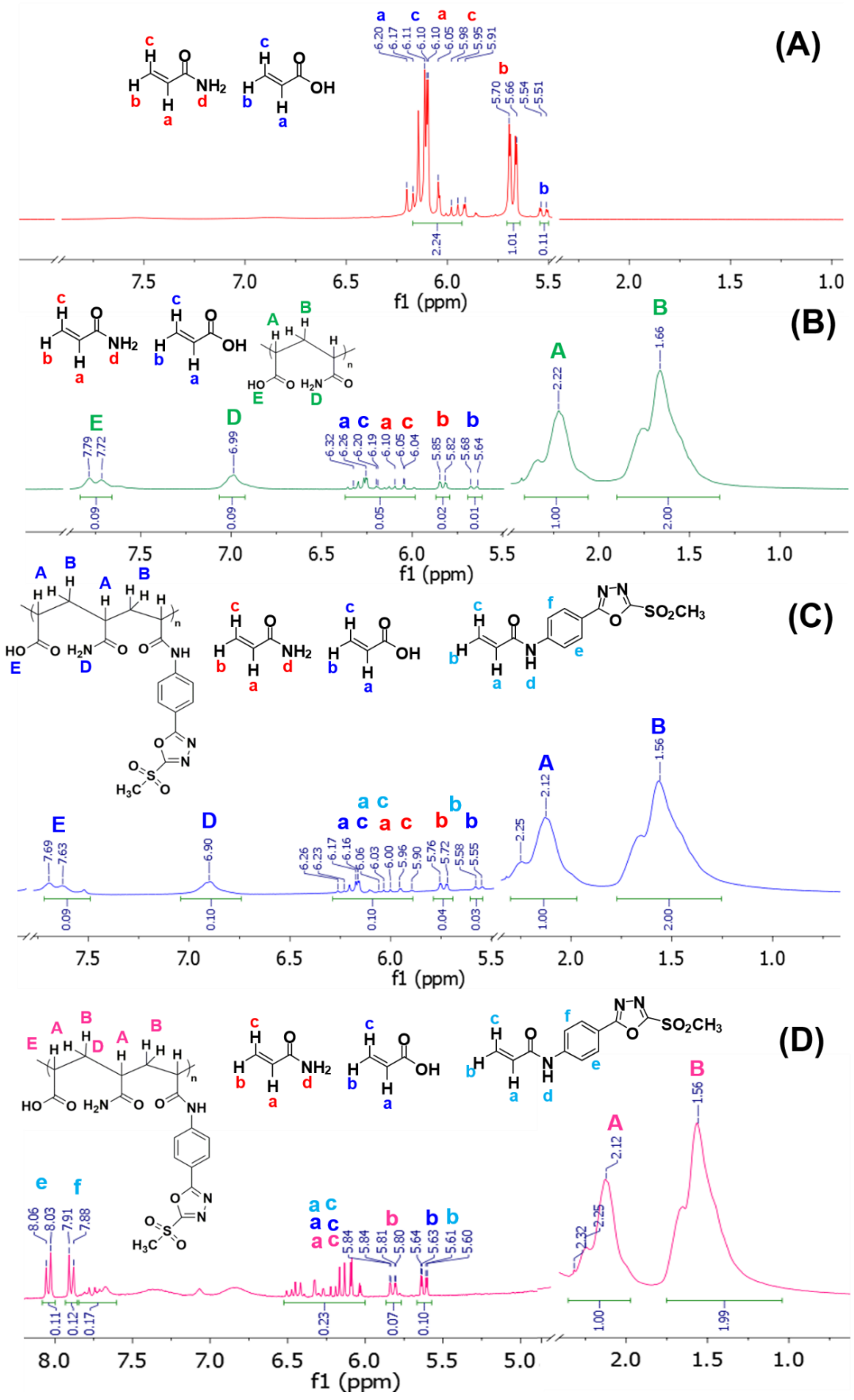
(A)
(B)
(C)
(D)
f1 (ppm)

Figure 1: ^{1}H NMR (D_2O, 300 MHz) of (A) mixture of AA + AAm without initiator (10:90mol%) (B) linear P(AAm-AA) (90:10mol%) (C) linear P(AAm-MS-AA) (89:2.2:8.8mol%) (D) linear P(AAm-AA-MS) (40:50:10mol%). Samples B-D were measured after 15 min of polymerization.

The linear P(AAm), P(Amm-AA) and P(AAm-MS-AA) copolymers obtained under identical polymerization conditions were subjected to GPC analysis. The molecular weight of the copolymer was slightly lower than the homopolymer while the polydispersity index was slightly higher, indicating a moderate widening of the molecular weight distribution in the terpolymer (Appendix Section 8.9.1). These small changes are presumably due to differences in the polymerization kinetics of the three monomers and different solubility of monomer in solvent (DMF/PBS). However, these small differences did not significantly affect the properties of the hydrogel (Table 1).

The copolymer network was obtained by mixing AA (8.8 wt%), MS (2.2 wt%), AAm (89 wt%) and bis-acrylamide (0.2wt%) as cross linker. The polymerization was initiated the by APS and catalyzed by TEMED in PBS pH 7.4. The solution of AA monomer decreases the pH of the polymerization mixture. Therefore, the pH of the monomer solution was pre-adjusted to pH 7.5 in order to avoid protonation of catalyst and initiator that would affect the polymerization reaction. A drop of the monomer mixture was sandwiched between a hydrophobic Sigmacote® slide and a APTS-coated slide to obtain thin films of hydrogel covalently attached to the APTS functionalized slide but releasable from the Sigmacoated one. The stable transparent hydrogels were obtained, with reproducible thickness (Appendix Section 8.9.3).

The mechanical properties of the hydrogel films were determined by dynamic mechanical analysis using a plate-plate rheometer. The stiffness was measured in presence of water filled in bottom plate of rheometer to avoid drying during measurement. The storage modulus of P(AAm-MS-AA) hydrogel was 23±0.8 kPa, slightly lower than that obtained for P(AAm) homopolymer (25±1.5kPa) (Table 1). Similar effect was also observed for P(AAm-AA) and P(AAm-MS) copolymers with 24±0.7 and 23±2 kPa stiffness respectively.

Table 1. Physical characterization of derived hydrogels, representing molecular weight distribution and polydispersity of linear polymers, swelling of crosslinked polymer in bulk and stiffness measurement of crosslinked hydrogel film.

Polymer	Linear		Hydrogel	
	Mw g/mol	Polydispersity (PD)	Swelling Ratio [mg water/mass polymer]	Elastic Modulus (kPA)
P(AAm)	75194	2.30	5.6±0.46	75±2
P(AAm-MS)	69852	2.38	6.3±0.28	69±3
P(AAm-AA)	79319	2.43	23±0.22	73±2
P(AAm-MS-AA)	60866	2.56	21±0.54	70±2

The swelling ratio of the bulk hydrogels was measured by polymerizing in an Eppendorf vial (Appendix Section 8.11). Bulk P(AAm-MS-AA) hydrogels showed three times higher swelling ratio than P(AAm). This can be explained by the presence of the charged carboxylic acid groups in AA. This behavior was also reflected during the measurements on thin films. The swelling ratio of thin films was evaluated by measuring the thickness of the dry and swollen films by confocal fluorescence microscopy after binding to a chromophore (Appendix Section 8.11). The thickness of P(AAm-MS-AA) hydrogels remained largely unaffected (205 µm) after binding of a fluorophore to MS monomer, but drop significantly to 63 µm after coupling fluorophore to the AA monomer since the ionizable carboxylic groups were reacted to ester groups (Figure 2). Therefore, despite similar stiffness and crosslinking degrees in the different hydrogel compositions, the swelling degree changes among them mostly depending on the presence of ionizable AA groups.

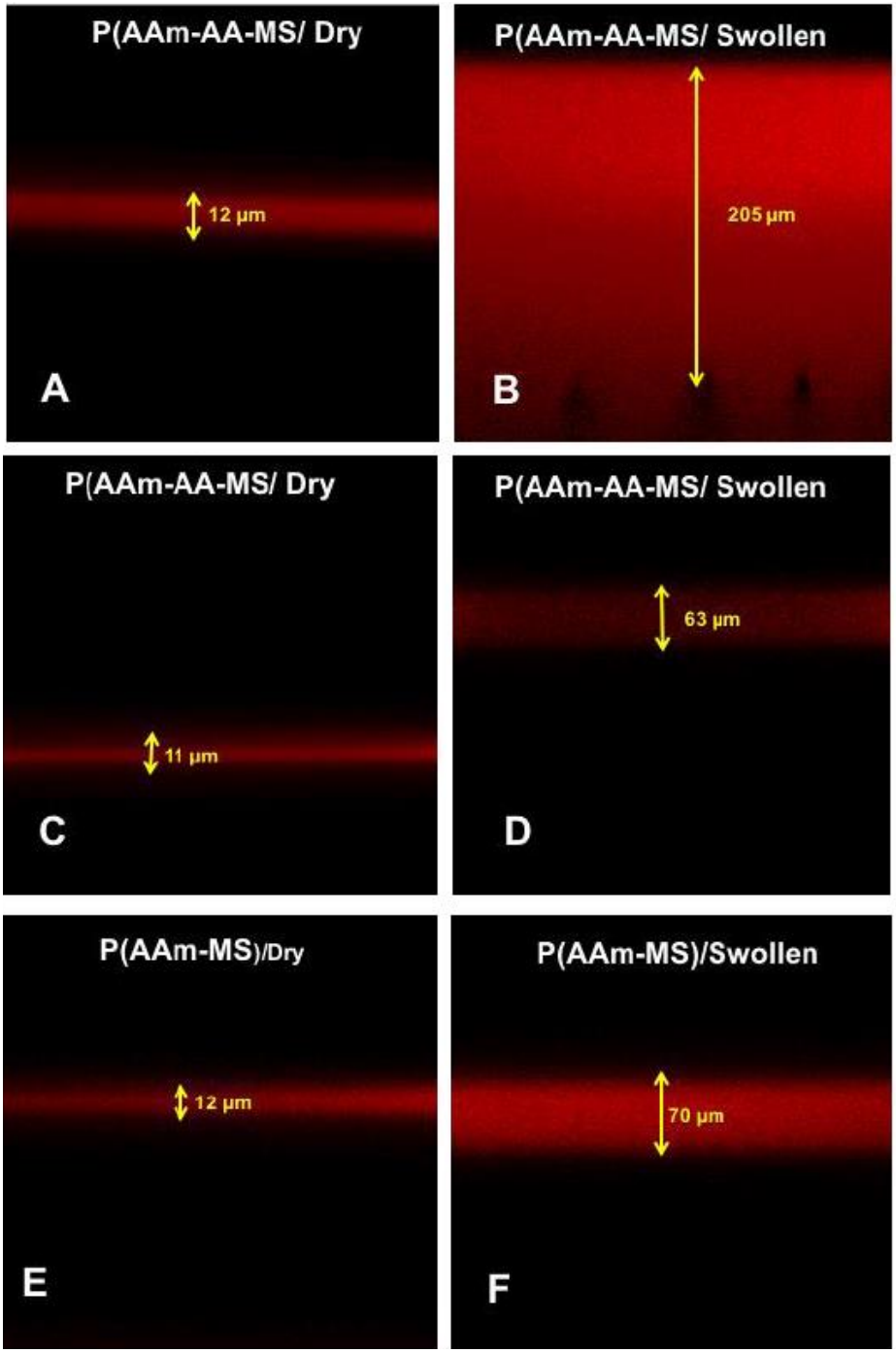

Figure 2. Thickness, swelling and distribution of ligands bound to gels (2kPa) measured by confocal LSM microscope. (A-B and E-F) after thiol-coupling using thiol-Streptavidin/Biotin Atto 425 (0.5 mg/mL), and (C-D) after amine coupling using 1 mgmL^{-1} c[RGD(Coum)fK] after EDC/NHS activation.

The morphology of the copolymer and terpolymers was imaged by SEM and compared to P(AAm). The hydrogel samples were prepared in bulk, freeze dried and

coated with conductive layer for imaging. All systems showed a porous network with pore size in nanometer to micrometer range (Figure 3). These results show that copolymerization did not affect the topographical properties and that the morphology of P(AAm-MS-AA) was comparable to P(AAm) and P(AAm-AA) hydrogels.

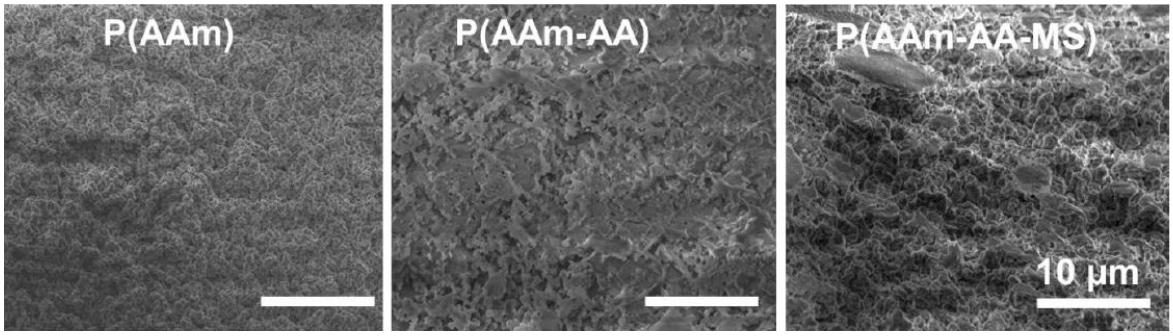

Figure 3. SEM images of freeze dried bulk hydrogels.

4.3 Orthogonal coupling of two different ligands to P(AAm-MS-AA) hydrogels

The specific coupling of amine and thiol biomolecules to the P(AAm-MS-AA) hydrogels was evaluated by UV spectroscopy analysis of the samples after reacting with chromophores. The cyclic peptides c[RGD(coum)fC] and c[RGD(coum)fK] chromophores were used for this purpose. These molecules show an absorbance band at λ_{max} = 390 nm corresponding to the Coum chromophore attached to the Aspartic acid (D) rest and were available in the group.[15] c[RGD(coum)fC] and c[RGD(coum)fK] present a cysteine or lysine as probes for thiol or amine coupling respectively. The P(AAm-MS-AA) gels were coupled with increasing concentration of these peptides for 1h. Coupling of thiol derivative was one-step whereas coupling of the amine required a previous EDC/NHS activation step. The mechanism involves attack of oxygen on electro-deficient carbodiimide making unstable O-acylisourea intermediate (Scheme 3). The NHS attacks on activated carbonyl carbon of acid, making -NHS ester and releasing carbodiimide isourea. The NHS is better leaving group, therefore nucleophilic attack on carbonyl carbon by amine displaces NHS and forms the amide bond.[16]

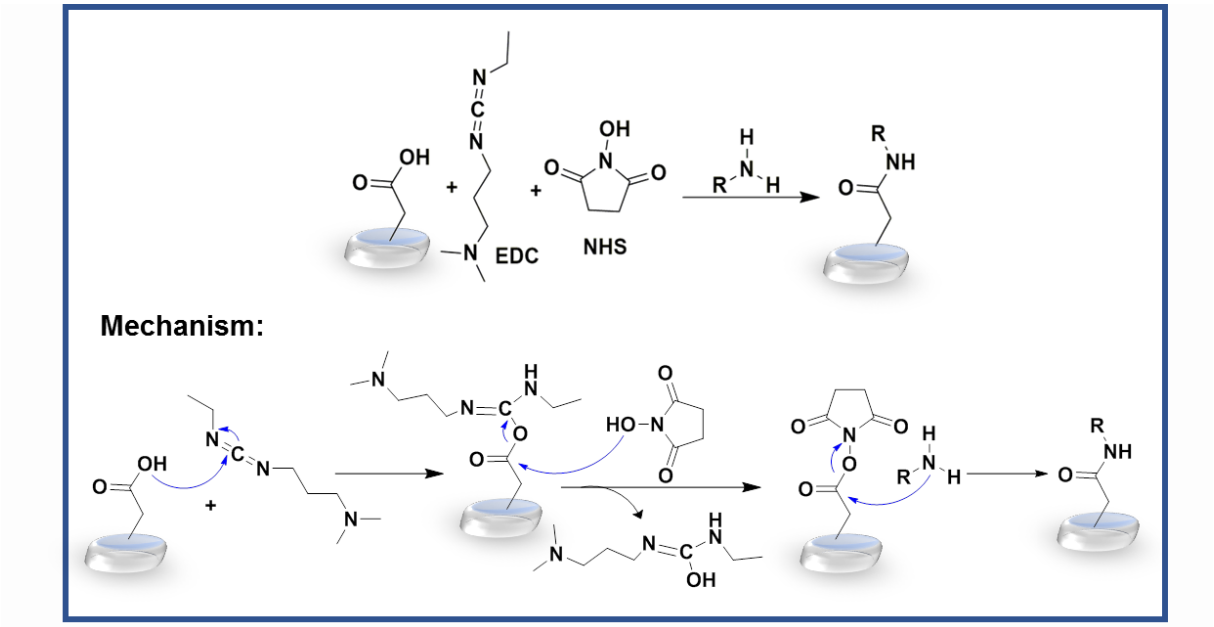

Scheme 3. The amide bond formation by EDC/NHS activation on surface of hydrogels.

An increase in absorbance in the spectra of the hydrogels was observed after coupling reaction with the individual chromophores. The absorbance increased with increasing coupling concentration of the peptide (Figure 4a-b). The copolymer hydrogels showed selective functionalization of amine and thiol molecules at tunable concentration. The coupling efficiency on surface was calculated by Beer-Lambert law (c=A/lε) (Table 2). The absorbance values were obtained from UV spectra, extinction coefficient of chromophore from literature RGD(coum)fC λ_{max} 390 nm, ε_{390}= 20000$M^{-1}cm^{-1}$ and thickness of hydrogel was measured by fluorescence microscopy (Appendix Section 8.11).[15] The coupling yield for both amine and thiol were calculated from initial concentration of incubation solution and final concentration obtained on surface by Beer Lambert law (Table 2). Thiol coupling was more efficient than amine considering there are only 2% of MS groups for thiol coupling vs 9% of –COOH groups for amine but still higher coupling yield was obtained. Generally the MS coupling (>90%) as established in Chapter 3 section 3.4 is more efficient than EDC/NHS (~70%) due to the partial hydrolysis of reactive NHS ester by water.[17]

The coupling kinetics for both types of reactions was evaluated by following the increase in absorbance for increasing coupling times between 1 and 24 hours. Longer coupling times resulted in higher absorbance values (Figure 4c-d). This trend was more pronounced for amine coupling, indicating thiol coupling is faster than amine coupling. The thiol coupling in P(AAm-MS-AA) platform at 1mgmL^{-1} was slightly less efficient (89.48%) than on P(AAm-MS) biopolymer (93%) (Chapter 3 Section 3.4), this was attributed to the higher swelling of the terpolymer.

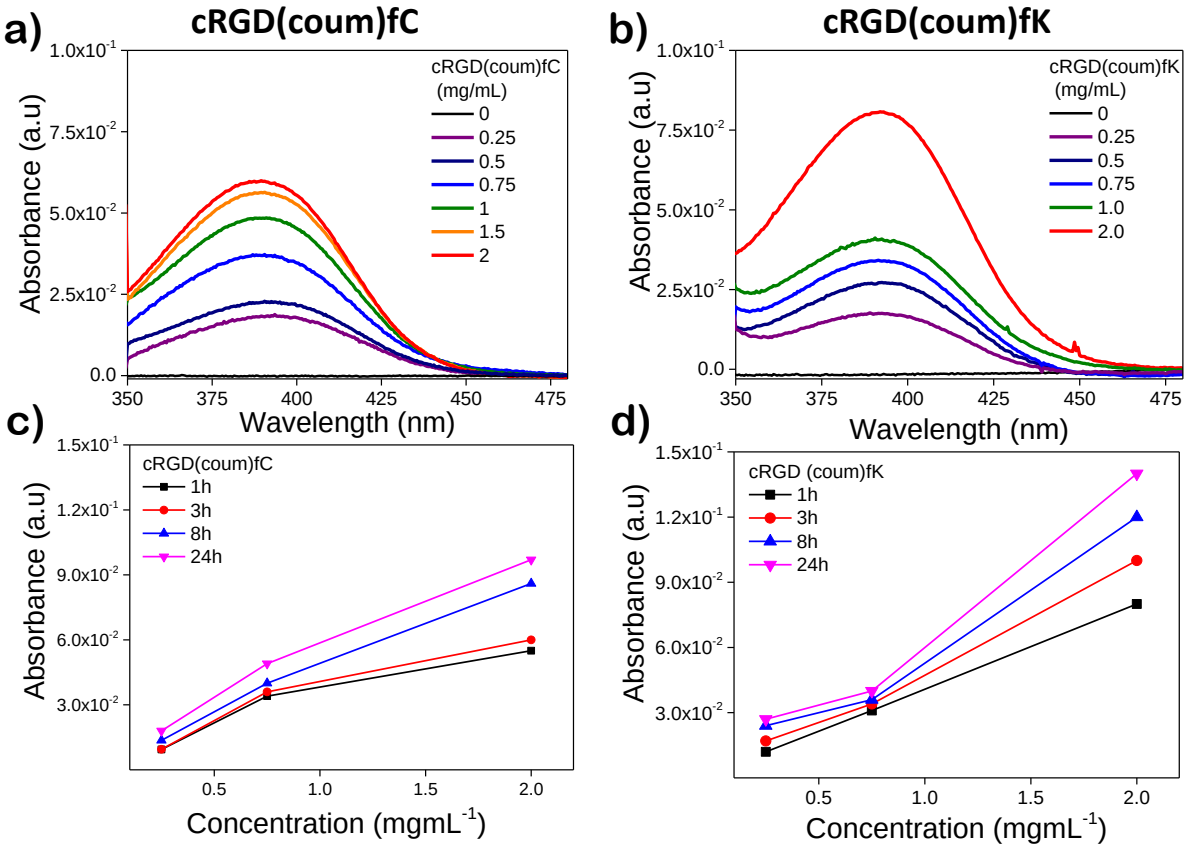

Figure 4. UV spectra of P(AAm-MS-AA) hydrogels (a-b) increasing peptide solution concentrations for 1h, (c-d) coupling at increasing coupling times (1 to 24h, λ_{max}= 390 nm).

The stability of the covalently bounded thiol and amine derivatized molecules was tested by keeping the functionalized hydrogels for 8 weeks in PBS and measuring the UV spectra afterwards. No drop in absorption was observed, indicating the stability of functionalization chemistry. However, similar experiments performed in cell culture medium displayed some differences. The decrease in absorbance of chromophore after 10 days was compared with initial absorbance value (Appendix

Section 8.7.11). In thiol less than 50% decrease in absorbance was observed while ~95% decrease in absorbance intensity was seen for EDC/NHS coupled ligand (Chapter 3, Section 3.4).

Table 2. Coupling efficiency of amine and thiol coupling on P(AAm-MS-AA) hydrogels with peptide solutions of increasing concentrations after 1h of coupling. The efficiency was calculated from Beer Lambert expression with corresponding λ_{max} absorbance values at 390 nm, thickness from confocal microscopy and ε_{390}= 20000$M^{-1}cm^{-1}$

Concentration of c[RGD(coum)fC/fK] solution		**Coupling Efficiency (%)**	
mgmL^{-1}	**Molar**	**RGD(coum)fK**	**RGD(coum)fC**
0.25	2.96x10^{-4}	52.06	84.77
0.5	5.91x10^{-4}	63.34	86.56
0.75	8.87x10^{-4}	68.04	87.84
1.0	1.18x10^{-3}	71.80	89.48
1.5	1.77x10^{-3}	72.15	92.10
2.0	2.36x10^{-3}	74.80	93.65

Different control experiments were carried out to demonstrate the chemo-selectivity between MS and AA coupling chemistries in the orthogonal hydrogels. The RGD(coum)fC (1mgmL^{-1}) in the absence of MS monomer on P(AAm-AA) hydrogel failed to bind on surface. P(AAm-AA) hydrogels incubated with RGD(coum)fK without EDC activation showed a very high absorption band. This high non-specific adsorption was due to electrostatic interaction of the lysine side chain amine with negatively charged acrylic acid. The nonspecifically adsorbed RGD(coum)fK could not be washed away with water, but with 0.05 M aq. acetic acid solution (pH = 4) (Figure 5A). This non-specific adsorption of amine chromophore on acrylic acid hydrogel was significantly reduced after EDC activation due to decrease in surface charge. The RGD(coum)fK coupled after EDC activation show 15% drop in absorbance after washing with 0.05 M aq. acetic acid solution (pH = 4) (Figure 5B).

However, to avoid non-specific adsorption, a final washing step with acetic acid solution after peptide coupling was always included in the procedure.

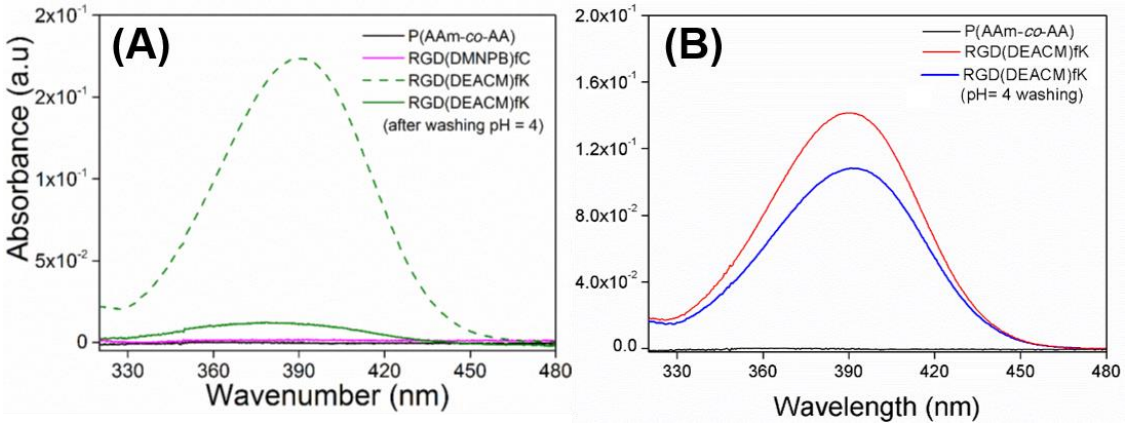

Figure 5. UV spectra of P(AAm-AA) gels after incubation with (A) c[RGD(coum)fC] and c[RGD(coum)fK] peptides (A) without EDC activation, (B) after EDC activation and washing with acetic acid.

The bifunctionalization of thiol and amine containing molecules on the P(AAm-MS-AA) hydrogel was demonstrated by sequential immobilization of thiol and amine containing molecules with two different chromophores. The RGD(coum)fC (λ_{max} 390 nm, ε_{390}= 20000$M^{-1}cm^{-1}$) and cRGD(DMNPB)fK, (λ_{max} 360 nm, ε_{360}= 4100$M^{-1}cm^{-1}$) were employed as UV probes (Figure 6).[18] The UV spectra of aqueous solution of chromophores (1mgmL^{-1}) showed distinct absorbance bands corresponding to λ_{max}. A 1:1 solution of the chromophores shows a broad absorbance band at λ_{max} =375 nm, due to the overlap of the individual absorbance bands of DMNPB and Coum chromophores.

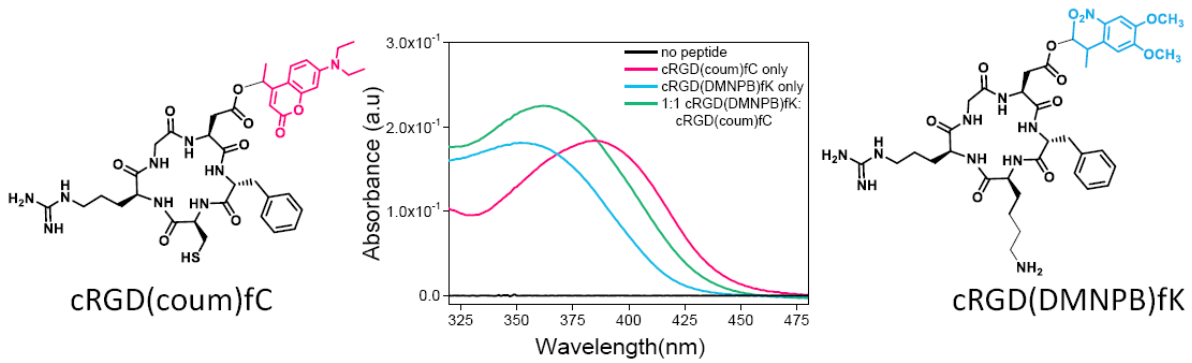

Figure 6. UV spectra of c[RGD(DMNPB)fK], c[RGD(coum)fC] and of a 1:1 mixture of both peptides in solution.

Two pathways for sequential binding were explored: (i) EDC activation and amine coupling followed by washing and then thiol binding (green curve) (ii) thiol coupling followed by washing, EDC activation and then amine binding (orange curve) (Figure 7). Both routes provided successful immobilization of the two peptides, as observed from shift in absorbance to λ_{max} 375-385 nm due to the overlapping of chromophores. This shift corresponds to the expected position for the absorbance band observed in the solution for 1:1 mixture of both chromophores (Figure 6). The one-pot coupling strategy was also tested by incubating with a solution of 1:1 peptide mixture (purple curve). The thiol coupling efficiency prevailed in this pathway but amine coupling efficiency was significantly reduced. This result is in agreement with the higher coupling efficiency in the thiol coupling observed in the previous experiments (Figure 4A).

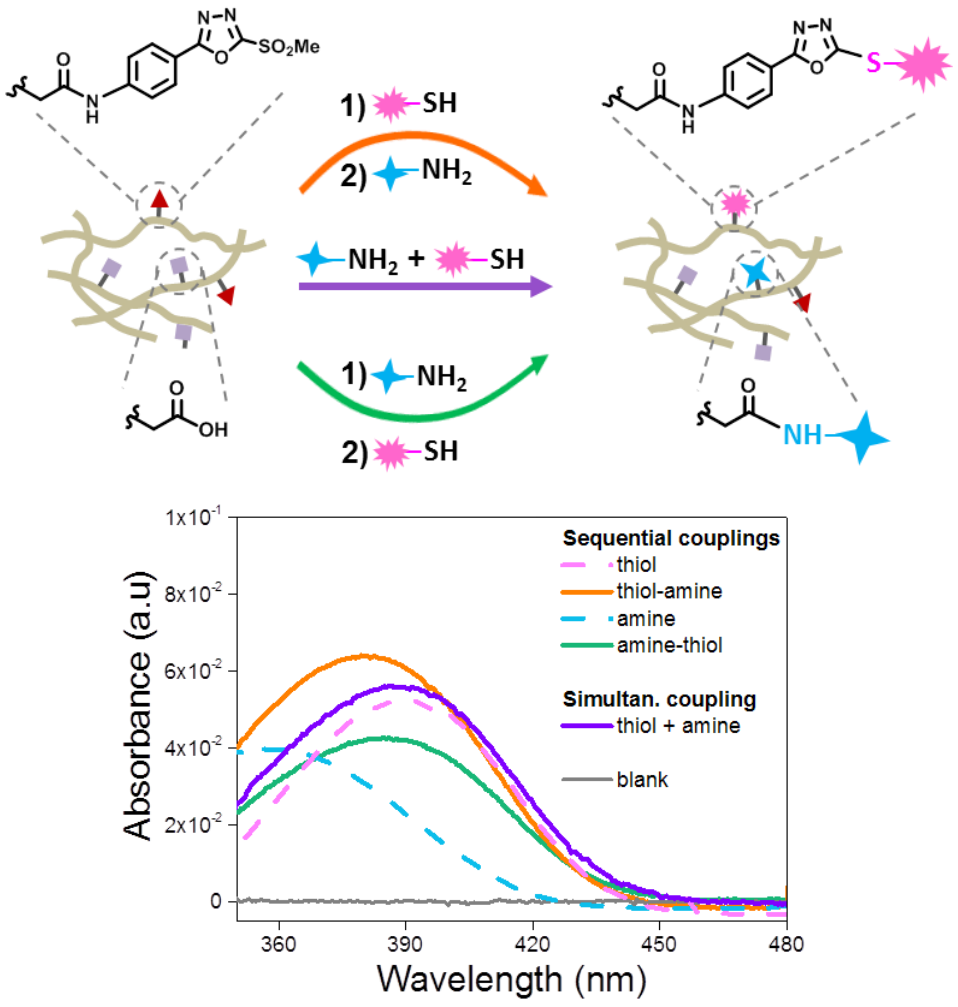

Figure 7. Reaction scheme and UV spectra of P(AAm-MS-AA) hydrogels with thiol and amine containing molecules at 1 $mgmL^{-1}$ concentration for 1h.

The bifunctional coupling was successfully extended to binding of two bulky proteins to the hydrogels. The laminin (LN) protein with Hylite fluorophore was immobilized on P(AAm-MS-AA) hydrogel by amine binding, followed by incubation with streptavidin on the surface by thiol coupling. The functional streptavidin recognized Atto-425 biotin forming color complex on the surface as demonstrated by UV absorbance curve (Figure 8).

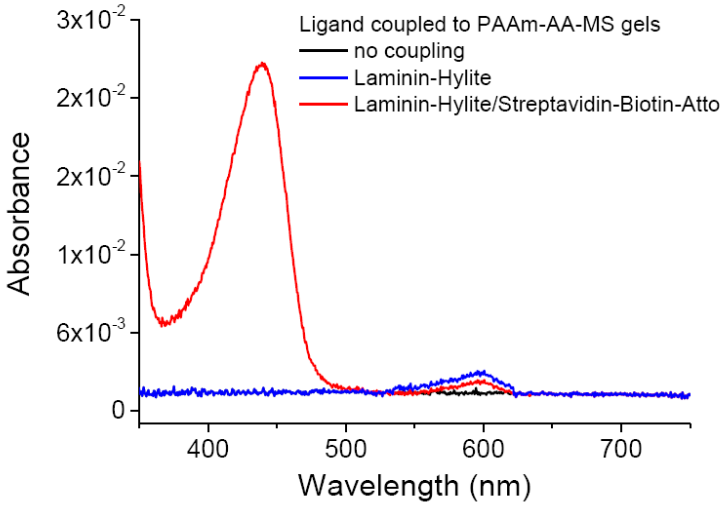

Figure 8. UV spectra of P(AAm-MS-AA) gel sequentially functionalized with laminin-Hilyte and streptavidin-biotin-Atto425.

4.4 Differentiation of neural progenitor cells on bifunctionalized P(AAm-MS-AA)

P(AAm-MS-AA) hydrogels were used as culture substrates for differentiation of neural stem cells. For this purpose, the gels were functionalized with PDL, in order to support nonspecific interaction of the neurons with the gel, and with the laminin mimetic peptide CSRARKQAASIKVAVSADR (IK-19) that supports neuronal lineage and promotes extension of neurites (Chapter 5 Section 5.2).[19] P(AAm-MS-AA) hydrogels were functionalized either by *sequential* binding or by *one-pot* coupling of a pre-mixed solution of these two molecules (Scheme 4). The P(AAm-MS-AA) hydrogels (70 kPa) were functionalized with either PDL (introduced through amine coupling after EDC/NHS activation) or IK-19 (through MS-Cys thiol conjugation).

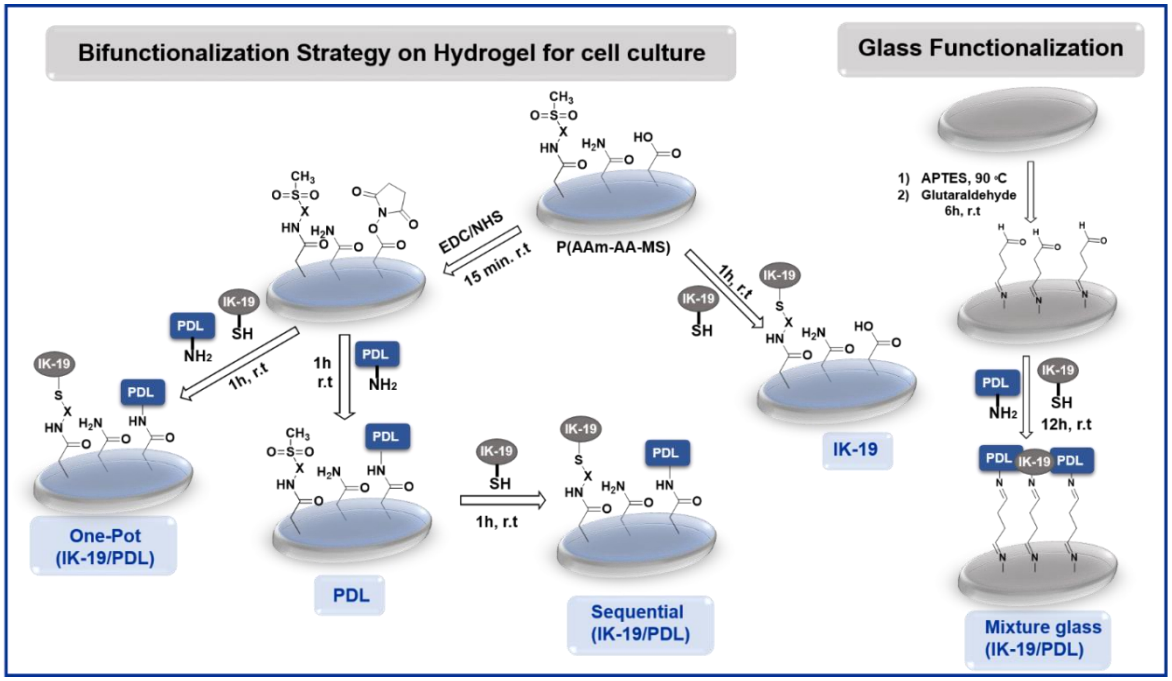

Scheme 4. The bifunctionalization route on P(AAm-MS-AA) hydrogels for NSCs culture. The IK-19 and PDL were reacted either in *sequential* binding (first PDL and then IK-19) or by *one-pot* coupling of pre-mixed IK-19/PDL.

The IK-19 peptide was coupled on the P(AAm-MS-AA) hydrogel surface by the MS groups while PDL was immobilized to the AA monomer after EDC/NHS-activation. The *one-pot coupling* was performed by incubation with a premixed solution of IK-19/PDL (10:1) after EDC/NHS activation. During *sequential* coupling, PDL was immobilized first to AA units after EDC/NHS activation, followed by washing and binding of IK-19 to MS. The used IK-19/PDL 10:1 concentration was selected from typical ratio of LN/PDL used in literature for neuronal cell culture.[20]

Neural progenitor cells (eNCPs) isolated from cerebral cortex of embryonic mouse (E 14.5) were seeded on the hydrogels. As control experiments, cortical progenitors were also cultured on glass modified with PDL/IK-19 after APTES activation and glutaraldehyde coupling. The glutaraldehyde forms imine linkage with amine side groups at the glass and at the biomolecule (Scheme 4).

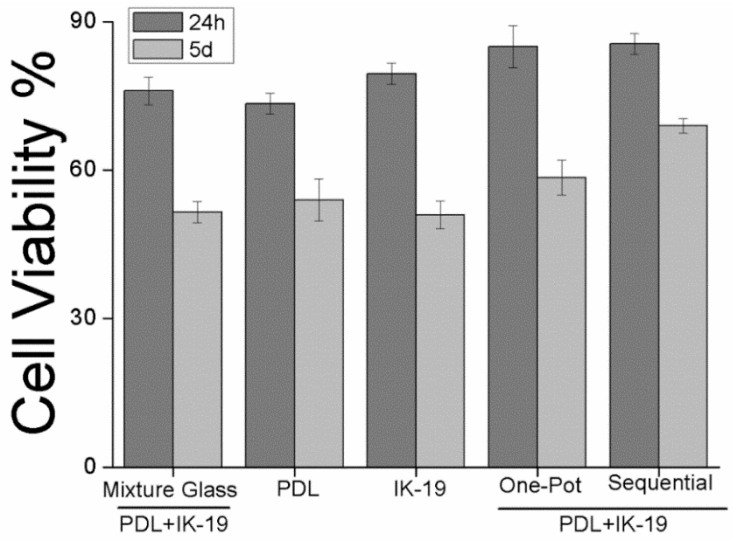

Figure 9. NPCs survival after 24h and 5 days on 70 kPa P(AAm-AA-MS) hydrogels with different surface functionalization.

Cytocompatibility was the first parameter to test the bifunctional P(AAm-MS-AA) hydrogels platform for cell culture. The cells were seeded on different functionalized surfaces and cell viability and proliferation was followed by time-lapse microscopy during 5 days. The protocols for cell culture are provided in Appendix Section 8.12.3. No notable difference in cell viability was observed after 24 h of cell culture, however after 5 days *sequential* coupling surface supported 23% higher cell survival (Figure 9) than all other conditions. Hence the significance of specific coupling and binding density is already depicted by initial experiments.

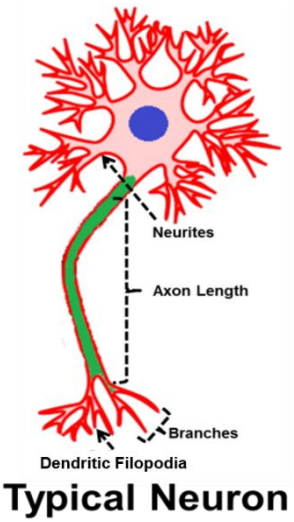

Scheme 5. Schematic representation highlighting morphological features of a typical neuron.

Neuronal differentiation was characterized by immunostaining of various morphological features on the different gels after 5 days in vitro (DIV). During neurogenesis, several processes originates from cell body called neurites. After polarization, one process differentiates into an axon and the other process are called dendrites. In addition, there are secondary branches originating from axon and dendrites termed as branches. The small actin protrusions on neurites and branches are known as dendritic filopodia or spines (Scheme 5). The dendritic filopodia are a morphological feature of neurons leading to synapsis formation and increase neuronal complexity.[21] The dendrites, branches and dendritic filopodia of one cell facilitates synapsis formation with axonal process of the other cell building a neural network. These morphological features were identified by immunostaining makers, SMI-312, DCX and DAPI. The axon is identified by SMI-312 anti-neurofilament maker which binds to neurofilaments (NF), a major part of neuronal cytoskeleton providing support to axon.[22] The doublecortin (DCX) maker binds to microtubule cytoskeleton in neurons and stains cell body, processes and branches. DCX is an early marker to identify immature neurons from glial cells, and therefore widely used to identify neurogenesis.[23] The nucleus is stained by typical nuclear marker DAPI, which binds at adenine (A)- thymine (T) nucleotides rich region in nuclear DNA.[24]

The cell differentiation features as axonal length, dendritic filopodia, number of neurites and branches were evaluated after 5d of cell culture. The axonal length remained substantially unaffected by all surface modifications (Figure 10A). However, neurite outgrowth and development of secondary branches were significantly higher in gels modified by *sequential* binding. Neurons on gels with *sequential* coupling showed enhanced multipolarity and supported a 2-fold increase in the number of branches *versus* all other conditions. In addition, neural progenitors on *sequentially* functionalized gels showed a 3-fold enhancement in the number of dendritic filopodia (Figure 10B). The improvement in neuronal features on *sequentially* coupled gels is either due to higher binding density of IK-19 or due to the chemo-selective coupling to MS. The IK-19 molecule has two lysine residues among which one is part of the IKVAV motif (the active site of the ligand), and binding through IKVAV site can lead to functional impairing of the sequence. Therefore, despite higher availability of functional groups for binding, non-selective

immobilization of IK-19 during *one-pot* coupling through amine binding apparently leads to loss of bioactivity (Figure 10C). The site selective binding, controlled surface density and bifunctional modification in P(AAm-MS-AA) hydrogels lead to advanced substrate platforms to explore and facilitate neural development in an effective, reliable and reproducible manner.

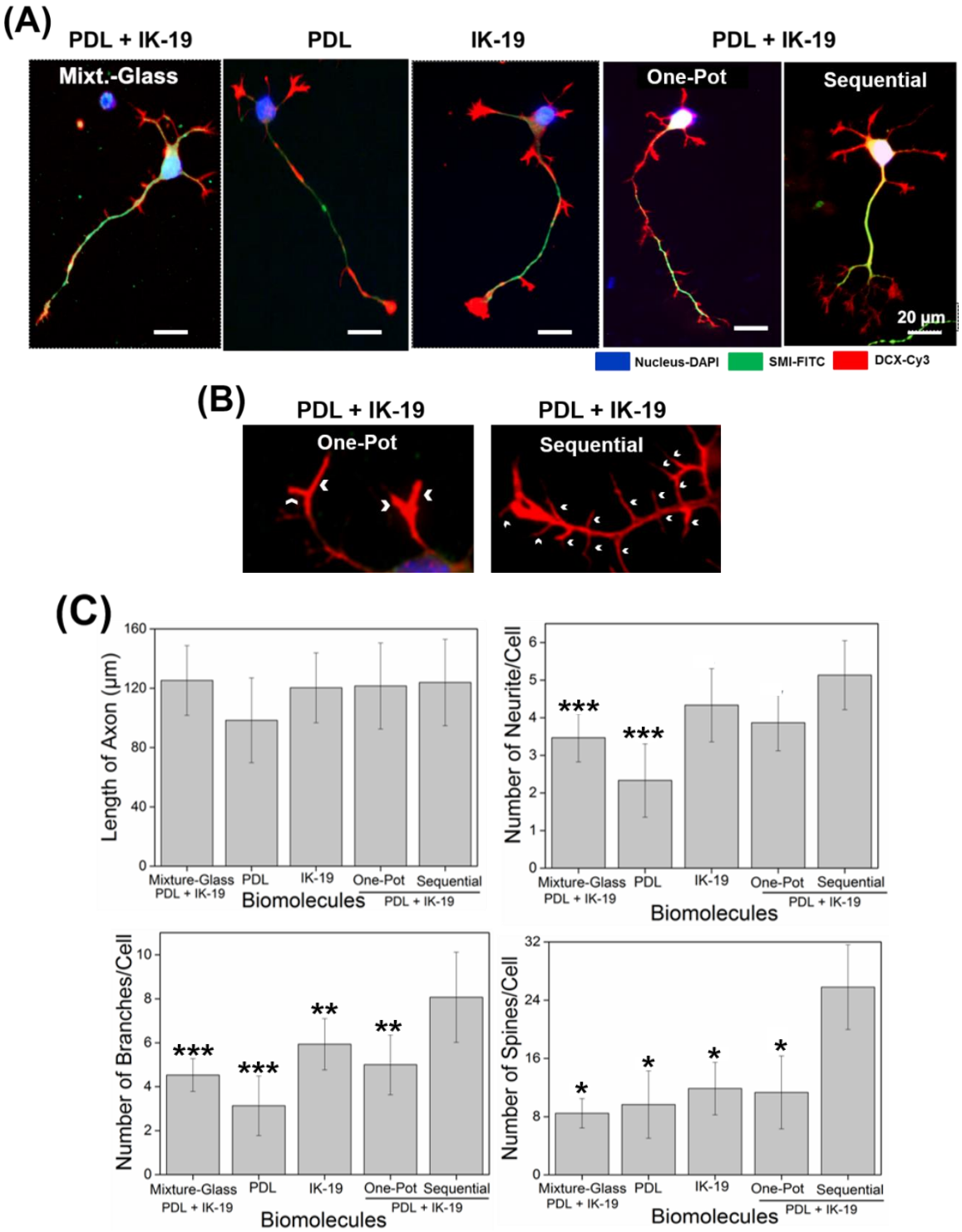

Figure 10. NPCs on 70 kPa P(AAm-MS-AA) hydrogel 5 days after cell seeding (a) Representative pictures of single neuron on different samples (b) distributions of dendritic filopodia on neurite, arrows show type of counted filopodia (c) Quantification of neuronal features. Significant differences showed in the graphics are compared against *sequential* substrate by Tukey- test (mean ± SD, ANOVA, ** p <0.01, *** p <0.001).

4.5 Influence of substrate stiffness on differentiation of neural progenitor cells culture

The soft brain tissue has low stiffness in the range of 0.1-1kPa.[7] Neuronal differentiation and growth have been shown to be favored on substrates with stiffness in the sub kPa range.[25] P(AAm-MS-AA) hydrogels with varying stiffness of 0.2 - 20 kPa and *sequential* coupling of PDL and IK-19 were used to explore the development and fate of embryonic (E 14.5) NPCs in culture. Glass slides functionalized with IK-19/PDL were used as control (stiffness in the GPa range). The neuronal cell viability on substrates with different stiffness, *sequentially* functionalized with IK-19/PDL was evaluated by time-lapse microscopy at 1 and 4 DIV. The cell viability was higher on 2kPa hydrogels after 24h and this effect was more pronounced after 4d of cell culture (Figure 11). Therefore, 2kPa hydrogel was identified as the best platform for eNPCs culture *in vitro*.

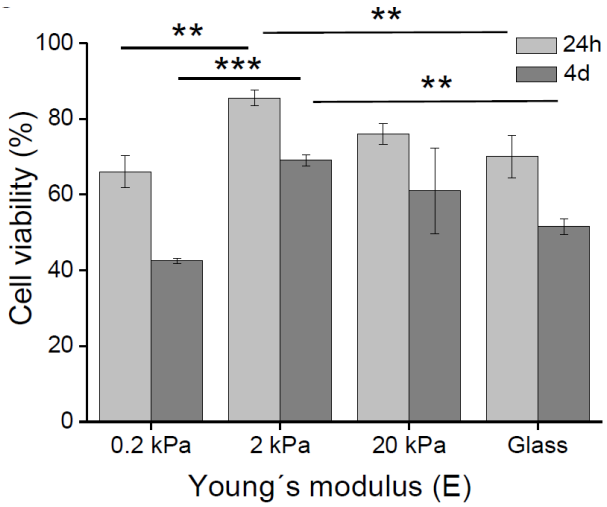

Figure 11. Cell viability of eNPCs on P(AAm-MS-AA) hydrogels of different stiffness functionalized with PDL/IKVAV (sequential coupling). The significance of 2 kPa samples was analyzed by Tukey- test (mean ± SD, ANOVA, ** p <0.01, *** p <0.001).

The neuronal morphological features (axonal length, neurites, branches and dendritic filopodia) were monitored at 4d. Axons were significantly longer on 2 kPa bifunctional hydrogel, in particular when compared to glass. This result shows the benefit of soft culture substrates for neuronal development (Figure 12A). A similar trend was observed for development of branches, with hydrogels with 2kPa showing the best performance. The sprouting of primary neurites was favored on softer substrates (0.2 – 2kPa) (Figure 12 C). Intriguingly, the density of dendritic filopodia on 2 kPa hydrogel was 3- fold higher than on the other substrates (Figure 12 B).

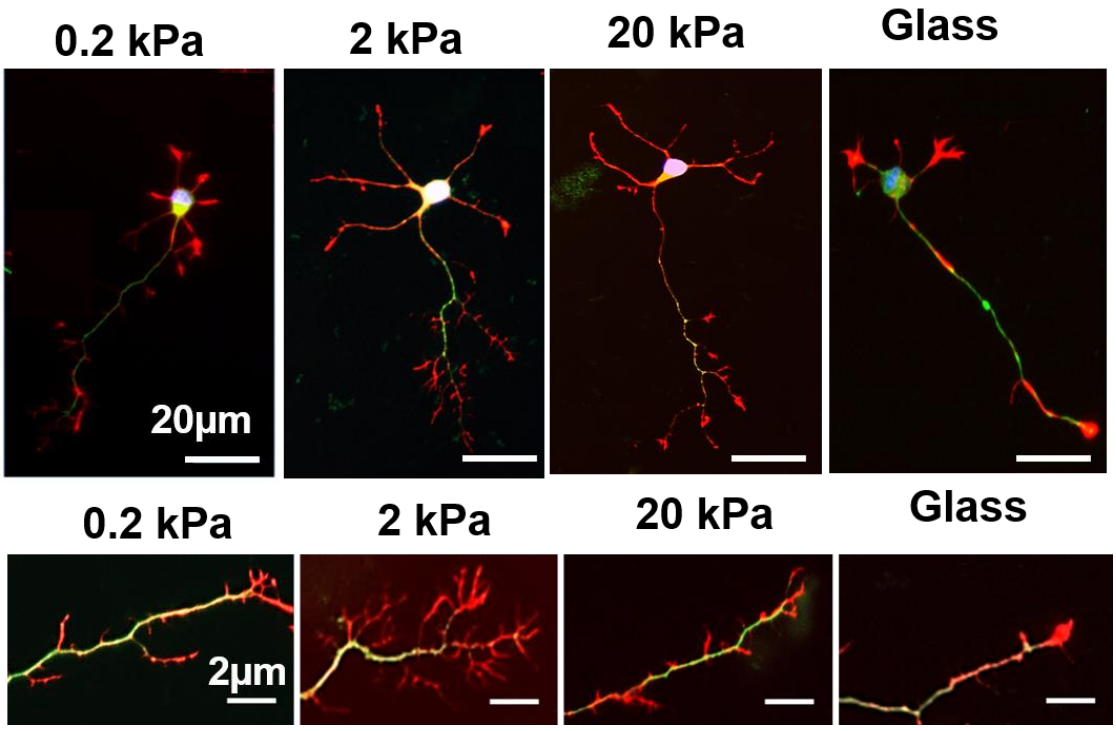

Figure 12. Representative pictures of the development of single eNPC after 5 days on substrates at different stiffness.

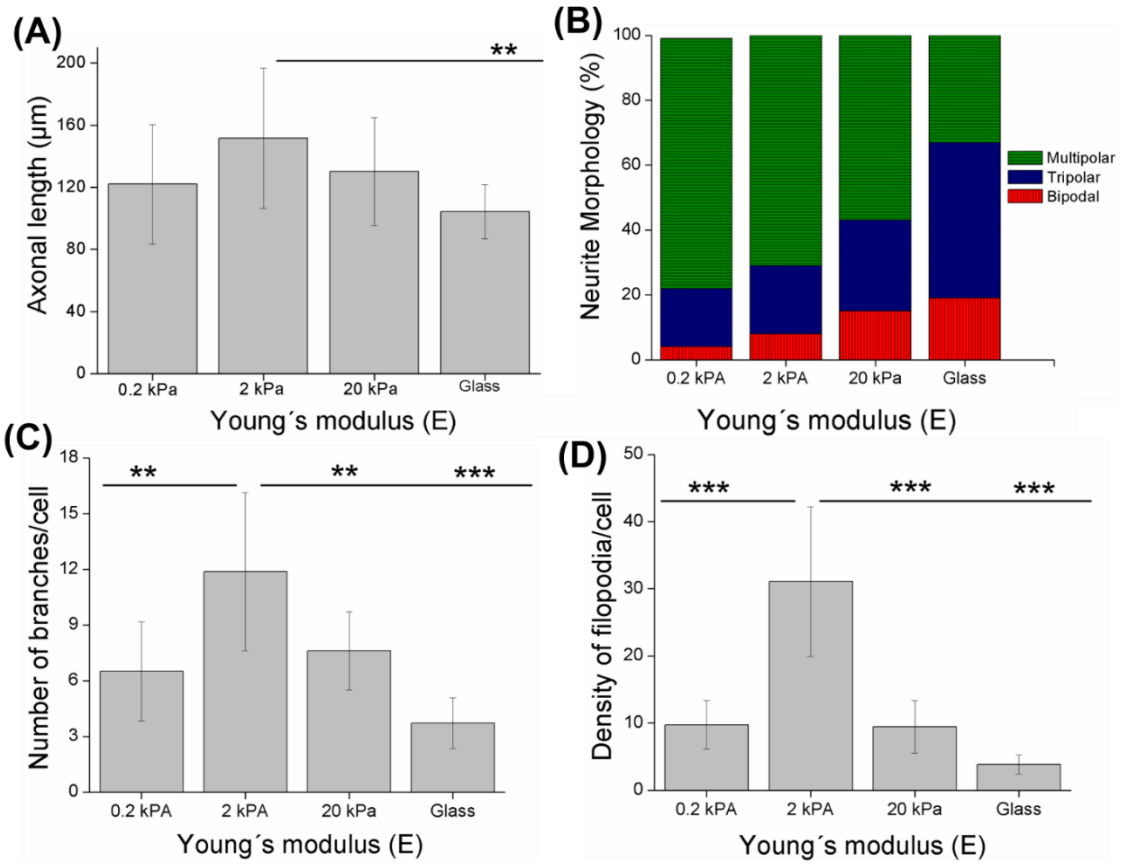

Figure 12 A-D. The Graph A-D show quantification of neuronal features. All significance was contrasted against substrates with 2 kPa (data are represented as mean ± SD, Tukey post hoc test ** p <0.01, *** p <0.001).

The neuronal morphological features obtained on 2kPa substrate with *sequential* coupling of IK-19/PDL were compared to the morphologies obtained on LN, LN/PDL, IK-19 and PDL functionalized hydrogels (2kPa). The LN/PDL was covalently bond through *sequential* coupling on hydrogel similar to IK-19/PDL functionalization. The neuronal features obtained on 2 kPa-gels bifunctionalized with IK-19/PDL were comparable to those observed on LN or LN/PDL functionalized gels, and significantly better than those observed on PDL or IK-19 functionalized samples (Figure 13). The differentiation on IK-19 and PDL samples was significantly less than on IK-19/PDL, in accordance with results observed on 70kPa hydrogels in Section 4.4, highlighting the relevance of bifunctionalization. The *sequential* coupling of LN/PDL significantly enhanced neural differentiation *versus* LN.

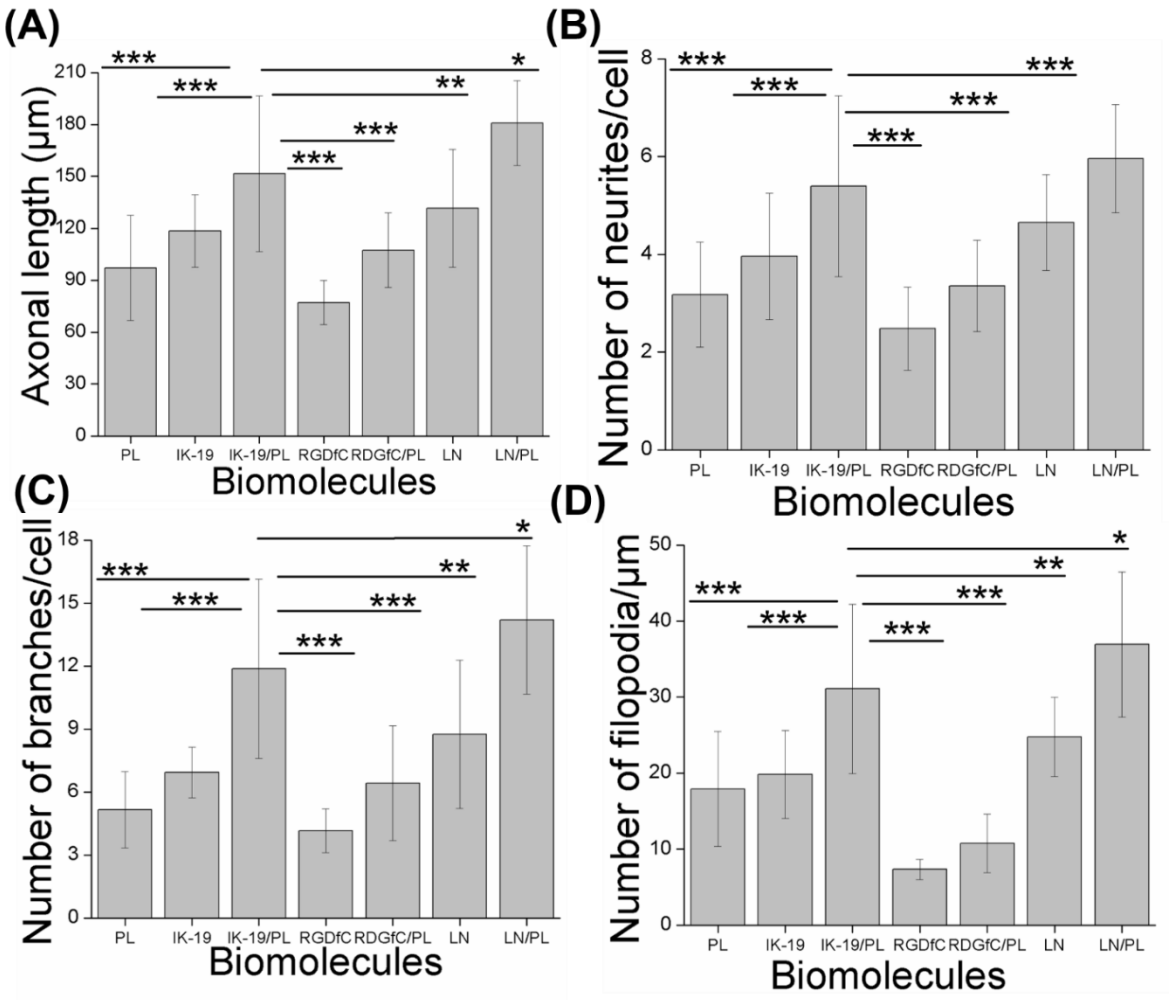

Figure 13. Comparative effect of coupling cRGDfC or IK-19 on 2 kPa hydrogels for neuronal development. Ligands were coupled to the hydrogels by *sequential* reaction. Neuronal features were analyzed after 5 days of cell cultures. The statistical significance was compared with IK-19/PDL sample and calculated by mean ± SD, ANOVA, Tukey- test ** $p < 0.01$, *** $p < 0.001$.

The improvement in neuronal morphological features on IK-19 functionalized gels is attributed to cell-integrin specific interactions. The laminin peptidomimetic IK-19 sequence is recognized by $\alpha_3\beta_1$, $\alpha_4\beta_1$ and $\alpha_6\beta_1$ classes of integrins. To emphasize the importance of IKVAV motif for neuronal differentiation, IK-19 was substituted by RGDfC adhesive motif derived from fibronectin protein.[26] The neural development on RGD and RGD/PDL samples was much lower than on IK-19/PDL samples, demonstrating the specificity of IK-19 for neurogenesis on the hydrogels (Figure 13).

This observation is further supported by immunocytochemistry results revealing the expression of β1 Integrin on cell focal adhesions. The β1 class of integrin receptor modulates neurite outgrowth in response to ECM components via activation of focal adhesion kinase.[27] The β1 integrin, upon binding with laminin, regulates microtubule assembly and stabilizes neuronal polarity and axonal development.[28] An increase expression of anti- β1 marker on axonal filament displays higher density of focal adhesions containing integrin β1 complex on IK-19 functionalized surface. Cells on IK-19/PDL substrates showed a high density of beta-1 integrin mediated focal adhesions complexes on axonal filament and neurites (Figure 14).[2a, 29] The other substrates showed very weak density of β1 strongly supporting the benefits of bifunctional modification of P(AAm-MS-AA) hydrogels. The quantification of β1 density on focal adhesion in neurites highlights the upregulation of β1 expression on IK-19/PDL substrate.

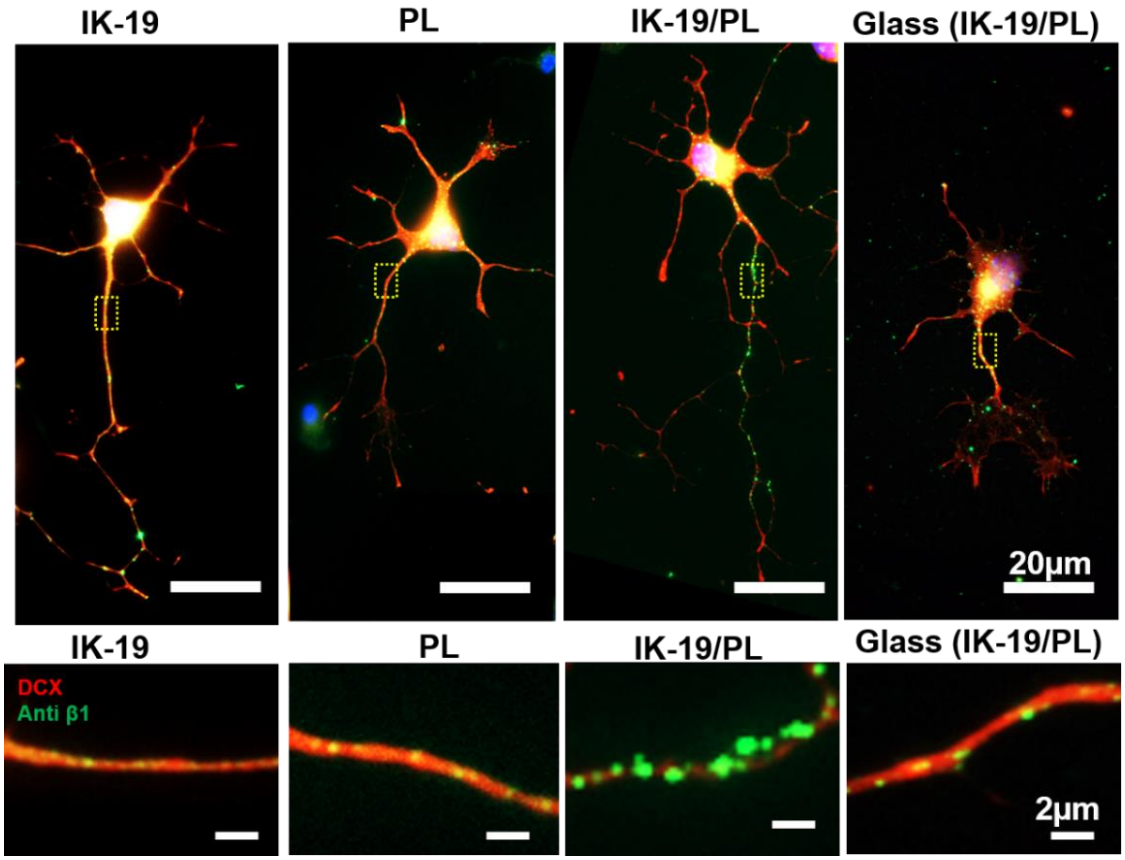

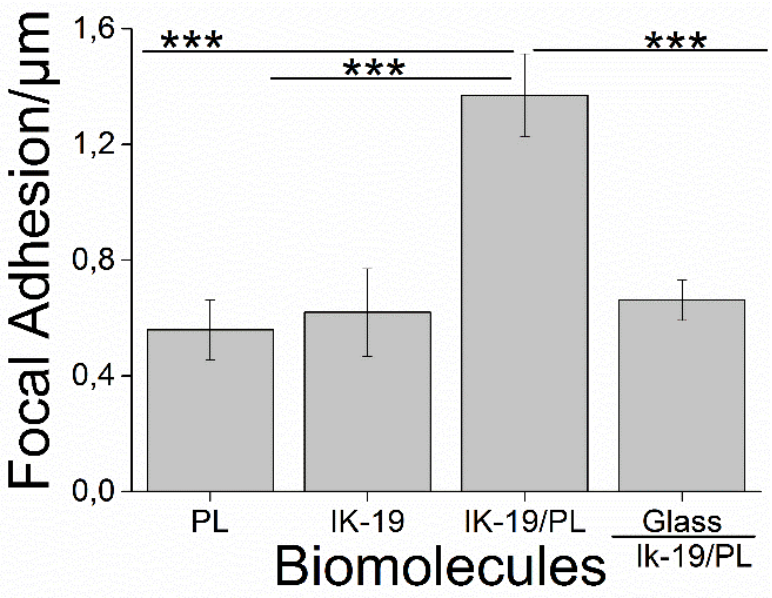

Figure 14. eNPCs culture: Representative images of neurons after 5 DIV showing an increased density of focal adhesion containing β1 along the axon on the bifunctional IK-19/PDL substrates.

4.6 Bifunctional hydrogels platform to controls fate of Adult NSCs

The bifunctional P(AAm-MS-AA) hydrogels were explored to direct cell lineage selection in adult NSCs (aNSCs) culture. aNSCs isolated from mouse subependymal zone (SEZ) can differentiate into either neuronal progenitor cell or glial progenitor cells lineage. The IKVAV motif in combination with soft substrates have been shown to favor neuronal lineage over glial proliferation.[30] [19, 31] The 20 kPa P(AAm-MS-AA) hydrogels functionalized with PDL, IK-19 and *sequentially* with IK-19/PDL and LN/PDL were tested to support neuronal lineage. Glass substrates functionalized with PDL and IK-19/PDL were used as controls, as glial lineage is expected to proliferate faster on a hard surface. The aNSCs were seeded on the substrate for 5 days and counted after immunofluorescence staining. The neurons were specifically stained by β-III tubulin, astrocytes by glial fibrillary acidic protein (GFAP) and oligodendrocytes by NG2 antibodies. The percentage of each cell type was quantified in all substrates by taking images with epifluorescence microscope and counting the number of different cell types.

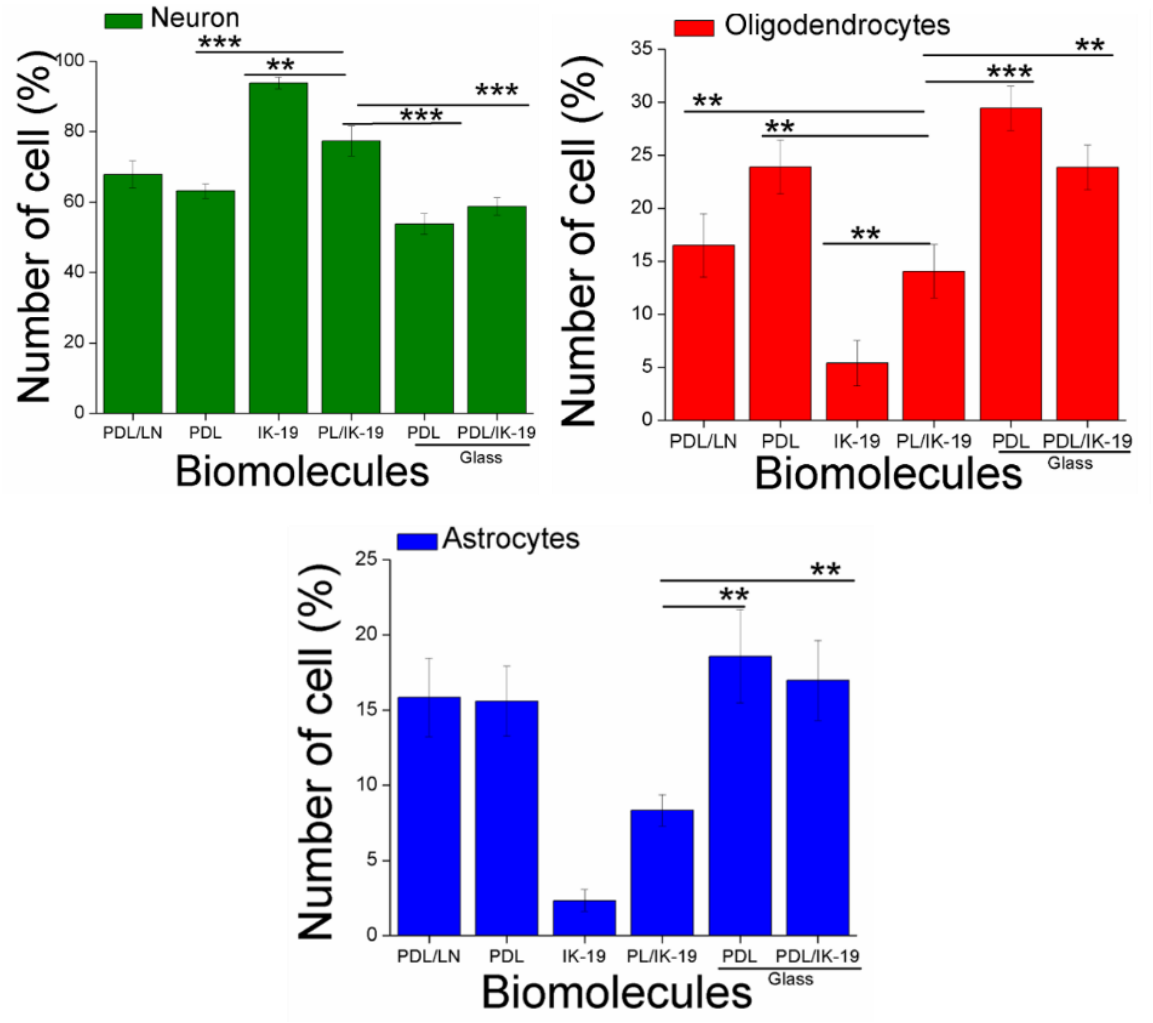

Figure 15. aNSCs on 2kPa P(AAm-AA) hydrogel: Percentage of neurons, oligodendrocytes and astrocytes in aNSCs cultures after 5 DIV on 20 kPa gel substrates. Data are represented as mean ± SD, Tukey-test ** p <0.01, *** p <0.001.

The IK-19 modified hydrogel preferentially promoted neuronal cell fate, while the presence of PDL in IK-19/PDL hydrogels led to an increase in the percentage of glial lineages (i.e. astrocytes and oligodendrocytes). The neuronal lineage on IK-19 substrate was in response to IKVAV motif as reported in literature.[2c, 25b, 31-32] No significant difference in neuronal lineage was observed in cultures on IK-19/PDL and LN/PDL modified hydrogels, although LN/PDL sample also supported proliferation of glial cells (Figure 15). The higher stiffness of glass samples supported glial lineage. In conclusion, IK-19 in combination with soft substrates exclusively supports neuronal lineage in aNSCs cultures.

4.7 Conclusions

The differentiation and fate of neural progenitor cells are crucial for development and regeneration of brain. The role of ECM-cell interactions in the differentiation of progenitor cells can be investigated by using P(AAm-MS-AA) model substrates functionalized with relevant ligands of the brain ECM. The P(AAm-MS-AA) hydrogels facilitated coupling of amine and thiol containing compounds with high chemical selectivity, efficiency and functionality. The laminin peptidomimetic IK-19 and the positively charged PDL were sequentially coupled to P(AAm-MS-AA) hydrogels of varied stiffness (0.2 - 70 kPa). The coupling of two biomolecules using two independent and orthogonal coupling chemistries on the same surface provided bifunctional ligation that efficiently supported the neural development studies in a controlled and reliable manner. Instead of simple mixing and coating on the surfaces, orthogonally controlled coupling and adjusted mechanical cues supported the maturation of progenitors. The orthogonal coupling enhanced cell viability and accelerated differentiation of embryonic cortical progenitor stem cells into mature neuron in *in vitro* cultures by regulating the chemical and mechanical cues. This platform directed the fate of SEZ aNSCs into neuronal linage and promoted neuronal proliferation and maturation. The regeneration of brain requires repopulation of NSCs and their differentiation into neuronal lineage at the site of injury. This bifunctional platform is an ideal *in vitro* model to selectively direct neuronal lineage amplification and differentiation.

References

[1] M. Dihné, C. Bernreuther, M. Sibbe, W. Paulus, M. Schachner, *Journal of Neuroscience* **2003**, *23*, 6638-6650.

[2] aM. Nomizu, W. H. Kim, K. Yamamura, A. Utani, S.-Y. Song, A. Otaka, P. P. Roller, H. K. Kleinman, Y. Yamada, *Journal of Biological Chemistry* **1995**, *270*, 20583-20590; bE. Hohenester, P. D. Yurchenco, *Cell adhesion & migration* **2013**, *7*, 56-63; cS. Raghavan, R. R. Gilmont, K. N. Bitar, *Biomaterials* **2013**, *34*, 6649-6658.

[3] aS. Joo, J. Y. Kim, E. Lee, N. Hong, W. Sun, Y. Nam, *Scientific reports* **2015**, *5*, 13043; bM. Pacifici, F. Peruzzi, *JoVE (Journal of Visualized Experiments)* **2012**, e3965-e3965; cJ. Li, D. Feng, Y. Huang, F. Ye, *Zhongguo xiu fu chong jian wai ke za zhi= Zhongguo xiufu chongjian waike zazhi= Chinese journal of reparative and reconstructive surgery* **2010**, *24*, 172-179.

[4] M. Ho, D. Yu, M. C. Davidsion, G. A. Silva, *Biomaterials* **2006**, *27*, 4333-4339.

[5] A. Farrukh, J. I. Paez, M. Salierno, W. Fan, B. Berninger, A. del Campo, *Biomacromolecules* **2017**, *18*, 906-913.

[6] aA. K. Denisin, B. L. Pruitt, *ACS applied materials & interfaces* **2016**, *8*, 21893-21902; bB. Trappmann, J. E. Gautrot, J. T. Connelly, D. G. T. Strange, Y. Li, M. L. Oyen, M. A. Cohen Stuart, H. Boehm, B. Li, V. Vogel, J. P. Spatz, F. M. Watt, W. T. S. Huck, *Nat. Mater.* **2012**, *11*, 642-649; cR. S. Fischer, K. A. Myers, M. L. Gardel, C. M. Waterman, *Nature protocols* **2012**, *7*, 2056-2066; dA. J. Engler, S. Sen, H. L. Sweeney, D. E. Discher, *Cell* **2006**, *126*, 677-689.

[7] B. Mammadov, M. Sever, M. O. Guler, A. B. Tekinay, *Biomaterials Science* **2013**, *1*, 1119-1137.

[8] aK. Franze, J. Gerdelmann, M. Weick, T. Betz, S. Pawlizak, M. Lakadamyali, J. Bayer, K. Rillich, M. Gögler, Y. B. Lu, A. Reichenbach, P. Janmey, J. Käs, *Biophysical Journal* **2009**, *97*, 1883-1890; bY. B. Lu, K. Franze, G. Seifert, C. Steinhäuser, F. Kirchhoff, H. Wolburg, J. Guck, P. Janmey, E. Q. Wei, J. Käs, A. Reichenbach, *Proceedings of the National Academy of Sciences of the United States of America* **2006**, *103*, 17759-17764; cP. C. Georges, W. J. Miller, D. F. Meaney, E. S. Sawyer, P. A. Janmey, *Biophysical Journal* **2006**, *90*, 3012-3018.

[9] aP. Moshayedi, L. Da F Costa, A. Christ, S. P. Lacour, J. Fawcett, J. Guck, K. Franze, *Journal of Physics Condensed Matter* **2010**, *22*; bJ. M. Stukel, R. K. Willits, *Tissue Engineering - Part B: Reviews* **2016**, *22*, 173-182; cJ. Lantoine, T. Grevesse, A. Villers, G. Delhaye, C. Mestdagh, M. Versaevel, D. Mohammed, C. Bruyère, L. Alaimo, S. P. Lacour, L. Ris, S. Gabriele, *Biomaterials* **2016**, *89*, 14-24.

[10] aC. Pande, A. Sharma, *Journal of applied polymer science* **2002**, *84*, 2613-2620; bV. Damljanovic, B. C. Lagerholm, K. Jacobson, *BioTechniques* **2005**, *39*, 847; cP. Moshayedi, L. da F Costa, A. Christ, S. P. Lacour, J. Fawcett, J. Guck, K. Franze, *Journal of Physics: Condensed Matter* **2010**, *22*, 194114; dT. Grevesse, M. Versaevel, G. Circelli, S. Desprez, S. Gabriele, *Lab on a Chip* **2013**, *13*, 777-780; eJ. H. Wen, L. G. Vincent, A. Fuhrmann, Y. S. Choi, K. C. Hribar, H. Taylor-Weiner, S. Chen, A. J. Engler, *Nat. Mater.* **2014**, *13*, 979-987.

[11] O. F. Zouani, J. Kalisky, E. Ibarboure, M.-C. Durrieu, *Biomaterials* **2013**, *34*, 2157-2166.

[12] A. Farrukh, J. I. Paez, M. Salierno, A. del Campo, *Angewandte Chemie* **2016**, *128*, 2132–2136.

[13] aM. Karow, R. Sánchez, C. Schichor, G. Masserdotti, F. Ortega, C. Heinrich, S. Gascón, M. A. Khan, D. C. Lie, A. Dellavalle, *Cell stem cell* **2012**, *11*, 471-476; bF. Ortega, S. Gascon, G. Masserdotti, A. Deshpande, C. Simon, J. Fischer, L. Dimou, D. C. C. Lie, T. Schroeder, B. Berninger, *Nat Cell Biol* **2013**, *15*, 602-+.

[14] A. Louvi, S. Artavanis-Tsakonas, *Nature Reviews Neuroscience* **2006**, *7*, 93-102.

[15] S. Weis, Z. Shafiq, R. A. Gropeanu, A. del Campo, *Journal of Photochemistry and Photobiology A: Chemistry* **2012**, *241*, 52-57.
[16] M. J. Fischer, *Surface plasmon resonance: methods and protocols* **2010**, 55-73.
[17] N. Dafader, M. Adnan, M. Haque, D. Huq, F. Akhtar, *African Journal of Pure and Applied Chemistry* **2011**, *5*, 111-118.
[18] S. Petersen, J. M. Alonso, A. Specht, P. Duodu, M. Goeldner, A. del Campo, *Angew Chem Int Ed Engl* **2008**, *47*, 3192-3195.
[19] X. Li, X. Liu, B. Josey, C. J. Chou, Y. Tan, N. Zhang, X. Wen, *Stem Cells Transl Med* **2014**, *3*, 662-670.
[20] W. Ma, T. Tavakoli, E. Derby, Y. Serebryakova, M. S. Rao, M. P. Mattson, *BMC developmental biology* **2008**, *8*, 90.
[21] N. E. Ziv, S. J. Smith, *Neuron* **1996**, *17*, 91-102.
[22] N. Ulfig, J. Nickel, J. Bohl, *Cell and tissue research* **1998**, *291*, 433-443.
[23] J. G. Gleeson, P. T. Lin, L. A. Flanagan, C. A. Walsh, *Neuron* **1999**, *23*, 257-271.
[24] A. Coleman, M. Maguire, J. Coleman, *Journal of Histochemistry & Cytochemistry* **1981**, *29*, 959-968.
[25] aH. Lv, L. Li, Y. Zhang, Z. Chen, M. Sun, T. Xu, L. Tian, M. Lu, M. Ren, Y. Liu, Y. Li, *Cell and Tissue Research* **2015**, *361*, 657-668; bW. Sun, T. Incitti, C. Migliaresi, A. Quattrone, S. Casarosa, A. Motta, *Journal of tissue engineering and regenerative medicine* **2017**, *11*, 1532-1541.
[26] M. Aumailley, M. Gurrath, G. Müller, J. Calvete, R. Timpl, H. Kessler, *FEBS letters* **1991**, *291*, 50-54.
[27] X. Wu, D. S. Reddy, *Pharmacology & therapeutics* **2012**, *134*, 68-81.
[28] W.-L. Lei, S.-G. Xing, C.-Y. Deng, X.-C. Ju, X.-Y. Jiang, Z.-G. Luo, *Cell research* **2012**, *22*, 954-972.
[29] E. Agius, Y. Sagot, A. Duprat, P. Cochard, *Neuroscience* **1996**, *71*, 773-786.
[30] J. M. Stukel, R. K. Willits, *Tissue Engineering Part B: Reviews* **2016**, *22*, 173-182.
[31] G. A. Silva, C. Czeisler, K. L. Niece, E. Beniash, D. A. Harrington, J. A. Kessler, S. I. Stupp, *Science* **2004**, *303*, 1352-1355.
[32] J. M. Banks, L. C. Mozdzen, B. A. C. Harley, R. C. Bailey, *Biomaterials* **2014**, *35*, 8951-8959.
[33] F. Ortega, S. Gascón, G. Masserdotti, A. Deshpande, C. Simon, J. Fischer, L. Dimou, D. C. Lie, T. Schroeder, B. Berninger, *Nat Cell Biol* **2013**, *15*, 602-613.
[34] aF. Ortega, M. R. Costa, T. Simon-Ebert, T. Schroeder, M. Götz, B. Berninger, *Nature protocols* **2011**, *6*, 1847-1859; bO. Hilsenbeck, M. Schwarzfischer, S. Skylaki, B. Schauberger, P. S. Hoppe, D. Loeffler, K. D. Kokkaliaris, S. Hastreiter, E. Skylaki, A. Filipczyk, *Nature biotechnology* **2016**, *34*, 703-706.

Chapter 5

Photo-activatable Laminin Peptidomimetics for Directional Neuronal Growth

5.1 Introduction

Neural injuries due to trauma, accidents or neurodegenerative diseases are critical due to low self-regenerative ability of brain.[1] Neural regeneration therapies are mainly based on stem cell transplant at the injury site.[2] In addition to grafting and generation of new born cells at the injured area, neurons need to grow and wire in spatially defined manner so that information transfer occurs in the proper direction. Therefore neural regeneration does not only require generation of new-born cells, but also oriented axonal re-branching and directional synapses formation between adjacent neurons.[3] *In vivo,* directionality for axon extension is provided by the spatial arrangement of adhesive proteins (i.e. Laminin) of the extracellular matrix (ECM), neighboring cells in the neural microenvironment, and gradients of soluble growth factors.[4] Laminin is an abundant adhesive protein in neuronal ECM, fundamental for neural migration, differentiation and neurite development.[5] Different integrin membrane receptors present in neural cells can bind to Laminin, such as $\alpha_6\beta_1$, $\alpha_7\beta_1$, $\alpha_3\beta_1$ and $\alpha_4\beta_1$.Therefore, spatial organization of Laminin is an appropriate route to direct axon growth.[6]

The IKVAV peptide sequence is present at the globular region of the α-chain in Laminin-1 protein and interacts with integrin receptors $\alpha_3\beta_1$, $\alpha_4\beta_1$ and $\alpha_6\beta_1$[7]. When immobilized on the culture plate, this peptide has been shown to stimulate neurite growth, branching and maturation of neurons.[8] This peptide is frequently used as adhesive ligand for neuronal cultures to replace Laminin.[9] In order to spatially arrange adhesive proteins or peptides, different methods have been applied, such as microcontact printing, electro-spinning or photopatterning.[4, 9-10] The group of A. del Campo pioneered the use of photoactivatable groups to control the activity of surface bounded RGD cell adhesive peptide at cell friendly wavelengths and generate light-triggered micropatterns of adhesive proteins to guide cell attachment and migration.[11] In this chapter, this approach is particularized for the IKVAV peptide.

A non-cell adhesive IKVAV derivative containing a photocleavable protecting group was developed. Upon exposure to light at appropriate wavelength and intensity, the chromophore can be removed from the peptide and activity can be restored (Chapter 2 Section 2.3 - 2.5). The photo-activatable Laminin mimetic peptides will be used to control the directionality over the spatial localization and activity of neurons in artificial matrices. The soft polyacrylamide gels described in Chapter 4 Section 4.2-4.3 will be used in these studies.[12] In this chapter the activity of photoactivatable Laminin peptidomimetics for supporting neural progenitor cell culture and their ability to spatiotemporally control neuronal cell attachment and development is described.

5.2 Bioactivity of Laminin Peptidomimetics

5.2.1 Bioactivity of IKVAV variants

Different Laminin peptidomimetics including the sequence IKVAV were presented in Chapter 2 Section 2.2.1 as possible candidates with improved water solubility *versus* the short hydrophobic IKVAV sequence. All these variants were coupled to P(AAm-*co*-AA) hydrogels and their ability to support neuronal differentiation was tested. These studies will display how aggregation effects observed in Chapter 2 Section 2.2.1 Table 1 influence the bioactivity of the immobilized ligand and consequently the integrin binding and the attachment of cells.

Soft 2 kPa P(AAm-*co*-AA) hydrogels were selected for these studies, based on experiments showing positive effects of soft hydrogels in supporting neuronal development in Chapter 4, Section 4.5.[13] Coupling of the Laminin peptidomimetics to the pendent carboxyl groups of the hydrogel was performed as described in Chapter 4 Section 4.4 and Appendix Section 8.5.3. Control substrates functionalized with standard LN and LN/PDL functionalized hydrogels were also prepared. Neural progenitor cells (eNPCs) isolated from cortex of mouse embryo (E 14.5) were seeded on the functionalized gels for 24 h and cell development was followed by imaging and quantifying typical neuronal features analogously as described in Chapter 4 section 4.4.

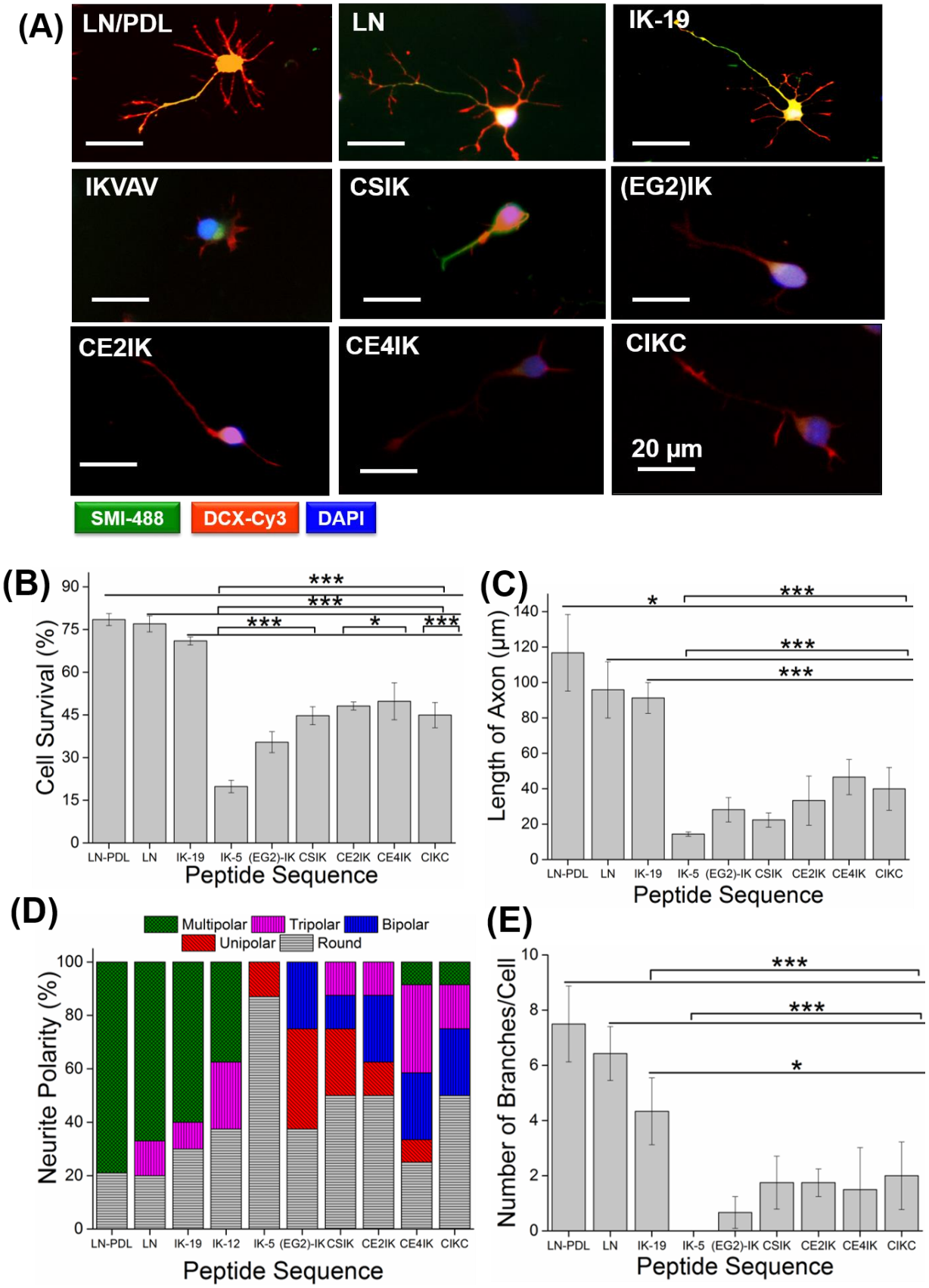

Figure 1. Morphological analysis of neural progenitor cells (E 14.5) seeded on 2 kPA P(AAm-*co*-AA) hydrogel functionalized with Laminin derived peptidomimetic

sequences. (A) Immunofluorescence images of representative cells on different peptide modified hydrogels, Quantification of neuronal morphological parameters (B) cell survival (C) length of axon, (D) neurites polarity and (E) number of branches, after 24 h of cell culture. The DCX stains cell body, SMI marks axonal filament and nucleus is stained by DAPI. The significance of data obtained for the different samples was analysed by Tukey- test (mean ± SD, ANOVA, ** $p < 0.01$, *** $p < 0.001$) and compared to LN/PDL, LN and IK-19 controls.

Hydrogels modified with IK-19 support neuronal survival and developed typical neuronal morphological features as long axon, multipolar neurites and dendrites at comparable levels to typical LN and LN/PDL substrates (Figure 1). The cells seeded on substrates functionalized with all other Laminin peptides showed significantly lower viability and very poor development of the neuronal phenotype. The formation of aggregates, which was found to be particularly strong in IKVAV (Chapter 2, Table 1), presumably hinders effective coupling of the peptides to the surface. Although the addition of ethylene glycol chain in (EG_2)-IK and the polar amino acid in CSIK improved solubility (Table 1) and bioactivity, the obtained results were not comparable to IK-19 modified gels. These variants enhanced the cell viability in comparison with IKVAV, but no significant development of neurites or branches were observed (Figure 1). CE2IK and CE4IK peptides, with negatively charged amino acids included in their sequences, were most effective in reducing the size of the aggregates (Chapter 2, Table 1), although aggregation was not completely prevented. However, these sequences showed poor cell viability, a major percentage of unipolar phenotypes and very less branching. This low bioactivity might be attributed to net negative charge on these peptides, which could lead to repulsion of the negatively charged cell membrane and hinder the interaction of the Laminin ligands with the integrins at the membrane.[14] The positively charged CIKC with large aggregates in DLS studies (Chapter 2, Table 1) showed low cell viability, short axonal process, less branches and mostly bipolar neurites (Table 1). However, in general the results with CIKC were better than on negatively charged more water solubility variants.

Table 1. Quantification of NPCs differentiation parameters on hydrogels modified with the different Laminin peptidomimetics. Results on LN and LN/PDL modified hydrogels are also included.

Peptide Sequence	Net charge on peptide (pH 7.0)	Cell survival (%)	Number of process	Number of branches	Axonal length
IKVAV	1	19.87	1.0	0.0	14.40
(EG_2)-IKVAV	1	35.43	1.4	0.66	28.14
CSIKVAV	0.9	44.73	2.0	1.75	22.37
CEEIKVAV	-1.1	48.15	1.75	1.75	33.33
CEEEIKVAV	-3.1	49.79	2.55	1.77	42.46
CCRRIKVAVWLC	2.8	44.95	2.66	1.83	43.24
CSIKVAVSADR	0.9	68.75	4.0	4.8	77.57
CSRARKQAASIKVAVSADR	3.9	71.14	4.42	4.33	91.22
LN	-	77.0	4.87	6.42	95.86
LN/PDL	-	78.5	6.37	7.5	116.77

IK-12, a shorter version of IK-19 lacking the positively charged amino acids, showed comparable bioactivity to IK-19 and supported significantly higher cell viability than all other IKVAV variants (Table 1). On IK-12 ~50% cells develop multipolar neurites and multiple branches, the characteristics neuronal features.

The time scales for the development of the different phenotypic features on IKVAV, IK-12 and IK-19 was analyzed by time-lapse microscopy (Figure 2). Cells on IK-19 and IK-12 attached within 4h of culture and extend neurites. Cells showed axonal differentiation and develop dendrites and dendritic filopodia within 1DIV.

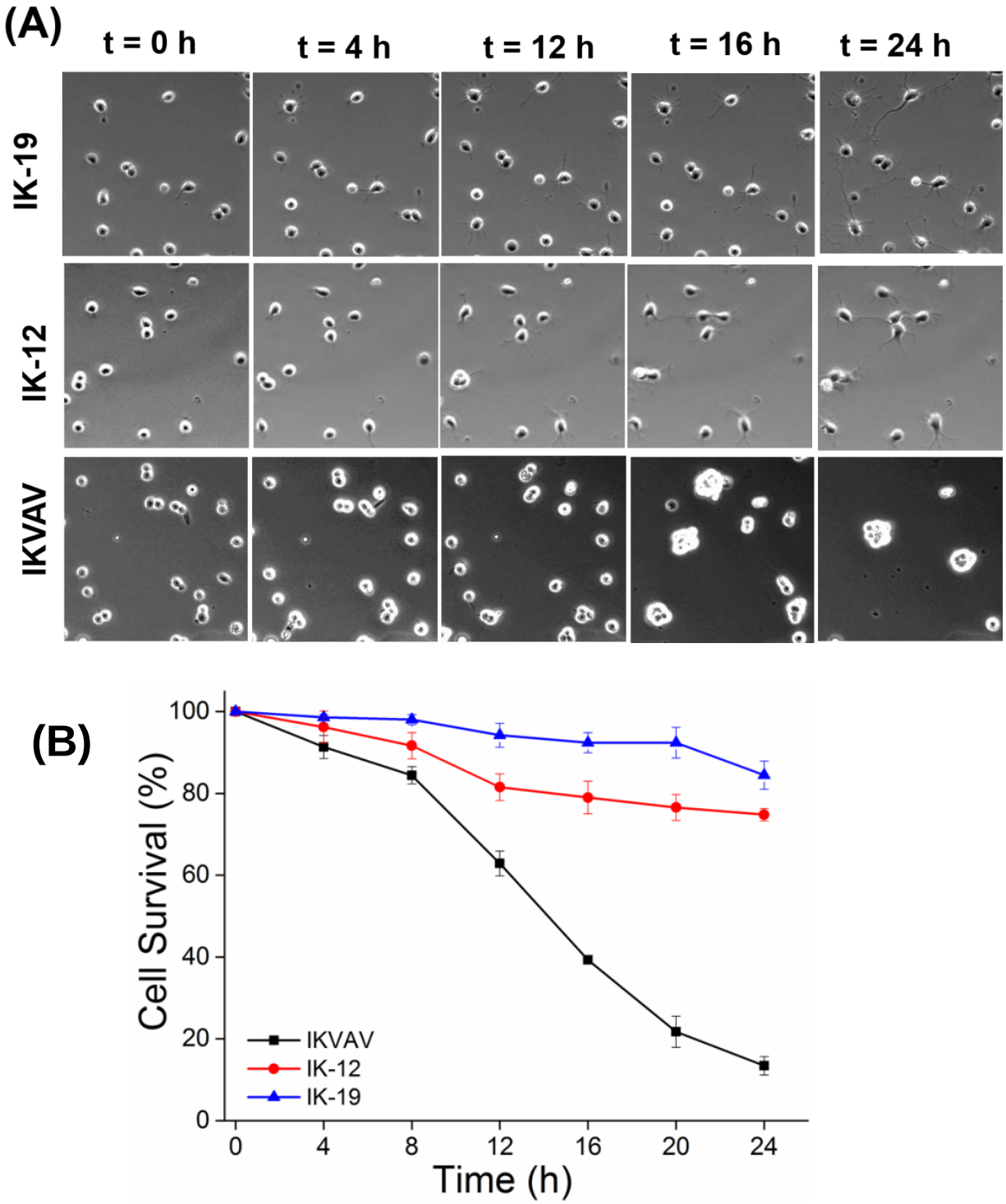

Figure 2. Comparison of the bioactivity of embryonic NPCs culture (E-14.5) on P(AAm-*co*-AA) gels (2 kPa) modified with IKVAV, IK-12 and IK-19 during 24 hours (A) Time-lapse images showing neural development at regular intervals (B) cell survival percentage with time.

5.2.2 Bioactivity of IK-12 photoactivatable variants

The photoactivatable Laminin peptidomimetics described in Chapter 2 Section 2.3 were tested to confirm the inhibition of activity in the caged forms and the restoration of activity upon light exposure. In the initial experiments, the negative peptide sequence CASIEVAVSADR (IE-12), where lysine (K) was replaced by glutamate (E), was tested.[15] Hydrogels functionalized with IE-12 failed to support NPCs. Cell survival decreased to 28% (Figure 3), the differentiation of neurites was strongly retarded, and the ability to trigger axonal process was lost in comparison to cells cultured on IK-12 and IK-19 modified gels.[15] This shows that the lysine residue of the IKVAV epitope is crucial for the integrin recognition and deactivation of IK-12. The suitability of caging IK-12 by introducing modifications at the Lys position is therefore confirmed.

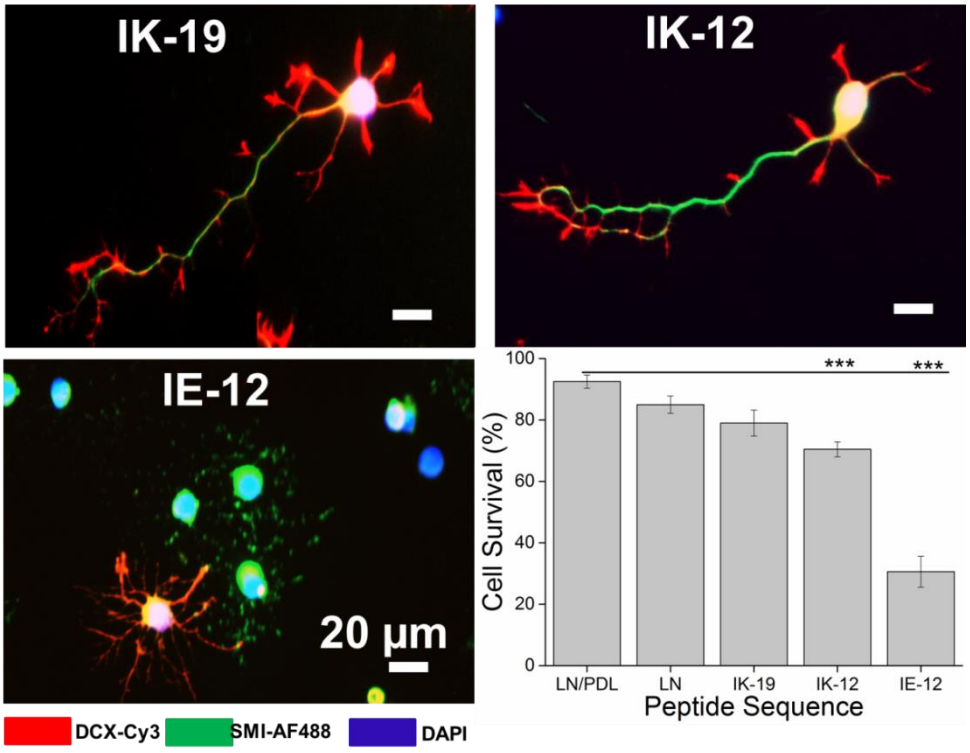

Figure 3. Embryonic NPCs (E-14.5) on 2 kPa P(AAm-*co*-AA) hydrogels modified with IK-12, IK-19 and IE-12 (A) Immunofluorescence images of cells, (B) Cell survival on different substrates 24h after seeding. The significance of 2 kPa samples was analyzed by Tukey- test (mean ± SD, ANOVA, ** p <0.01, *** p <0.001) in comparison with LN/PDL substrates.

The ability of the photoactivatable peptides IK-12(NVOC), IK-12(DMNPB) and IK-12(HANBP) described in Chapter 2 Section 2.3 to photo-trigger neuronal differentiation was tested. Neural progenitor cells (eNPCs) were seeded on 2 kPa P(AAm-*co*-AA) hydrogels functionalized with the caged IK-12 peptides. Only few cells attached on caged substrates, confirming the inhibition of the bioactivity of the peptides as a consequence of the introduction of the chromophore in the Lys rest. Cell viability was poor (19-28%), similar to the values observed on hydrogels modified with the IE-12 peptide (Table 2). The functionalized hydrogels were irradiated for 15 min at λ_{max}: 345 nm for NVOC, 365 nm for DMNPB, and 420 nm for HANBP chromophore in order to activate the immobilized peptide by photocleavage of the chromophore. Cells attached to the irradiated samples (Figure 4A), indicate effective light-triggered activation of peptide functionality. Moreover, cells seeded on the photoactivated substrates showed cell survival ratios (61-63%) close to those observed in IK-12 modified samples (Table 2). IK-12(HANBP) proved to be more effective than the other caged analogues, giving statistically the highest difference among samples before and after irradiation.

Table 2: Quantification of NPCs differentiation on thin gels (P(AAm-co-AA) hydrogels functionalized with different peptides.

Peptide Sequence	Cell Survival (%)	Number of Process	Number of Branches	Length of axon (μm)	Number of spines
IK-19	79.05	5.42	8.3	122.42	17.6
IK-12	70.45	5.15	6.8	111.66	13.8
IK-12(NVOC)	26.18	0.8	0.4	15.00	0.6
IK-12(NVOC) Irradiated	63.65	4.6	4.2	57.67	7.9
IK-12(DMNPB)	28.07	0.6	0.4	9.67	0.6
IK-12(DMNPB) Irradiated	61.50	4.3	5.0	51.55	9.0
IK-12(HANBP)	19.14	1.0	0.8	18.57	1.2
IK-12(HANBP) Irradiated	63.15	5.0	6.0	108.44	10.2

The figure 4B shows the quantification of cell morphological parameters indicative of neuronal differentiation on the different substrates, i.e. the number of neurites and branches, the length of axon and number of dendritic filopodia. Irradiated IK-12NVOC/DMNPB/HANBP hydrogels supported attachment of NPCs and promoted the growth of neurites, branches and dendritic filopodia after 48h of cell culture.

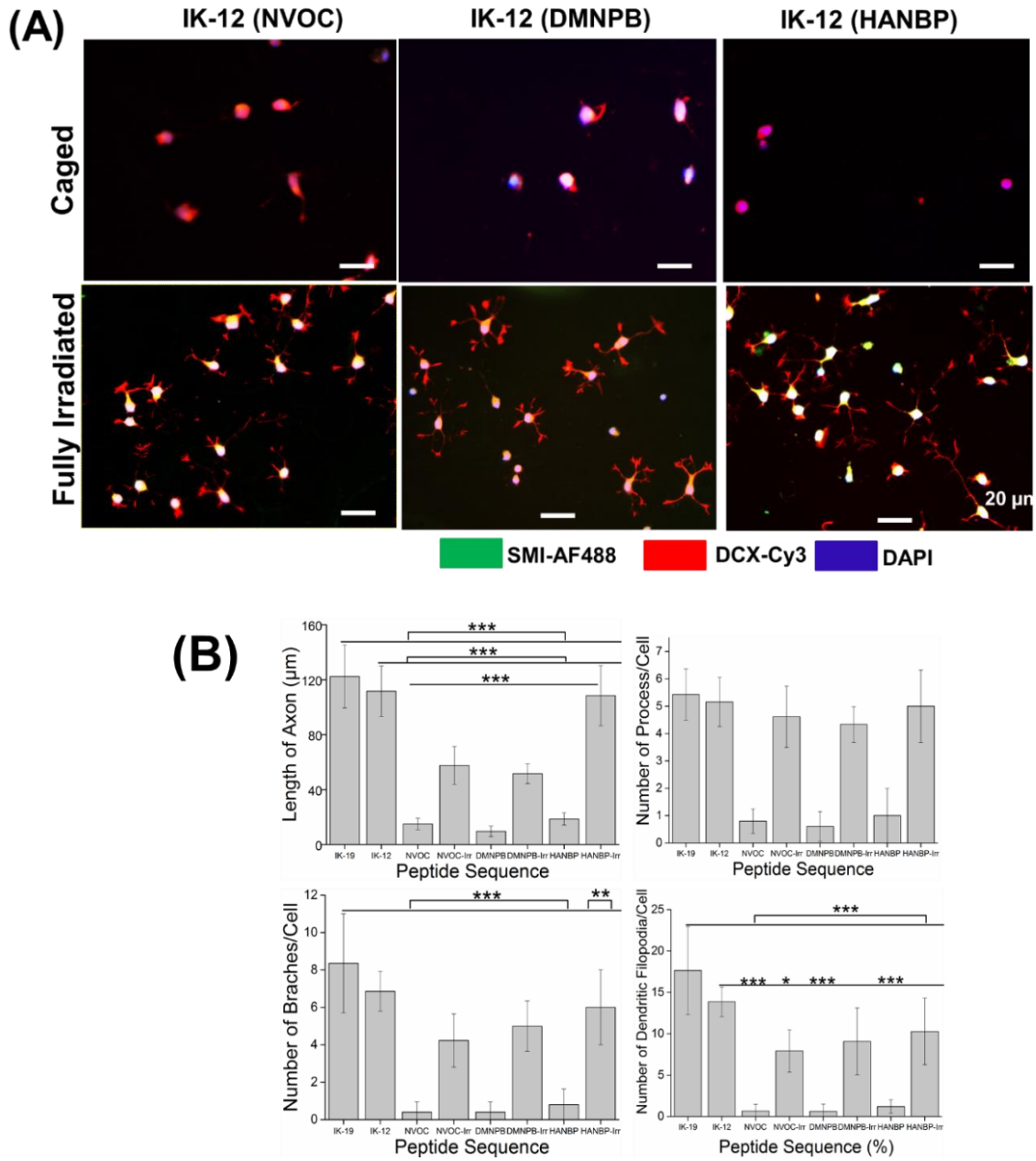

Figure 4: Post-mitotic NPCs seeded on hydrogel (A) caged and after 15 min pre-irradiation of caged IK-12 sequence at λ_{max}: 345 nm for NVOC, 365 nm for DMNPB, and 420 nm for HANBP (B) Quantification of axonal length, number of neurites, branches and dendritic filopodia developed in newborn neurons after 48 h. The

significance of samples was analyzed by Tukey- test (mean ± SD, ANOVA, ** p <0.01, *** p <0.001) in comparison to IK-19, IK-12 and fully uncaged IK-12(HANBP).

The axonal length on IK-12(HANBP) was comparable to control IK-19 and significantly longer than on irradiated IK-12 NVOC/DMNPB substrates. Cells on IK-12NVOC/DMNPB/HANBP hydrogels before irradiation showed short axons and growth of very few processes. Light exposure lead to a 4-5 fold increase in axon length and number of processes, up to values observed on IK-12 hydrogels. Similarly, the number of branches increased 8-13 folds and the number of dendritic filopodia increased 10-15 fold upon light exposure. IK-12 hydrogels showed slightly better development of morphological features, suggesting that the density of IK-12 peptide after irradiation might be lower as a consequence of incomplete photolysis or photolytic side reactions. Among all irradiated samples IK-12(HANBP) hydrogels showed the best results. Taking into account that all three caged peptides showed similar water solubility and hydrolytic stability (Chapter 2 Section 2.3), the higher performance can be associated to the higher photolysis efficiency of the HANBP caging group.

5.3 Directional neuronal migration on IK-12(HANBP) patterned substrates

IK-12(HANBP) modified hydrogels were used to test the possibility to spatially organized neurons on substrates by patterned activation of the peptide. For this purpose, hydrogels were irradiated through a quartz photo-mask patterned with chrome stripes. The irradiation creates a micro-pattern of lines with activated IK-12 (width 10µm) and caged IK-12(HANBP) peptide (100 µm width) corresponding to the exposed and non-exposed areas respectively. The NSCs isolated from NPCs and cultured as neurosphere were used for these experiments. Neurospheres are clusters of undifferentiated stem cells, frequently used for studying differentiation of neurons on biomaterials.[16] These cells are kept in undifferentiated status on a non-adhesive surface in the presence of growth factors (EGF, FGF), and undergo differentiation once seeded on a cell adhesive surface. The neurosphere were dissociated into single cells and seeded on hydrogel in the absence of growth factors.

Cells from neurosphere showed no attachment on caged IK-12(HANBP) substrate after 24 of cell culture. However, cells showed attachment and differentiation into neurons on irradiated IK-12 (HANBP) sample (Figure 5 A-B). Cells survival ratio on irradiated samples was similar to IK-12 and IK-19 controls. The cells showed formation of neurites, develop branches and extend an axonal process with length similar to controls. On patterned hydrogels, cells attached and migrated specifically on the irradiated area, i.e. where the IK-12 was active. Cells followed the patterned geometry already within 2 h of cell seeding, and remained organized in patterns during 4 days of cell culture (Figure 5 C-D). These results demonstrate that the IK-12(HANBP) peptide allows light-triggered positioning of neuronal cells on a biomaterial surface, and eventually construction of neuronal networks with desired geometries.

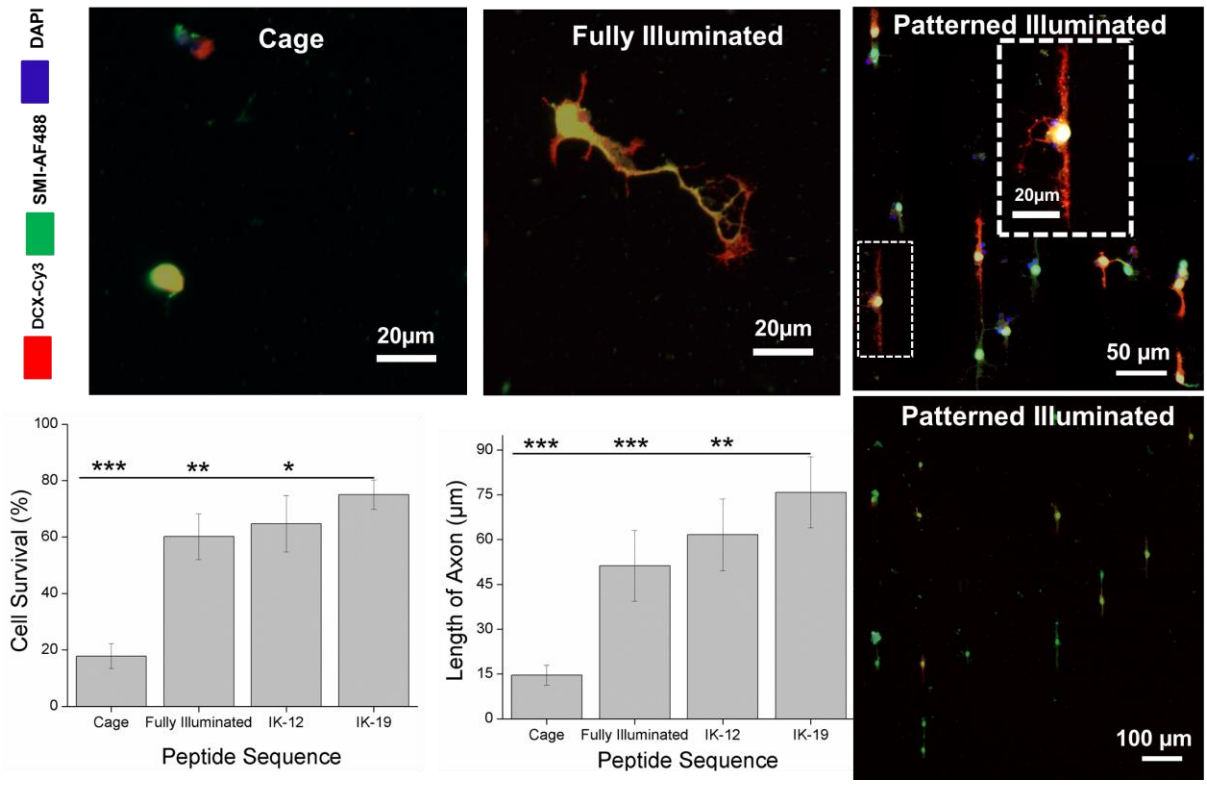

Figure 5. NSCs from dissociated neurospheres (Passage 3) seeded on 2 kPa P(AAm-*co*-AA) hydrogel functionalized with IK-12(HANBP) peptide, 24h after cell seeding. (A) Non-irradiated (B) fully irradiated, (C-D) mask-illuminated substrate (mask: 10 µm strips separated by a 100 µm gap). The graph shows cell survival ratio and length of axon with statistical significance analyzed by Tukey- test in comparison to IK-19 (mean ± SD, ANOVA, ** p <0.01, *** p <0.001).

5.4 Neuronal differentiation and localization on light-activated IK(HANBP)VAV hydrogels

Chapter 2 Section 2.4 described the good solubility and enhanced photolysis efficiency of IK(HANBP)VAV peptide vs longer caged IK-12 variants. In this section, the performance of IK(HANBP)VAV modified hydrogels in supporting differentiation and localizing of NPCs at predefined positions on a substrate will be described.

IK(HANBP)VAV modified 2 kPa P(AAm-*co*-AA) hydrogels did not support the attachment and viability of NPCs (Figure 6A). After full light exposure at 405 nm, cells attached to IK(HANBP)VAV modified gels and 82% of cell viability was observed, higher than IK-19 controls(Figure 6D). The improved performance is attributed to the improved solubility of IK(HANBP)VAV vs. IK-19, leading to higher peptide densities on the hydrogel for comparative coupling conditions. The photo-activated peptide supported differentiation of NPCs, multipolar neurites, high number of branches and densely distributed dendritic filopodia (Figure 6C). When cells were seeded on IK(HANBP)VAV line micropatterns, they preferentially attached to the activated regions and aligned along the activated lines (Figure 6B).

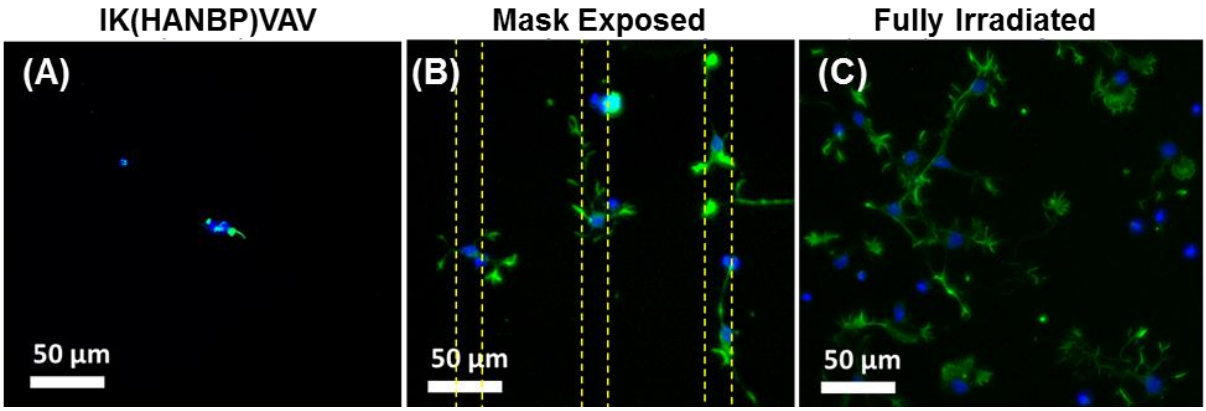

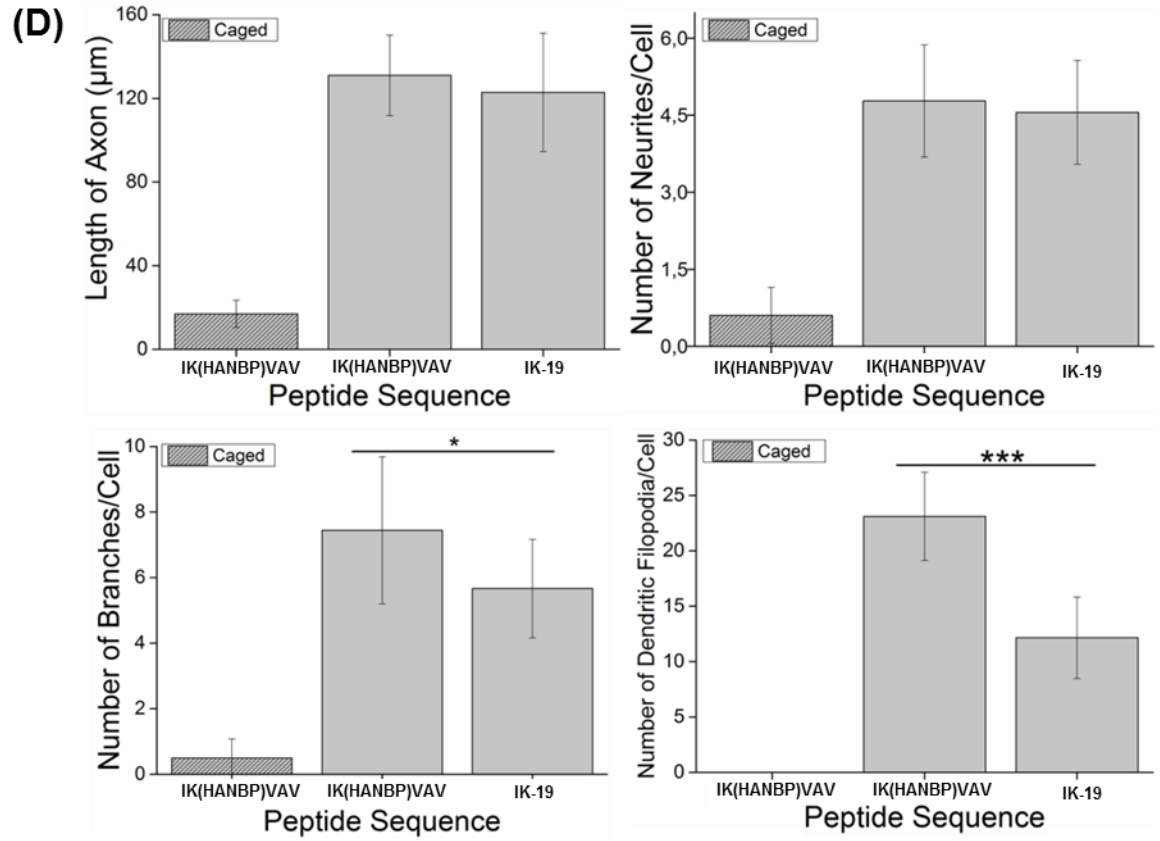

Figure 6. NPCs from embryonic cortex (E 14.5) seeded on IK(HANBP)VAV on P(AAm-*co*-AA) hydrogel (A) non-illuminated (B) irradiated (C) pre-irradiated patterns. The IK(HANBP)VAV modified substrate was illuminated through photomask with strips of illuminated (15 µm) and non-illuminated (50 µm) areas. (D) graph showing quantification of length of axon, number of neurites, branches and dendritic filopodia with statistical significance analyzed by Tukey- test in comparison to IK-19 (mean ± SD, ANOVA, ** p <0.01, *** p <0.001).

The morphological features of NPCs on photoactivated IK(HANBP)VAV hydrogels was followed by time-lapse microscopy over 4 days and compared with IK-19. Cells showed comparable fast maturation on IK-19 and IK(HANBP)VAV and maintained high survival ratios of 83 and 87% respectively until 48 h. On IK-19 hydrogels cell survival drops after 72 h (74%), whereas IK(HANBP)VAV successfully keeps high cell survival (81%) even after 6 days of cell culture. The cells on both substrates develop fully differentiated neuronal phenotypes, with long axons, multipolar neurites, branches and dendritic filopodia (Figure 7).

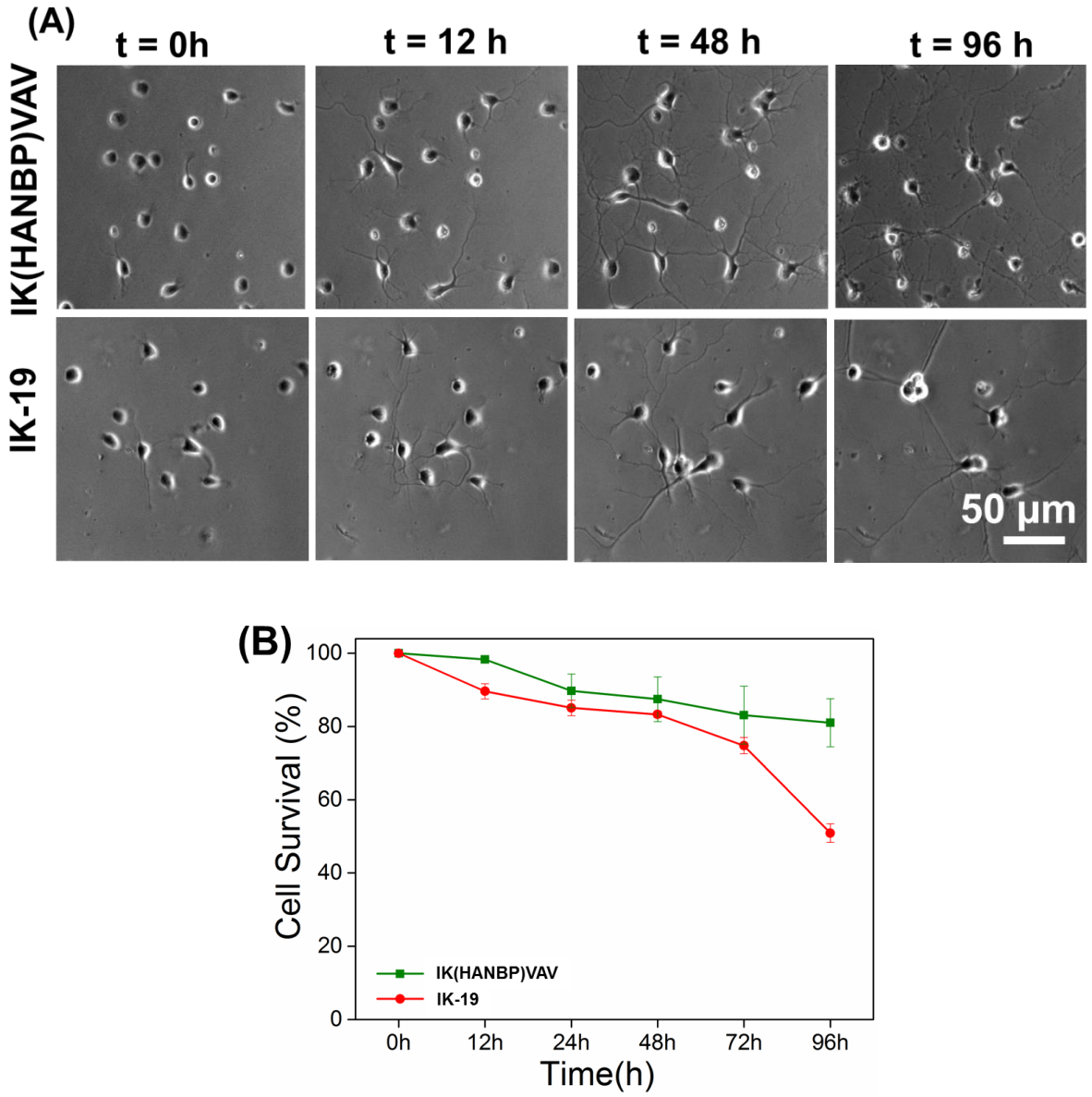

Figure 7. Neural progenitor cells followed at different culture times by time-lapse on P(AAm-*co*-AA) hydrogel (A) Images at different time intervals from 0 - 4d cell culture (B) quantification of cell survival over time.

Neurospheres and cortical explants cultures were also seeded on activated IK(HANBP)VAV substrates. For these experiments, self-assembled monolayers (SAMs) of COOH/CH_3 terminated mixed layers of PEGylated thiols on gold substrates were used. These are standard surfaces in the study of cell-materials interactions that provide flexibility in the composition and density of functional groups.[17] Neurosphere and cortical explants are known to be less sensitive towards material stiffness.[18] and, therefore, this type of substrates are expected to support

neuronal differentiation in spite of the hard gold surface. The details about the surface modification are described in Appendix Section 8.15.2 Neurospheres were seeded as spheroids on the substrates modified with IK(HANBP)VAV substrates, without previous dissociation into single cells. Before light exposure, cells failed to migrate out of neurosphere. Once irradiated, neurospheres grow and proliferate on the substrates (Appendix section 8.16.1). Neurospheres seeded on IK(HANBP)VAV with pre-irradiated strips of 15 µm with 50 µm gap migrated from the neurosphere into the activated IKVAV strips. The cells developed neuronal process in the direction of irradiation and differentiated into neurons. This process can be seen in Figure 8. Time lapse videos showed the persistent growth of the neurons in the pre-irradiated direction. The cell after first 7.5h of attachment showed fast extension, at an average rate of ~0.90 µm/min, and reach maximum length of 243 µm in 24h (Figure 8). The neural process did not develop on the not exposed areas, showed very low persistence and process got retracted in 1h (Figure 8).

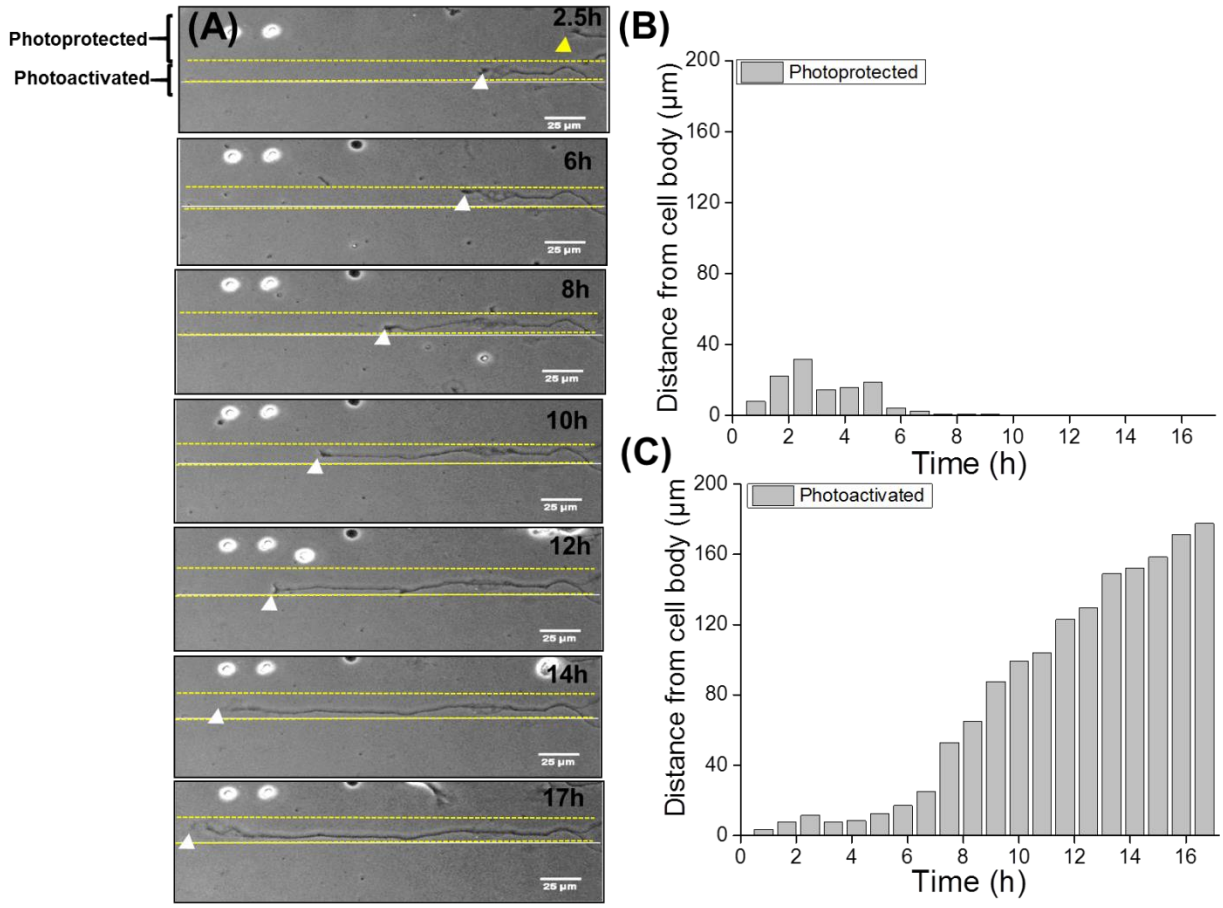

Figure 8. Neurosphere (Passage 1) from embryonic cortex (E 14.5) seeded on pre-patterned IK(HANBP)VAV functionalized SAMs (A) Axon development on irradiated

area at different times after initial attachment. White arrow show axon extension on irradiated area while yellow arrow show process on cage area. The persistence of neurite growth from neurosphere culture was quantified (B) on photoprotected and (C) on photoactivated areas on the same sample.

Finally, the IK(HANBP)VAV functionalized gold surfaces were seeded with cortical explants. In *vivo,* during development or injury, chains of neural progenitor migrate from sub-ventricular zone (SVZ) to injured area of the brain to repair. The persistence of chain migration indicates successful migration of cells to injured site.[19] It has been reported that high expression levels of β1 integrin on interaction with Laminin support chain migration. Taking into account that IKVAV interacts with β1 integrin class, the photoactivatable peptide IK(HANBP)VAV is expected to allow control and chain migration.[20] The cells cultured on IK(HANBP)VAV failed to migrate out of explant after 24h and only few single cells visible after 48 h. On irradiated IK(HANBP)VAV, cells showed strong chain migration out of explant within 24 hours, and continue to undergo chain migration even after 48 h. Interestingly, prepatterned substrates by masked illumination also support chain migration in the defined geometries.

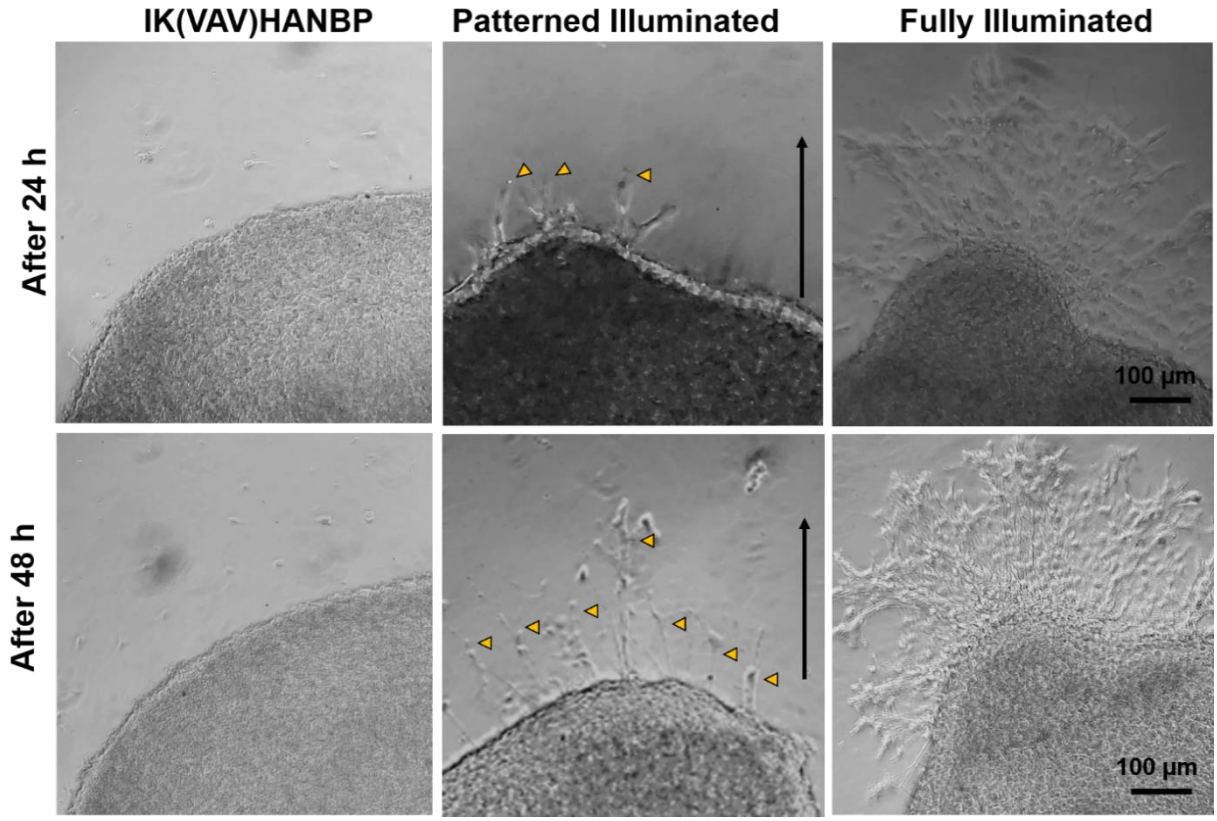

Figure 9. Subventricular zone explants from neo-natal (7days) mouse seeded on SAMs supported on gold, modified with caged, irradiated and pre-irradiated patterns of IK(HANBP)VAV. The black arrow show the direction of irradiation (15µm irradiated and 50µm non-irradiated strips), while yellow arrow indicates chain migration on photo-patterned area.

5.4 *In-situ* activation of IK(HANBP)VAV for light guided axonal growth

Reported works with photoactivatable peptides have demonstrated the possibility to activate cellular attachment and migration *in situ*, i.e. in the presence of cells. [11, 17c, 21] This possibility is particularly interesting for IK(HANBP)VAV modified hydrogels due to observed higher photo-efficiency. It would allow directional growth of neurites with temporal resolution, selection of neurite polarity and can be extended to create customized neuronal circuity.

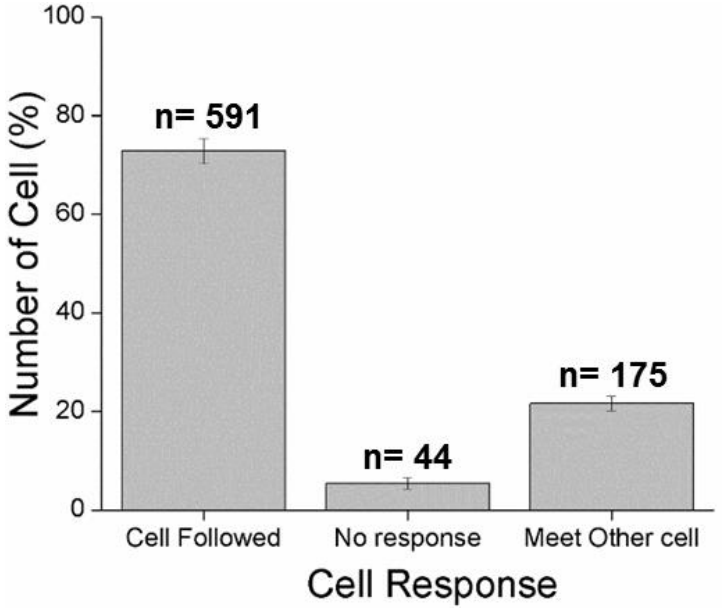

Figure 10. Graphical representation of response of embryonic (E 14.5) NPCs seeded on IK(HANBP)VAV after *in-situ* irradiation. Only viable cells after irradiation were quantified.

Neural progenitor cells (eNPCs) cells were seeded on IK(HANBP)VAV modified hydrogels at low cell densities and left for 2h to sediment on the substrate in an incubation chamber at the microscope. Using a 405nm laser, areas of 10µmx100µm were scanned in the vicinity of cells in 10 sec. The behavior of the cells was followed

during 24 hours. More than 70% of the cells that were close to the irradiated lines extend leading process in the direction of irradiation. Only ~ 5% of cells did not respond to the exposed area and ~ 22% cells connect with other cells and change direction (Figure 10).

A representative image of a growing process after *in-situ* exposure is shown in Figure 11. The neurite grew persistently along the irradiated area at 0.12 µm/min speed during the first two hours and at speed of 0.20 µm/min in the next 4 hours. In 8 hours, the neurite extended to 83 µm and reached the maximum length of 91µm in 24h of cell culture. This length matches the dimension of the activated pattern. The neurite did not extend outside of the pattern. The cells were fixed after 24h and stained with SMI to corroborate the axonal character of the extended neurite and with DCX to confirm the neuronal lineage of differentiated cell. The IKVAV peptide was successfully uncaged with short irradiation dosage and cell followed only the irradiated area and no neurite extension was observed outside the irradiated area. The cell changes the polarity and extends the longer process in the direction of irradiation and leading process was differentiated into axon. These results demonstrate that IK(HANBP)VAV modified substrates allow *in situ* determination of cell polarity and the direction of extension of the axonal process. These experiments will further extend to build neural circuit with spatiotemporal resolution. The HANBP chromophore possesses high two photon cross section and thus enables *in-situ* neurite networking in 3D as well.

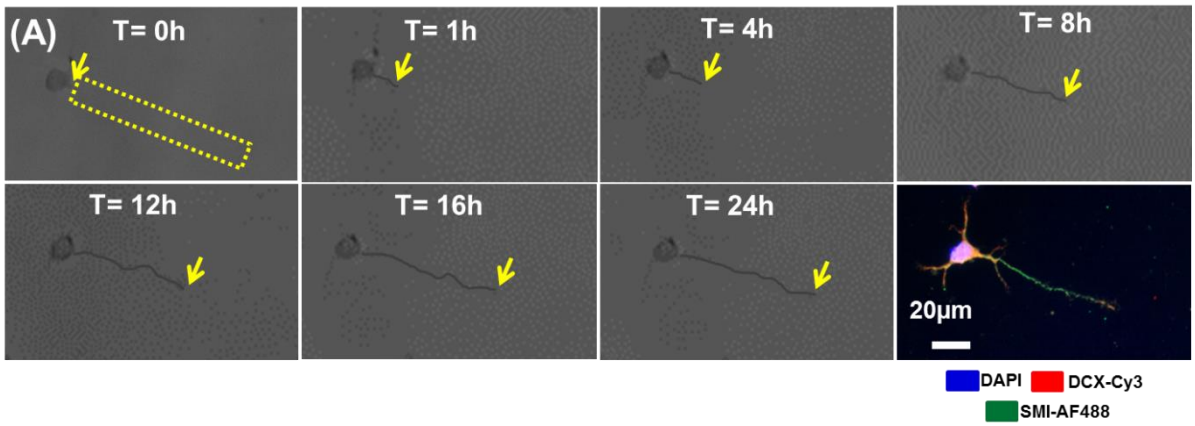

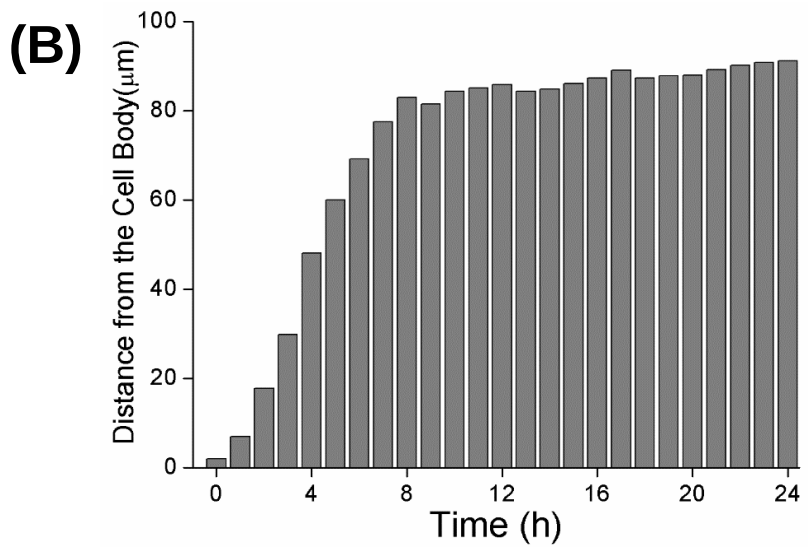

Figure 11. Growth of NPCs (E 14.5) on IK(HANBP)VAV after *in situ* activation of the peptide using a scanning laser in a microscope (A) Microscope image of a representative cell after *in-situ* irradiation during 24 hours. The arrow indicates the growth cone (B) Persistence of neurite extension over time, on *in-situ* photo-activated pattern. The axon shows stable increase in axon length and not retraction of axonal process was observed. A false trace is added to neurite to increase visibility.

5.5 Conclusions

Biomaterials functionalized with photo-activatable Laminin peptidomimetics allow light-directed activation and control over neurite growth and support neuronal differentiation *in vitro*. Neurons can be assembled on predetermined patterns and the growth of neurites can be guided in preselected directions. Screening among several reported IKVAV variants allowed identification of best candidates on the basis of good water solubility and bioactivity to support NPCs. This photo-activatable Laminin mimetic peptides coupled to soft hydrogels provide spatial control over neuronal cell differentiation. IK-12(DMNPB/NVOC/HANBP) and IK(HANBP)VAV peptides were proven to be inactive towards cell attachment and neuron maturation, and were activated upon light exposure. IK-12(HANBP) allowed spatial arrangement of neuronal cells derived from neurosphere. The short IK(HANBP)VAV peptide supported spatial arrangement of neuronal cells from neural progenitor cells (eNPCs), neurospheres and cortical explants. The *in-situ* activation of photoresponsive Laminin peptidomimetic by using scanning lasers provided

spatiotemporal control of neurite extension. Photo-activatable Laminin mimetic peptides in combination with soft hydrogels allow site-selective neurite outgrowth in neural progenitor cells (NPCs) culture.

References

[1] K. Liu, A. Tedeschi, K. K. Park, Z. He, *Annual review of neuroscience* **2011**, *34*, 131-152.

[2] aJ. S. Lunn, S. A. Sakowski, J. Hur, E. L. Feldman, *Annals of neurology* **2011**, *70*, 353-361; bS. Casarosa, Y. Bozzi, L. Conti, *Molecular and cellular therapies* **2014**, *2*, 31; cJ. Della Rocca, D. Liu, W. Lin, *Accounts of chemical research* **2011**, *44*, 957-968; dF. H. Gage, S. Temple, *Neuron* **2013**, *80*, 588-601.

[3] W. Lee, C. W. Frank, J. Park, *Adv. Mater.* **2014**.

[4] W. Lee, C. W. Frank, J. Park, *Advanced Materials* **2014**, *26*, 4936-4940.

[5] aP. Liesi, *The EMBO journal* **1985**, *4*, 1163; bW.-L. Lei, S.-G. Xing, C.-Y. Deng, X.-C. Ju, X.-Y. Jiang, Z.-G. Luo, *Cell research* **2012**, *22*, 954-972; cM. Pesaresi, R. Soon-Shiong, L. French, D. Kaplan, F. Miller, T. Paus, *Neuroimage* **2015**, *115*, 191-201; dM. A. Wolman, V. K. Sittaramane, J. J. Essner, H. J. Yost, A. Chandrasekhar, M. C. Halloran, *Neural development* **2008**, *3*, 6.

[6] A. Domogatskaya, S. Rodin, K. Tryggvason, *Annual review of cell and developmental biology* **2012**, *28*, 523-553.

[7] J. E. Frith, R. J. Mills, J. E. Hudson, J. J. Cooper-White, *Stem cells and development* **2012**, *21*, 2442-2456.

[8] aM. C. Kibbey, M. Jucker, B. S. Weeks, R. L. Neve, W. E. Van Nostrand, H. K. Kleinman, *Proceedings of the National Academy of Sciences* **1993**, *90*, 10150-10153; bE. Agius, Y. Sagot, A. Duprat, P. Cochard, *Neuroscience* **1996**, *71*, 773-786; cH. Hosseinkhani, Y. Hiraoka, C.-H. Li, Y.-R. Chen, D.-S. Yu, P.-D. Hong, K.-L. Ou, *ACS chemical neuroscience* **2013**, *4*, 1229-1235; dW. Sun, T. Incitti, C. Migliaresi, A. Quattrone, S. Casarosa, A. Motta, *Journal of tissue engineering and regenerative medicine* **2017**, *11*, 1532-1541; eH. Kleinman, R. C. Ogle, F. Cannon, C. Little, T. Sweeney, L. Luckenbill-Edds, *Proceedings of the National Academy of Sciences* **1988**, *85*, 1282-1286; fM. Nomizu, W. H. Kim, K. Yamamura, A. Utani, S.-Y. Song, A. Otaka, P. P. Roller, H. K. Kleinman, Y. Yamada, *Journal of Biological Chemistry* **1995**, *270*, 20583-20590.

[9] aB. Zhu, S.-C. Luo, H. Zhao, H.-A. Lin, J. Sekine, A. Nakao, C. Chen, Y. Yamashita, H.-h. Yu, *Nature communications* **2014**, *5*; bY.-P. Lu, C.-H. Yang, J. A. Yeh, F. H. Ho, Y.-C. Ou, C. H. Chen, M.-Y. Lin, K.-S. Huang, *International journal of pharmaceutics* **2014**, *463*, 177-183.

[10] aE. J. Berns, S. Sur, L. Pan, J. E. Goldberger, S. Suresh, S. Zhang, J. A. Kessler, S. I. Stupp, *Biomaterials* **2014**, *35*, 185-195; bS. Tasoglu, C. Yu, H.

Gungordu, S. Guven, T. Vural, U. Demirci, *Nature communications* **2014**, *5*; cJ. C. Rose, M. Cámara-Torres, K. Rahimi, J. Köhler, M. Möller, L. De Laporte, *Nano Letters* **2017**; dW. Zhu, F. Masood, J. O'Brien, L. G. Zhang, *Nanomedicine: Nanotechnology, Biology and Medicine* **2015**, *11*, 693-704.

[11] M. Wirkner, S. Weis, V. San Miguel, M. Álvarez, R. A. Gropeanu, M. Salierno, A. Sartoris, R. E. Unger, C. J. Kirkpatrick, A. del Campo, *ChemBioChem* **2011**, *12*, 2623-2629.

[12] A. Farrukh, J. I. Paez, M. J. Salierno, W. Fan, B. Berninger, A. del Campo, *Biomacromolecules* **2017**.

[13] aD. E. Koser, A. J. Thompson, S. K. Foster, A. Dwivedy, E. K. Pillai, G. K. Sheridan, H. Svoboda, M. Viana, L. da F Costa, J. Guck, *Nature Neuroscience* **2016**, *19*, 1592-1598; bA. M. Hopkins, L. De Laporte, F. Tortelli, E. Spedden, C. Staii, T. J. Atherton, J. A. Hubbell, D. L. Kaplan, *Advanced Functional Materials* **2013**, *23*, 5140-5149; cQ.-Y. Zhang, Y.-Y. Zhang, J. Xie, C.-X. Li, W.-Y. Chen, B.-L. Liu, X.-a. Wu, S.-N. Li, B. Huo, L.-H. Jiang, *Scientific reports* **2014**, *4*; dJ. Lantoine, T. Grevesse, A. Villers, G. Delhaye, C. Mestdagh, M. Versaevel, D. Mohammed, C. Bruyère, L. Alaimo, S. P. Lacour, *Biomaterials* **2016**, *89*, 14-24; eM. M. Pathak, J. L. Nourse, T. Tran, J. Hwe, J. Arulmoli, T. L. Dai Trang, E. Bernardis, L. A. Flanagan, F. Tombola, *Proceedings of the National Academy of Sciences* **2014**, *111*, 16148-16153.

[14] M. Mela, S. Toivonen, *Differentiation* **1977**, *7*, 61-63.

[15] M. Yamada, Y. Kadoya, S. Kasai, K. Kato, M. Mochizuki, N. Nishi, N. Watanabe, H. K. Kleinman, Y. Yamada, M. Nomizu, *FEBS letters* **2002**, *530*, 48-52.

[16] aG. Wang, Q. Ao, K. Gong, A. Wang, L. Zheng, Y. Gong, X. Zhang, *Acta biomaterialia* **2010**, *6*, 3630-3639; bY.-J. Ren, Z.-Y. Zhou, F.-Z. Cui, Y. Wang, J.-P. Zhao, Q.-Y. Xu, *Journal of Bioactive and Compatible Polymers* **2009**, *24*, 56-62; cJ. R. Thonhoff, D. I. Lou, P. M. Jordan, X. Zhao, P. Wu, *Brain research* **2008**, *1187*, 42-51.

[17] aN. Faucheux, R. Schweiss, K. Lützow, C. Werner, T. Groth, *Biomaterials* **2004**, *25*, 2721-2730; bJ. C. Love, L. A. Estroff, J. K. Kriebel, R. G. Nuzzo, G. M. Whitesides, *Chemical Reviews* **2005**, *105*, 1103-1170; cM. J. Salierno, A. J. García, A. Del Campo, *Advanced Functional Materials* **2013**, *23*, 5974-5980.

[18] I. Singec, R. Knoth, R. P. Meyer, J. Maciaczyk, B. Volk, G. Nikkhah, M. Frotscher, E. Y. Snyder, *Nature methods* **2006**, *3*, 801-806.

[19] L. Cao, J. Pu, R. H. Scott, J. Ching, C. D. McCaig, *Stem Cell Reviews and Reports* **2015**, *11*, 75-86.

[20] R. Belvindrah, S. Hankel, J. Walker, B. L. Patton, U. Müller, *The Journal of neuroscience* **2007**, *27*, 2704-2717.

[21] M. Wirkner, J. M. Alonso, V. Maus, M. Salierno, T. T. Lee, A. J. García, A. Del Campo, *Advanced Materials* **2011**, *23*, 3907-3910.

Chapter 6

Two photon photoactivatable c[RGD(PMNB)fC] for spatially controlled cell migration in 3D

6.1 Introduction

The cellular niche is a dynamic environment where biochemical (adhesive ligands, growth factors, cytokines, ions) and mechanical factors undergo changes in a highly regulated manner.[1] These changes are sensed by cells and elicit relevant cell responses like adhesion, migration or differentiation. Typical biomaterials used for cell cultures hardly mimic this situation.[2] The properties of natural and synthetic hydrogels used for 3D cell culture (alginate, hyaluronic acid, collagen, matrigel, fibrin or PEG) can be tuned to be close to the properties of the natural environment. However, there is no possibility of active regulation after cell encapsulation to guide cellular responses.

In the last years, a few synthetic approaches to obtain dynamic hydrogels with the ability to change properties on demand have been reported. Most of them are based on the incorporation of photosensitive groups into the 3D network to achieve tunable mechanical properties by photo-degradation, or on orthogonal photocoupling of relevant ligands for cell membrane receptors (Figure 1). For example, the stiffness of alginate hydrogels were tuned by UV assisted release of calcium from photoactivatable DM-nitrophen to guide differentiation of hMCSs.[3] Anseth *et al.* incorporated *o*-nitrobenzyl ether photocleavable groups into a PEG network to soften the hydrogel after cell encapsulation.[4] These reaction generated channels in the hydrogel by photo-degradation and enable migration of cells embedded in 3D PEG hydrogels (Figure 1A).[4-5] *In situ* changes in the biochemical composition of a hydrogel have also been realized using photoactivatable chemistries. Application of photoinitiated thiol-ene chemistry to PEG hydrogels allowed triggering of fibroblast attachment to the gels after encapsulation (Figure 1B).[6] A similar strategy allowed photo-triggered differentiation of hMSCs on vitronectin photoligated patterns.[7] The incorporation of a photocleavable linker between peptide and substrate or hydrogel network was demonstrated for photo-release peptide and detachment of cells (Figure 1C).[8]

In addition to photo-ligation and photocleavable crosslinkers, phototriggerable adhesive ligands are effective in tuning cellular response with molecular precision. The del Campo group pioneered the use of phototriggerable adhesive ligands to *in situ* change the adhesion, detachment and migratory decisions of cells, *in vitro* and *in vivo*.[8b, 9] Light-responsive biomolecules provided spatiotemporal control over cell processes at cell friendly wavelength, in a non-invasive manner and in the absence of chemical additives, *in vitro* and *in vivo*. [8b, 9a-c, 9e, 10]

Photoactivation with single photon processes does not allow site-selective activation in a 3D context. Two photon (2P) activation in the near infra-red region (720-990 nm) enables 3D resolution of the activation process in biological contexts due to high penetration, low scattering of near infra-red light and reduced photodamage.[11] The photocleavage reaction by 2P laser is based on the absorption of two similar energy photons, leading to bond cleavage or rearrangements. The photochemical properties of two photon photolabile groups are defined by the two-photon absorption cross section (σ^2) and the quantum yield (φ). σ^2 represents the probability of simultaneous absorption of two photons of similar energy to reach the molecular transition energy, and it is measured in Goeppert-Mayer units, 1 GM = 10^{-50} cm^4 s.[12] The photo-patterning by 2P activation at 720 nm has been demonstrated by Lee *et al.* by crosslinking FITC-RGDSK-PEG-acrylate with free acrylates of pre-gelated PEG-DA hydrogel network. Migration of fibroblasts has been demonstrated inside the 3D hydrogel confined to photo-conjugated adhesive RGD ligand (Figure 1D).[13] In this chapter, photo-activatable adhesive ligands will be combined with 2P photolabile groups to allow modulation of cellular response in 3D hydrogels with defined z-resolution.

The terpeptide RGD(Arg-Gly-Asp) is integrin specific mimetic peptide display binding to $\alpha_5\beta_1$ and $\alpha_v\beta_3$ integrins and supporting cell adhesion, differentiation, angiogenesis, and metastasis.[9b, 14] The cyclic version of RGD with pentapeptide units (RGDfV) has been reported to enhance the proteolytic resistance and to improve the binding affinities to integrin receptors.[15] The aspartic acid (D) in RGD interacts with divalent cations and acts as integrin-selective binding site by ion-dependent adhesion.[16]

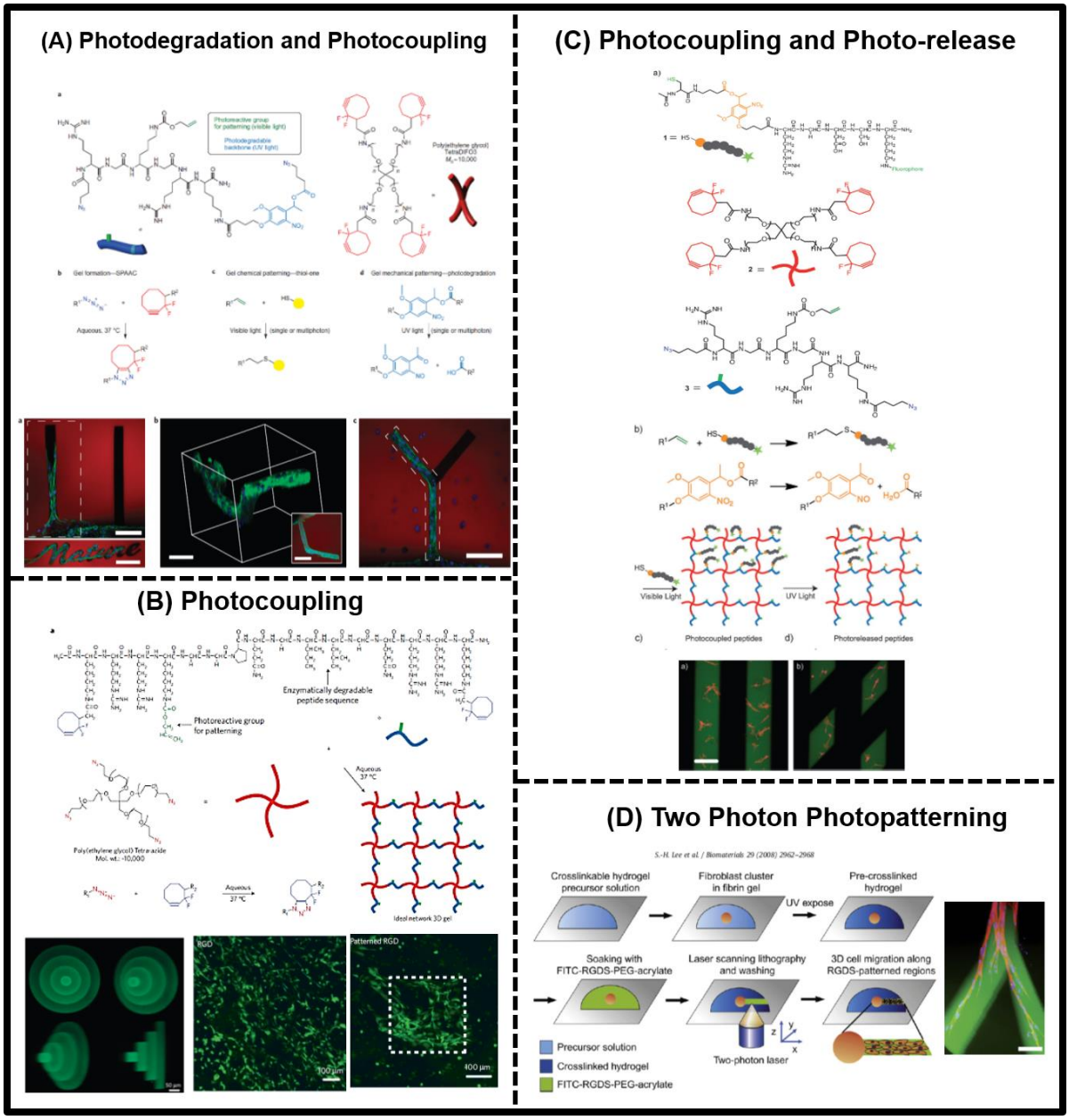

Figure 1. Light modulated patterning in 3D hydrogels (A) Photoinitiated thiol-ene coupling reaction and light triggered degradation of PEG hydrogel containing *o*-nitrobenzyl crosslinker for adhesion and migration of fibroblast cells[4] (B) Photoinitiated thiol-ene coupling in SPAAC PEG hydrogels for spatial cell attachment of fibroblast[6a] (C) Step by step photocoupling of peptide, attachment of fibroblast cells and light triggered detachment of cells[8a] (D) Two photo-mediated patterning and spatial migration of fibroblast inside hydrogel. [13]

The selectivity of binding site in RGD has been explored in different accounts by insertion of photocaged DMNPB moieties at aspartic acid lead to recognition failure by cell.[8b, 9a-c, 9e] The chromophore shows better photosensitivity and hydrolytic

stability than nitrobenzyl based chromophore used in all other studies as photocrosslinker. However, 2-(o-nitrophenyl)propyl DMNPB shows poor two-photon absorption cross sections (GM =0.17), like the other o-nitrobenzyl ether chromophores (0.013).[11a] This issue limits the extensive application of these approaches to 3D cultures at doses compatible with living cells. In this chapter, advanced photoactivatable versions of cyclic RGDfC adhesive ligand containing a chromophore for effective two-photon activation is presented.

Different photo-protecting groups with 2P cross-section are explored in terms of solubility, stability and photo-efficiency. Recently reported derivatives of the *o*-nitrobiphenylpropyl family, with an extended conjugation system, have shown significantly better σ^2 (GM = 3.2 to 11) depending on substitution at biphenyl backbone. These 2P activatable chromophores are used by our group to control the crosslinking degree of polymeric materials.[17] RGD(PMNB)fC was used to spatiotemporally control cell adhesion within 3D hydrogels at low exposure doses. Adhesion and invasive behavior of embedded cells was photo-triggered by using PEG-based 3D cell cultures.

6.2 Synthesis of two-photon activatable RGD(cage)fC

6.2.1 Selection of chromophores and synthesis of photoactivatable variants of aspartic acid

The photoactivatable group in RGD is selected to be introduced at aspartic acid residue based on previous accounts.[8b, 9] The photo-protecting derivatives from *o*-nitrobiphenylpropyl family with higher 2P cross sections were explored. The methoxynitrobiphenyl (PMNB) derivative with substituted methoxy on biphenyl back bone (GM = 3.2 at 740 nm) and dialkyl amine substituted derivatives *p*-dialkylaminonitrobiphenyl (ANBP) and 2-(4'-amino-4-nitro-[1,1'-biphenyl]-3-yl)propan-1-ol (HANBP) were selected. The ANBP and HANBP have similar reported 2P cross sections GM = 11 at 800 nm, but latter derivative is reported to have higher water solubility.[17-18]

The HANBP is adapted from reported 4-nitro-[1,1’-biphenyl]-3-yl)propan-1-ol (EANBP) derivative by replacing 2-(methoxyethoxy)ethyl with free hydroxyl group for enhanced water solubility. The scheme 1 shows the structural difference of all derivatives.

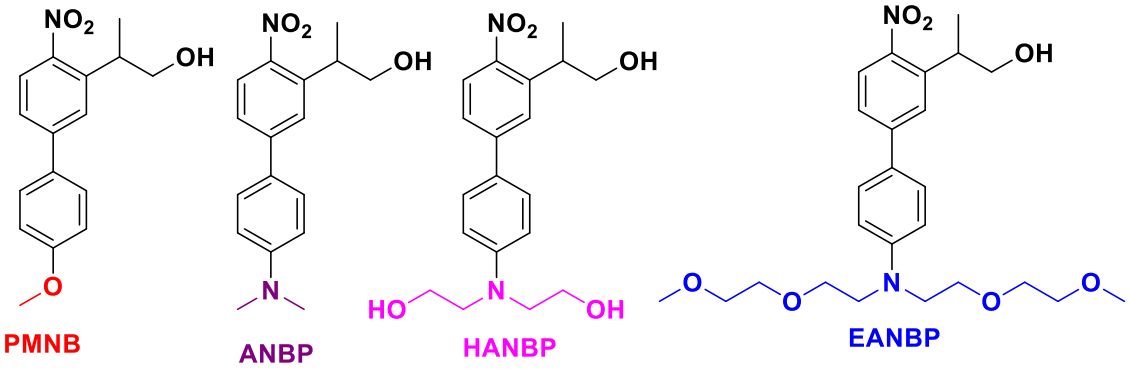

Scheme 1. Molecular structure of selected 2P chromophores.

The chromophores were designed to be coupled to the carboxylic side chain of an aspartic acid. The HANBP, ANBP and PMNB derivatized aspartic acids were synthesized by adaptation of reported protocols.[17-19] The PMNB, ANBP and HANBP groups were obtained by a microwave-assisted Suzuki coupling. The 2-(5-bromo-2-nitrophenyl)-propan-1-ol (**d**) intermediate was obtained as explained in Chapter 2 Section 2.2.3. The obtained product (**d**) was subjected to Suzuki coupling with iodo-anisole to obtain PMNB and iodo-dimethylaniline for ANBP according to reported protocols.[18-19] The aspartic with ^{t}Bu protected alpha carboxylic unit was introduced at hydroxyl group by forming ester link assisted by DMAP and DCC.[9b] The ^{t}Bu protection on alpha carbon was deprotected by acidic cleavage in DCM to obtain Fmoc-Asp(cage)-OH with PMNB or ANPB cage (Figure 2).

The introduction of fmoc aspartic acid in HANBP derivative after Suzuki coupling could lead to competition in selection of hydroxyl position for substitution. In HANBP the aspartic acid was coupled with compound **(c)** prior to Suzuki coupling, similar to the strategy adopted in Chapter 2 section 2.2.3 for synthesis of Fmoc-Lys(HANBP)-OH. The detailed synthetic scheme for HANPB and NMR characterization is included in Appendix sections 8.17.3

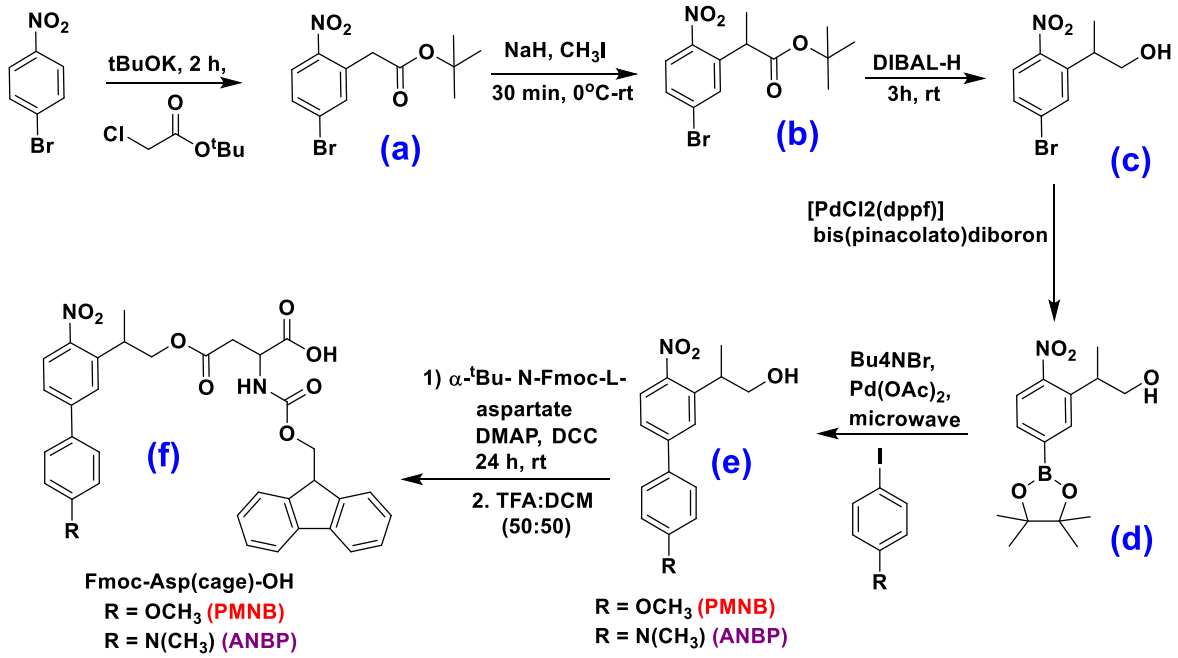

Figure 2. Synthetic pathway for Fmoc-Asp(ANBP/PMNB)-OH.

Fmoc-Asp(PMNB/ANBP/HANBP)-OH were purified by flash column chromatography and obtained in high purity and in 62, 56 and 45% yields respectively. The ^{1}H-NMR of PMNB and ANPB are in agreement with reported data displaying methoxy signals (3.84 ppm) in PMNB and dimethylamine signals in ANBP (3.09 ppm).[18-19] The insertion of fmoc aspartic acid lead to appearance of Fmoc signals in the aromatic range (7.28-7.72 ppm), doublet for benzylic methyl (1.27 ppm) and signal for ^{t}Bu protecting group at (1.38 ppm). The ^{t}Bu signal disappearance on TFA deprotection leading to final products. The ESI-MS measurements confirmed the mass of the final products at 647.68 [M+Na]+ for PMNB, at 637.59 [M+Na]+ for ANBP and 754.54 [M+H]+ and 777.34 [M+Na]+ for HANBP.

6.2.2 Synthesis of photoactivatable RGDfC peptide.

A cyclic RGDfC peptide with photolabile group was synthesized. The Cys containing version of the cyclic peptide was selected for reaction with maleimide derivatized PEG hydrogels in later experiments. The RGD(Cage)fC peptide was synthesized manually by Fmoc solid-phase peptide synthesis (SPPS) with sequential addition of amino acids to H-Gly-2-Cl-Trt resin.[9b]

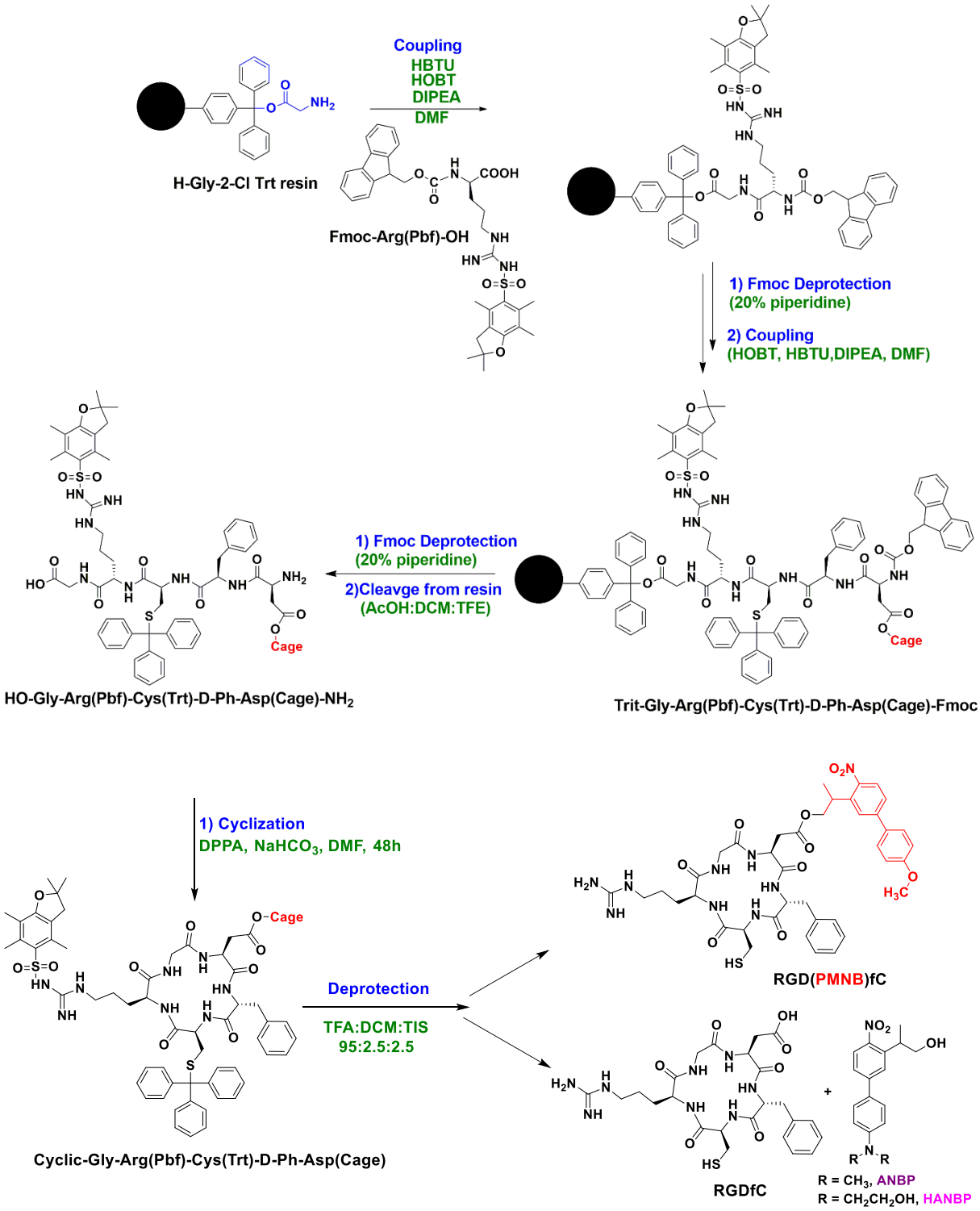

Figure 3. The synthetic route for caged RGDfC peptide by SPPS

The linear peptide chain was extended by repeated coupling cycles and caged aspartic (Cage= PMNB, ANBP or HANBP) was introduced as the final unit of the linear sequence. This route was adopted to avoid hydrolysis of the photoprotecting group during repeated coupling cycles. The linear peptide was cleaved from the

resin in mild acidic conditions (AcOH:DCM:TFE, 6:3:1) and no hydrolysis of the side chain protecting groups was observed. The linear protected peptide was subjected to cyclization using DPPA. This step was performed at high dilution conditions (ca 1mM) to favor intramolecular cyclization *vs*. intermolecular reactions. Deprotection of side chains was performed at acidic conditions (Figure 3) and the peptides were purified by RP-HPLC. Under these conditions the RGD(PMNB)fC was obtained in high yield 54% while RGD(ANPB)fC and RGD(HANPB)fC underwent hydrolysis and only 6% and 9% of pure product was obtained respectively.

6.2.3 Physicochemical properties of RGD(Cage)fC derivatives

According to reported data the ANBP and HANPB showed similar photoactivity, while the 2P efficiency of PMNB was 3 folds lower than ANBP derivatives (Table 1).[17-19] The solubility and stability of RGD(PMNB/ANBP/HANBP)fC peptides in PBS was studied. RGD(HANBP)fC peptide showed 10 times better water solubility than RGD(PMNB)fC due to the hydrophilic diethanolamine substituents, while RGD(ANBP)fC display comparable solubility to RGD(PMNB)fC (Table 1).

Table 1. The comparison of chromophore properties in term of different parameters.

Properties	RGD(PMNB)fC	RGD(HANBP/ANBP)fC
One photon photolysis efficiency *	λ_{max} 317 nm, 90% photo-release	λ_{max} 397 nm, 95 % photo-release
Two photon photolysis efficiency*	λ_{max} 740 nm (3.2 GM), 9% quantum yield	λ_{max} 800 nm (11 GM), 15% quantum yield
Hydrolytic Stability in PBS (pH 7.4) at r.t	Stable for more than one month	63% for hydrolysis ANBP and 58% hydrolysis for HANBP in 1 week
Solubility of Caged RGD in PBS (pH 7.4)	0.5 mg/ml	0.5 mg/ml for ANBP 5 mg/ml for HANBP

* values taken from literature.[17-18]

The hydrolysis of HANPB and ANBP in acidic conditions was observed during SSPS, suggesting lower hydrolytic stability of HANPB/ANBP caged aspartic acid vs PMNB containing variant. In fact, RGD(ANBP)fC kept in PBS at room temperature in one week showed a 63% and RGD(HANBP)fC show 58% cleavage of ANBP/HANBP chromophore respectively (Table 1). Under the same conditions, RGD(PMNB)fC remained stable for 1 month. The electron donating dialkylamine

derivative in ANBP and HANBP were effective in enhancing photo-efficiency of these donor-acceptor based derivative, but on the other hand the hydrolytic efficiency was compromised. The electronegative methoxy substituted *o*-nitrobiphenyl derivatives showed lower photo-efficiency, but it was a better candidate in terms of hydrolytic stability than dialkylamine family. Despite the reported higher photolytic efficiency and observed higher water solubility of RGD(HANBP/ANBP)fC, the RGD(PMNB)fC was selected as photo-triggerable RGD for further studies. The hydrolytic stability is relevant for later biological experiments and was the key factor for the selection.

6.3 Photochemical Properties of RGD(PMNB)fC

The reported photolysis mechanism for PMNB-caged carboxylic groups under UV irradiation predicts a *β*–elimination reaction resulting in the release of the COOH group and p-methoxybiphenyl 2-(o-nitrophenyl)propene as photo by-product (Figure 4).[20] The extinction coefficient of the chromophore is reported to be 9900 $M^{-1}cm^{-1}$.[17] The UV spectrum of RGD(PMNB)fC showed an absorption maximum at λ_{max}=345 nm (Figure 4), which corresponds to the reported absorption maximum of PMNB chromophore. The photolysis of RGD(PMNB)fC was followed by UV spectroscopy after irradiation of peptide solutions at 360 nm for increasing times. The photolysis efficiency was calculated from the decrease in UV absorbance at 345 nm. The photochemical yield was calculated from analytical HPLC of the irradiated solutions (Figure 5). Photolysis products were detected by ESI-MS measurements.

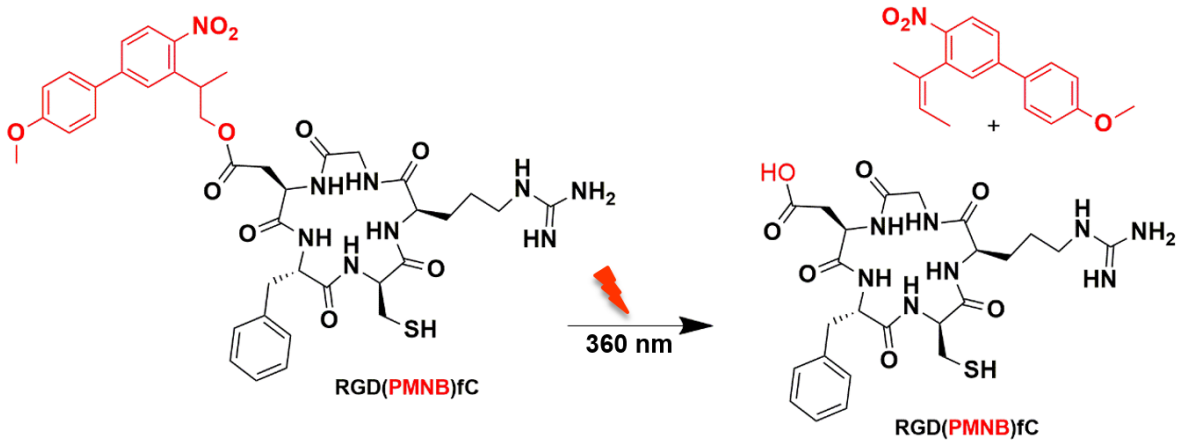

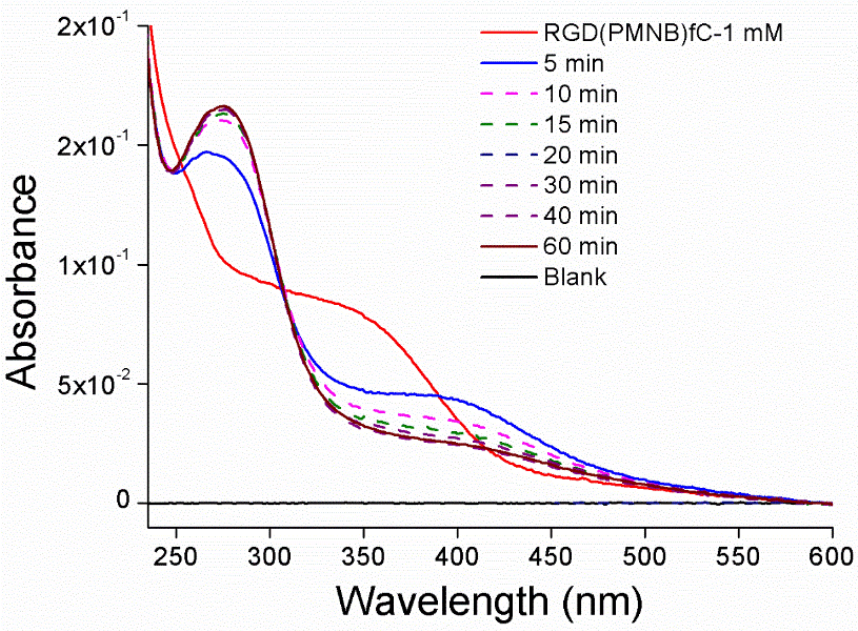

Figure 4. Photochemical reaction expected for RGD(PMNB)fC and corresponding UV-Vis spectra of 1mM RGD(PMNB)fC solution in water with increasing exposure times after irradiation at 360 nm with LUMSO 43 lamp source.

Upon irradiation, the UV spectrum of RGD(PMNB)fC solution showed a decrease in the absorbance at 345 nm and the appearance of two other maxima at 400 nm and 275 nm, already after 5 min of exposure. No further changes were observed in UV profile after 30 min of irradiation indicating completion of the photolysis reaction.

The HPLC profile of RGD(PMNB)fC solution after 30 min of irradiation showed complete disappreance of caged peptide signal and appearnce of RGDfC peptide signal. The ESI-MS also confirmed the presence of RGDfC peptide after irradiation. RGD(PMNB)fC showed efficient photo-conversion with 86% yield in only 5 min, emphasizing suitability of PMNB chromophore as photo-protecting group for next studies. The predicted photolysis reaction on the basis of literature reports, proceed through β-1 elimination, and the photolyzed side product o-nitro phenyl alkene at 306.48 $[M+ Na]^+$ was confirmed with ESI-MS results.[9a, 18, 21]

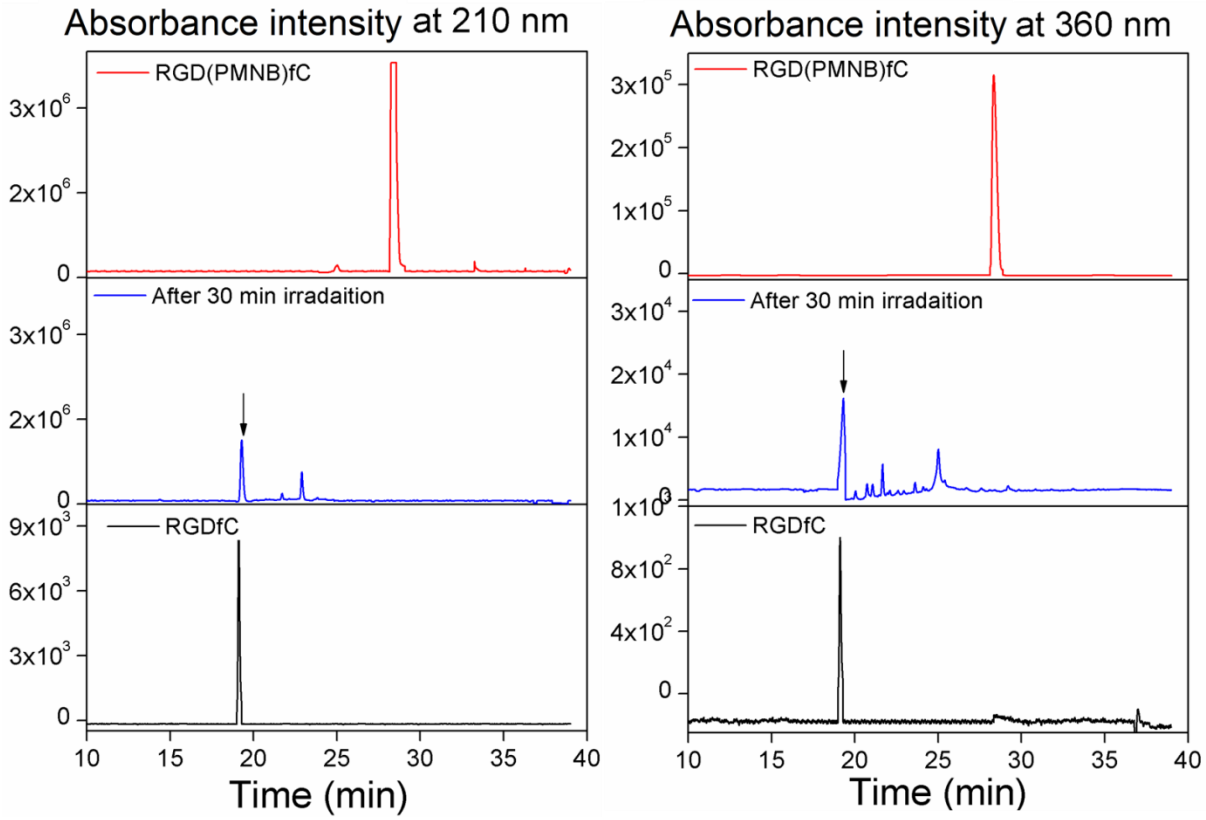

Figure 5. Analytical HPLC chromatograms of RGD(PMNB)fC (1mM) solution before and after irradiation at 360 nm for 30 min. The HPLC profile is shown for 210 and 360 nm absorbance channels. For comparison, the HPLC profile of RGDfC is shown as well.

6.4 Spatiotemporally controlled cell adhesion and migration in 2D cell culture

Cell experiments were performed in order to test the efficiency of PMNB chromophore to block the activity of RGDfC and to reactivate it upon light exposure. First the cytocompatibility of RGD(PMNB)fC peptide was tested in a 2D cell culture using Fibroblast L929. The P(AAm-MS) hydrogels developed in Chapter 3 Section 3.2 were selected and were derivatized with RGD(PMNB)fC.[22] The gel stiffness of 10 kPa was selected as the optimized stiffness for fibroblast from published reports.[23] The RGD(PMNB)fC was covalently immobilized on P(AAm-MS) by nucleophilic substitution of methyl sulfone with thiol. Samples not exposed, fully exposed (6 min at 360 nm using Till photonic polychrome 5000) or exposed through a mask and were incubated with cells for 24 h. Cells seeded on RGD(PMNB)fC samples showed no cell attachment while cells attached and spread on fully

irradiated samples. This demonstrates the effective inhibition of the peptide activity upon attachment of the PMNB chromophore to the aspartic acid, the photo-removal of PMNB chromophore and the reactivation of RGDfC peptide at the surface of the gel (Figure 6 A-B). Cells on patterned irradiated samples showed preferential adhesion to the exposed areas. No cell attachment was observed on unexposed areas after 24 h of cell culture (Figure 6 C-D). The spatial selectivity was retained during 4 days of culture and no attachment was observed on unexposed area during this time. The surface functionalization and cell culture protocols are described in Appendix Section 8.12

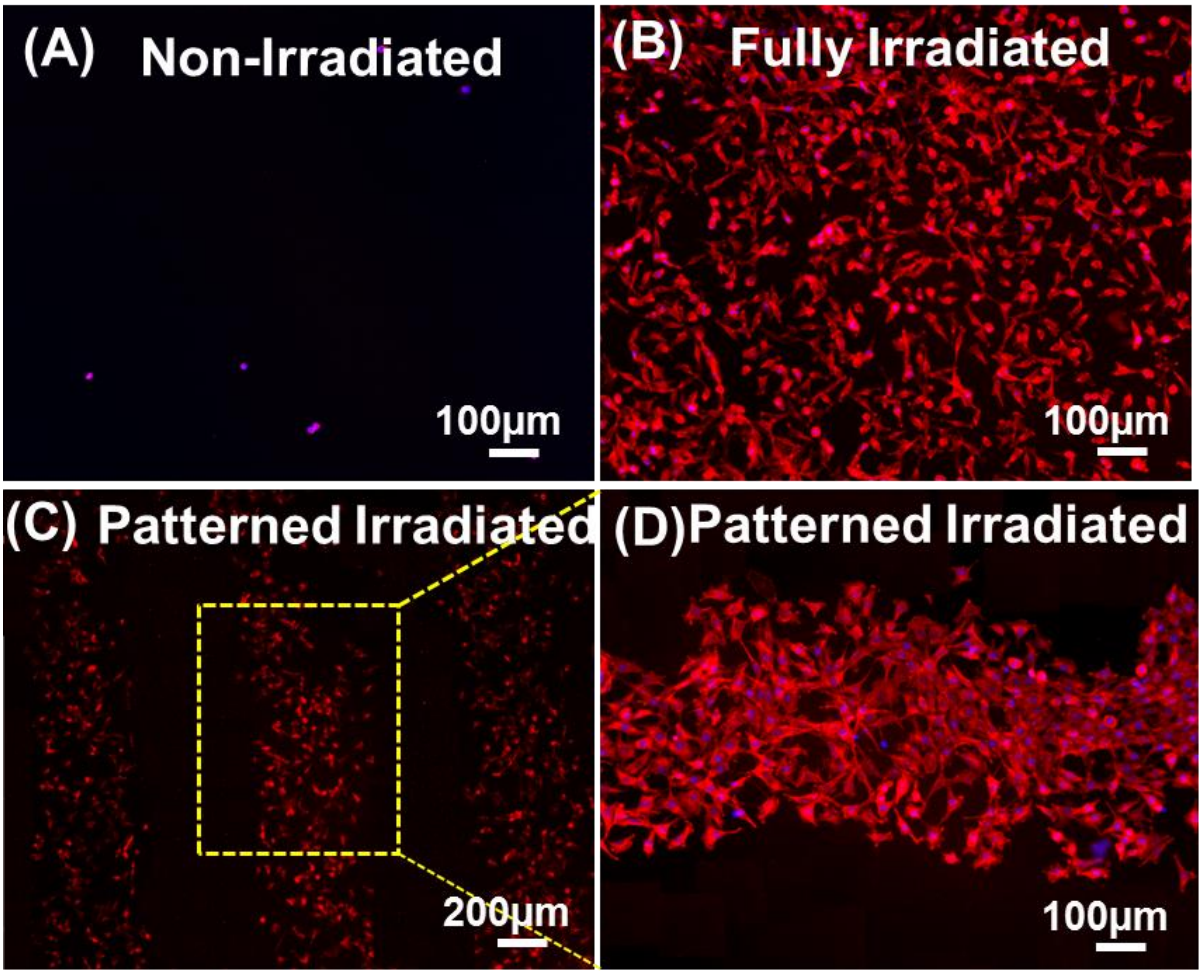

Figure 6. Photo-activatable cell adhesion: Immunoflourescence images of fibroblast L929 cell line, 24 hours after seeding on P(AAm-MS) gel functionalized with (A) RGD(PMNB)fC (B) fully irradiated RGD(PMNB)fC and (C-D) RGD(PMNB)fC irradiated through mask (Strips of 300 µm illuminated area with 600 µm unexposed area preserving caged peptide). The DAPI in blue stained nucleus while F-actin was stained in red by Phalloidin TRITC.

In order to test the possibility of activating the peptide using 2P excitation, lines of 15 µm width and 580 µm length were scanned across the RGD(PMNB)fC modified regions between the activated areas using a Ti:sapphire laser at 740 nm (Figure 7).[9c] After 2P exposure, cells close to the scanned line started to leave the monolayer and migrate into the illuminated pathway, demonstrating the ability of RGD(PMNB)fC modified gels to spatiotemporally control cell attachment and migration upon *in situ* exposure. The RGD(PMNB)fC dependent migration could be extended from single cell to collective migration by adjusting the geometry of activation path (data not shown). These results are in accordance with similar studies with RGD(DMNBP)fK, but extend the applicability to more cell-friendly longer wavelengths by exploiting 2P sensitivity of the PMNB chromophore.[9c]

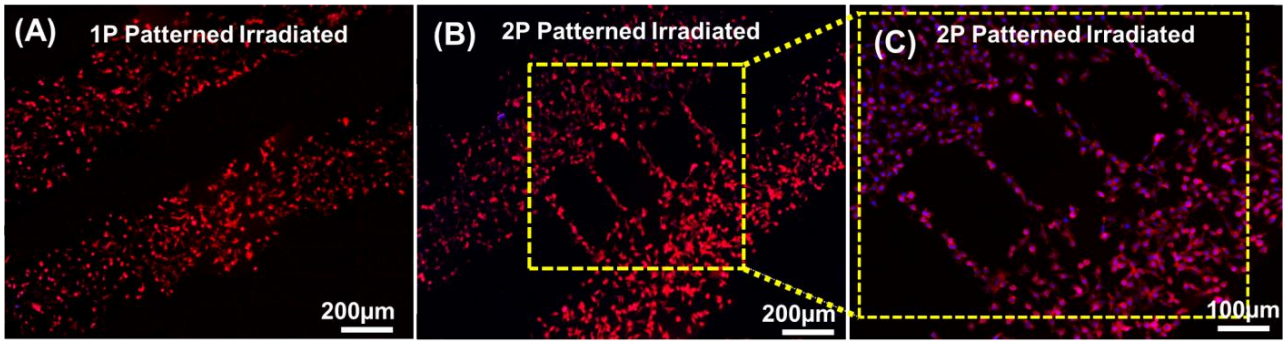

Figure 7. Photo-triggered cell migration on RGDfC adhesive patterns by *in situ* activation of migratory paths with 2P laser at 740 nm for 30 secs at 95% intensity. (A) RGD(PMNB)fC pre-pattern with strips of cells obtained after 1P activation 24h after cell seeding (B-C) 15 µm x 580 µm^2 migratory path was opened between strips of cells by 2P activation, 24 h after 2P activation.

6.5 Cell migration in 3D pathways defined by 2P activation

6.5.1 Synthesis and physicochemical properties of thiol/maleimide PEG hydrogels for cell encapsulation

The PEG thiol/maleimide system was selected to build 3D PEG gels for culturing cells. This system is well established among hydrogels for 3D cell cultures and is reported to show fast crosslinking kinetics, bio-orthogonality of thiol-maleimide reaction, gelation at physiological conditions and cytocompatibility.[24] The thiol group undergoes Michael addition with maleimide in the presence of nucleophilic HEPES

buffer.[25] The PEG network is non-degradable. However, enzymatic degradability can be implemented by incorporating degradable peptide sequences, eg. GCRDVPMSMRGGDRCG (VPM) to be selectively cleaved by matrix metalloproteinases (MMPs).[26]

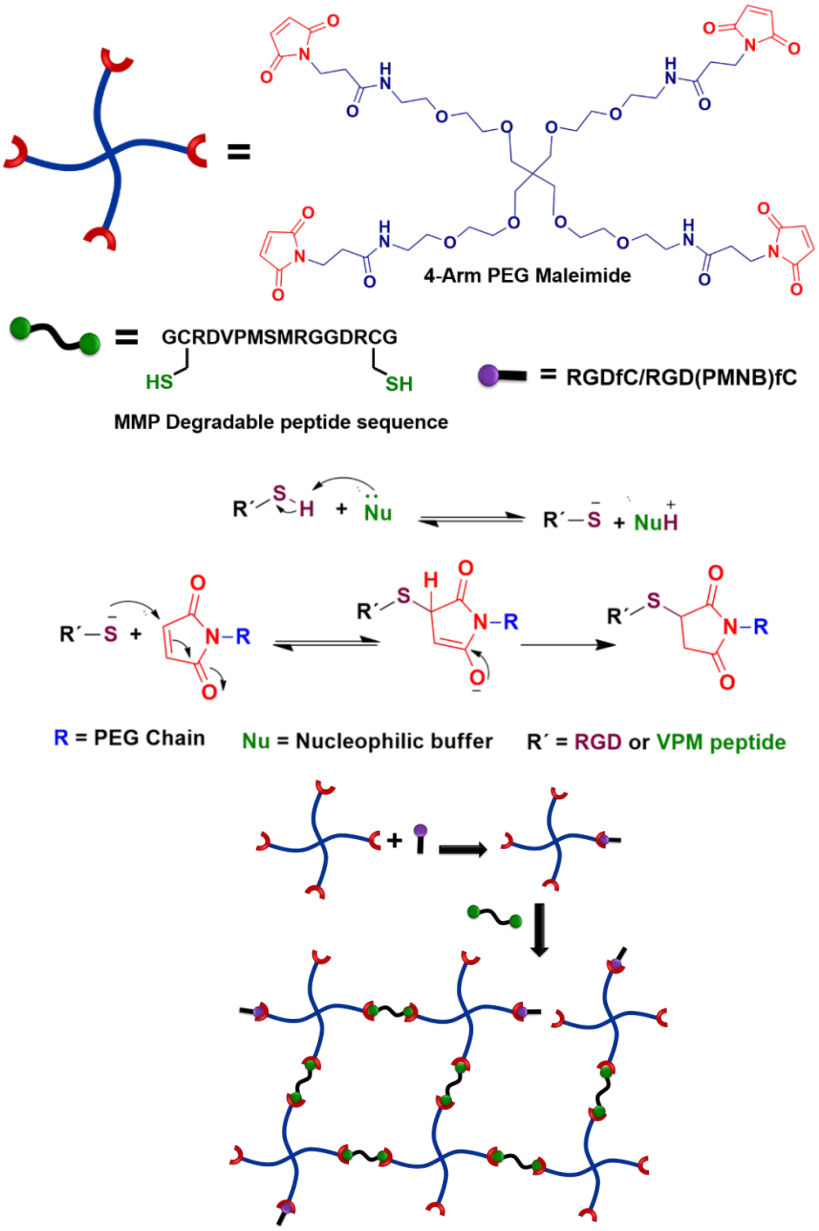

Figure 8. Schematic representation of the structure and synthesis of PEG maleimide-thiol hydrogels.

PEG hydrogels functionalized with adhesive ligands were prepared in a one pot reaction by mixing 4-Arm PEG maleimide with RGDfC and the degradable dithiol peptide as cross-linker at pH 7.4. The properties of PEG hydrogels can be adjusted

by changing the amount of PEG monomer and the cross-linker. A polymer content of 4wt% PEG, 1 mM of RGD ligand and 3 mM of crosslinking peptide were selected from previous reports.[24]

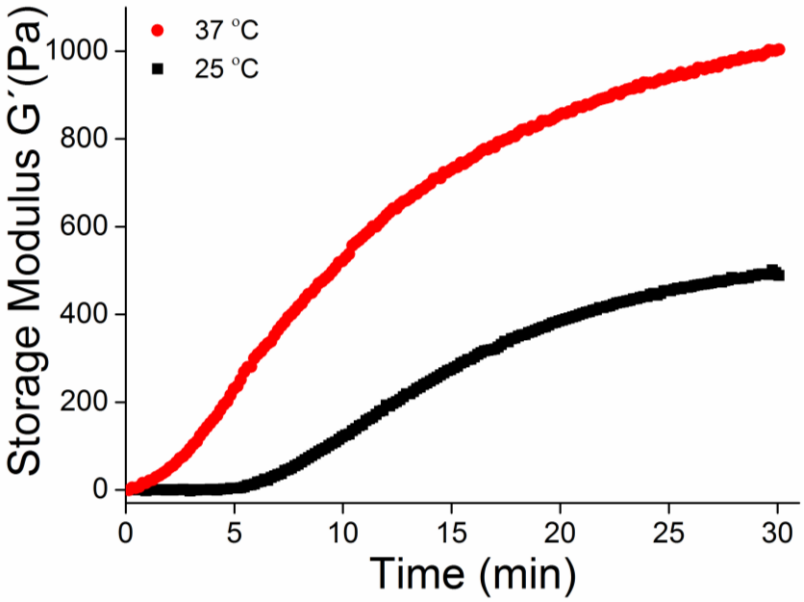

Figure 9. Polymerization kinetics of PEG hydrogel by dynamic mechanical analysis at different polymerization temperatures.

The physicochemical properties of PEG hydrogels, i.e swelling ratio, thickness and stiffness, obtained at different temperatures (25 and 37°C) were characterized. The stiffness of the gels was measured in a parallel plate rheometer. The curing kinetics of the hydrogel was followed by time sweep (0- 30 min). The shear modulus showed a continuous increase up to 760 Pa in 15 mins, indicative of rapid formation of a soft gel. The final storage modulus was temperature dependent: the storage modulus at 37°C was 2 folds higher than obtained at 25°C (~ 1 kPa vs 0.5 kPa Figure 9). The gelation kinetics was also temperature dependent and gelation was faster at 37°C presumably due to higher reactivity of maleimide-thiol reaction. The swelling degree of the hydrogel was measured after crosslinking of hydrogel for 30 min at 37°C. The water content of polymerized hydrogel was measured before and after drying. A swelling ratio of 162% was obtained for the hydrogel network. The thickness of the obtained hydrogel was dependent on the size of the mold used for the preparation (see Appendix Section 8.19.2) and the initial volume of monomer solution used during gelation. For these studies, a thickness of 800 µm was selected owing transparency under microscope. The thickness of free standing hydrogel was

determined directly by micrometer. The details of gel preparation and characterization are described in Appendix Section 8.19.

Table 2. The physicochemical properties of 4wt% PEG hydrogel.

Properties	**Results**
Storage Modulus (G´) at 25 °C	480± 70 Pa
Storage Modulus (G´) at 37 °C	1065 ± 120 Pa
Swelling ratio (mg water/mg gel)	162±14
Swollen Thickness	800µm

6.5.2 3D patterning of cell adhesive ligands in PEG hydrogels

In order to test the possibility to generate spatially defined 3D patterns of activated adhesive ligands inside the PEG hydrogel using a scanning two-photon laser, a commercially available photoactivatable fluorescein was incorporated into the gel composition. This molecule carries a bis-(5-carboxymethoxy-2-nitrobenzyl) ether (CMNP) chromophore that can be removed at 740 nm by 2P excitation laser to become fluorescent (Figure 10 A). This permits the visualization of the irradiated volume by the local increase in the reporting fluorescence signal. gels were scanned with the 2P laser and the 3D fluorescence pattern was imaged.

Different patterns with increasing exposure time were first scanned and evaluated. The hydrogel was subjected to irradiation at 10mWcm^{-2} intensity for increasing exposure times (30-120 sec) by adjusting 100-170µm/sec writing speed. Patterns with identical dimensions were scanned in the x,y and z plane (100 µm x 10 µm x 50 µm) (Figure 10 B). Patterns obtained with longer irradiation time showed higher fluorescence, demonstrating the dose-dependent uncaging of the fluorophore with 3D resolution. The dimensions of the patterns were comparable, reflecting the precise local activation of the chromophore at the focal plane of the TP laser.

The resolution of patterning in z-axis was evaluated by writing a pre-defined patterns with defined (x, y) dimension but different z-resolution in 3D. The caged fluorescein labeled PEG hydrogels were irradiated with 170µm/sec writing speed but with different penetration depth in z-axis from 5 to 60 µm at 10mWcm^{-2} laser intensity. The resolution in z-axis was qualitatively controlled and defined patterns from 5-60

µm were obtained (Figure 10C). These results demonstrate that the photoactivation of PEG hydrogels can be finely tuned with micrometer resolution (≥ 2 µm) by 2P activation.

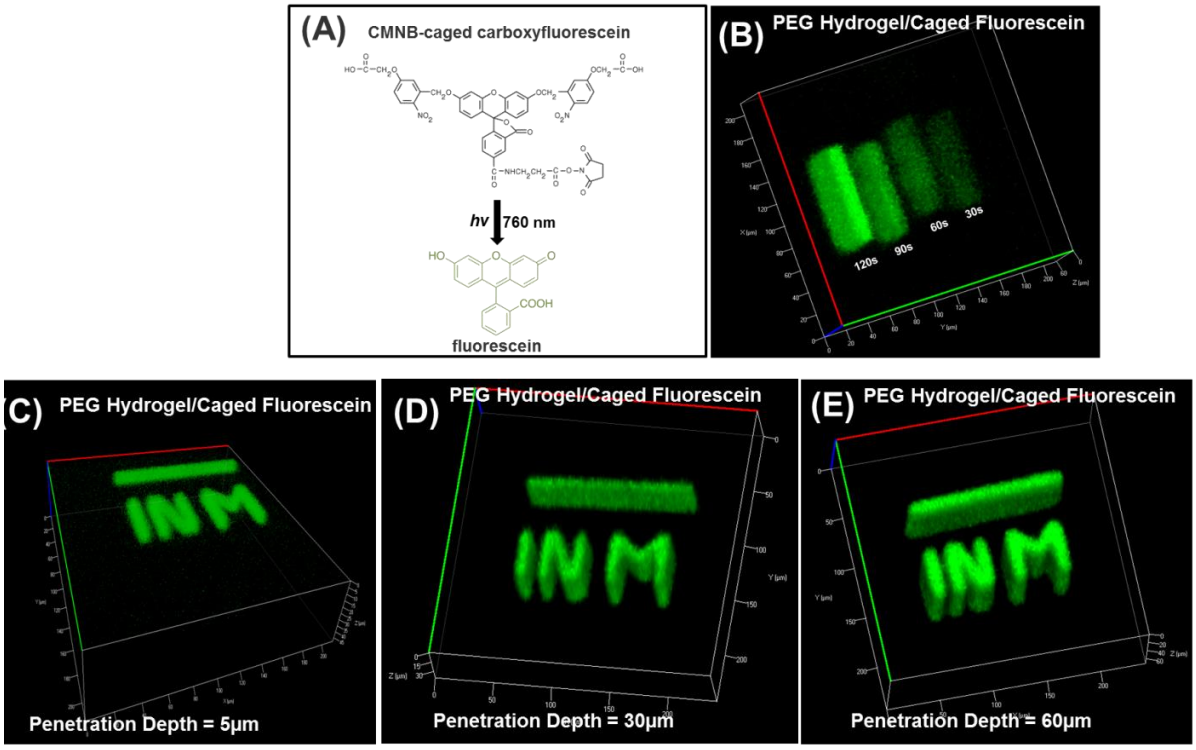

Figure 10. 3D patterning by 2P activation: (A) structure and photoactivation of caged fluorescein, Confocal microscopy z-stack of written structure (B) Scanned lines on PEG hydrogels at increasing exposure times. The longer exposure time increase the intensity of reporting fluorophore without effecting dimensions (C-E) Photo-patterning in 3D with different penetration depth.

6.5.3 Cell migration on gels after two-photon activation of RGD(PMNB)fC

The 3D activation of RGD(PMNB)fC mediated cell migration was demonstrated using Fibroblasts L929 embedded in a fibrin clot. The 4-Arm PEG was incubated with RGD(PMNB)fC or RGDfC, followed by addition of Fibroblast L929 fibrin clot with medium and crosslinking of hydrogel, initiated by addition of VPM peptide at 37 °C. The cells encapsulated in the hydrogels were transferred into cell culture medium and incubated for 1 week.

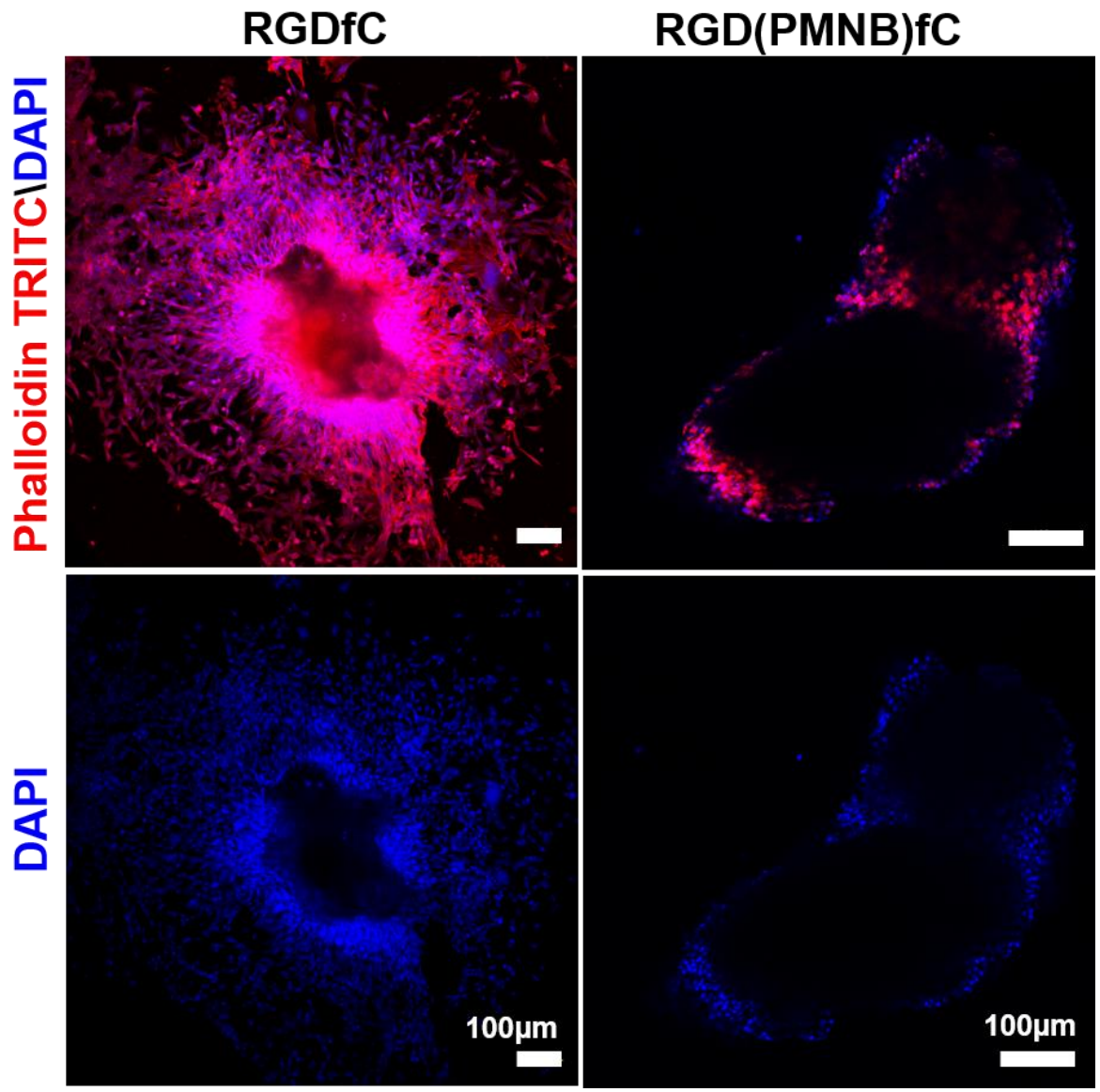

Figure 11. Cell laden fibrin clot of Fibroblast L929 encapsulated in 3D cell culture: Immunofluorescence images of cells in PEG hydrogels modified with RGDfC and RGD(PMNB)fC, 7 days after cell culture. Nucleus was stained by DAPI while actin fibers were stained with Phalloidin.

The cells were stained with phalloidin and DAPI for imaging the actin cytoskeleton and the nucleus respectively after 1 week of culture (Figure 11). The cells incubated in RGD(PMNB)fC gels remained confined inside the fibrin clot and no attachment or migration into the surrounding PEG gel was observed. These results indicate that RGD(PMNB)fC ligand cannot be recognized by the integrin membrane receptors and remains inactive and hydrolytically stable during at least 1 week under cell culture conditions, in accordance with 2D cell culture studies in section 6.2.2. The cells

inside the fibrin clot showed no DAPI staining indicating fragmentation of nuclei and apoptosis. On the contrary, cells encapsulated in RGDfC modified gels showed proliferation and migration out of fibrin clot into the hydrogel network after 3 days of cell culture. Cells inside the clot also displayed visible actin network and intact nucleus, indicating that cells remained viable only when surrounded by a gel with the adhesive RGDfC ligand.

Using a Ti-sapphire laser, a circular pattern was scanned in front of the cell clot encapsulated in RGD(PMNB)fC hydrogel (Figure 12). The circular pattern was written in 2 mins by 2P laser with 100µm/sec speed at 740 nm (Appendix Section 8.20). Cells migrated from the spheroid into the illuminated region within 3 days and remained confined to the illuminated space (Figure 12). This result demonstrates the successful two-photon mediated, spatiotemporal activation of RGD(PMNB)fC peptide and the consequent site-and time-specific cell response.

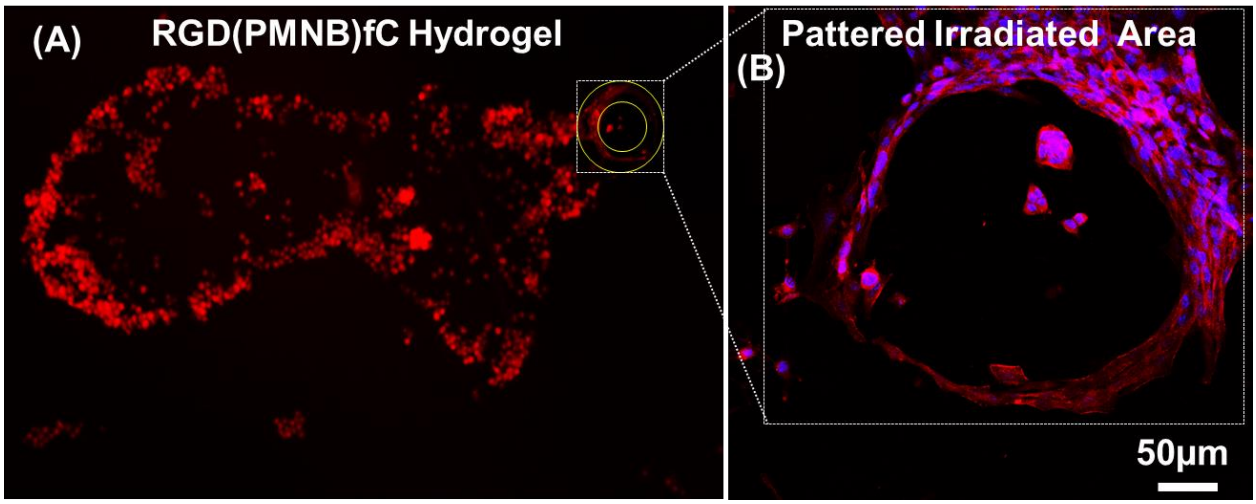

Figure 12. Encapsulated Fibroblast laden fibrin clot in 3D hydrogel (A) Embedded in RGD(PMNB)fC with small photoactivated area marked with yellow circles in front of spheroid (B) The cell migration on light activated RGD(PMNB)fC modified PEG hydrogels, 5 days after cell culture. The photo-patterning was written in 400x400x50 μm^3 volume in x, y and z dimensions respectively.

6.6 Conclusions

The temporal and 3D spatial distribution down to micron scale of ECM adhesive ligands into a hydrogel can be controlled by two-photon activatable RGD mimetic peptides. In this chapter, a 2P activatable version of the RGDfC peptide was

obtained with high purity and in milligram scale. PEG-maleimide hydrogels functionalized with RGD(PMNB)fC were employed for cell encapsulation and *in situ* activation of cell migration in predefined 3D patterns. Fibroblast spheroids encapsulated in 3D hydrogels functionalized with RGD(PMNB)fC showed migration of cells into pre-exposed areas. The patterns could be maintained over several days, demonstrating the selectivity and stability of the method. These hydrogels provide the possibility of 4D control, i.e. in 3D space and in time, of adhesive-ligand mediated cell behavior and can be regarded as dynamic mimics of *in vivo* remodeling of the extracellular space.

References

[1] A. Higuchi, Q.-D. Ling, S.-T. Hsu, A. Umezawa, *Chemical Reviews* **2012**, *112*, 4507-4540.

[2] A. M. Rosales, K. S. Anseth, *Nature Reviews Materials* **2016**, *1*, 15012.

[3] B.-h. Chueh, Y. Zheng, Y.-s. Torisawa, A. Y. Hsiao, C. Ge, S. Hsiong, N. Huebsch, R. Franceschi, D. J. Mooney, S. Takayama, *Biomedical microdevices* **2010**, *12*, 145-151.

[4] C. A. DeForest, K. S. Anseth, *Nature chemistry* **2011**, *3*, 925-931.

[5] aA. M. Kloxin, K. J. Lewis, C. A. DeForest, G. Seedorf, M. W. Tibbitt, V. Balasubramaniam, K. S. Anseth, *Integrative Biology* **2012**, *4*, 1540-1549; bM. A. Azagarsamy, I. A. Marozas, S. Spaans, K. S. Anseth, *ACS macro letters* **2015**, *5*, 19-23; cR. Y. Tam, L. J. Smith, M. S. Shoichet, *Accounts of Chemical Research* **2017**.

[6] aC. A. DeForest, B. D. Polizzotti, K. S. Anseth, *Nature materials* **2009**, *8*, 659-664; bP. M. Kharkar, K. L. Kiick, A. M. Kloxin, *Polymer Chemistry* **2015**, *6*, 5565-5574; cC. Zhu, C. J. Bettinger, *Journal of Materials Chemistry B* **2014**, *2*, 1613-1618.

[7] aC. A. DeForest, E. A. Sims, K. S. Anseth, *Chemistry of materials* **2010**, *22*, 4783-4790; bC. A. DeForest, D. A. Tirrell, *Nature materials* **2015**, *14*, 523-531.

[8] aC. A. DeForest, K. S. Anseth, *Angewandte Chemie* **2012**, *124*, 1852-1855; bM. Wirkner, J. M. Alonso, V. Maus, M. Salierno, T. T. Lee, A. J. García, A. Del Campo, *Advanced Materials* **2011**, *23*, 3907-3910.

[9] aS. Petersen, J. M. Alonso, A. Specht, P. Duodu, M. Goeldner, A. del Campo, *Angew Chem Int Ed Engl* **2008**, *47*, 3192-3195; bM. Wirkner, S. Weis, V. San Miguel, M. Álvarez, R. A. Gropeanu, M. Salierno, A. Sartoris, R. E. Unger, C. J. Kirkpatrick, A. del Campo, *ChemBioChem* **2011**, *12*, 2623-2629; cM. J. Salierno, A. J. García, A. Del Campo, *Advanced Functional Materials* **2013**, *23*, 5974-5980; dM. J. Salierno, L. García-Fernandez, N. Carabelos, K. Kiefer, A. J. García, A. del Campo, *Biomaterials* **2016**, *82*, 113-123; eT. T. Lee, J. R.

García, J. I. Paez, A. Singh, E. A. Phelps, S. Weis, Z. Shafiq, A. Shekaran, A. del Campo, A. J. García, *Nature Materials* **2015**, *14*, 352-360.

[10] aS. Weis, Z. Shafiq, R. A. Gropeanu, A. del Campo, *Journal of Photochemistry and Photobiology A: Chemistry* **2012**, *241*, 52-57; bJ. Iturri, L. García-Fernández, U. Reuning, A. J. García, A. Del Campo, M. J. Salierno, *Scientific reports* **2015**, *5*.

[11] aD. Warther, S. Gug, A. Specht, F. Bolze, J.-F. Nicoud, A. Mourot, M. Goeldner, *Bioorganic & medicinal chemistry* **2010**, *18*, 7753-7758; bS. Piant, F. Bolze, A. Specht, *Optical Materials Express* **2016**, *6*, 1679-1691.

[12] M. Drobizhev, N. S. Makarov, S. E. Tillo, T. E. Hughes, A. Rebane, *Nature methods* **2011**, *8*, 393-399.

[13] S.-H. Lee, J. J. Moon, J. L. West, *Biomaterials* **2008**, *29*, 2962-2968.

[14] C. Mas-Moruno, R. Fraioli, F. Rechenmacher, S. Neubauer, T. G. Kapp, H. Kessler, *Angewandte Chemie* **2016**, *128*, 7162-7183.

[15] aM. Aumailley, M. Gurrath, G. Müller, J. Calvete, R. Timpl, H. Kessler, *FEBS letters* **1991**, *291*, 50-54; bR. Haubner, R. Gratias, B. Diefenbach, S. L. Goodman, A. Jonczyk, H. Kessler, *Journal of the American Chemical Society* **1996**, *118*, 7461-7472.

[16] S. Petersen, J. M. Alonso, A. Specht, P. Duodu, M. Goeldner, A. del Campo, *Angewandte Chemie International Edition* **2008**, *47*, 3192-3195.

[17] L. García-Fernández, C. Herbivo, V. S. M. Arranz, D. Warther, L. Donato, A. Specht, A. del Campo, *Advanced Materials* **2014**, *26*, 5012-5017.

[18] L. Donato, A. Mourot, C. M. Davenport, C. Herbivo, D. Warther, J. Léonard, F. Bolze, J. F. Nicoud, R. H. Kramer, M. Goeldner, *Angewandte Chemie International Edition* **2012**, *51*, 1840-1843.

[19] S. Gug, S. Charon, A. Specht, K. Alarcon, D. Ogden, B. Zietz, J. Léonard, S. Haacke, F. Bolze, J. F. Nicoud, *ChemBioChem* **2008**, *9*, 1303-1307.

[20] A. Specht, F. Bolze, L. Donato, C. Herbivo, S. Charon, D. Warther, S. Gug, J.-F. Nicoud, M. Goeldner, *Photochemical & Photobiological Sciences* **2012**, *11*, 578-586.

[21] S. Walbert, W. Pfleiderer, U. Steiner, *Helvetica Chimica Acta* **2001**, *84*, 1601-1611.

[22] A. Farrukh, J. I. Paez, M. Salierno, A. del Campo, *Angewandte Chemie* **2016**, *128*, 2132–2136.

[23] J. Solon, I. Levental, K. Sengupta, P. C. Georges, P. A. Janmey, *Biophysical journal* **2007**, *93*, 4453-4461.

[24] E. A. Phelps, N. O. Enemchukwu, V. F. Fiore, J. C. Sy, N. Murthy, T. A. Sulchek, T. H. Barker, A. J. García, *Advanced Materials* **2012**, *24*, 64-70.

[25] B. H. Northrop, S. H. Frayne, U. Choudhary, *Polymer Chemistry* **2015**, *6*, 3415-3430.

[26] M. A. Azagarsamy, K. S. Anseth, *ACS macro letters* **2013**, *2*, 5-9.

Chapter 7

Conclusion and Outlook

In this PhD thesis novel, photoactivatable peptidomimetics of laminin have been developed and applied to guide neuronal growth in *in vitro* cell cultures. The peptidomimetics were IKVAV-containing sequences that have been reported to support neurite extension. Different photoremovable protecting group were attached to a Lys rest of the sequence to temporally inhibit bioactivity and allow light-triggered activation in the presence of cells. The obtained photoactivatable peptides were conjugated to soft polyacrylamide films using a new coupling strategy to functionalize PAAm with thiol-containing molecules and eventually amine containing molecules as well. The modified gels efficiently supported growth of neuronal cultures. *In situ* directional neurite extension was realized. A similar strategy was also tested in 3D gels using two-photon sensitive chromophores and a scanning laser. Light guided migration of fibroblasts embedded in a 3D degradable gel was demonstrated.

The following are the major conclusions of this work:

1) The hydrophobicity of IKVAV-containing peptidomimetics constitutes an important limitation for their use as cell adhesive ligands on hydrogels. All reported peptides showed poor performance in the cell assays, presumably as a consequence of their aggregation in solution at any tested condition. The peptide IK(HANBP)VAV synthesized in this Thesis was a fortunate exception. The presence of the hydrophilic HANBP group prevented aggregation, improved solubility and showed a remarkable better performance after light exposure than all other peptidomimetics with longer sequences in the performed biological assays.

2) Light-activatable peptidomimetics of cell adhesive molecules allow effective and precise activation of cell adhesion, migration and differentiation in time and space. This Thesis demonstrated that photoactivation is possible in 2D and 3D contexts using appropriate chromophores and single and two-photon photochemical processes. In this Thesis IK(HANBP)VAV enabled light guided

neural growth and directional axon growth in 2D. The c[RGD(PMNB)fC] enabled directional migration of fibroblasts within a 3D hydrogel previously scanned with a two-photon laser.

3) Phototriggerable biological ligands allow specific and quantitative activation of interactions at molecular scale with light. However, when those ligands are immobilized on biomaterials, this precision and the consequent control over biological processes can be partially lost if conjugation strategies are less precise. In this Thesis, new conjugation strategies based on methylsulfones chemistry for specific and quantitative covalent immobilization of thiolated biomolecules to widely used poly(acrylamide) hydrogels were developed. This chemical strategy is orthogonal to well established EDC/NHS coupling chemistry for COOH and NH_2 groups, allowing selective immobilization of two different ligands in independent concentrations to P(AAm) gels. A demonstration of how coupling chemistry impacts cell-biomaterials interactions is provided in this Thesis in the context of neuronal development on Poly(lysine)/IKVAV modified gels. This biomaterial is envisioned as an ideal platform for *in vitro* studies of the impact and crosstalk between biochemical and mechanical factors in the responses of cells to biomaterials.

4) This Thesis demonstrates the potential of IK(HANBP)VAV to guide neuronal growth and spatially direct axon development. This is the first step towards biomaterials able to *in situ* control neural network formation and circuitry. This work can be further extended in the future to 3D and *in vivo* contexts, and eventually end in novel scaffolds for directed nerve regeneration in the clinic.

Chapter 8

Appendix[1]

The section entails photocage, acrylate and peptide synthesis, preparation and characterization of hydrogels, surface functionalization and cell culture protocols.

Appendix Chapter 2	**Section 8.2 - 8.6**
Appendix Chapter 3	**Section 8.6 - 8.8**
Appendix Chapter 4	**Section 8.9- 8.14**
Appendix Chapter 5	**Section 8.15 - 8.16**

Experimental Section

8.1 Materials and Methods

DIBAL-H (Diisobutylaluminium hydride 1M in THF), methyl iodide (MeI), sodium hydride (NaH), potassium tert-butoxide (^{t}BuOK), potassium carbonate (K_2CO_3), triphosgene, [1,1'-Bis(diphenylphosphino)ferrocene]palladium(II) dichloride ($PdCl_2$(dppf), palladium acetate (PdOAc), trifluoroacetic acid (TFA), iodo-anisole, iodo-dimethylaniline, 1-Hydroxybenzotriazole hydrate (HOBt), *N,N,N′,N′*-Tetramethyl-*O*-(1*H*-benzotriazol-1-yl)uronium hexafluorophosphate (HBTU), *N*,*N*-Diisopropylethylamine (DIPEA), N-(3-dimethylaminopropyl)-N′-ethylcarbodiimide hydrochloride) (EDC), N-hydroxysuccinimide (NHS), acrylamide (AAm), bisacrylamide, tetramethylethylenediamine TEMED, ammonium persulfate (APS), 4-(2-hydroxyethyl)-1-piperazineethanesulfonic acid (HEPES), and 2-(N-morpho)-ethanesulfonic acid (MES) were purchased from Sigma-Aldrich and used as received, unless specified. Dry THF, DCM, toluene, acetonitrile, and DMF were purchased from Acros (Geel, Belgium). All Fmoc/tBu protected amino acids were acquired from Merck Novabiochem (Darmstadt, Germany) and used without purification.

[1]The content of this chapter was published in Angewandte Chemie International Edition (2016), Volume 128 (6), page 2132–2136, A. Farrukh, J. I. Paez, M. Salierno, A. del Campo, “Bioconjugating Thiols to Poly(acrylamide) Gels for Cell Culture Using Methylsulfonyl Co-monomers’’ and with permission from American chemical Society, published in Biomacromolecules (2017), Volume 18, page 906-913. A. Farrukh, J. I. Paez, M. Salierno, W. Fan, B. Berninger, A. del Campo, “Bifunctional poly(acrylamide) hydrogels through orthogonal coupling chemistries’’[1]

CSRARKQAASIKVAVSADR (IK-19) was obtained from alfa asear and CCRRIKVAVWLC (C-C) from Eurogentec (köln Germany). Solid phase peptide synthesis (SSPS) was performed manually using 10-mL syringes as reaction vessels equipped with PE-filters (CEL- 053 and CEL-1016), (Roland Vetter Laborbedarf OHG, Ammerbuch, Germany) for washing steps. Trityl-linker (TCP) resin, TCP-L-Val-Fmoc (loading 0.42 mmol/g), TCP-L-Arg(Pbf)-Fmoc (loading 0.37 mmol/g) and H-Gly-2-Cl-Trt resin (0.56 mmol/g) were obtained from Intavis AG Bioanalytical Instruments (Tübingen, Germany). Fmoc-NH_2-(EG_2)-COOH was obtained from Novabiochem (Darmstadt, Germany). The RGDfC was purchased from peptide international (Kentucky, USA). The peptides containing chromophores for the quantitative determination of ligand density within the hydrogels were synthesized by Dr. Julieta Paez by using previously reported protocols: cyclo[RGD(DMNPB)fK],[2] cyclo[RGD(DMNPB)fC],[3] cyclo[RGD(coum)fK],[4] and cyclo[RGD(coum)fC. Thiols for SAMs TH 001-m11.n3-0.2 and TH 003-m11.n6-0.1 were purchased from (ProChimia,Gdansk, Poland). 4-Arm-PEG Maleimide 20K was purchased from Creative PEG work (North Carolina, USA) and GCRDVPMSMRGGDRCG from Proteogenix (Schitigheim, France). UV/VIS Spectra were recorded with a Varian Cary 4000 UV/VIS spectrometer (Varian Inc. Palo Alto, USA). ^{1}H-NMR spectra were measured at 298K in a Bruker Avance 300 (300 MHz) spectrometer. ESI-MS spectra were recorded using a QTos Ultima 3. HPLC analysis and purification of the compounds was performed with a HPLC JASCO 4000 (Japan) equipped with a diode array UV-Vis detector and fraction collector. Reprosil C18 columns were used for semi-preparative (250 × 25 mm) and analytical (250 × 5 mm) runs.

Appendix Chapter 2

8.2 Synthesis of Caged Lysine

8.2.1 NVOC caged Lysine [Fmoc-Lys-(NVOC)-OH]

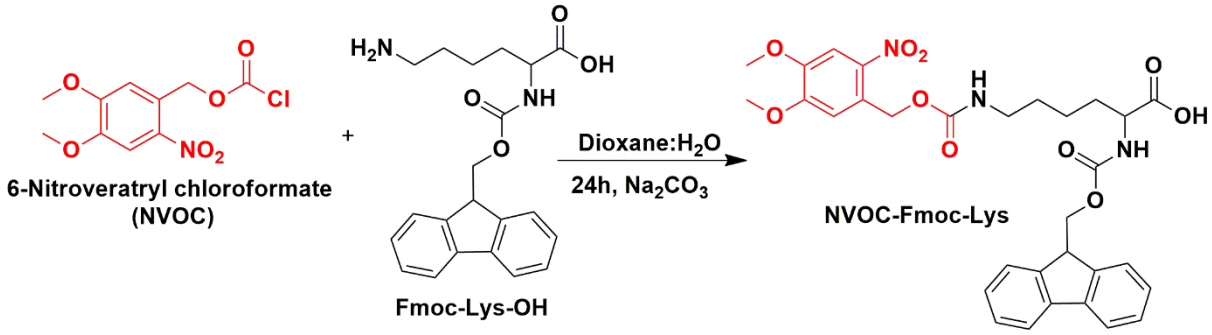

Scheme A1. Synthetic pathway for Fmoc-Lys(NVOC)-OH

a. 4,5-dimethoxy-2-nitrobenzyl)oxy)carbonyl)N-Fmoc-L-lysine

4,5-dimethoxy-2-nitrobenzyl)oxy)carbonyl)N-Fmoc-L-lysine synthesis was adapted from previous report.[5] Fmoc-Lysine-OH (368 mg, 1 mmol) was dissolved in water:dioxane (1:1, 10 mL) and Na_2CO_3 (233 mg, 2.2 mmol) was added at 0°C. 2-(2-nitrophenyl)propyl chloroformate (275 mg, 1 mmol) was dissolved in THF (1 mL) and slowly added to above solution, stirred for 20 min at 0°C and then stirred for 24h at room temperature. The solvent was evaporated and water (5 mL) was added, followed by extraction with EtOAc to remove unreacted NVOC. The aqueous layer was acidified by addition of 5% HCl (10 mL) at 0 °C to precipitate out unreacted Fmoc-Lys-OH and product was extracted with EtOAc. The volatiles were evaporated and the obtained product (orange solid) was used directly without further purification (0.55 g, 91%).

^{1}H-NMR (300 MHz, $CDCl_3$): δ/ppm = 1.43-1.46 (m, 2H); 1.52-1.56 (m, 2H); 1.82-1.92 (m, 2H); 3.21-3.24 (m, 2H); 3.72-3.78 (m, 1H); 3.92 (s, 3H); 4.15-4.20 (m, 1H); 4.36-4.39 (m, 2H); 5.22-5.28 (m, 1H); 6.98 (s, 1H); 7.23-7.38 (m, 6H); 7.54-7.57 (d, J=7.0 Hz, 2H); 7.66 (s, 1H); 7.72-7.55 (d, J=9.0 Hz, 2H).

^{13}C-NMR (75 MHz, $CDCl_3$): δ/ppm = 22.1 ($-CH_2$); 29.2 ($-CH_2$); 30.9 (-CH); 40.6 ($-CH_2$); 47.1 (-CH); 53.5 (-CH); 56.3 ($-CH_3$); 63.6 ($-CH_2$); 67.3 ($-CH_2$); 77.3 ($-CH_2$); 108.2 (-CH); 110.3(-CH); 119.5 (-CH); 125.4 (-CH); 127.1 (-CH); 127.7 (-CH); 127.9

(-C); 139.7 (-CH); 141.2 (-C); 143.6 (-C); 143.7 (-C); 148.6 (-C); 153.5 (-C); 155.9 (-C=O); 156.43 (-C=O); 175.1 (-C=O)

ESI-MS: 607.22 [M +H]+ , 630.28 [M+Na]+

8.2.2 DMNPB caged Lysine [Fmoc-Lys-(DMNPB)-OH]

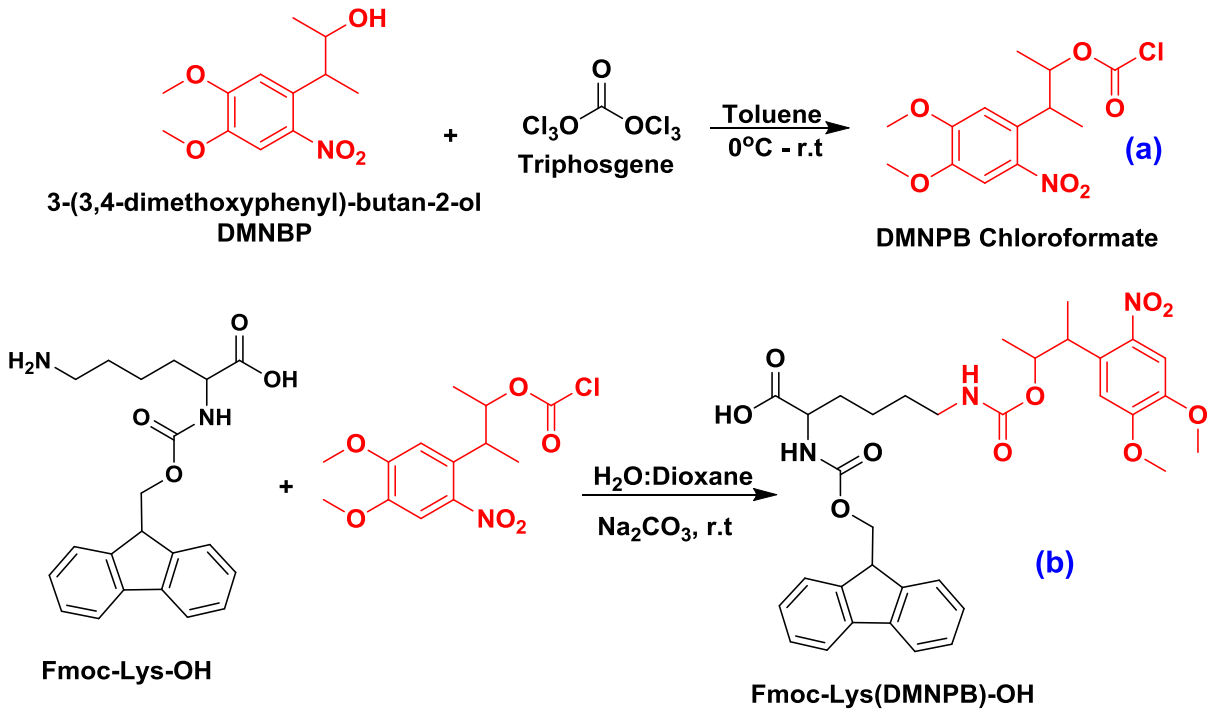

Scheme A2. Synthetic pathway for Fmoc-Lys(DMNPB)-OH

a. 3-(4,5-dimethoxy-2-nitrophenyl)butan-2-yl carbonochloridate

Triphosgene (50 mg) was dissolved in toluene (2 mL), followed by addition of K_2CO_3 (45 mg), and catalytic amount of DMF. The mixture was stirred for 30 min at 0°C. 3-(4,5-dimethoxy-2-nitro-phenyl)-butan-2-ol (200 mg, 0.78 mmol) obtained according to previously described procedure[6] was dissolved in toluene (2 mL) and added to the above mixture at 0°C. The mixture was stirred for 8h at room temperature. The volatiles were evaporated under nitrogen and the obtained product was used directly for the next reaction without further purification.

b. 3-(4,5-dimethoxy-2-nitrophenyl)butan-2-yl)oxy)carbonyl)N-Fmoc-L-lysine

Fmoc-Lys(4,5-dimethoxy-2-nitrobenzyl)oxy)carbonyl) synthesis was adapted from a previous report.[5] Fmoc-Lys-OH (368 mg, 1 mmol) was dissolved in water:dioxane (1:1, 10 mL) and Na_2CO_3 (233 mg, 2.2 mmol) was added at 0°C. 3-(4,5-dimethoxy-2-nitrophenyl)butan-2-yl carbonochloridate (317 mg, 1 mmol) was dissolved in THF (1 mL) and slowly added to above solution, stirred for 20 min at 0°C and then stirred for 24h at room temperature. The solvent was evaporated and water (5 mL) was added, followed by extraction with EtOAc to remove unreacted DMNPB-OH. The aqueous layer was acidified by addition of 5% HCl (10 mL) at 0 °C to precipitate out unreacted Fmoc-Lys-OH and extracted with EtOAc. The product purified by preparative RP-HPLC using water/acetonitrile containing 0.1% TFA as eluent with 20 to 95% increase in acetonitrile gradient (564 mg, 87%).

^{1}H-NMR (300 MHz, $CDCl_3$): δ/ppm = 1.23-1.26 (m, 3H); 1.29-1.33 (m, 3H); 1.43-1.45 (m, 2H); 1.53-1.57 (m, 2H); 1.73-1.78 (m, 2H); 3.19-3.21 (m, 2H); 3.72 (s, 6H); 3.91-3.97 (m, 1H); 4.15-4.20 (m, 1H); 4.35-4.39 (m, 2H); 5.14-5.22 (m, 1H); 5.45-5.54 (m, 1H); 7.23-7.38 (m, 6H); 7.41-7.49 (m, 2H); 7.54.7.57 (d, J=7.0 Hz, 1H); 7.70-7.54 (d, J=9 Hz, 2H).

^{13}C-NMR (75 MHz, $CDCl_3$): δ/ppm = 17.6 ($-CH_3$); 18.3 ($-CH_3$); 22.2 ($-CH_2$); 29.2 ($-CH_2$); 31.8 (-CH); 40.7 ($-CH_2$); 53.6 (-CH); 56.4 (-CH); 63.8 ($-CH_3$); 67.8 ($-CH_2$); 77.3 ($-CH_2$); 108.2 (-CH); 110.4(-CH); 120.5 (-CH); 125.1 (-CH); 127.1 (-CH); 127.8 (-CH); 139.9 (-CH); 141.3 (-C); 143.7 (-C); 153.5 (-C); 151.7 (-C); 155.9 (-C=O); 157.8 (-C=O); 174.7 (-C=O)

ESI-MS: 649.26 [M +H]+ , 672.52 [M+Na]+

8.2.3 HANBP caged Lysine [Fmoc-Lys-(HANBP)-OH]

a. Tert-butyl 2-(5-bromo-2-nitrophenyl)acetate (a)

4-Bromonitrobenzene (3.67 g, 18.2 mmol) and tert-butyl chloroacetate (4.26 g, 28.3mmol) were dissolved in DMF (50 mL) and slowly added to a stirred solution of *t*-BuOK (12.8 g, 114 mmol) in anhydrous DMF (50 mL). The reaction was stirred under argon at room temperature for 2h, followed by the addition of 5 % HCl (50 mL) at 0°C. The product was extracted with EtOAc and washed twice with excess amount of water. The organic layer was dried over $MgSO_4$, solvent was evaporated and

crude product was subjected to silica gel column chromatography (10% EtOAc/n-Hexane) to obtain a light-yellow solid (4.77 g, 83%).

^{1}H-NMR (300MHz, CDCl3): δ/ppm = 1.41 (s, 9H), 3.89 (s, 2H), 7.48 (d, J=2.0 Hz, 1H), 7.57 (dd, J=8.5/2.0 Hz, 1H), 7.96 (d, J=8.5 Hz, 1H)

^{13}C-NMR (75 MHz, CDCl$_3$): δ/ppm = 27.7 (-CH$_3$); 37.1 (CH); 81.8 (-C); 126.3 (-CH); 127.9 (-CH); 131.0 (-C); 132.8 (-C); 137.7 (-CH); 147.9 (-C); 171.6 (C=O).

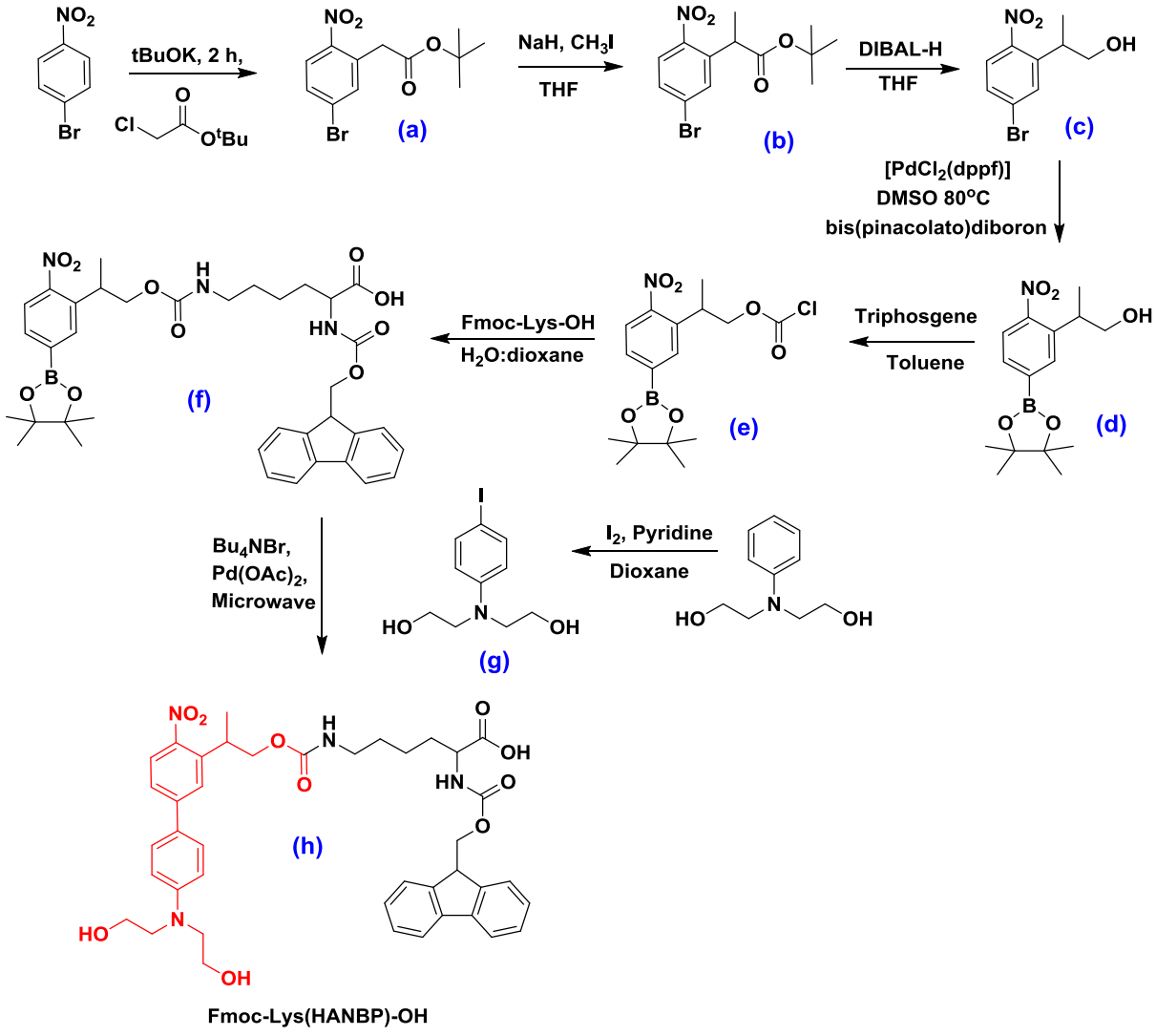

Scheme A3. Synthetic pathway for Fmoc-Lys(HANBP)-OH

b. Tert-butyl 2-(5-bromo-2-nitrophenyl)propanoate (b)

tert-butyl 2-(5-bromo-2-nitrophenyl)acetate **(a)** (1.0 g, 3.17 mmol) was dissolved in dry THF (15 mL) and maintained under argon for 5 min at 0°C. Methyl iodide (2 mL, 30 mmol) was added to above solution followed by addition of NaH (60 % in

suspension in oil, 400 mg, 10 mmol) at 0°C. Ice batch was removed and the mixture was stirred at room temperature under argon for 30 min, then reaction was quenched with water and extracted with EtOAc. The organic layer was dried over $MgSO_4$, then evaporated and the crude product was subjected to silica gel column chromatography (5% EtOAc/n-Hexane) to obtain a light yellow solid (0.92 g, 88%).

^{1}H-NMR (300MHz, CDCl3): δ/ppm = 1.40 (s, 9H), 1.57 (d, J=7.1 Hz, 3H), 4.21 (q, J=7.1 Hz, 1H), 7.54 (dd, J=8.5/2.0 Hz, 1H), 7.62 (d, J=2.0 Hz, 1H), 7.81 (d, J=8.5 Hz, 1H).

^{13}C-NMR (75 MHz, $CDCl_3$): δ/ppm = 17.4 ($-CH_3$); 27.7 ($-CH_3$); 36.8 (CH); 81.8 (-C); 126.3 (-CH); 127.9 (-CH); 131.0 (-C); 132.8 (-C); 137.7 (-CH); 147.9 (-C); 171.6 (C=O).

c. 2-(5-bromo-2-nitrophenyl)propan-1-ol (c)

tert-butyl 2-(5-bromo-2-nitrophenyl)propanoate **(b)** (0.5 g, 1.51 mmol) was dissolved in dry THF (19 ml) and DIBAL-H (4.5 ml, 4.5 mmol, 1 M in THF) was slowly added to the solution at 0°C. The mixture was stirred for 3h at the same temperature and 38 ml of an HCl solution (5 N) were added dropwise at 0°C followed by extraction with EtOAc. The organic layer was washed with brine and dried over anhydrous $MgSO_4$, evaporated and the crude was submitted to column chromatography on silica (10 and 30% EtOAc/n-Hexane) to obtain a pale red oil (200 mg, 52%).

^{1}H-NMR (300MHz, $CDCl_3$): δ/ppm = 1.32 (d, J=7.0 Hz, 3H), 3.55 (m, 1H), 3.78 (m, 2H), 7.49 (dd,J=8.5/2.1 Hz, 1H), 7.63 (d, J=2.1 Hz, 1H), 7.651 (d, J=8.5 Hz, 1H)

^{13}C-NMR (75 MHz, $CDCl_3$): δ/ppm = 17.4 ($-CH_3$); 36.4 ($-CH_2$); 67.6 (-CH); 125.7 (-CH); 127.5 (-CH); 130.4 (-C); 131.6 (-C); 140.5 (-CH); 149.4 (-C).

d. 2-(2-nitro-5-(4,4,5,5-tetramethyl-1,3,2-dioxaborolan-2-yl)phenyl)propan-1-ol (d)

A mixture of 2-(5-bromo-2-nitrophenyl)propan-1-ol **(c)** (346 g**,** 1.33 mmol), $PdCl_2$(dppf) (97 mg, 0.1mmol), KOAc (163 mg, 1.66 mmol), and bis(pinacolato)diboron (372 mg, 1.46 mmol) in DMSO (10 mL) was heated at 80 °C overnight. The reaction mixture was poored into 50 mL ice-water slush and extracted with EtOAc (3x100 mL) and dried over $MgSO_4$. After evaporation of solvent, crude

product was purified by flash chromatography using gradient elution of 20-50% EtOAc/n-Hexane to obtain a dark red oil (200 mg, 49%).

^{1}H-NMR (300MHz, $CDCl_3$): δ/ppm = 1.31-1.34 (m, 14H), 3.41 (q, J=6.8 Hz, 1H), 3.80 (m, 2H), 7.65 (d, J=8.4 Hz, 1H), 7.74 (dd, J=8.4/1.2 Hz, 1H), 7.85 (d, J=1.2 Hz, 1H)

^{13}C-NMR (75 MHz, $CDCl_3$): δ/ppm = 17.6 ($-CH_3$); 24.9 ($-CH_3$), 36.5 ($-CH_2$); 68.1 (-CH); 84.5 (-C); 122.9 (-CH); 133.6 (-CH); 133.7 (-CH); 134.4 (-C); 136.8 (-C); 162.6 (-C).

e. 2-(2-nitro-5-(4,4,5,5-tetramethyl-1,3,2-dioxaborolan-2-yl)phenyl)propylcarbonochloridate (e)

Triphosgene (50 mg) was dissolved in toluene (2 mL), followed by addition of K_2CO_3 (45 mg), and catalytic amount of DMF. The mixture was stirred for 30 min at 0°C. 2-(2-nitro-5-(4,4,5,5-tetramethyl-1,3,2-dioxaborolan-2-yl)phenyl)propan-1-ol **(d)** (200 mg, 0.65 mmol) solution in toluene (2 mL) was added to above mixture at 0°C and stirred for 8h at room temperature. The volatiles were evaporated under nitrogen. The formed chloroformate was confirmed by TLC and used directly for the next reaction without further purification.

f. 2-(2-nitro-5-(4,4,5,5-tetramethyl-1,3,2-dioxaborolan-2-yl)phenyl)propoxy)carbonyl), Fmoc-lysine (f)

Fmoc-Lysine-OH (368 mg, 1 mmol) was dissolved in water:dioxane (1:1, 10 mL) and Na_2CO_3 (233 mg, 2.2 mmol) was added at 0°C. Compound **(e)** (300 mg, 0.81 mmol) was dissolved in THF (1 mL) and slowly added to above solution, stirred for 20 min at 0°C and then stirred for 24h at room temperature. The solvent was evaporated and water (5 mL) was added, followed by extraction with EtOAc to remove (e). The product was purified by silica gel column chromatography (80% Ethyl Acetate: n-Hexane) to obtain a pure orange product.

^{1}H-NMR (300 MHz, $CDCl_3$): δ/ppm = ^{1}H-NMR (300 MHz, $CDCl_3$): δ/ppm = 1.24-1.27 (m, 12H); 1.33-1.39 (m, 2H); 1.43-1.48 (m, 2H); 1.52-1.59 (m, 2H); 1.76-1.88 (m, 2H); 3.18-3.22 (m, 2H); 3.42 (q, J=6.8 Hz, 1H); 3.82-3.91 (m, 2H); 4.15-4.19 (m, 1H); 4.35-4.38 (m, 2H); 5.16-5.28 (m, 1H); 7.28 (m, 2H); 7.33 (m, 2H); 7.54-7.57 (d, J=1.2 Hz, 2H); 7.67-7.72 (m, 3H); 7.76 (dd, J=8.4/1.2 Hz, 1H); 7.88 (d, J=7.5 Hz, 1H).

^{13}C-NMR (75 MHz, $CDCl_3$): δ/ppm = 16.8 ($-CH_3$); 22.1 ($-CH_2$), 24.7 ($-CH_3$); 29.2 ($-CH_2$), 31.4 ($-CH_2$), 36.2 (-CH); 40.6 ($-CH_2$), 47.0 (-CH); 54.3 (-CH); 65.6 ($-CH_2$); 67.3 ($-CH_2$); 88.7 (-C); 121.5 (-CH); 123.6 (-CH); 125.2 (-CH); 126.4 (-CH); 126.9 (-CH); 133.1 (-CH); 137.4 (-C); 140.8 (-C); 142.2 (-C); 143.6 (-C); 151.5 (-C); 156.7 (-C=O); 154.8 (-C=O); 172.3 (-C=O).

ESI-MS: 702.8 $[M+H]^+$, 724.6 $[M+Na]^+$

g. 2,2'-((4-iodophenyl)azanediyl)bis(ethan-1-ol) (g)

N-phenyldiethanolamine (600 mg, 3.31 mmol) was dissolved in dioxane (15 mL) and pyridine (15 mL) and the solution was cooled to 0 °C. Iodine (1.76 g, 6.15 mmol) was added in one portion. The solution progressively turned dark brown color. After 1h, the ice bath was removed and a supplementary portion of iodine (566 mg, 2.31 mmol) was added. The solution was further stirred for 1h at room temperature. A saturated solution of sodium thiosulfate was then added until the brown color disappeared. The mixture was extracted with dichloromethane (200 mL) and washed with water (200 mL). After evaporation, the product was filtered through a short plug of silica, eluted with 50% EtOAc, to afford 827mg of (**g**) (81 %) as a light brown solid.

1H-NMR (300MHz, $CDCl_3$): δ/ppm = 3.73-3.85 (m, 4H); 4.18-4.27 (m, 4H); 6.50 (d, J=9.2 Hz, 2H); 7.36 (d, J=9.2 Hz, 2H)

^{13}H-NMR (75 MHz, $CDCl_3$): δ/ppm = 58.6 ($-CH_2$); 61.5 ($-CH_2$); 89.4 (-C); 117.1 (-CH); 138.5 (-CH); 148.6 (-C).

ESI-MS: 308.18$[M+H]^+$

h. 2-(4'-amino-4-nitro-[1,1'-biphenyl]-3-yl)propan-1-ol (h)

2,2'-((4-iodophenyl)azanediyl)bis(ethan-1-ol) **(g)** (165 mg, 0.53 mmol), Fmoc-lysine-pinacolato complex **(f)** (100 mg, 0.14 mmol), K_2CO_3 (70 mg, mmol), and Bu_4NBr (360 mg, mmol) were dissolved in EtOH (10 mL) and water (5 mL), and flushed with argon for 10 min. A catalytic amount of $Pd(OAc)_2$ was added and mixture was further purged with Argon for 15 min. The mixture was heated under microwave conditions at 150 °C for 10 min. Water (100 mL) was added and the aqueous phase was extracted with EtOAc (200 mL). Purification was performed by flash chromatography using a gradient elution of 50% EtOAc/n-Hexane to obtain the title compound in 82% yield.

^{1}H-NMR (300 MHz, $CDCl_3$): δ/ppm = 1.20-1.23 (m, 12H); 1.36-1.39 (m, 2H); 1.53-1.58 (m, 2H); 1.72-1.84 (m, 2H); 3.19-3.22 (m, 2H); 3.52 (q, J=7.0 Hz, 1H); 3.63-3.78 (m, 2H); 3.72-3.84 (m, 2H); 4.19-4.23 (m, 1H); 4.33-4.39 (m, 2H); 5.19-5.28 (m, 1H); 3.85-3.98 (m, 2H); 7.23-7.38 (m, 6H); 7.41-7.49 (m, 2H); 7.52-7.59 (d, J=7.0 Hz, 2H); 7.67-7.72 (m, 3H); 8.21 (d, J=7.0 Hz, 1H); 8.42 (d, J=7.5 Hz, 1H).

^{13}C-NMR (75 MHz, $CDCl_3$): δ/ppm = 17.8 ($-CH_3$); 22.6 ($-CH_2$), 29.1 ($-CH_2$), 30,9 ($-CH_2$), 35.6 (-CH); 41.4 ($-CH_2$), 44.2 (-CH); 54.9 (-CH); 65.3 ($-CH_2$); 67.8 ($-CH_2$); 112.8 (-CH); 119.3 (-CH); 123.4 (-CH); 125.0 (-CH); 126.8 (-CH); 127.0 (-CH); 133.7 (-CH); 137.3 (-C); 139.5 (-C); 142.4 (-C); 143.6 (-C); 146.4 (-C); 148.3 (-C); 151.9 (-C); 156.3 (-C=O); 154.2 (-C=O); 175.4 (-C=O).

ESI-MS: 777.58 [M+Na]+

8.3 Synthesis of Peptidomimetics by SPPS

8.3.1 Coupling of Amino acids

All peptides were synthesized manually by Fmoc solid-phase peptide synthesis (SPPS) from preloaded TCP-L-Val-Fmoc (0.042 mmol, 100 mg resin) or TCP-L-Arg(Pbf)-Fmoc (0.037 mmol, 100 mmol) resin (Table A1). Fmoc protecting group from the resin and from subsequent amino acids were cleaved by treating resin twice with 20% piperidine in DMF (10 min x 2) with vigorous shaking followed by washing five times with DMF.

Next amino acids were sequentially coupled by adding solution of the Fmoc-amino acid (2 equivalents, 0.084 mmol), HOBt (2 equivalents, 0.084 mmol), HBTU (2 equivalents, 0.084 mmol), and DIPEA (5.6 equivalents, 0.084 mmol) in DMF (10-15 ml/g of resin) with shaking vigorous for (1-3 h). The coupling solution was then filtered out and the resin was washed five times with DMF.

In the case (EG_2)-IKVAV last coupling solution contains Fmoc-NH_2-(EG_2) -COOH (2 equivalents, 0.084 mmol), HOBt (2 equivalents, 0.084 mmol), HBTU (2 equivalents, 0.084 mmol), and DIPEA (5.6 equivalents, 0.084 mmol) in DMF (10-15 ml/g of resin) with shaking vigorous for (2.5 h).

8.3.2 Cleavage from Resin

The linear protected peptide was cleaved from the resin by treating the resin with trifluorethanol/acetic acid/DCM (1/3/6) three times with 6 ml of solution 30 min each.

Toluene was added to the filtrate and the solvents were removed in vacuum to obtain crude peptide.

8.3.3 Deprotection of side chain protection

In the case of Lys(Boc), Asp(O^{t}Bu), Ser(^{t}Bu), Cys(Trt), Glu(O^{t}Bu), Arg(pbf) deprotection of lateral chains was performed. The peptide was dissolved in 3 mL of 95% TFA/H_2O and stirred for 2h. Solvent was evaporated to 20% of the initial volume and 15 mL of diisopropyl ether was added. The precipitates were centrifuged and dried in high vacuum to obtain the deprotected crude product.

8.3.4 Purification of peptide by HPLC

The crude product was purified by RP-HPLC using water/acetonitrile containing 0.1% TFA as eluents. All peptides were purified by increasing the volume fraction of acetonitrile after a 3 min run gradually from 5 to 95% acetonitrile fraction till 40 min run. The pure fractions were collected and freeze dried to obtained pure solid peptide confirmed by Mass ESI. Purity of the obtained peptides was confirmed by analytical HPLC.

Table A1: Peptide sequence synthesis and characterization

Peptide Sequence	**TCP- Resin**	**HPLC purification profile**	**Mass (Da)**	**Abbreviation**
IKVAV	Val-Fmoc	32 min	528.69	IK-5
(EG_2)-IKVAV	Val-Fmoc	26 min	915.45	(EG_2)-IK
IK(HANBP)VAV	Val-Fmoc	4 min	731.92	IK-5-(HANBP)
CSIKVAV	Val-Fmoc	22 min	718.31	CSIK
CEEGIKVAV	Val-Fmoc	17 min	947.11	CE2IK
CEEEEGIKVAV	Val-Fmoc	16 min	1205.34	CE4IK
CASIKVAVSADR	Arg(Pbf)-Fmoc	16 min	1187.35	IK-12
CASIEVAVSADR	Arg(Pbf)-Fmoc	15 min	1188.29	IE-12
CASIK(NVOC)VAVSADR	Arg(Pbf)-Fmoc	22 min	1457.32	IK-12(NVOC)
CASIK(DMNPB)VAVSADR	Arg(Pbf)-Fmoc	23 min	1499.73	IK-12(DMNPB)
CASIK(HANBP)VAVSADR	Arg(Pbf)-Fmoc	28 min	1573.65	IK-12(HANBP)
CSRARKQAASIKVAVSADR	Purchased			IK-19
CCRRIKVAVWLC	Purchased			CIKC

8.4 Solubility and Photolysis of Peptides

8.4.1 Dynamic Light Scattering

The aggregation formation in peptide solutions was analyzed by measuring light scattering of peptide solutions at working concentrations (0.2 $mgmL^{-1}$) in PBS. Dynamic light scattering (DLS) measurements were performed on an ALV spectrometer consisting of a goniometer and an ALV-5004 multiple-tau full-digital co-relator (320 channels) which allows measurements over an angular range from 30° to 150 equipped with He-Ne Laser (wavelength of 632.8 nm) is used as light source. For temperature controlled measurements the light scattering instrument is equipped with a thermostat from Julabo. The size of aggregates was calculated by plotting mean value of the hydrodynamic radius against the scattering vector, corresponding to the angles 30°, 60°, 90° and 120° at room temperature. The DLS samples measurement and data analysis was performed by Christine Rosenauer at MPIP.

8.4.2 Photolysis of caged peptides in solution

The photolysis in solution was performed by irradiating 1mM peptide solution in phosphate buffer at pH 7.4 using LUMOS 42 and 43 (Atlas Photonics Inc.) at 345, 365 and 420 nm for NVOC, DMNPB and HANBP chromophores respectively. Photolytic conversion of caged peptide was calculated from the decrease in UV absorbance at λ_{max} of chromophore with increasing irradiation time. The percentage of uncaged peptide in solution was quantified by analytical HPLC profiles as well (Figure A1).

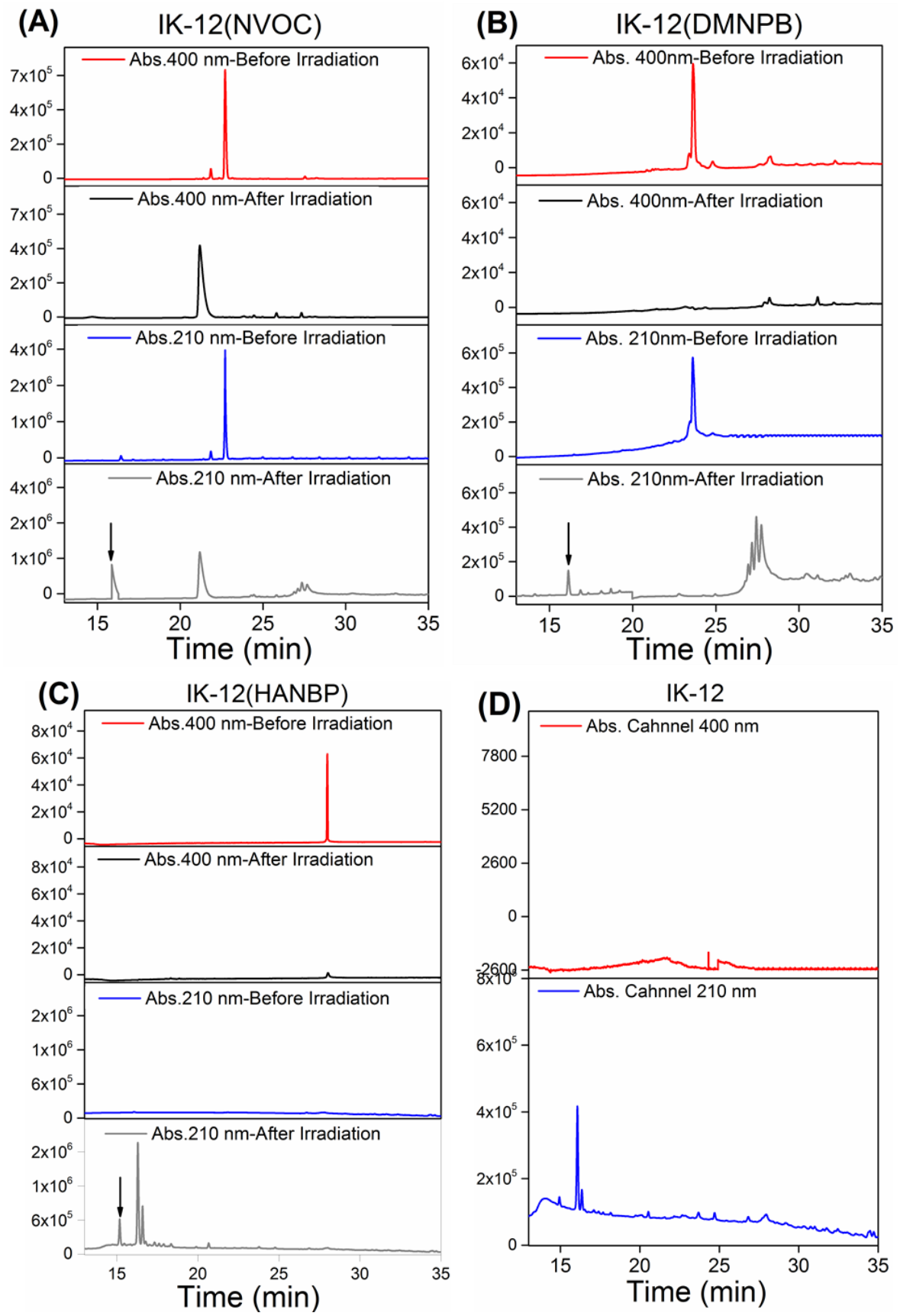

Figure A1. (A-C) Analytical HPLC chromatograms of 1mM solution of IK-12(HANBP), IK-12(DMNPB) and IK-12(NVOC), before and after irradiation,

appearance of IK-12 peptide is indicated by arrow. Light irradiation was performed as follows: IK-12(HANBP) at 420nm for 60 min, IK-12(DMNPB) at 365nm for 120 min, and IK- 12(NVOC) at 345 nm for 120 min, respectively. (D) For comparison, HPLC profile of IK-12 at different absorbance channels is shown as well.

8.5 Photolysis on Hydrogel Surface

8.5.1 Gel Preparation Protocols

P(AAm-AA) gels hydrogel was prepared and characterized by following reported procedures.[7] Briefly, acrylamide (60 mg) was dissolved in PBS (1 mL), acrylic acid (6 µL), and N,N-methylene-bis-acrylamide (0.4 mg) were added and the pH of solution was adjusted to pH 8 by using 0.1M NaOH aq. solution. The solution was degassed to remove oxygen and the free radical initiator ASP (10% solution, 1/100 of total volume) and TEMED catalyst (1/1000 of total volume) were added. 10 µL drops of the polymer solution were placed on hydrophobic Sigmacote coated glass slides and covered with 3-acryloxypropyl-trimethoxysilane (APTS) functionalized coverslips. The thin film of gel obtained has stiffness of 2 kPa as characterized by DMA (dynamic mechanical analysis) measurement section 8.7.5.

8.5.2 Functionalization of hydrogels

Peptides were coupled on surface of hydrogels by activation of pendant carboxyl groups for amine coupling by using by EDC/NHS chemistry. Briefly gels were covered with aqueous solution of EDC (0.2M) and NHS (0.1M) in MES buffer (0.1M, containing 0.5 M NaCl) for 15 min. After activation, gels were washed with water and incubated with drop (30 µL) of peptide solution (1mM in PBS pH 7.4) for 1 h at room temperature and washed 3 times with water.

8.5.3 Photoactivation of Hydrogel films

Gels functionalized with caged IK-12 variants were irradiated at the corresponding λ_{max} for the different chromophores (i.e. 345, 365 and 420 nm for NVOC, DMNPB, and HANBP, respectively). A Xe-lamp coupled to a monochromator (Polychrome V, TILL Photonics GmbH, Gräfelting, Germany) was used for irradiation. The irradiance values were comparable at the different wavelengths: 0.28 mW at 345 nm, 0.22 mW at 365 nm, and 0.34 mW at 420 nm. The IK-12 caged (NVOC/DMNPB/HANPB) functionalized gels were irradiated at respective wavelengths for different time

intervals, followed by washing with PBS to remove photolyzed by-product. The concentration of photo-protected ligand bound to hydrogel thin films was calculated from UV absorbance by Beer-Lambert law:

$$\boldsymbol{C = \frac{A}{l\varepsilon}} \qquad (\boldsymbol{Equation\ 1})$$

The extinction coefficient ε_{max} values were taken from literature (NVOC: 6210 $M^{-1}cm^{-1}$ at 365 nm[8], DMNPB: 4100 $M^{-1}cm^{-1}$ at 346 nm [2], and HANBP: 7500 $M^{-1}cm^{-1}$ at 397 nm [9]), the absorbance values at respective λ_{max} was determined from UV/vis spectra and the path length *l* = swollen thickness of hydrogel film (~ 0.007 cm) was obtained from fluorescence correlation spectroscopy. The binding efficiency was the ratio between the absorbance of peptide after coupling on hydrogel (*Aa*) and the absorbance of initial incubation solution (*Ai*).

$$\boldsymbol{Binding\ Efficiency\ \% = \frac{Ai - Aa}{Ai}\ x\ 100} \qquad (\boldsymbol{Equation\ 2})$$

Appendix Chapter 3

8.6 Synthesis of Methylsulfone Acrylates

8.6.1 Synthesis of N-(4-(5-(methylsulfonyl)-1,3,4-oxadiazol-2-yl)phenyl) acrylamide (1)

a. Tert-butyl (4-(5-mercapto-1,3,4-oxadiazole-2-yl)phenyl)carbamate (SI-1)

To the solution of 5-(4-aminophenyl)1,3,4-oxadiazole-2-thiol (100 mg, 0.517 mmol) in EtOH (1 mL), Boc_2O was added (452 mg, 2.068 mmol).[10] The reaction mixture was stirred overnight at 45 °C, accompanied by regular monitoring of reaction progress by TLC (40% EtOAc/n-Hexane). After the formation of product solvent was evaporated and crude product was subjected to silica gel column chromatography (15-20% EtOAc/n-Hexane) to obtain desired compound as white solid product (127 mg, 84% yield).

^{1}H-NMR (300 MHz, CD_2Cl_2): δ/ppm = 1.44 (9H, s, $-CH_3$, O^{t}Bu); 6.77 (1H, s, NH); 7.46 (2H, d, *J* = 8.7, CH); 7.77 (2H, d, *J* = 8.7, CH); 10.27 (1H, brs, SH).

^{13}C-NMR (75 MHz, CD_2Cl_2): δ/ppm = 28.33 ($-CH_3$); 81.44 (O-C); 118.54 (-CH); 127.88 (-CH); 144.69 (-C); 148.38 (-C); 154.59 (-C=O); 162.51 (-C); 179.73 (-C).

ESI-MS: 316.07 $[M + Na]^+$, 609.15 $[2M+Na]^+$

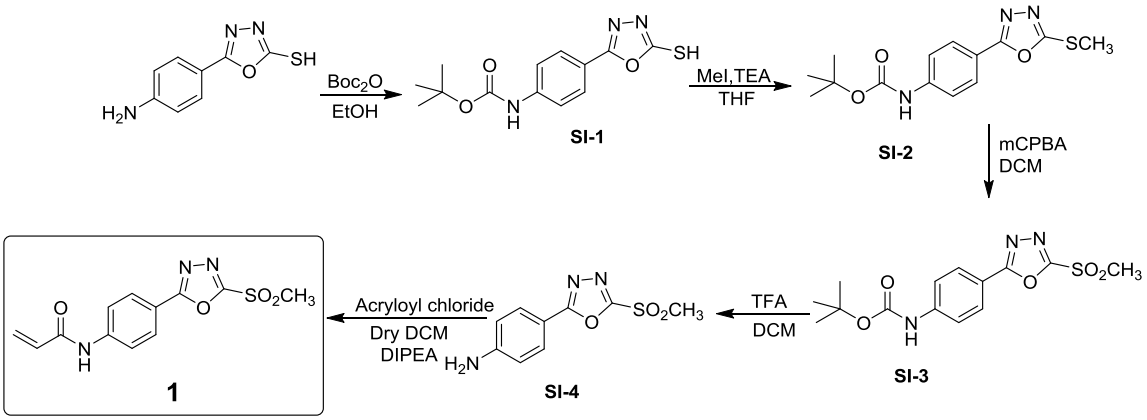

Scheme A4. Synthetic pathway for compound **1**

b. Tert-butyl (4-(5-(methylthio)-1,3,4-oxadiazole-2-yl)phenyl)carbamate (SI-2)

Compound SI-1 (80 mg, 0.273 mmol) was subjected to S-methylation by dissolving it in dry THF (1.2 mL), and subsequently adding TEA (57 µL, 0.41 mmol) and MeI (23 µL, 0.375 mmol) at 0°C.[11] The mixture was stirred for 2 h at room temperature, followed by addition of water and extraction of organic layer with ethyl acetate. The combined organic layers were washed with brine and dried over $MgSO_4$, to obtain pure white product (76 mg, 90%), which was used for next step without further purification.

^{1}H-NMR (300 MHz, CD_2Cl_2): δ/ppm = 1.43 (9H, s, -CH_3, O^{t}Bu); 2.67 (3H, s, -CH_3); 6.77 (1H, s, NH); 7.45 (2H, d, *J* = 9.0, CH); 7.83 (2H, d, *J* = 8.7, CH).

^{13}C-NMR (75 MHz, CD_2Cl_2): δ/ppm = 14.97 (S-CH_3); 28.36 (-CH_3); 81.34 (O-C); 118.31 (-C); 118.51 (-CH); 127.88 (-CH); 147.12 (-C); 152.58 (-C=O); 164.78 (-C); 165.94 (-C).

ESI-MS: 308.10 $[M+H]^+$, 330.07 $[M+Na]^+$, 637.15 $[2M+Na]^+$

c. Tert-butyl (4-(5-(methylsulfonyl)-1,3,4-oxadiazole-2-yl)phenyl)carbamate (SI-3)

To the cooled solution of SI-2 (70 mg, 0.228 mmol) in dry DCM (15 mL) at 0°C, meta-Chloroperoxybenzoic acid (mCPBA) (77wt%, 215 mg, 0.96 mmol) was added and reaction mixture was stirred overnight at room temperature.[11] After overnight reaction, the product was washed with 0.1M NaOH, 5% $NaHCO_3$ and finally with water, followed by drying of organic layer over $MgSO_4$. The crude product was

purified by silica gel column chromatography (30% EtOAc/n-Hexane) to obtain title compound as yellow solid (48 mg, 62% yield).

^{1}H-NMR (300 MHz, CD_2Cl_2): δ/ppm = 1.44 (9H, s, $-CH_3$, O^{t}Bu); 3.39 (3H, s, $-CH_3$); 6.79 (1H, s, NH); 7.51 (2H, d, *J* = 9.0, CH); 7.97 (2H, d, *J* = 8.7, CH).

^{13}C-NMR (75 MHz, CD_2Cl_2): δ/ppm = 28.32 ($-CH_3$); 43.55 (SO_2-CH_3); 81.74 (O-C); 116.38 (-C); 118.57 (-CH); 129.20 (-CH); 143.7 (-C); 152.23 (-C=O); 161.04 (-C); 164.42 (-C).

ESI-MS: 362.03 $[M+Na]^+$, 679.05 $[2M+H]^+$

d. 4-(5-(methylsulfonyl)-1,3,4-oxadiazole-2-yl)phenyl)aniline (SI-4)

The compound SI-3 (40 mg, 0.118 mmol) was dissolved in DCM (1 mL) followed by addition of TFA (230 µL, 3 mmol) and stirring for 3.5 h at room temperature. After completion of reaction the solvent was evaporated and excess TFA was evaporated in the presence of toluene by forming azeotropic mixture to obtain pure product as white solid (25 mg, 88.6% yield).[12]

^{1}H-NMR (300 MHz, CD_2Cl_2): δ/ppm = 3.37 (3H, s, $-CH_3$); 6.69 (2H, d, *J* = 8.7, CH), 7.81 (2H, d, *J* = 8.7, CH).

^{13}C-NMR (75 MHz, CD_2Cl_2): δ/ppm = 47.39 (SO_2-CH_3); 111.51 (-C), 114.88 (-CH); 129.85 (-CH); 148.64 (-C); 161.08 (-C); 164.50 (-C).

ESI-MS: 240.05 $[M+H]^+$, 262.02 $[2M+Na]^+$

e. N-(4-(5-(methylsulfonyl)-1,3,4-oxadiazol-2-yl)phenyl)acrylamide (1)

To the solution of SI-4 (24 mg, 0.1004 mmol) in dry DCM (8 mL), DIPEA (225 µL, 1.30 mmol) was added and solution was cooled to 0°C. Acryloyl chloride (150 µL, 1.97 mmol) was slowly added to it, followed by stirring overnight at room temperature. After completion of reaction, it was diluted with DCM (10 mL) and washed with 0.1M NaOH, 5% $NaHCO_3$ and brine solution, and subsequent drying of organic phase on $MgSO_4$. The product was subjected to silica gel column chromatography (70% EtOAc/n-Hexane) to obtain pure product as white solid (18 mg, 62% yield).

^{1}H-NMR (500 MHz, $CDCl_2$): δ/ppm = 3.47 (3H, s, $-CH_3$); 5.74 (1H, dd, *J* = 9.5 and 2.5 Hz, *cis,* $=CH_2$); 6.21 (1H, dd, *J* =17.0 and 9.0 Hz, =CH); 6.34 (1H, dd, *J* = 17.0 and 3.0, trans, $=CH_2$); 7.71 (1H, brs, NH); 7.83 (2H, d, *J* = *8.5,* CH); 8.01 (2H, d, *J* = *8.5,* CH).

^{13}C-NMR (126 MHz, $CDCl_2$): δ/ppm = 41.95 (SO_2-CH_3); 117.41 (-C); 119.86 (-CH); 127.43 (-CH_2), 128.26 (-CH); 130.72 (-CH); 143.14 (-C); 162.00 (-C=O); 164.83 (-C), 166.25 (-C).

ESI-MS: 294.06 $[M+H]^+$, 316.06 $[M+Na]^+$

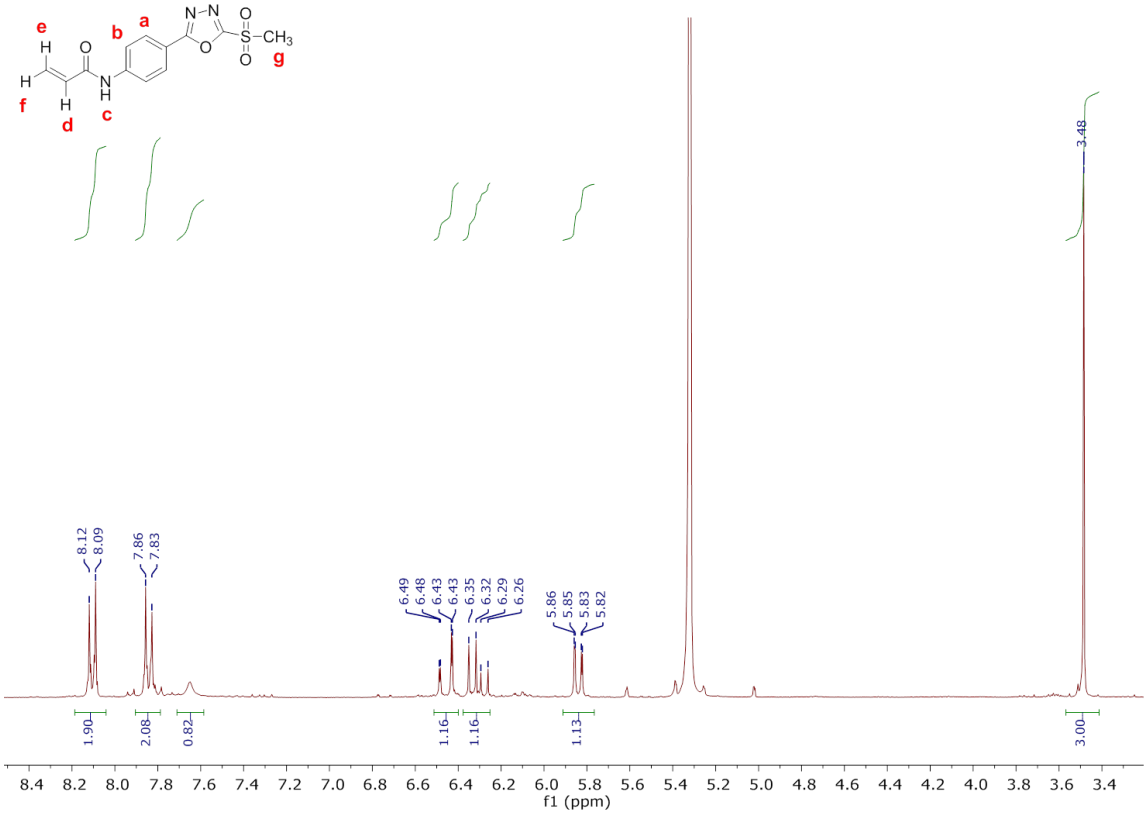

Figure A2. ^{1}H NMR spectrum of **1**

8.6.2 Synthesis of N-(2-(methylsulfonyl)benzo[*d*]thiazol-6-yl)acrylamide (2)

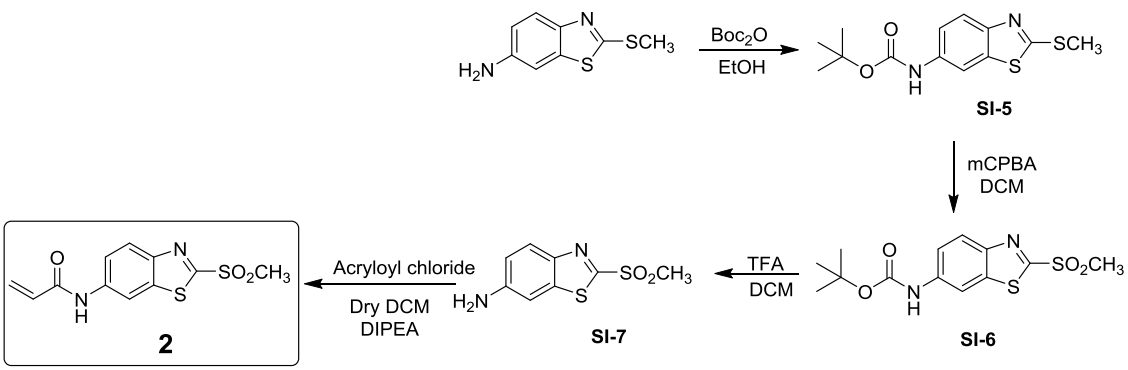

Figure A5. Reaction Scheme for the synthesis of compound **2**.

a. Tert-butyl (2-(methylthio)benzo[*d*]thiazol-6-yl)carbamate (SI-5)

2-(methylthio)benzo[*d*]thiazol-6-amine (100 mg, 0.510 mmol) was dissolved in EtOH (750 µL), followed by addition of Boc_2O (197 mg, 0.90 mmol).[10] The reaction mixture was stirred at room temperature and the progress of reaction was monitored by TLC (40% EtOAc/n-Hexane). The reaction was completed after 2h, followed by evaporation of solvent and purification of product by silica gel column chromatography (15-20% EtOAc/n-Hexane) to obtain title compound as yellow solid product (138 mg, 91% yield).

^{1}H-NMR (300 MHz, CD_2Cl_2): δ/ppm = 1.44 (9H, s, -CH_3, O^{t}Bu); 2.68 (3H, s, S-CH_3); 6.61 (1H, brs, NH); 7.10 (1H, dd, *J* = 8.7 and 2.1 Hz, CH); 7.63 (1H, d, *J* = 8.7 Hz, CH), 8.02 (1H, d, *J* = 2.1 Hz, CH).

^{13}C-NMR (75 MHz, CD_2Cl_2): δ/ppm **=** 16.18 (S-CH_3); 28.40 (-CH_3); 81.30 (O-C); 110.59 (-CH); 117.97 (-CH); 121.47 (-CH); 136.58(-C); 135.77 (-C); 149.66 (-C); 153.11 (-C=O); 166.62 (-C).

ESI-MS: 319.01 $[M+Na]^+$, 615.08 $[2M+Na]^+$

b. Tert-butyl (2-(methylsulfonyl)benzo[*d*]thiazol-6-yl)carbamate (SI-6)

To a solution of SI-5 (91 mg, 0.307 mmol) in dry DCM (15 mL) cooled at 0°C, mCPBA (77wt%, 250 mg, 1.115 mmol) was added while stirring.[11] The mixture was then stirred overnight at room temperature, followed by evaporation of solvent under vacuum. The crude green colored product was washed with 0.1M NaOH, 5% $NaHCO_3$ and water, and subsequent drying of organic layer over $MgSO_4$. Silica gel column chromatography was employed (30% EtOAc/n-Hexane) to obtain pure product (72 mg, 71.4% yield).

^{1}H-NMR (300MHz, CD_2Cl_2): δ/ppm = 1.45 (9H, s, -CH_3, O^{t}Bu); 3.34 (3H, s, SO_2-CH_3); 6.83 (1H, brs, NH); 7.29 (1H, dd, *J* = 9.0 and 2.1 Hz, CH); 7.99 (1H, d, *J* = 9.0 Hz, CH); 8.34 (1H, d, *J* = 2.1 Hz, CH).

^{13}C-NMR (75 MHz, CD_2Cl_2): δ/ppm = 28.35 (-CH_3); 42.94 (SO_2-CH_3); 81.29 (O-C); 110.20 (-CH); 119.36 (-CH); 125.72 (-CH); 137.20 (-C); 139.20 (-C); 149.77 (-C); 152.55 (-C=O); 164.79 (-C).

ESI-MS: 351.04 $[M+H]^+$, 679.08 $[2M+Na]^+$

c. 2-(methylsulfonyl)benzo[*d*]thiazol-6-amine (SI-7)

The deprotection of Boc was carried out by stirring SI-6 (64 mg, 0.195 mmol) in DCM (1 mL) by addition of TFA (250 µL, 3.18 mmol) for 4 h at room temperature. The solvent was evaporated and excess TFA was evaporated in the presence of toluene to obtain pure product as white solid (36 mg, 81% yield).[12]

^{1}H-NMR (300 MHz, CD_2Cl_2): δ/ppm = 3.24 (3H, s, SO_2-CH_3); 6.91 (1H, dd, *J* = 9.0 Hz*,* CH); 7.09 (1H, d, *J* = 2.1 Hz, CH); 7.86 (1H, d, *J* = 9.0 and 2.2 Hz*,* CH).

^{13}C-NMR (75 MHz, CD_2Cl_2): δ/ppm = 42.70 (SO_2-CH_3); 107.90 (-CH); 119.80 (-CH); 126.61 (-CH); 140.22 (-C); 146.20 (-C); 147.63 (-C); 156.41 (-C).

ESI-MS: 228.99 $[M+H]^+$, 250.99 $[M+Na]^+$

d. N-(2-(methylsulfonyl)benzo[*d*]thiazol-6-yl)acrylamide (2)

Compound SI-7 (32 mg, 0.140 mmol) was dissolved in dry DCM (10 mL), followed by addition of DIPEA (320 µL, 1.840 mmol). The solution was cooled to 0°C, and subsequently acryloyl chloride (225 µL, 2.77 mmol) was added to it. The reaction mixture was stirred overnight at room temperature. The reaction mixture was diluted with DCM (20 mL) and product was washed with 0.1M NaOH, 5% $NaHCO_3$ and brine solution. Organic layer was dried over $MgSO_4$, and purified further with silica gel column (70% EtOAc/n-Hexane) to obtain pure product as white solid (26 mg, 66% yield).

^{1}H-NMR (500 MHz, $CDCl_2$): δ/ppm = 3.43 (3H, s, SO_2-CH_3); 5.73 (1H, dd, *J* = 9.5 and 2.5 Hz*, cis,* =CH_2); 6.19 (1H, dd, J = 17.0 and 9.0 Hz, =CH); 6.34 (1H, dd, *J* =17.0 and 2.5 Hz , *trans ,* =CH_2); 7.65 (1H, dd, J = 9.0 and 2.0 Hz, CH); 8.04 (1H, d, *J* = 9.0 Hz, CH); 8.65 (1H, d, *J* = 2.0 Hz, CH).

^{13}C-NMR (126 MHz, $CDCl_2$): δ/ppm = 41.19 (SO_2-CH_3); 112.12 (-CH); 120.66 (-CH); 124.77 (-CH); 127.24 (-CH_2), 130.75 (-CH); 137.69 (-C); 138.74 (-C), 149.03 (-C); 164.90 (-C), 165.58 (C=O).

ESI-MS: 283.04$[M+H]^+$, 305.17 $[M+Na]^+$

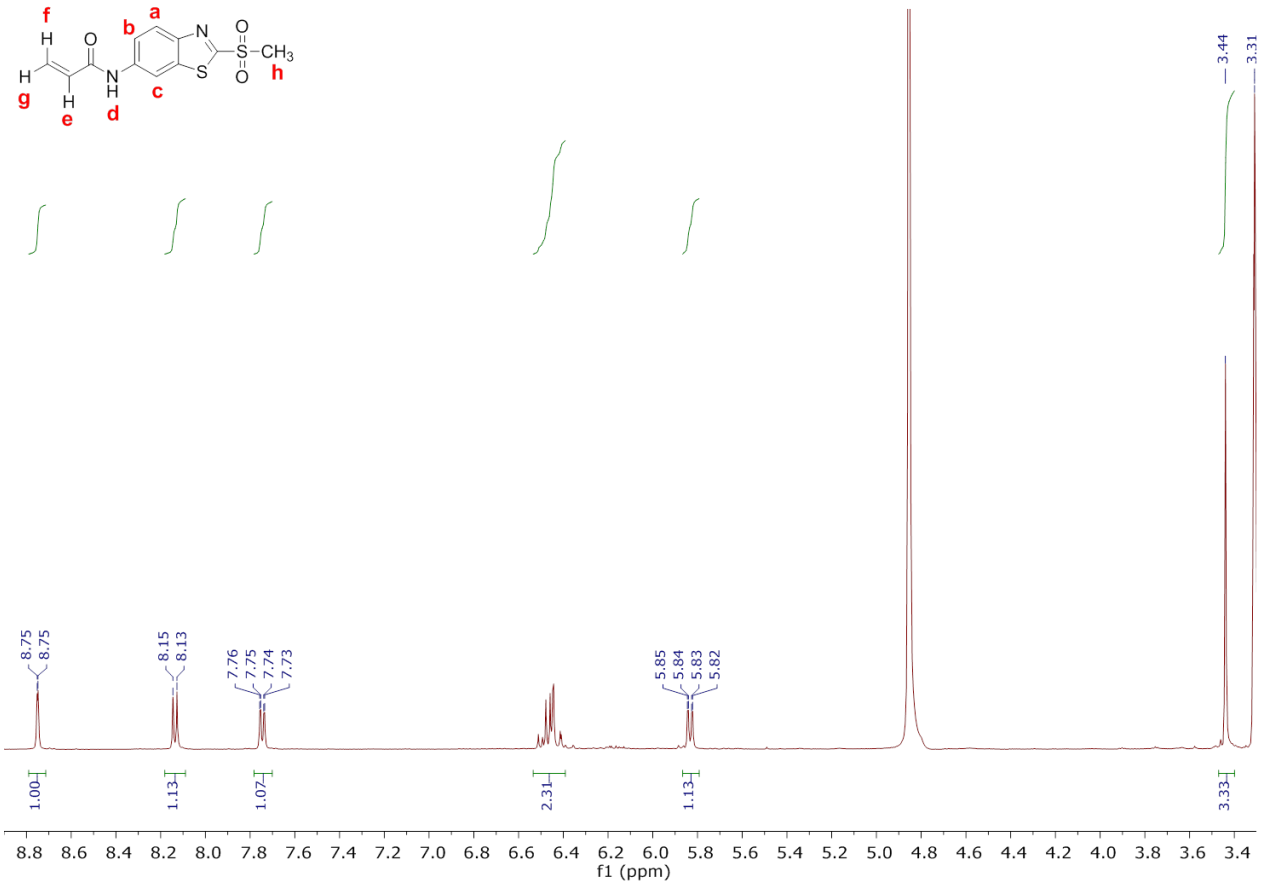

Figure A3. ^{1}H spectrum of compound **2**

8.7 Polymerization and functionalization of hydrogel

8.7.1 Linear copolymers for GPC

Compound **1** or **2** (4 mg, ~ 2 mol%) was dissolved in DMF (125 µL) and mixed with the solution of AAm (60 mg mL^{-1} in PBS. 98 mol%). The solution was degassed for 15 min with positive flow of N_2 in a Schlenk flask, followed by addition of initiator APS (10% solution, 1/100 of total volume) and TEMED (catalyst, 1/1000 of total volume). The polymerization was carried out for 1 h at room temperature and quenched by exposing the mixture to air. The control linear P(AAm) polymer was also prepared in similar way. The GPC was measured by using Suprema Linear M column, 0.1 M $NaNO_3$ eluent and calibrated by employing PAANa.

8.7.2 Linear polymers for NMR

Compound **1** (0.4 mg in 12.5µL DMF for 2 mol%) and (5 mg in 50 µL of DMF for 50 mol%) was mixed with the solution of AAm in PBS (87.5 mL or 50 µL respectively).

The solution was degassed for 2 min with N_2 in Eppendorf tube followed by addition of ammonium persulfate (10% solution, 1/100 of total volume) and N,N,N′,N′-tetramethylethylenediamine (catalyst, 1/1000 of total volume). The polymerization was carried out for 15 min at room temperature and quenched by exposing the mixture to air. The control linear P(AAm) polymer was also prepared in similar way. The internal standard DMS (1 mM in D_2O) was added to all samples. The linear polymer was dissolved in 650 µL of D_2O for 2 mol% and in mixture of D_2O:DMF (60:40) for 50mol% polymer and ^{1}H-NMR was measured at 300 MHz.

8.7.3 Preparation of gel films

Acrylamide (60 mg) was dissolved in PBS (1 mL), N,N-methylene-bis-acrylamide (10 mg) was added. Compound **1** or **2** (4 mg) was dissolved in DMF (125 µL) and mixed with the monomer solution. The solution was degassed to remove oxygen and the free radical initiator ammonium persulfate (10% solution, 1/100 of total volume) and N,N,N′,N′-tetramethylethylenediamine (catalyst, 1/1000 of total volume) were added.[7a] 10 µL drops of the polymer solution were placed on Sigmacote coated glass slides and covered with 3-acryloxypropyl-trimethoxysilane (APS) functionalized coverslips.[13] The hydrogel forms between both glass slides and bound to APS-functionalized slides. After 10 min, the gel bound to the APS coated coverslip was separated from the Sigmacote slide and kept in cold deionized water until further use. Films of P(AAm) gels were prepared with the same method, in the absence of compounds **1** or **2**. The stiffness of obtained hydrogel was 10 kPa, measured by DMA Section 8.7.5.

8.7.4 Determination of swelling ratio

The swelling ratio of the gels was determined by gravimetric method. The gels were polymerized and swollen by keeping in water for 24 h at room temperature and weighted (swollen weight =W_s) followed by drying at 40 °C for 24 h under vacuum and weighted again (dry weight = W_d). The swollen ratio (SR) was calculated after three replicates by the following equation:

$$\mathbf{SR} = \frac{(\boldsymbol{W_s} - \boldsymbol{W_d})}{\boldsymbol{W_d}} \qquad (\boldsymbol{Equation\ 3})$$

8.7.5 Characterization of mechanical properties of the gel

The stiffness of hydrated samples was measured by dynamic mechanical analysis at 25°C, and at frequency of 0.1 rad/sec. The hydrogel samples were prepared between two 25 mm coverslips previously functionalized with APTS and Sigmacote® following the above mention gel preparation protocol. The Sigmacote® coated slide was removed and rheology was performed in presence of water to avoid drying of hydrogel. The elastic modulus was calculated from the obtained storage modulus (G´) by using following expression.

$$\boldsymbol{E = 2Gx(1 + v)\ (Equation\ 4)}$$

where the poisson number was v = 0.5.

8.7.6 Characterization of gel morphology by Scanning Electron Microscopy (SEM)

Gel samples were prepared and lyophilized for SEM imaging. Gel samples prepared in an Eppendorf tube or as hydrogel films were swollen in water, freezed in liquid nitrogen followed by freeze drying. Dried gels were fractured and the cross section was imaged. Samples were coated with 2.5 nm thick coating of Pt before SEM imaging.

8.7.7 Functionalization of gels and UV-Vis spectroscopy characterization

Coupling of c[RGD(DMNPB)fC] to P(AAm-*co*- **1** or **2**) gels was done by incubating the gel films with a solution of the peptide at defined concentration for 1 h at room temperature. A 30 µL drop of the peptide solution was placed on a parafilm surface and covered with methylsulfone copolymer gel. After coupling, the gel was washed with water to rinse out non-specifically adsorbed peptide, followed by drying under nitrogen stream for measurement of UV absorbance.

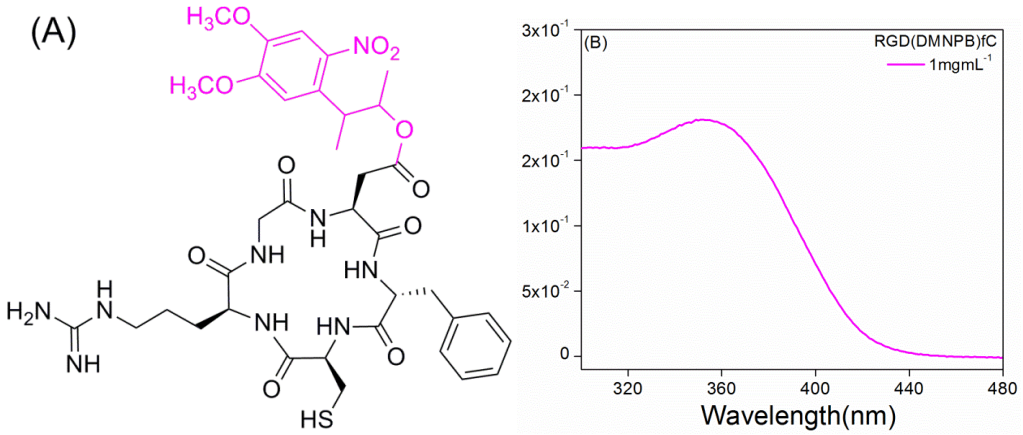

Figure A4. Chemical structure and UV spectrum of c[RGD(DMNPB)fC] in solution (1 mg mL^{-1} in water).

8.7.8 Peptide concentration on P(AAm-*co*-1) and P(AAm-*co*-2) gels

The peptide concentration *C* in the methylsulfone gels was estimated from the UV absorbance *A* as described above in section 8.5.3. The path length *l*= swollen thickness of the gel (~ 0.007 cm obtained from fluorescence correlation spectroscopy (FCS) while reported ε_{max} for DMNPB chromophore is 4100M^{-1}cm^{-1} at λ_{max} 346 nm.[14]

8.7.9 P(AAm) functionalization with sulfo-SANPAH

P(AAm) gels were coupled with RGD(DMNPB)fC and RGD(DMNPB)fK (1 mg mL^{-1}) *via* sulfo-SANPAH.[13] A 100 µL-drop of sulfo-SANPAH solution (0.2 mg mL^{-1}) was placed on hydrogel surface, followed by irradiation at 365 nm using BLX-E 254 UV Lamp, 8W (LFT-Labortechnik) for 8 min. The gel was rinsed by water and the activation step was repeated. The gel was immediately washed, and incubated overnight with the solution of peptide (30 µL) at 37°C. After coupling, the gel was washed with water and dried under nitrogen stream prior to the measurement by UV.

8.7.10 Functionalization of gels with Streptavidin-Biotin

P(AAm)/sulfo-SANPAH and P(AAm-co-**1**) gels were incubated overnight with 20 µL of 300 µgmL^{-1} streptavidin solution in PBS, followed by washing with PBS and overnight incubation with 20 µL of Atto 425 biotin solution (0.3 mgmL^{-1}) in PBS. The gels were repeatedly washed with PBS, dried with N_2 stream and the biotin density was characterized by UV spectroscopy. P(AAm) and P(AAm-*co*-**1**) gels were

incubated only with Atto 425 biotin solution (0.3 mg mL^{-1}) in PBS for establishing negative controls.

In a second assay, 120 µL of streptavidin (500 µgmL^{-1}) were mixed with 80 µL of Atto 425-biotin (0.75 mg mL^{-1}) in PBS for 2 min. 20 µL of this mixture were incubated with P(AAm)/sulfo-SANPAH and P(AAm-co-**1**) gels. After successive washing and drying with N_2, UV spectra of the gels were measured.

8.7.11 Stability of Coupled Peptide

The hydrogel functionalized with RGD(DMNPB)fC (0.5 mgmL^{-1}) on P(AAm-co-**1**) and on P(AAm)/sulfo-SANPAH, while RGD(DMNPB)fK (0.5 mgmL^{-1}) on P(AAm-co-AA)/EDC were place in DMEM medium with 10% FBS. The samples were kept in dark at 37°C in 5% CO_2 inside the incubator. The samples were removed from medium after 3 or 10 days, washed with water and UV of dried hydrogel was measured.

8.8 Cell Culture Experiment

8.8.1 Cell culture Protocol

HeLa cells were cultivated at 37°C in 5% CO_2 in DMEM medium (Invitrogen) supplemented with 10% fetal bovine serum (Invitrogen), 1% L-glutamine from Invitrogen and Penicillin/Streptavidin (Invitrogen). P(AAm-*co*-**1**/**2**) gels were prepared as described above and incubated with c[RGDfC] (0.1 mgmL^{-1}) or with fibronectin (FN1, from human plasma, 0.01mgmL^{-1}) solutions in PBS overnight at room temperature. P(AAm) gels were activated with sulfo-SANPAH (see protocol above) and incubated overnight with c[RGD]fC or c[RGDfK] solution or fibronectin solution (0.01 mgmL^{-1}) in PBS at 37 °C.[13] As negative controls, P(AAm) and P(AAm-co-**1**/**2**) gels were incubated overnight with c[RGDfK] solution in PBS. All gels were washed thoroughly with water after incubation.

The samples were placed in 24 well plate, sterilized by ethanol and washed 3 times with PSB. The samples were incubated with 500 µL of 1× 10^5 cells/well suspension of HeLa at 37 °C and 5% CO_2. After 3 h substrates were rinsed with PBS and fresh medium to remove unattached cells, imaged and further incubated overnight. Cells were fixed with 4% PFA solution, permeabilized with 0.1% Triton, actin fibers were

stained with TRITC-phalloidin (1:200) and the nucleus was stained with DAPI using standard protocols. Fluorescence images were taken with an Olympus IX81 epi-fluorescence microscope.

8.8.2 Live/Dead assay

The cytocompatibility of the gels was determined by incubating them for 3 days with 400 µL of suspension of HeLa (1 × 10^5 cells) at 37 °C and 5% CO_2. The LIVE/DEAD assay was performed with Viability/Cytotoxicity Kit for mammalian cells (Invitrogen) based on Calcein AM and Ethidium homodimer-1 following standard protocol, and subsequent imaging after 30 min by epi-fluorescence microscopy. Live cells were stained green while dead cells appeared in red color

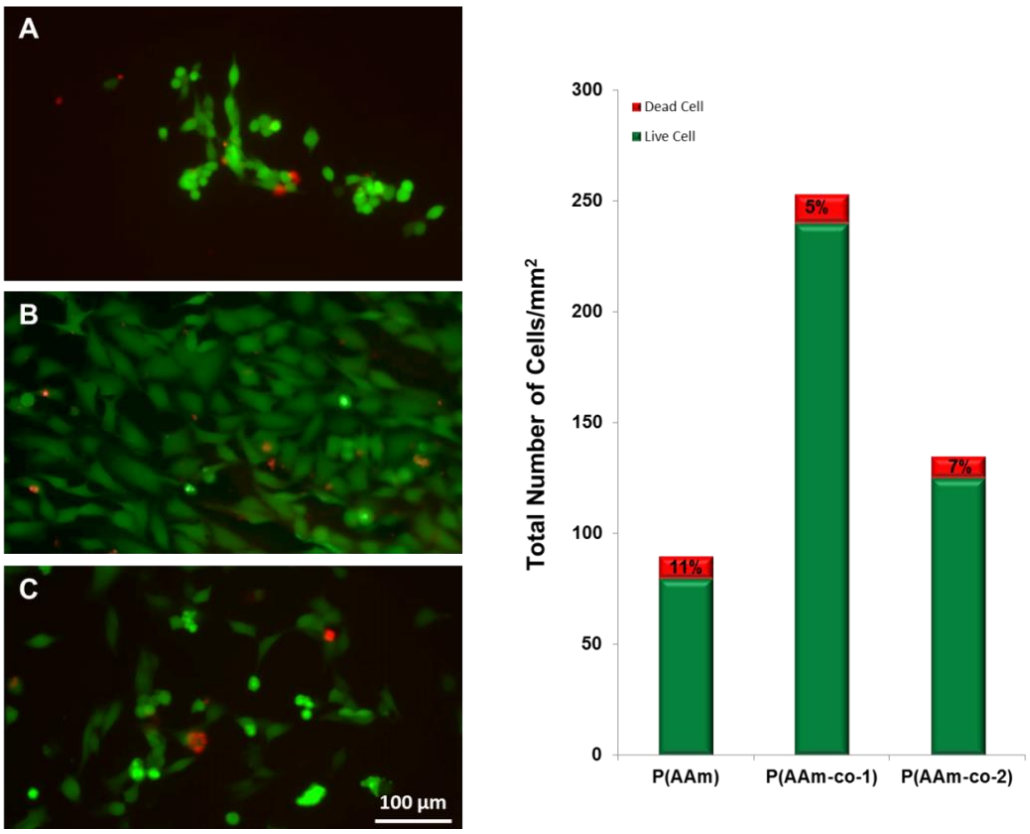

Figure A5. Viability assay. (A-C) Fluorescence image of HeLa cells cultured on P(AAm) (a), P(AAm-*co*-**1**) (b) and P(AAm-*co*-**2**) (c) gels functionalized with c[RGDfC] 3 days after cell seeding. The graph shows the quantification of the microscopic pictures.

8.8.3 Cell experiments on P(AAm)/sulfoSANPAH/c[RGDfK] and P(AAm-*co*-1)/c[RGDfC] gels with equal density of adhesive peptide

P(AAm-co-**1**) gel was incubated with 20 µL of 20 µgmL^{-1} solution of c[RGDfC] in PBS, while P(AAm)/sulfo-SANPAH gels were incubated with 20 µL 100µg mgmL^{-1} solution of c[RGDfK] in PBS for 24 hours. Peptide density was estimated 8µM in both cases, through Lambert-Beer's law (l ~ 0.007 cm, corresponding to the swollen thickness of the gel; ε_{max} = 4100M^{-1}cm^{-1} at λ_{max} 346 nm; and A=2.5 10^{-4}, value extrapolated from the Figure A6). A homogenous distribution of the peptide across the gel was assumed.

The gel samples were placed in 24-well plates and incubated with 500 µL of 1× 10^5 cells/well suspension of HeLa at 37 °C and 5% CO_2. After 3 h substrates were rinsed with PBS and fresh medium to remove unattached cells and further incubated till 6 h or 24 h. Cells were fixed with 4% PFA solution, permeabilized with 0.1% Triton, actin fibers were stained with TRITC-phalloidin and the nucleus was stained with DAPI using standard protocols. Confocal fluorescence images were taken with Leica TCS SP5.[13]

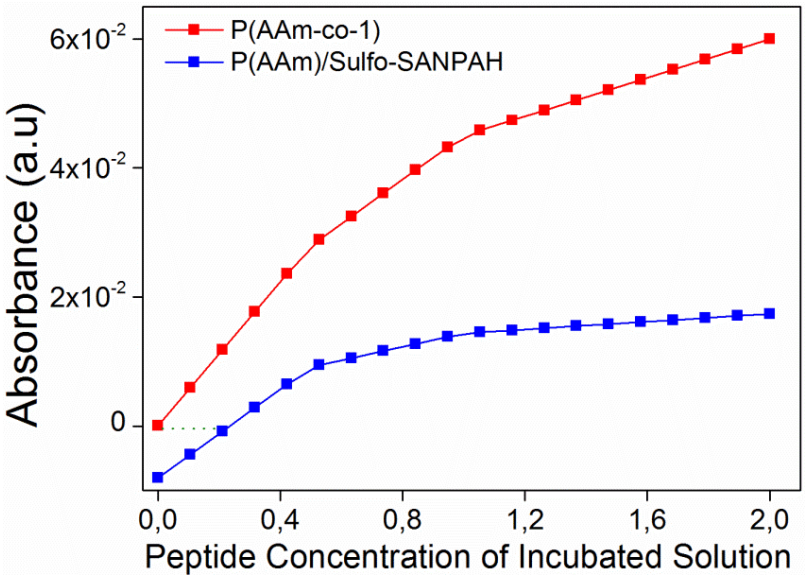

Figure A6. Absorbance values at 350 nm measured on gels after incubation with different concentrations of peptides (0.01 -2 mgmL^{-1}).

Appendix Chapter 4

8.9 Polymerization and Functionalization of Hydrogel

8.9.1 Linear copolymers for GPC

Methylsulfonyl comonomer (4 mg) was dissolved in DMF (100 µL) and mixed with the solution of acrylamide (60 $mgmL^{-1}$) and acrylic acid (6µL) in PBS. The pH of solution was adjusted to pH = 8, and the solution was degassed for 15 min with positive flow of N_2 in a Schlenk flask, followed by addition of ammonium persulfate (10% solution, 1/100 of total volume) and *N,N,N′,N′*-tetramethylethylenediamine (catalyst, 1/1000 of total volume). The polymerization was carried out for 1 h at room temperature, followed by quenching of reaction by exposing the content of flask to air. A solution of polymer was prepared (5 $mgmL^{-1}$in H_2O) and GPC elugram was measured by using Suprema Linear M column, 0.1 M $NaNO_3$ eluent and calibrated by employing PAANa.

8.9.2 Linear polymers for NMR

Compound **1** (0.4 mg in 12.5 µL DMF for 2 mol%) and (5 mg in 50 µL of DMF for 50 mol%) was mixed with the solution of AA:AAm (8.8:89 mol%) in PBS (87.5 mL or 50 µL respectively) at pH 8. The solution was degassed for 2 min with N_2 in Eppendorf tube followed by addition of ammonium persulfate (10% solution, 1/100 of total volume) and N,N,N′,N′-tetramethylethylenediamine (catalyst, 1/1000 of total volume). The polymerization was carried out for 15 min at room temperature and quenched by exposing the mixture to air. The control linear P(AAm-AA) polymer was also prepared in similar way. The internal standard DMS (1 mM in D_2O) was added to all samples. The linear polymer was dissolved in 650 µL of D_2O for 2 mol% and in mixture of D_2O:DMF (60:40) for 50 mol% polymer and ^{1}H-NMR was measured at 300 MHz.

8.9.3 Preparation of gel films

Hydrogel with different stiffness (0.2 -70 kPA) were prepared by following a previously reported protocol by free radical copolymerization of methylsulfone acrylate, acrylamide and acrylic acid with varying amount of N,N′-methylene-bis-acrylamide crosslinker (Table A2). Briefly, acrylamide (60 mg, 6%w/v), acrylic acid

(6 µL, 0.6% w/v) and N,N-methylene-bis-acrylamide was dissolved in PBS (1 mL), and pH of solution was adjusted to pH 8. Methylsulfone comonomer (N-(4-(5-(methylsulfonyl)-1,3,4-oxadiazol-2-yl)phenyl)acrylamide) (4 mg, 0.4% w/v) was dissolved in DMF (100 µL) and mixed with above solution. The APS (initiator, 10% solution, 1/100 of total volume) and TEMED (catalyst, 1/1000 of total volume) was added to it under nitrogen. One drop of monomer solution (6 µL for 0.2, 10 µL for 2 and 20 kPa) was immediately placed on Sigmacote-coated glass slide and covered with 3-acryloxypropyl-trimethoxysilane functionalized coverslips.

Table A2: Amount of crosslinker and crossponding young's modulus

Quantity of Cross-linker ($mgmL^{-1}$)	**Young's modulus E (kPa)**
0.04	0.2 ± 0.1
0.4	2 ± 0.4
17	20 ± 0.3
28	70 ± 0.3

8.9.4 Characterization of Hydrogels

Hydrogels are denoted in the following as PAAm-AA for poly(acrylamide-*co*-acrylic acid) and PAAm-AA-MS for poly(acrylamide-*co*-acrylic acid-*co*-methylsulfonyl). The complete characterization of the hydrogels, including measurement of swelling ratio, hydrogel stiffness (by DMA), and surface morphology by scanning electron microscopy (SEM) was performed as described in section 8.7.4- 8.7.6.

8.10 Functionalization of gels for UV-Vis spectroscopy

8.10.1 Coupling of thiol- or amine- peptides

Coupling of thiol-peptides to hydrogels was done by incubating the hydrogels with a peptide solution of different concentrations (0.25, 0.5, 0.75, 1.0, 1.5, and 2 $mgmL^{-1}$) in PBS for 1h at room temperature. 30 µL of the peptide solution were placed on a parafilm surface and covered with the hydrogel. After coupling, the hydrogel was washed with water and with 0.05 M aq. acetic acid solution (pH = 3) to rinse out non-specifically adsorbed peptide, followed by drying under nitrogen stream and measurement of UV absorbance. Coupling of amine-peptides required prior

activation of the -COOH groups of the hydrogel Section 8.5.2. After EDC activation, the hydrogels were incubated with peptide solutions of different concentrations (0.25 - 2 $mgmL^{-1}$) in PBS for 1 h. The hydrogel was washed with water and 0.05 M aq. acetic acid solution (pH = 3) to rinse out non-specifically adsorbed peptide, followed by measurement of UV absorbance in dry state.

8.10.2 Orthogonal sequential coupling of thiol- and amine-containing peptides

It was carried out by using cRGD(coum)fC and cRGD(DMNPB)fK(1$mgmL^{-1}$) as probes. For testing thiol/amine coupling pathway, hydrogel was functionalized with cRGD(coum)fC followed by washing with water and measurement of UV absorbance. Subsequently, on the same hydrogel, carboxylic groups were activated by EDC/NHS followed by coupling with cRGD(DMNPB)fK and UV measurement. The amine/thiol route was also tested by first coupling amine peptides using EDC/NHS activation and subsequent coupling of thiol peptide.

8.10.3 One-pot orthogonal coupling of thiol- and amine- peptides

For one pot coupling PAAm-AA-MS hydrogel was first activated with EDC/NHS (section 8.5.2) and then incubated with a 1:1 mixture of 1 $mgmL^{-1}$ cRGD(coum)fC and cRGD(DMNPB) aqueous solution for 1h, followed by washing and measurement of UV spectra.

8.10.4 Determination of ligand binding efficiency to hydrogels

The concentration *C* of ligand coupled to hydrogels was estimated from the UV absorbance *A* using the Lambert-Beer law section 8.5.3. The path length *l*= swollen thickness of the hydrogel and reported ε_{max} for *coum* chromophore is 20000$M^{-1}cm^{-1}$ at λ_{max} 390 nm.

8.10.5 Non-specific binding controls of peptide coupling to PAAm gels

PAAm-AA gels (without MS comonomer), were incubated with 1 $mgmL^{-1}$ solution of c[RGD(DMNPB)fC] for 1h, followed by washings with water and 0.05 M aq. acetic acid solution (pH = 3), and UV characterization. PAAm-AA hydrogels, without EDC/NHS activation, were incubated with 1 $mgmL^{-1}$ solution of c[RGD(coum)fK] for 1h, washed with water and then with 0.05 M aq. acetic acid solution, and

characterized by UV. Washing with 0.05 M aq. acetic acid solution (pH = 3) proved necessary to wash out the non-specifically adsorbed peptide, since only washings with water were not enough to remove it. This effect was more pronounced when cRGD(coum)fK was used. Therefore, a final washing with acetic acid solution after peptide coupling was always included in the procedure.

8.10.6 Studies of RGD peptide binding kinetics

PAAm-AA-MS gel was incubated with cRGD(coum)fC or cRGD(coum)fK solutions at 0.25, 0.75 and 2 $mgmL^{-1}$ concentration for 1, 3, 8 and 24 h. The gels were washed with water and 0.05 M aq. acetic acid solution (pH = 3) followed by UV spectroscopy measurement in dry state.

8.10.7 Bifunctionalization of gels with larger proteins

PAAm-AA-MS gel was activated with EDC/NHS and then incubated with laminin-Hilyte solution in PBS (0.75 $mgmL^{-1}$) for 1h. After rinsing with PBS, UV spectrum was measured. The same gel was subsequently incubated with Streptavidin-SH solution in PBS (1 $mgmL^{-1}$) for 1h, rinsed and then incubated overnight with Atto425-biotin solution in PBS (1 $mgmL^{-1}$). After washing, UV spectrum was measured.

8.11 Study of thickness, swelling and distribution of ligands in PAAm-AA-MS gels by confocal microscopy

Hydrogels were functionalized with ligands containing fluorophores. On the one hand, PAAm-AA-MS gels were incubated with a 0.1$mgmL^{-1}$ thiol-Steptavidin solution for 1h at room temperature followed by incubation with Atto-425 biotin (0.5 $mgmL^{-1}$) for 1 h. Subsequent gel washings removed non-bound ligand. On the other hand, PAAm-AA-MS gels were activated with EDC/NHS and then coupled with cRGD(coum)fK (0.5 $mgmL^{-1}$) for 1 h followed by washings. Thickness of gel was measured by performing Z-stack using Zeiss-LSM 880 with Airyscan. The samples were measured first in dry state in Z-axis by following the fluorescent signal from the corresponding chromophore (either Atto-425 or Coum group). The hydrogel was allowed to swell for 5 min by placing a drop (100 µL) of Fe_3O_4 nanoparticles (ca 1$mgmL^{-1}$) dispersed in PBS on the surface of gel. The signal from the chromophore in the swollen gel was tracked in Z-axis to measure the thickness of the gel.

The EDC/NHS activation step had a big impact on the thickness of swollen gels (Table A3). While dry gels without or with EDC/NHS activation showed a similar thickness (12 and 11 µm, respectively), swollen gels without EDC treatment were approximately 3 times thicker (205 µm) than activated gels (63 µm).

Table A3. Summary of thickness measurements of thin film PAAm-AA-MS hydrogels determined by confocal fluorescent microscopy.

Hydrogel	Treatment of gel for measurement			Thickness	
	EDC/NHS Pre-activation	Fluorescent labeling by		Dry	Swollen
		thiol coupling[(a)]	amine coupling[(b)]		
P(AAm-AA-MS)	no	yes	--	12 µm	205 µm
	yes	--	yes	11 µm	63 µm
P(AAm-MS) (control)	no	yes	--	12 µm	70 µm

(a) Thiol-Streptavidin/Biotin Atto 425

(b) cRGD(coum)fK

8.12 Bio-functionalization and cells culture

8.12.1 Sequential functionalization of hydrogels

For binding PDL, the gel was activated by EDC/NHS (section 8.5.2) for 15 min, followed by 1 h coupling with (10 µgmL^{-1}) PDL solution in PBS. Bioconjugation of CSRARKQAASIKVAVSADR (IK-19) (100 µgmL^{-1}) was performed by placing a drop (20 µL) of peptide solution in PBS, on the P(AAm-MS-AA) gel surface and coupling for 1 h at r.t. For orthogonal coupling hydrogel was activated with EDC/NHS and incubated with PL solution (10 µgmL^{-1}) for 1 h followed by washing and coupling with IK-19 solution (100 µgmL^{-1}). The RGD/PDL (100/10 µgmL^{-1}) and LN/PDL (100/10 µgmL^{-1}) were functionalized by similar procedure, while for RGD (100 µgmL^{-1}) and LN (100 µgmL^{-1}) ligand solutions were incubated with hydrogel for 1 h followed by washing with water.

8.12.2 Functionalization of glass substrates with an IK-19/PDL mixture

The IK-19/PDL mixture was covalently bonded on APTES functionalized glass, activated by incubation with aq. glutaraldehyde solution (8%) for 6 h, subsequent washing and incubation with IK-19/PL (100/10 µgmL^{-1}) solution.

8.12.3 Cell isolation and Seeding

The hydrogel samples functionalized with different biomolecules were placed in 24-well plates, kept for 10 min in ethanol and washed with sterilized milliQ water for 3 times. The samples were seeded with 2.6 x 10^4/cm^2 of NPCs or aNSCs. Cell growth was followed by regular intervals (6-12 h) and cells were fixed after 24 h or 5 days.

The neural progenitor cells (NPCs) isolation from cerebral cortex of C57BL/6 mice embryo (E14.5) and seeding on sample were performed by Wenqiang Fan and Dr. Felipe Ortega at Institute of Physiological Chemistry JGU, Mainz, according the reported protocol.[1] The SEZ cultures containing aNSCs were prepared from the lateral wall of the adult SEZ of young adult (8-12 weeks) C57/Bl6 and seeded by Dr. Felipe Ortega as previously reported.[15]

8.13 Immunostaining

All neural cell cultures were fixed with 4% paraformaldehyde (PFA) solution for 10 min, followed by 3 times washing with PBS pH 7.4. The cells were stained according to following protocols:

8.13.1 Neural progenitor cells (NPCs)

The fixed NPCs were respectively blocked and permeabilized with 2% bovine serum albumin (BSA) and 0.2% Triton in PBS for 45 min at room temperature. The cells were incubated at room temperature with (1:700 DCX (guinea pig, neuronal lineage marker, dianova) and 1:1000 SMI-312 (Anti Pan-axonal Neurofilament mouse IgG1, Biolegend) for 2h. Cells were washed 3 times with PBS followed by incubation for 2h at room temperature with (1:800 Cy3 anti-guinea pig and 1:1000 alexa-488 anti-mouse). The nucleus was stained by DAPI and mounted by following standard protocols. Images were taken with Zeiss Axio Observer microscope at 0.22 and 0.42 µm and per px. Time lapse videos were recorded in order to calculate cell viability and proliferation. The length of axon was measured using FIJI software. The number of branches, process and dendritic filopodia were quantified manually.

8.13.2 Neural progenitor cells (NPCs) focal adhesion staining

The fixed NPCS were permeabilization for 15 min with 0.5 % triton in PBS and washed with PBS. The cells were incubated at room temperature for 2h with DCX 1:700 (guinea pig, neuronal lineage marker, dianova) and anti-integrin β_1 antibody

(1:500, abcam) in 1% BSA. Cells were washed 3 times with PBS followed by incubation for 2h at room temperature with (1:800 Cy3 anti-guinea pig and 1:500 alexa-488 anti-mouse). The nucleus was stained by DAPI and mounted by following standard protocols. Images were taken with Zeiss Axio Observer microscope at 0.22 and 0.42 µm and per px. The focal adhesion density was counted manually.

8.13.3 Adult Neural Stem Cells (aNSCs)

The fixed aNSCs were permeabilization with 0.5 % (v/v) triton X-100 in PBS for 15 min and washed with PBS. The cells were incubated with primary antibodies prepared in 30 % (v/v) horse serum (Gibco) overnight at 4°C. The following antibodies were used anti-beta III tubulin (1:800, mouse, neuronal marker, Sigma), NG2 (1:500, rabbit, oligodendrocyte marker, Millipore) and GFAP (1:500, mouse, astrocyte marker, Sigma). The cells were washed with PBS and incubated with secondary antibodies (1:500 alexa-488 anti-mouse for neuron, 1:500 Cy3-anti rabbit for oligodendrocytes and 1:1500 Cy5 anti mouse for astrocytes). The nucleus was stained by DAPI and mounted by following standard protocols. Images were taken with Zeiss Axio Observer microscope at 0.22 µm per px and different cell types were counted manually.

8.14 Analysis and Quantification

8.14.1 Cell Proliferation

Cell proliferation was followed by time lapse experiment by taking pictures every 1 min. The number of cell was counted at t=0 and the percentage of surviving cells after t=24h and t=5 days was calculated from two independent experiments.

8.14.2 Statistical Analysis

Data were expressed as mean ± standard deviation. For each condition, a minimum of three independent experiments were performed with sample size larger than 25 fields in all cases. The value of $p < 0.05$ was used for statistical significance. A one-way ANOVA with a Tukey test of the variance was used to determine the statistical significance between groups. The statistical significance difference was set to* $\alpha < 0.05$, **$\alpha < 0.01$, ***$\alpha < 0.001$.

Appendix Chapter 5

8.15 Surface Functionalization and Photoactivation

8.15.1 Biofunctionalization of Hydrogels.

The 2 kPa hydrogels were activated by EDC/NHS (details in section 8.5.2) and incubated for 1h for functionalization with IKVAV photo-protected or native variants (200 μgmL^{-1}), IK-19 (100 μgmL^{-1}), LN (100 μgmL^{-1}) and LN/PDL (100/10μgmL^{-1}).

8.15.2 Self-assembled monolayers (SAMs) on gold substrates

SAMs monolayers were prepared on gold-coated substrates (13 mm glass, 2 nm Ti and 20 nm Au) according to previously described protocol briefly,[6] gold-coated coverslips were incubated in mixture of $HS(CH_2)_{11}$-$(OCH_2CH_2)_3OH$ (90%) and $HS(CH_2)_{11}(OCH_2CH_2)_6OCH_2COOH$ (10%) 1.0 mM thiol solution in absolute ethanol and incubated overnight. Cell culture experiments were performed on 10% COOH SAMs, rinsed with ethanol and Milli-Q water, activated by EDC/NHS (section 8.52), washed with water and coupled with peptide solutions (200 μgmL^{-1}).

8.15.3 Photo-activation of Substrates

Hydrogel functionalized with caged IK-12 peptides were irradiated for 15 min at λ= 345, 365 and 420 nm respectively for NVOC, DMNPB, and HANBP using a Xe-lamp coupled to a monochromator (Polychrome V, TILL Photonics GmbH, Gräfelting, Germany). The patterned irradiation was performed by using quartz slides with chrome patterned stripes of 10 µm width and 100 µm spacing, were placed on substrates during light exposure.

The hydrogel and SAMs samples modified with IK(HANBP)VAV was irradiated for 7 min by using a Xe-lamp at 420 nm and for strip patterns mask of 15 µm width and 50 µm spacing was used.

8.16 Cell culture experiment

8.16.1 Neural progenitor cells (NPCs) and neurosphere culture

The isolation of NPCs from cerebral cortex of E14.5 C57BL/6 mice embryo (E 14.5) and formation of neurosphere from isolated cells were performed by Wenqiang Fan according to literature reports.[1, 16]

The sterilized samples placed in 24-well cell culture plate were seeded with $5x10^4$ NPCs or with 3-5 neurosphere in each well (Figure A7).

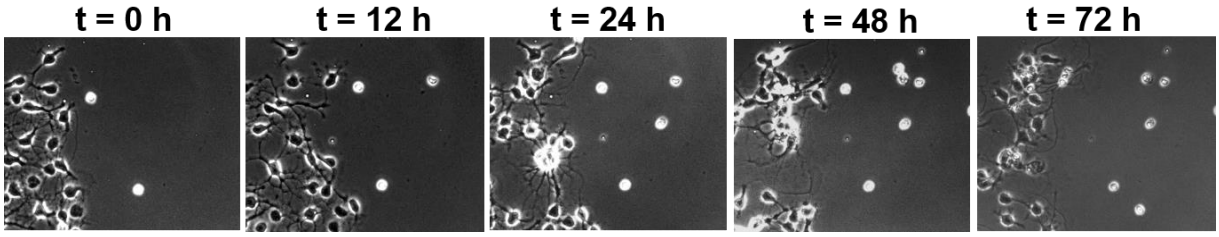

Figure A7. The neurosphere P-1 isolated from mouse embryonic (E 14.5) cortex seeded on caged IK(HANBP)VAV functionalized SAMs. The cells failed to migrate out of the explant during 4 days cell culture as observed from images after different time intervals.

8.16.2 Neo-natal explant culture

The slices from sub-ventricular zone of mouse pub (7day old) were performed by Dr. Marcelo Salierno according to reported protocol.[17] The 2-3 slices of explants (60µm) were seeded on each sample placed in 24-well plate.

8.16.3 Dissociated embryonic neural stem cells from Neurosphere Culture

The neural progenitor cells from cerebral cortex of C57BL/6 mice embryo (E14.5) were isolated and maintained as undifferentiated neurosphere by Shifang Zhao. The neurosphere were dissociated between P1 - 3 and NSCs were seeded (50,000 cells per well in 24-well plate) on caged IK-12 patterned hydrogel.

8.16.4 *In-situ* photo-activation cultures

The isolation of cerebral cortex of C57BL/6 mice embryo (E14.5) and seeding of cells on sample were performed by Shifang Zhao according to reported protocol. The samples were placed in 24-well cell culture plate and $1.2x10^4$ cells were seeded in each well. Cells were allowed to attach/sediment for 2 h at 37ºC. The samples were

placed in Zeiss Axio Observer microscope equipped with RAPP irradiation source with 405 nm laser source. The cells were irradiated for 30 sec by drawing different geometries with RAPP software. The laser power was kept at 90% and irradiation area was adjusted. The samples were followed by time-lapse microscope for 24 h. The samples were fixed and stained with SMI, DAPI and DCX as described in following section.

8.16.5 Immunostaining

The NPCs and dissociated neurosphere cultures were stained as described in Section 8.13. Images were taken with Zeiss Axio Observer microscope at 0.22 and 0.42 µm and per px. Time-lapse videos were recorded in order to follow cell survival by taking pictures after every 5 min on Zeiss Axio Observer microscope. The length of axon was measured by using FIJI software.

Appendix Chapter 6

8.17 Synthesis of Fmoc-Asp(PMNB)-OH and Fmoc-Asp(ANBP)-OH

8.17.1 Synthesis of PMNB and ANBP

The iodo-anisole was used for synthesis of PMNB while iodo-dimethylaniline was used for synthesis of ANBP according to previous reports.[9, 18] Briefly respective iodo-aryl (0.53 mmol) compounds were dissolved in mixture of EtOH (10 mL) and water (5 mL), followed by addition of compound **(d)** Section 8.2.3 (100 mg, 0.14 mmol), K_2CO_3 (70 mg, mmol), Bu_4NBr (360 mg, mmol). The mixture was flushed with argon for 10 mins and catalytic amount of $Pd(OAc)_2$ (10 mg) was added. The mixture was heated under microwave conditions at 150 °C for 10 min. Water (100 mL) was added and the aqueous phase was extracted by EtOAc (200 mL). Purification by flash chromatography using gradient elution of 50% EtOAc/n-Hexane to obtain of the title compound in 82% yield. The characterization data correlates with reported literature.

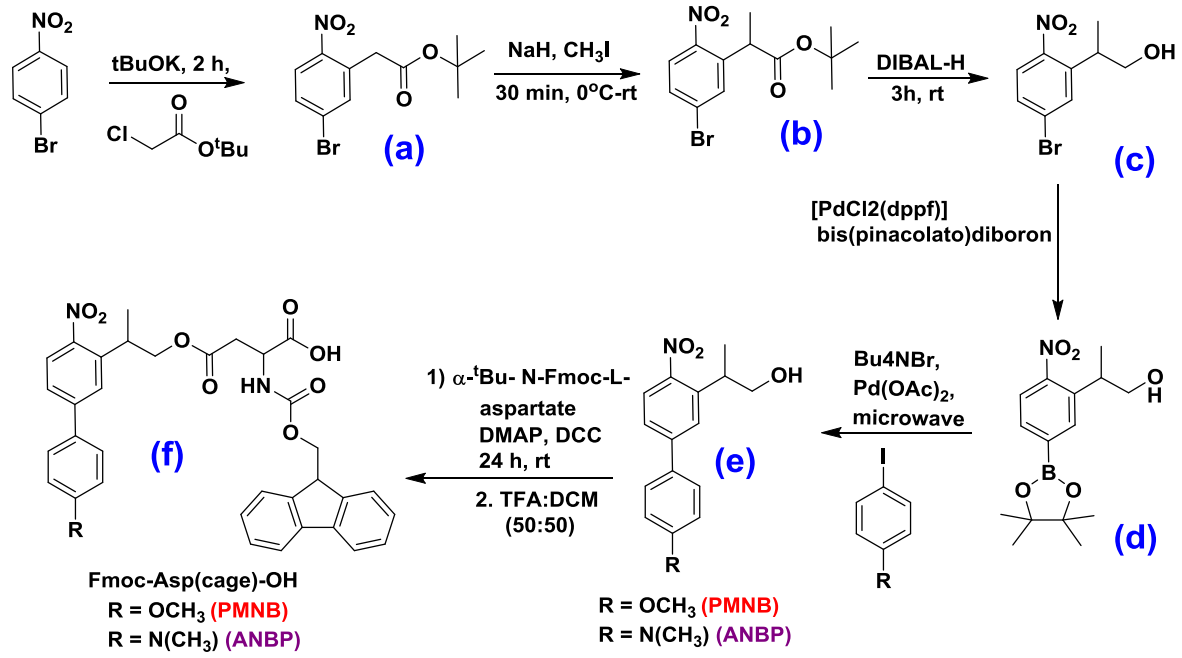

8.17.2 Fmoc-Asp(PMNB/ANBP)-OH

The PMNB (287 mg, 1 mmol) or ANBP (300mg, 1 mmol) was dissolved in dry DCM (10 mL), followed by addition of α-tert-butyl N-Fmoc-L-aspartate (411 mg, 1 mmol), DCC (200 mg, 1 mmol) and DMAP (10 mg, 81 µmol) under nitrogen. The reaction mixture was stirred overnight at room temperature followed by addition of 5% $NaHCO_3$ and product was extracted with ethylacetate. The organic layer was washed with brine and dried over $MgSO_4$. The crude product was purified by column chromatography on silica (70% EtOAc/n-Hexane) to obtain orange solid (500 mg, 77%). The product was confirmed by ESI-MS 680.47[$M+H^+$] for PMNB, at 694.63 [$M+Na^+$] for ANBP.

The compound Fmoc-(PMNB/ANBP)-OBt was dissolved in 2mL of TFA:DCM (50:50) and stirred for 1 h at room temperature, followed by evaporation of DCM. Toluene was added to the mixture and form azeotropic mixture with TFA and evaporated under vacuum. The product was used for next reaction without further purification.

Fmoc-Asp(PMNB)-OH

^{1}H-NMR (300 MHz, $CDCl_3$): δ/ppm = 1.29 (d, J=7.0 Hz, 3H); 2.83-2.94 (m, 2H); 3.84 (s, 3H); 3.43-3.60 (m, 1H); 4.16-4.27 (m, 1H); 4.31-4.38 (m, 1H); 4.41-4.46 (m, 2H); 5.47-5.56 (m, 1H); 6.92 (d, J=9.2 Hz, 2H); 7.23-7.39 (m, 6H); 7.57 (m, 3H); 7.61 (d, J=1.2 Hz, 1H); 7.72(d, J=8.4 Hz, 2H); 7.84 (d, J=1.2 Hz, 1H).

^{13}C-NMR (75 MHz, $CDCl_3$): δ/ppm = 16.7 ($-CH_3$); 33.4 (-CH); 36.7 ($-CH_2$); 55.9 ($-CH_3$); 47.5 (-CH); 51.6 (-CH); 67.3 ($-CH_2$); 114.8(-CH); 121.0(-CH); 124.4(-CH); 125.14(-CH); 127.1(-CH); 127.7(-CH); 131.4(-CH); 141.3 (-C); 143.7 (-C); 143.8(-C); 145.8 (-C); 156.2 (-C); 158.8 (-C); 159.0(-C=O); 171.4(-C=O); 175.1 (-C=O)

ESI-MS: 647.68 [M+Na]+

Fmoc-Asp(ANBP)-OH

^{1}H-NMR (300 MHz, $CDCl_3$): δ/ppm = 1.34 (d, J=7.0 Hz, 3H); 2.86-2.97 (m, 2H); 3.09 (s, 6H); 3.83-3.90 (m, 1H); 4.14-4.17 (m, 1H); 4.20-4.36 (m, 1H); 4.39-4.42 (m, 2H); 5.77-5.80 (m, 1H); 6.76 (d, J=9.2 Hz, 2H); 7.26-7.39 (m, 6H); 7.48 (m, 3H); 7.58(d, J=1.2 Hz, 1H); 7.67 (d, J=8.4 Hz, 2H); 7.84 (d, J=1.2 Hz, 1H).

^{13}C-NMR (75 MHz, $CDCl_3$): δ/ppm = 17.5 ($-CH_3$); 33.2 (-CH); 36.7 ($-CH_2$); 40.3 ($-CH_3$); 47.1 (-CH); 50.7(-CH); 67.3 ($-CH_2$); 112.5(-CH); 120.0(-CH); 124.4(-CH); 125.14(-CH); 127.1(-CH); 127.7(-CH); 128.0(-CH); 141.3 (-C); 143.7 (-C); 143.8(-C); 145.8 (-C); 156.0(-C=O); 156.2 (-C); 158.8 (-C); 169.4(-C=O); 176.1 (-C=O)

ESI-MS: 637.59 $[M+Na]^+$

8.17.3 Synthesis of Fmoc-Asp(HANBP)-OH

a. 4-(2-(5-bromo-2-nitrophenyl)propyl) α-tert-butyl N-Fmoc-L-aspartate (d´´)

The 2-(5-bromo-2-nitrophenyl)propan-1-ol (**c**) section 8.2.3 (260 mg, 1 mmol) was dissolved in dry DCM (10 mL), followed by addition of α-tert-butyl N-Fmoc-L-aspartate (411 mg, 1 mmol), DCC (200 mg, 1 mmol) and DMAP (10 mg, 81 µmol) under nitrogen. The reaction mixture was stirred overnight at room temperature followed by addition of 5% $NaHCO_3$ and product was extracted with ethylacetate. The organic layer was washed with brine and dried over $MgSO_4$. The crude product was purified by column chromatography on silica (70% EtOAc/n-Hexane) to obtain orange solid (500 mg, 77%) and confirmed by ESI-MS 654.43 $[M+H]^+$.

The obtained product was dissolved in 2 mL of TFA:DCM (50:50) and stirred for 1 h at room temperature, followed by evaporation of DCM. Toluene was added to the mixture and form azeotropic mixture with TFA and evaporated under vacuum. The compound **d´´** was used for next reaction without further purification.

^{1}H-NMR (300 MHz, $CDCl_3$): δ/ppm = 1.21 (d, J=7.0 Hz, 3H); 2.86-2.97 (m, 2H); 3.38-3.54 (m, 1H); 4.14-4.22 (m, 2H); 5.27-5.34 (m, 1H); 7.23-7.34 (m, 4H); 7.54-7.57 (d, J=1.2 Hz, 1H); 7.76 (dd, J=8.4/1.2 Hz, 1H); 8.20 (d, J=7.5 Hz, 1H).

^{13}C-NMR (75 MHz, $CDCl_3$): δ/ppm = 17.9 ($-CH_3$); 35.2 (-CH); 36.4 ($-CH_2$); 47.3 (-CH); 50.7(-CH); 59.4 ($-CH_2$); 67.3 ($-CH_2$); 113.6 (-CH); 121.5 (-CH); 125.2 (-CH); 126.4 (-CH); 126.9 (-CH); 133.1 (-CH); 139.4 (-C); 145.2 (-C); 148.6 (-C); 151.5 (-C); 156.7 (-C=O); 154.8 (-C=O); 172.3 (-C=O).

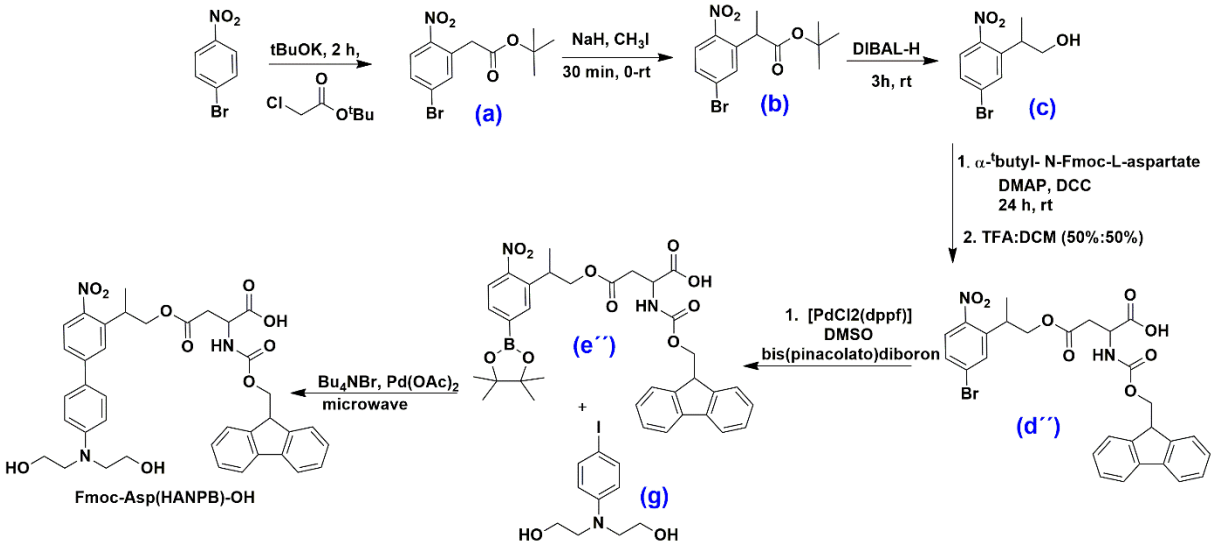

b. 4-(2-(5-bromo-2-nitrophenyl)propyl) (e´´)

The compound (**d´´**) (397 g**,** 0.67 mmol) was dissolved in DMSO (10 mL), followed by addition of PdCl2(dppf) (97 mg, 0.1mmol), KOAc (163 mg, 1.66 mmol), bis(pinacolato)diboron (372 mg, 1.46 mmol) and heated to 80 °C overnight. The reaction mixture was poor into 50 mL ice-water slush and extracted with ethyl acetate (3x100 mL) and dried over $MgSO_4$. The solvent was evaporated and crude product was purified by silica gel flash chromatography EtOAc/n-Hexane (20-50%) to obtain orange red solid (320 mg, 42%).

^{1}H-NMR (300 MHz, $CDCl_3$): δ/ppm = 1.22-1.29 (m, 12H); 1.23 (d, J=7.0 Hz, 3H); 2.86-2.97 (m, 2H); 3.58-3.74 (m, 1H); 4.14-4.17 (m, 1H); 4.27-4.43 (m, 1H); 4.39-4.42 (m, 2H); 5.27-5.34 (m, 1H); 7.23-7.34 (m, 4H); 7.54-7.59 (d, J=1.2 Hz, 1H); 7.76 (dd, J=8.4/1.2 Hz, 1H); 8.14 (d, J=7.5 Hz, 1H).

^{13}C-NMR (75 MHz, $CDCl_3$): δ/ppm = 17.9 ($-CH_3$); 24.6 ($-CH_3$); 34.2 (-CH); 36.4 ($-CH_2$); 47.1 (-CH); 50.7(-CH); 58.4 ($-CH_2$); 67.3 ($-CH_2$); 88.7 (-C); 113.6 (-CH); 121.5

(-CH); 125.2 (-CH); 126.4 (-CH); 126.9 (-CH); 133.1 (-CH); 137.4 (-C); 142.2 (-C); 143.6 (-C); 151.5 (-C); 156.7 (-C=O); 154.8 (-C=O); 172.3 (-C=O).

c. 4-(2-(5-bromo-2-nitrophenyl)propyl) α-tert-butyl N-Fmoc-L-aspartic acid

The compound **(g)** 2,2'-((4-iodophenyl)azanediyl)bis(ethan-1-ol) (165 mg, 0.53 mmol) was dissolved in mixture of EtOH (10 mL) and water (5 mL), followed by addition of compound **(e´´)**, K_2CO_3 (70 mg, mmol), Bu_4NBr (360 mg, mmol). The mixture for flushed with argon for 10 mins and catalytic amount of $Pd(OAc)_2$ (10mg) was added. The mixture was heated under microwave conditions at 150 °C for 10 min. Water (100 mL) was added and the aqueous phase was extracted by EtOAc (200 mL). Purification by flash chromatography using gradient elution of 50% EtOAc/n-Hexane to obtain of the title compound in 82% yield.

Fmoc-Asp(HANBP)-OH

^{1}H-NMR (300 MHz, $CDCl_3$): δ/ppm = 1.21 (d, J=7.0 Hz, 3H); 2.86-2.97 (m, 2H); 3.38-3.54 (m, 1H); 3.83-3.94 (m, 3H); 4.14-4.17 (m, 1H); 4.20-4.36 (m, 3H); 4.39-4.42 (m, 2H); 5.27-5.34 (m, 1H); 6.67 (d, J=9.2 Hz, 2H); 7.23-7.34 (m, 6H); 7.48 (m, 3H); 7.57(d, J=1.2 Hz, 1H); 7.69(d, J=8.4 Hz, 2H); 8.21 (d, J=1.2 Hz, 1H).

^{13}C-NMR (75 MHz, $CDCl_3$): δ/ppm = 17.9 ($-CH_3$); 34.2 (-CH); 36.4 ($-CH_2$); 47.1 (-CH); 50.7(-CH); 58.4 ($-CH_2$); 61.6 ($-CH_2$); 67.3 ($-CH_2$); 112.5(-CH); 120.0(-CH); 123.8(-CH); 125.42(-CH); 127.3(-CH); 127.7(-CH); 128.0(-CH); 141.3 (-C); 143.7 (-C); 144.8(-C); 147.8 (-C); 156.0(-C=O); 158.2 (-C); 159.2 (-C); 171.4(-C=O); 176.1 (-C=O)

ESI-MS: 637.59 $[M+Na]^+$

8.18 Synthesis of RGD(PMNB/ANBP/HANBP)fC

8.18.1 Coupling of Amino acids

All peptides were synthesized manually by Fmoc solid-phase peptide synthesis (SPPS) from preloaded H-Gly-2-Cl-Trt resin (0.54 mmol/g, 100 mg resin) adapting reported protocol. [6] Next amino acids were sequentially coupled by adding solution of the Fmoc-amino acid (2 equivalents, 0.084 mmol), HOBt (2 equivalents, 0.084 mmol), HBTU (2 equivalents, 0.084 mmol), and DIPEA (5.6 equivalents, 0.084 mmol) in DMF (10-15 ml/g of resin) with shaking vigorous for (1-3 h). The coupling solution was then filtered out and the resin was washed five times with DMF. Fmoc

protecting group from subsequent amino acids were cleaved by treating resin twice with 20% piperidine in DMF (10 min x 2) with vigorous shaking followed by washing five times with DMF. The linear peptide was grow in following order Gly-Arg(pbf)-Cys(Trit)-D-Ph-Asp (O^tBu).

8.18.2 Cleavage from Resin for

The linear protected peptide was cleaved from the resin by treating the resin with trifluorethanol/acetic acid/DCM (1/3/6) three times with 6 ml of solution 30 min each time. Toluene was added to the filtrate and the solvents were removed in vacuum to obtain crude peptide.

8.18.3 Cyclization of Peptide

The linear peptide was dissolved in high dilution in DMF (c = 5 $x10^{-3}$ mol), DPPA (3 eq) and $NaHCO_3$ (5 eq) and mixture was stir for 48h at r.t protected from light. The mixture was filtered to remove $NaHCO_3$ and DMF was evaporated under high vacuum. The cyclic peptide was precipitated in water and precipitates were collected by centrifugation at 4000 rpm for 30 min. The water was removed and precipitates were dried.

8.18.4 Deprotection of side chain protection

The deprotection of lateral chains from Arg(pbf) and Cys(Trt) was performed by dissolving the peptides in 3 mL of 95% TFA/H_2O and stirring for 2h at r.t. Solvent was evaporated to 20% of the initial volume and 15 ml diisopropyl ether was added. The precipitate was centrifuged and dried in high vacuum to obtain the deprotected crude product. Crude peptides were purified by RP-HPLC using 0.1% TFA-containing water/acetonitrile combination as eluents. The peptides were purified by 5 to 95% gradual increase of acetonitrile (over 40 min). The fractions were collected and freeze dried to obtained pure solid peptide confirmed by ESI-MS and analytical HPLC.

8.19 Preparation and Functionalization of PEG Hydrogel

The 4-Arm PEG Maleimide 20K (100 $mgmL^{-1,}$ 4.5 mM) was dissolved in HEPES buffer (pH 7.4, 10 mM) inside sterile Laminar flow. The stock solution of RGDfC (3.36 $mgmL^{-1}$, 5 mM), RGD(PMPB)fC (4.23 $mgmL^{-1}$,5 mM) and VPM peptide (GCRDVPMSMRGGDRCG, 26.6 $mgmL^{-1}$, 15.6 mM) were also prepared in sterile

HEPES buffer (pH 7.4). These concentrations were kept constant for all experiments.

8.19.1 Hydrogel for stiffness Measurements

The 4-Arm PEG Maleimide 20K (4.5 mM, 4 µL) was mixed with RGD (5 mM, 2 µL) and kept at 37°C for 30 min. The HEPES (2 µL, pH 7.4) was added to this mixture and the drop of mixture (8 µL) was placed on lower plate of rheometer (8 mm) arranged in parallel plate geometry. The VPM (15.6 mM, 2 µL) was added to the above mixture and mixed with pipette tip. The head plate was adjusted above the sample and the area surrounding the drop was sealed with silicone oil to avoid evaporation. The stiffness was measured by time sweep at 25 and 37°C, with 0.5% applied strain at 0.5N force and 0.1rad/sec oscillation amplitude. The stiffness was calculated from storage modulus by using equation **4** section 8.7.4.

8.19.2 Swelling and Thickness measurement

The 5 mM solution of 4-Arm-PEG Maleimide was mixed with RGDfC (2:1) at 37°C for 30 min. To the PEG mixture, HEPES and VPM were mixed (3:1:1) and allow to polymerize in Ibidi® 15 µwell angiogenesis slide for 30 min at 37°C. The obtained hydrogels were overnight kept in water and thickness of swollen hydrogel was measured by digital Vernier caliper.

The swelling ratio was determined by weighing swollen hydrogel (Ws) and the hydrogel was dried at 40°C for 24 h and weight of dry hydrogel was determined (Wd). The swelling ratio was obtained by using equation **3** section 8.7.5.

8.19.3 Photo-patterning PEG hydrogel modified with caged Fluorescein

The 4-Arm-PEG Maleimide (5 Mm,10 µL) was mixed with NH_2-PEG-SH (3.5 K, 1 mM in HEPES, 1 µL) and incubated for 15 min at 37°C. The CMNB-caged Fluorescein (2.4 mM in HEPES, 2 µL) was added to above solution and incubated further for 15 min at 37°C. The solution was placed in Ibidi® 15 well angiogenesis slide and mixed with VPM (5mM, 2 µL) and allow to gelate at 37°C for 30 min. The obtained hydrogels was transferred to Ibidi glass bottom petridish (35mm) and kept in water during photopatterning. The sample was placed in Zeiss LSM 800 microscope and scanned with Coherant two photon laser 10 mW, at 760 nm with different scanning speeds and time. The predefined patterns were drawn by Zeiss LSM 800 ROI tool.

The z-stack of obtained pattern was created by using confocal Zeiss LSM 800 microscope in GFP channel.

8.20 Cell Culture experiment in 2D and 3D

8.20.1 Functionalization of P(AAm-co-MS) hydrogel

The 10kPa P(AAm-co-MS) hydrogels were prepared according to protocol mentioned in Section 8.7.3. The hydrogels were incubated with 20 µL drops of RGD(PMPB)fC (0.25 $mgmL^{-1}$) solution in PBS pH 7.4 for 1h at r.t. The hydrogel were washed with water and samples were either fully uncaged or irradiated through a mask (300 µm glass with 600µm chrome) by illumination at 360 nm (0.22 mW) for 6 min by using Till Photonics Polychrome 5000 lamp. The samples were placed in 24 well plates, sterilized by ethanol, washed 3 times with PBS and incubated with cells.

8.20.2 Fibroblast L929 cell culture

Fibroblast L929 cell line were cultivated at 37° C in 5% CO_2 in RPMI medium (Gibco) supplemented with 10% fetal bovine serum (Invitrogen) and 1% P/S (Invitrogen). The peptide functionalized hydrogel samples were placed in 24-well plate and incubated with 500 µL of 1×10^5 cells/well suspension of Fibroblast L929 at 37 °C and 5% CO_2. After 6 h the medium was substituted with fresh medium to remove unattached cells, and further incubated for 24 h. The cells were fixed with 4% PFA solution, permeabilized with 0.1% Triton, actin fibers were stained with TRITC-phalloidin (1:200), the samples were mounted with DAPI containing mounting medium (Dinova) to stain nucleus by using standard protocols. Fluorescence images were taken with Zeiss Axio Observer epi-fluorescence microscope.

8.20.3 The *in-situ* photoactivation in 2D

The cell attached on pre-irradiated RGD(PMPB)fC patterns were irradiated by Zeiss LSM microscope with 10x objective equipped with Coherent two photon laser 10mW at 760 nm. The predefined patterns between two strips of cells were drawn by Zeiss LSM 800 ROI tool. The cells after irradiation were kept in incubator and observed after 2, 6 and 24 h to follow migration of cells on the predefined lines. The cells were fixed with 4% PFA solution, permeabilized with 0.1% Triton, actin fibers were stained

with TRITC-phalloidin (1:200), the samples were mounted with DAPI containing mounting medium (Dinova) to stain nucleus by using standard protocols.
Fluorescence images were taken with Zeiss Axio Observer epi-fluorescence microscope.

8.20.4 3D cell culture protocol

The Fibrin clot of Fibroblast L929 cell line was prepared by following literature report. [19] The cell pellet of $1X10^6$ cells was dissociated in 5 $mgmL^{-1}$ fibrinogen (Sigma, from human plasma) and 2 µL drops were placed on Sigmacote coated glass slide (Check section 8.7.5 for details). The 1 µL thrombin solution ($5UNmL^{-1}$, Sigma) was mixed with each drop of fibrinogen and the cells were placed in incubator for 15 min to get fibrin clot.

8.20.5 Photo-activation in 3D

The 4-Arm-PEG Maleimide 4.5 mM was mixed in 2:1 with 5mM RGDfC or RGD(PMPB)fC and incubated for 30 min at 37 °C. The cell culture medium was added to above solution in 1:3 and 8 µL drops of mixture were placed in Ibidi® 15µwell angiogenesis slide. One fibrin clot was picked up by tweezers and added to each well followed by addition of 15.6 mM VPM peptide. The gel was allowed to polymerized for 15 min at 37°C and with 5%CO_2 in incubator followed by addition of medium to each well. The samples, after 30 min of cell culture were irradiated by Zeiss LSM microscope as explained in section 8.19.3. The samples were observed regularly after every 12-24 h and kept in culture for 3-7 days. The cell culture medium was each day substituted with fresh medium. The samples were fixed with 4% PFA solution for 2h, washed with PBS and blocked with 1% BSA solution for 1h. The cells were permeabilized with 0.5% Triton for 1 h, actin fibers were stained with TRITC-phalloidin (1:200 in water) and nucleus was stained by Hoechst 33342, trihydrochloride, trihydrate (1:500 in water, life technology). The samples were washed with PBS and imaged by Zeiss Axio Observer epi-fluorescence microscope and by Zeiss LSM 800 confocal microscope.

References

[1] A. Farrukh, J. I. Paez, M. Salierno, W. Fan, B. Berninger, A. del Campo, *Biomacromolecules* **2017**, *18*, 906-913.

[2] S. Petersen, J. M. Alonso, A. Specht, P. Duodu, M. Goeldner, A. del Campo, *Angew Chem Int Ed Engl* **2008**, *47*, 3192-3195.

[3] T. T. Lee, J. R. García, J. I. Paez, A. Singh, E. A. Phelps, S. Weis, Z. Shafiq, A. Shekaran, A. del Campo, A. J. García, *Nature Materials* **2015**, *14*, 352-360.

[4] S. Weis, Z. Shafiq, R. A. Gropeanu, A. del Campo, *Journal of Photochemistry and Photobiology A: Chemistry* **2012**, *241*, 52-57.

[5] V. San Miguel, C. G. Bochet, A. del Campo, *Journal of the American Chemical Society* **2011**, *133*, 5380-5388.

[6] M. Wirkner, S. Weis, V. San Miguel, M. Álvarez, R. A. Gropeanu, M. Salierno, A. Sartoris, R. E. Unger, C. J. Kirkpatrick, A. del Campo, *ChemBioChem* **2011**, *12*, 2623-2629.

[7] aO. F. Zouani, J. Kalisky, E. Ibarboure, M.-C. Durrieu, *Biomaterials* **2013**, *34*, 2157-2166; bP. Moshayedi, L. da F Costa, A. Christ, S. P. Lacour, J. Fawcett, J. Guck, K. Franze, *Journal of Physics: Condensed Matter* **2010**, *22*, 194114; cA. Farrukh, J. I. Paez, M. Salierno, A. del Campo, *Angewandte Chemie - International Edition* **2016**, *55*, 2092-2096; dA. Farrukh, J. I. Paez, M. Salierno, A. del Campo, *Angew Chem Int Ed Engl* **2016**.

[8] F. Buhr, J. Kohl-Landgraf, C. Hanus, D. Chatterjee, A. Hegelein, E. M. Schuman, J. Wachtveitl, H. Schwalbe, *Angewandte Chemie International Edition* **2015**, *54*, 3717-3721.

[9] L. Donato, A. Mourot, C. M. Davenport, C. Herbivo, D. Warther, J. Léonard, F. Bolze, J. F. Nicoud, R. H. Kramer, M. Goeldner, *Angewandte Chemie International Edition* **2012**, *51*, 1840-1843.

[10] T. Vilaivan, *Tetrahedron Lett.* **2006**, *47*, 6739-6742.

[11] N. Toda, S. Asano, C. F. Barbas, *Angew. Chem., Int. Ed.* **2013**, *52*, 12592-12596.

[12] N. Delsuc, J. M. Léger, S. Massip, I. Huc, *Angew. Chem. Int. Ed.* **2007**, *119*, 218-221.

[13] J. R. Tse, A. J. Engler, *Current protocols in cell biology* **2010**, *10.1002/0471143030.cb1016s47*.

[14] S. Petersen, J. M. Alonso, A. Specht, P. Duodu, M. Goeldner, A. del Campo, *Angew. Chem. Int. Ed.* **2008**, *47*, 3192-3195.

[15] F. Ortega, M. R. Costa, T. Simon-Ebert, T. Schroeder, M. Gotz, B. Berninger, *Nat Protoc* **2011**, *6*, 1847-1859.

[16] M. R. Costa, R. Jagasia, B. Berninger, *Protocols for Neural Cell Culture: Fourth Edition* **2010**, 29-49.

[17] E. Mire, C. Mezzera, E. Leyva-Díaz, A. V. Paternain, P. Squarzoni, L. Bluy, M. Castillo-Paterna, M. J. López, S. Peregrín, M. Tessier-Lavigne, *Nature neuroscience* **2012**, *15*, 1134-1143.

[18] aL. García-Fernández, C. Herbivo, V. S. M. Arranz, D. Warther, L. Donato, A. Specht, A. del Campo, *Advanced Materials* **2014**, *26*, 5012-5017; bA. Specht, F. Bolze, L. Donato, C. Herbivo, S. Charon, D. Warther, S. Gug, J.-F. Nicoud, M. Goeldner, *Photochemical & Photobiological Sciences* **2012**, *11*, 578-586.

[19] aC. A. DeForest, K. S. Anseth, *Nature chemistry* **2011**, *3*, 925-931; bS.-H. Lee, J. J. Moon, J. L. West, *Biomaterials* **2008**, *29*, 2962-2968.

List of Scientific Contributions

Articles

1. Bioconjugating thiols to poly(acrylamide) gels for cell culture using methylsulfonyl co-monomers, **A. Farrukh**, J. I. Paez, M. Salierno, A. del Campo*, Angewandte Chemie*, 55, 2092–2096, **2016**.

2. Bifunctional poly(acrylamide) hydrogels through orthogonal coupling chemistries, **A. Farrukh,** J. I. Paez, M. Salierno, W. Fan, B. Berninger, A. del Campo, *Biomacromolecules*, 18, 906–913, **2017**.

3. Biofunctionalization of poly(acrylamide) gels, J.I. Paez, **A. Farrukh**, O. Ustahüseyin, A.del Campo, A chapter contributed to book Lab protocol series "*Methods in Molecular Biology*" (MiMB), Springer **2017**. Series Editor John M. Walker. ***In print***

4. Bifunctional hydrogels containing the laminin-motif IKVAV promote neurogenesis, **A, Farrukh,** F. Ortega, W. Fan, N. Marichal, J.I. Paez, B.Berninger, A. del Campo, M.J. Salierno, *Stem Cell Reports*, 9, 1432–1440, **2017**.

5. Light-guided neuronal growth using phototriggered adhesive ligands, **A, Farrukh,** W. Fan, S. Zhao, M. Salierno, J.I. Paez, A. del Campo, M.J. Salierno, **2017. Submitted.**

6. Two photon photoactivatable caged cyclic RGD for 3-D guided cell migration, **A.Farrukh**, J.Paez, A.del Campo. **Manuscript in preparation**

7. A bifunctional Platform to decouple cell-cell and cell-matrix forces, **A. Farrukh**, D. Joseph, R. Vakkeel, A. del Campo. **Manuscript in preparation**

8. *In situ* light-guided axon growth with photoactivatable laminin peptidomimetics, **A. Farrukh**, S. Zhao, J. Paez, M. Salierno, A. del Campo. **Manuscript in preparation.**

Scientific Talks

1. Light responsive laminin mimetic peptides for directional neural regeneration, **A. Farrukh**, M. Salierno, J. Paez, F. Ortega, B. Berninger, A. del Campo, WE-Heraeus-Seminar (622) on Neural Mechanics, August **2016**, Bad Honnef, Germany.

2. Directional neural regeneration by using photo-triggered laminin mimetic peptide, **A. Farrukh**, M. Salierno, J. Paez, F. Ortega, B. Berninger, A. del Campo, MPGC Annual Retreat, October **2015**, Munich, Germany.

3. Directional neural regeneration by using photo-triggerable laminin mimetic peptide, **A. Farrukh**, M. Salierno, J. Paez, F. Ortega, B. Berninger, A. del Campo. Biomaterials & Tissue Engineering, Gordon Research Conference, July **2015**, Girona, Spain.

4. Bioconjugation to poly(acrylamide) gels beyond Sulfo-SANPAH: thiol coupling with methylsulfone comonomers, **A. Farrukh**, Julieta I. Paez, Marcelo Salierno, Aránzazu del Campo, European Polymer Congress, June **2015**, Dresden, Germany.

Poster Presentations

1. Guiding neuronal networks with light, **A. Farrukh**, M. Salierno, J. Paez, F. Ortega, B. Berninger, A. del Campo, Leibniz PhD Workshop on Health Technologies, September **2016**, Berlin, Germany.

2. Photo-guided axon growth by using light responsive laminin mimetic peptide, **A. Farrukh**, M. Salierno, J. Paez, F. Ortega, B. Berninger, A. del Campo, WE-Heraeus-Seminar (623) on Cellular Dynamics, September **2016**, Bad Honnef, Germany.

3. Bioconjugation to Poly(acrylamide) gels beyond SulfoSANPAH: thiol coupling with methylsulfone co-monomers, **A. Farrukh,** J. Paez, A. del Campo, Gordon Research Seminar, July **2015**, Girona, Spain.

4. Directional Neural Regeneration by Using Photo-Triggerable Laminin Mimetic Peptide, **A. Farrukh,** M. Salierno, J. Paez, F. Ortega, B. Berninger, A. del Campo, Biomaterials & Tissue Engineering, Gordon Research Conference, July **2015**, Girona, Spain. **Poster Selected for Talk at GRC.**

5. Light triggered axon growth, **A. Farrukh,** M. Salierno, J. Paez, F. Ortega, B. Berninger, A. del Campo, 5th International Symposium: Interface Biology of Implants, May **2015**, Warnemünde, Germany.

6. Light triggered axon growth, **A. Farrukh**, M. Salierno, J. Paez, F. Ortega, B. Berninger, A. del Campo, Symposium "Vorbild Natur" Gesellschaft Deutscher Naturforscher und Ärzte (GDNÄ), September **2014**, Mainz, Germany.

Participation in exercises

1. Tutorial-ship: Organic Chemistry, 3rd Semester WS 2015/2016, at Institute for Pharmacy and Biochemistry, JGU, Mainz, Germany.

Participation in lectures

1. Modern techniques in neuroscience, MPI-Brain Research, Frankfurt (March-April **2015**), **European credit points 2.5.**
2. Biomaterials-Based Approaches to Personalized Medicine, Leibniz Health Tech Symposium, 22 March **2017**, Berlin, Germany.
3. Cell culture basic course, Promo-cell academy, 8 - 11 July **2014,** Heidelberg, Germany.

Participation in soft skills seminars

1. Public Speaking for Women, 3 - 4th September 2015 Sci Mento-Hessenweit, Goethe-Universität Frankfurt, Germany.
2. Communication in the academic context, 21st October 2015, Munich, Germany.
3. Conflict management for doctoral candidates, 22nd October 2015, Munich, Germany.
4. Scientific Presentation Skills, 17-19 September 2015, MPIP, Mainz, Germany.